Faculty of Computing, Engineering and Media

Institute of Energy and Sustainable Development

An investigation into the performance of a very shallow borehole thermal energy store for a solar-assisted ground source heat pump

A thesis submitted in partial fulfilment of the requirements for the degree of Doctor of Philosophy (Ph.D)

by

Carlos Andres Naranjo Mendoza

Leicester, UK

May 2020

To my parents:
This effort is minimal
compared to the sacrifice
they have made for me,
to be where I am.
Infinite thanks.

"A person who never made a mistake,
never tried anything new."
Albert Einstein

Acknowledgements

The journey throughout this investigation has not been easy, there have been stumbles and falls, but without a doubt, it has also been plenty of achievements, growth, and satisfaction.

First, I want to express my gratitude to my supervisor Prof. Rick M. Greenough, for his constant support and guidance. His practical way of seeing things has been a valuable contribution to my development as a researcher. Thank you.

Likewise, I would like to thank my second supervisor Dr. Andrew J. Wright, and my non-official supervisor Dr. Muyiwa A. Oyinlola for their technical support, advice and constructive suggestions that improved the academic quality of my work.

Thanks to my Alma Mater, Escuela Politécnica Nacional, for the financial support during the time of my studies.

To Jerko (†) and Ivan for being the first people to push me on this journey called doctorate. Thanks.

A special mention to my friends and colleagues from the Institute of Energy and Sustainable Development (IESD), for the pleasant and fun moments shared inside and outside the university.

To my family: parents, brothers, sisters, and nephews who, despite the distance, have always been opened to give me their support when I have needed it most.

Finally, I want to make a special thanks to those whom I consider my family in the UK, Pamela, Andrés, Isabel, and Nervo, for helping me to have a balance in my life that has been crucial during this adventure.

Abstract

Ground-source heat pumps (GSHP) have been used in building applications to meet heating needs at lower energy costs. Likewise, solar thermal systems have been integrated into conventional GSHP to reduce the size of the ground heat exchanger and provide seasonal heat storage. So far, this technology has mainly been used in large commercial or residential buildings due to its high installation costs.

The present work focuses on an experimental and numerical investigation on the thermal performance of a very shallow borehole heat exchanger for a solar-assisted ground source heat pump (SAGSHP) for small-scale applications. For the experimental part, energy analysis of a small domestic SAGSHP was conducted. The main innovation of this system is the use of an array of 16 very shallow (1.5-metre depth) boreholes to store heat seasonally into an underground earth energy bank (EEB). In the numerical investigation, different models were developed to study the thermal performance of the natural soil as well as the thermal response of very shallow borehole heat exchangers.

A comparison in accuracy and time of simulation was carried out between the Infinite Line Source (ILS) model, the Infinite Cylindrical Source (ICS) model, and a new model developed by the author based on the Finite Difference Method (FDM). To consider in the model the interaction between adjacent boreholes as well as the impact of the natural soil temperature, the superposition technique was applied.

Results show that the proposed model based on the FDM is faster and more accurate than the conventional analytical models (ILS and ICS) to study the thermal response of very shallow boreholes. Likewise, dimensionless graphical representations (a.k.a. G-functions) were developed for the study of very shallow boreholes for different types of soil thermal properties and different borehole diameters.

List of publications

Journal Publications

1. Naranjo-Mendoza, C., Wright, A. J., Oyinlola, M. A., & Greenough, R. M. (2018). A comparison of analytical and numerical model predictions of shallow soil temperature variation with experimental measurements. *Geothermics*, 76, 38–49. doi: https://doi.org/10.1016/j.geothermics.2018.06.003

2. Naranjo-Mendoza, C., Oyinlola, M. A., Wright, A. J., & Greenough, R. M. (2019). Experimental study of a domestic solar-assisted ground source heat pump with seasonal underground thermal energy storage through shallow boreholes. *Applied Thermal Engineering*, 162, 114218. doi: https://doi.org/10.1016/j.applthermaleng.2019.114218

Conferences Publications with Peer Review

1. Naranjo-Mendoza, C., Greenough, R. M., & Wright, A. J. (2018). Are shallow boreholes a suitable option for inter-seasonal ground heat storage for the small housing sector?. In *Proceedings of the IGSHPA Research Track 2018 (pp. 1–10). International Ground Source Heat Pump Association*. Stockholm, Sweden. doi: https://doi.org/10.22488/okstate.18.000040

2. Naranjo-Mendoza, C., Wright, A. J., Oyinlola, M. A., & Greenough, R. M. (2019). Application of the superposition technique in conduction heat transfer for analysing arrays of shallow boreholes in ground source heat pump systems. In *Proceedings of 16th UK Heat Transfer Conference*. Nottingham, UK.

3. Naranjo-Mendoza, C., Sakellariou, E., Wright, A. J., Oyinlola, M. A., & Greenough, R. M. (2019). Thermal Analysis of an Earth Energy Bank. In

Proceedings of 16th UK Heat Transfer Conference. Nottingham, UK.

4. Naranjo-Mendoza, C., Greenough, R. M., & Wright, A. J. (2019). Integrating solar to ground seasonal heat storage for the small domestic heating sector in the UK: Experiments from a research prototype. In *Proceedings of the International Conference on Energising the SDGs through appropriate technology and governance*, Institute of Energy and Sustainable Development, De Montfort University, Leicester, UK.

Others

1. Naranjo-Mendoza, C., (2017). HEATING FROM THE SOIL - Interseasonal Ground Heat Storage. In *Ph.D student poster competition*, De Montfort University, Leicester, UK.

2. Naranjo-Mendoza, C., (2019). Modelling of shallow geothermal boreholes. In *ASHRAE student competition*, Loughborough University, Loughborough, UK.

Awards

1. Best Poster Award at the Ph.D student poster competition, April, 2017, De Montfort University, Leicester, UK.

2. Second Price Award at the ASHRAE student presentation competition, March, 2019, Loughborough University, Loughborough, UK.

Contents

List of Figures

List of Tables

Nomenclature

Acronyms

ASHP Air source heat pump

ATES Aquifer thermal energy storage

BC Boundary condition

BES Building energy simulation

BTES Borehole thermal energy storage

COP Coefficient of performance

DHW Domestic hot water

EEB Earth energy bank

ETC Evacuated tubes solar collectors

FDM Finite difference method

FLS Finite line source

FPC Flat plate solar collectors

GCHP Ground coupled heat pump

GHE Ground heat exchanger

GSHP Ground source heat pump

GWHP Groundwater heat pump

HC Hydrofluorocarbon fluid

HFC Hydrofluorocarbon fluid

HGHE Horizontal ground heat exchanger

HP Heat pump

ICS Infinite cylindrical source

ILS Infinite line source

PCM Phase change materials

PTES Pit thermal energy storage

PV Photovoltaic

PVT Photovoltaic thermal

RTD Resistance temperature detector

SAGSHP Solar assisted ground source heat pump

SPF Seasonal performance factor

SWHP Surface water heat pump

TTES Tank thermal energy storage

UC Unglazed solar collectors

VGHE Vertical ground heat exchanger

Symbols

$\dot{m}$ Mass flow rate in kg/s

$\dot{V}$ Volume flow rate in m^3/s

A Surface in m^2

a Exponent of the primary variable

B Borehole spacing in m

c_p Specific heat in J/kgK

D Distance below the surface, diameter

$E1$ Exponential integral

EF Efficiency of the model

Fo Fourier number

G Heat flow in the ground surface in W/m^2

H Length in m

h Enthalpy in J/kg

J_0 Bessel function of first kind, zero order

J_1 Bessel function of first kind, first order

k Thermal conductivity in W/mK

L Length in m

m Mass in kg

N Number of boreholes

n Number of nodes

$NRMSE$ Normalised root mean square error

Nu Nusselt number

Pr Prandlt number

Q Heat in J

q Heat flow in J/m

R Thermal resistance in K/W

r Radius in m

R^2 Coefficient of determination

$RMSE$ Root mean square error

T Temperature in °C or K

t Timein s

U Global coefficient of heat transfer in W/m^2

W Work in J

x Variable

Y_0 Bessel function of second kind, zero order

Y_1 Bessel function of second kind, first order

z Axial distance in m

Greek letters

α Thermal diffusivity in m^2/s

β Shape coefficient

Δ Gradient or variation

δ Penetration depth in m

η Efficiency

γ Euler constant = 0.5772

ω Uncertainty

ϕ Time in radian cycle

ρ Density in kg/m^3

Θ Dimensionless time

ε Effectiveness of heat exchangers

Subscripts

a Air

b Borehole

$build$ Building

$comp$ Compressor

conv	Convection
EEB	Earth energy bank
ele	Electricity
eq	Equivalent
eva	Evaporator
f	Fluid
gen	Generated
geo	Geothermal
ghe	Ground heat exchanger
gr	Ground
grout	Grouting material
HX	Heat exchanger
i	Spatial element
in	Inlet
j	Temporal element
loss	Losses
m	M element
nat	Natural soil
o	Initial
out	Outlet
p	pipe
po	Outer pipe
r	Radial

s	Soil, surface
solar	Solar
surr	Surroundings
tot	Total
u	Useful

1. Introduction

1.1 Research Background

As a result of the decline of heavy industry production, more efficient technology and policies focused on the reduction of greenhouse gases, in the last 20 years the final energy consumption in the UK has been reduced, from 156 million tons of oil equivalent (Mtoe) in 1998 to 142 Mtoe in 2018 [3]. In the domestic sector the reduction in final energy use went from 46 Mtoe in 1998 to 41 Mtoe in 2018 [3]. However, from 2014 to 2018, the domestic sector has increased its energy consumption by 7%. Heating consumption is the main reason for this increase since 80% of the final energy consumption of the domestic sector is for space heating and domestic hot water [3].

One of the reasons for this trend is the high dependence of the domestic sector's energy consumption on outdoor environmental conditions. The UK has a heating-dominated climate where the challenges are related to the design of more energy-efficient housing and the use of heating systems with renewable energy sources. On the one hand, energy-efficient homes allow heating demands to be lower and thus require smaller active systems to meet those demands. On the other hand, renewable energy systems are more sustainable and operate with minimal environmental impact [4].

In the UK, renewable technologies with the most significant potential for domestic heating are solar systems and ground source heat pumps (GSHP). However, solar systems have greater potential in summer when the demand for heating is minimal, while geothermal systems have the problem that they cannot recover in summer all the heat extracted during winter, causing a thermal imbalance and reduction in the COP of the GSHP [5]. For this reason, the combination of the two technologies to create a more efficient system with seasonal heat storage has great potential to develop a sustainable system, with a low long-term environmental impact. This type of system makes use of what is

known as Borehole Thermal Energy Storage (BTES), and its principle is to store heat in the soil during summer to extract it in winter either directly or through a GSHP [6].

GSHP has advantages over a conventional (air source) heat pumps, mainly because the ground is a source of higher temperature heat than the air in winter, which increases the coefficient of performance (COP) of the heat pump [7]. GSHPs are classified according to the type of geothermal heat exchanger (GHE) used. Horizontal heat exchanger systems are typically installed between 1.5 and 2 meters deep, and pipe arrangements are placed on a large surface of land [8]. On the other hand, borehole heat exchangers are composed of double or single U-tube boreholes, installed at depths between 40 and 300 meters [9]. The limitation in the large-scale use of vertical systems is the high cost of installing the GHEs. In horizontal systems, it is required to remove large volumes of soil, while in vertical systems, robust machinery is needed for drilling deep into the ground [10].

Nevertheless, as previously mentioned, improvements in building construction methods plus the use of more efficient technologies such as solar assisted ground source heat pumps (SAGSHP) systems or dual-source heat pumps systems, have allowed a reduction in the size of the GHE, with very shallow boreholes (shorter than 5 metres deep) appearing as an alternative [11]. Even though very shallow boreholes are affected by the seasonal and short-term temperature variations in the shallow soil [12], this concept presents an advantage since the use of shallow systems makes this type of technology much cheaper than conventional borehole drilling. In fact, for very shallow systems drilling can be done with a fence post auger [13]. An example of this is the concept of the solar house developed by Caplin Homes, which uses an array of very shallow boreholes (only 1.5 metres deep) assisted by solar energy to store heat within the boundary of a dwelling's foundations. Another example is the development at Priors Hall Park in Corby which is heated by using a very shallow geothermal system [14].

The use of solar energy allows an increase in the temperature of the ground, and this also contributes to the reduction in the size of the vertical boreholes [13]

and allows seasonal heat storage. This concept is profitable when applied in new buildings where the machinery to build the foundations is already on-site, which minimises the drilling cost. Undoubtedly, in the UK the potential of this type of systems is high. In fact, according to the Ministry of Housing, Communities and Local Governments, in the last four years, in average 153400 homes are built in England each year [15]. Considering the increasing heating demand in the domestic sector due to the increase in the number of homes, it can be predicted that there is much potential for the implementation of the technology of very shallow GSHP systems.

1.2 Problem definition

While the use of geothermal systems with very shallow boreholes shows many advantages there is little published research into this technology. For this reason, the thermal behaviour of this type of systems in the long term is not known, nor is the way that the natural temperature variation of the shallow soil affects the thermal response of this type of systems or what theory can be used to size these systems. Moreover, when using very shallow boreholes along with solar systems for seasonal heat storage, it is still unknown what the optimal configuration of this type of system is to maximise the overall efficiency. For this reason, it is necessary to maintain active research in the area to be able to contribute design methodologies and develop a theory of the thermal behaviour of very shallow geothermal boreholes. In this way, one can contribute by filling research gaps in this area and generating results that can be used by building services engineers who intend to use this type of system.

For such reasons, it is necessary to develop models that are suitable for studying the thermal response of very shallow geothermal boreholes. The peculiarity of the shallow soil is that it cannot be considered to be undisturbed (constant temperature throughout the year), so the natural temperature variations in the soil will have an impact on its thermal response. Figure 1.1 shows the typical variation of soil temperature as a function of depth. In the very shallow soil (less than 5 metres deep), the soil temperature cannot be treated as constant.

Conventional models, such as the Infinite Line Source (ILS), Infinite Cylindrical Source (ICS) or Finite Line Source (FLS), have been tested as simple and accurate models for the study of conventional vertical boreholes (depth greater than 30 metres) [16]. However, these types of models do not consider seasonal variations in the natural temperature of the soil. On the other hand, software-based on complex numerical methods such as ANSYS, OpenFoam and Comsol can be used to model very shallow systems. Nevertheless, the use of such systems has a high computational cost, in addition to the need for expensive licenses and specialised training. Therefore, this is not an ideal approach for the design or parametric studies of very shallow boreholes.

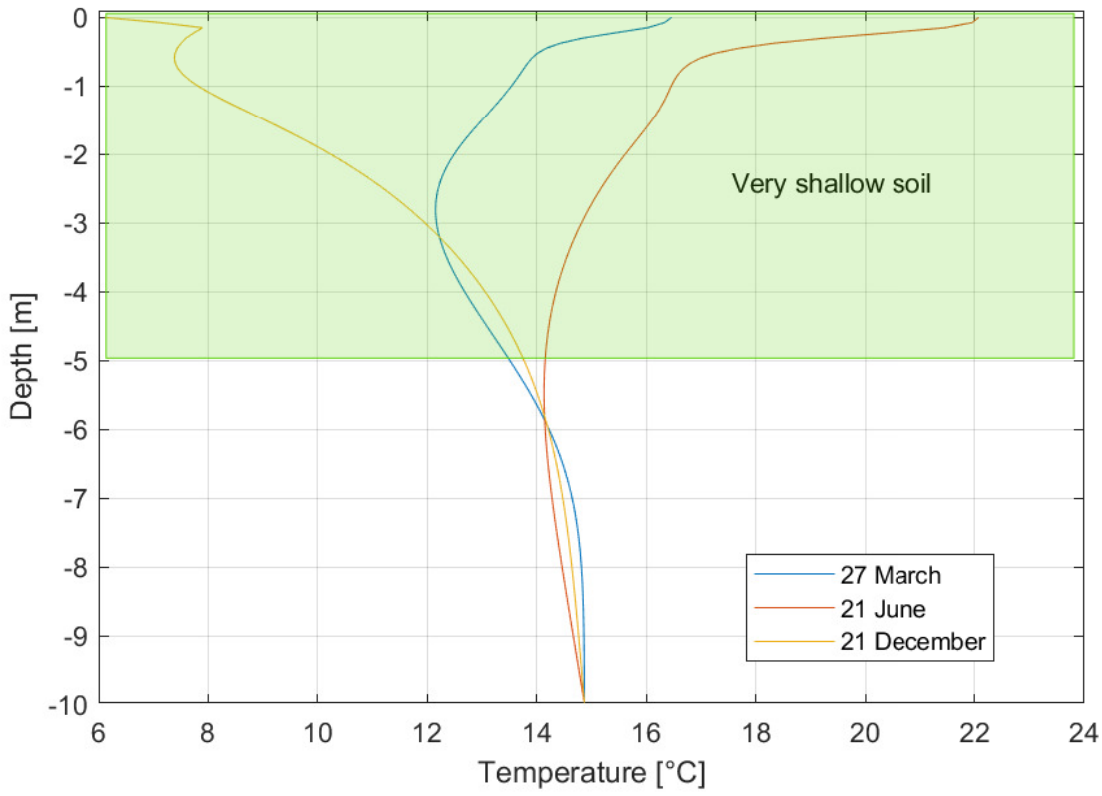

Figure 1.1: Natural soil temperature variation (for illustration only)

One approach to deal with this problem is to use simpler numerical methods such as the finite difference method (FDM). This method has been widely used in studies of heat transfer to solve complex systems accurately and quickly [17]. The application of this model can be done through any programming language.

Additionally, to deal with more complex problems that include multiple

boreholes and the natural temperature variation in the soil, the superposition technique that simplifies the treatment of complex heat transfer problems can be applied [18]. This technique is key to deal with multidimensional heat transfer problems, like an array of boreholes, in a simple way. It should be noted that to validate any model of very shallow boreholes, an experimental system that serves as a reference is needed. To this end, a refurbished Victorian house was used at De Montfort University to investigate the performance of a SAGSHP that uses a geothermal heat exchanger with very shallow boreholes. This is part of the Grasmere Street project [4, 19]. This system is based on a design from Caplin Homes that uses photovoltaic thermal (PVT) collectors coupled to a GSHP via an array of very shallow boreholes (1.5-metre deep) for heat injection and extraction [13].

Finally, in order to contribute to the practical creation of new designs of very shallow borehole arrays, the model must be simple and easy to use. For this, the most common form for the presentation of the results of geothermal heat exchanger models is a series of graphical representations called G-functions. These graphs allow a practical study of the thermal response of vertical boreholes at different time scales and for different soil thermal properties. The problem to be solved in the current investigation focuses on the development of models to determine the thermal response of very shallow geothermal boreholes when heat is added or removed, while also considering the natural temperature variation of the soil.

1.3 Aim and objectives

The aim of this research is to develop a practical model that is accurate enough to evaluate the thermal response of very shallow boreholes in the short and long term.

To achieve this aim, the following objectives are proposed:

- To analyse the current performance of the SAGSHP system of the Grasmere Street Project from the experimental data.
- To develop an accurate dynamic model to estimate the heat diffusion in

the soil under variable ambient conditions.

- To develop a dynamic model to study the thermal response of very shallow borehole heat exchangers.
- To perform a parametric or sensitivity study to analyse the impact of the different variables of the model in the performance of a very shallow borehole heat exchanger.
- To develop G-functions or graphical representations of the thermal response of very shallow boreholes.

1.4 Research scope

The scope of this research is the development of a computationally efficient model that is accurate enough to study the thermal response of very shallow geothermal boreholes from an engineering point of view or for engineering applications. Although the model will be developed based on the physical principles of heat transfer, simplifications will be made to accelerate the resolution time of the model with only a minimal and acceptable reduction in accuracy. The model to be developed is not intended to be of a specific application in the very short term (range of a few seconds). That is, it will not consider the transient effects within the working fluid.

Also, since the research will be based on an experimental retrofitted low carbon heating system featuring seasonal thermal storage (developed and installed by Caplin Homes) the model will be validated using experimental data from this system. The scope of the modelling approach is flexible enough to be extrapolated to other applications since it is based on a physical model. However, the model will not be validated with experimental data from another type of system. In the same way, although the model is intended to offer the flexibility to be applied for generic heat extraction and injection systems under different climate conditions, the case study will be based on a domestic heating system in Leicester, UK. Finally, the application of this very shallow system is intended to satisfy the thermal demands of small buildings such as dwellings or small

offices. Given the nature of this system, it is not suitable for use in tall buildings.

1.5 Thesis structure

This thesis is structured according to the specific objectives defined in section 1.3. This chapter introduces the topic and justifies the need for this research. In addition, it defines the aim and objectives to be achieved.

Chapter 2 presents a detailed literature review that focuses primarily on three topics: a) seasonal heat storage; b) small-scale solar assisted ground source heat pumps and c) thermal response models for geothermal boreholes. These are the primary fields that must be addressed in order to meet the objectives.

Chapter 3 presents the proposed methodology to address the aim of the present research, that is based on an experimental and numerical investigation. This chapter shows the methodology from a general perspective since the specific resolution methods are shown in the corresponding chapters.

The experimental investigation is shown in Chapter 4. This chapter describes the operation of the experimental system of the Grasmere Street project. Emphasis is placed on the behaviour of the seasonal energy storage system known as an Earth Energy Bank (EEB). This chapter is based on the paper published in Applied Thermal Engineering by the author of this thesis [4].

Chapter 5 shows different analytical and numerical models to estimate the natural temperature of the shallow soil since this is very relevant in storage systems with very shallow boreholes. This chapter is based on the paper published in Geothermics by the author of this thesis [12].

The model for estimating the thermal response of very shallow boreholes is developed in Chapter 6. The results of applying two different analytical models (ILS and ICS) are compared with the results of applying numerical models by the finite difference method (FDM). The results are validated by comparison with the experimental data from the Grasmere Street project.

In Chapter 7 the developed model is applied, and the EEB thermal response is evaluated over the long term and under different thermal properties of materials. Also, G-functions are developed to estimate the thermal response of arrays of

very shallow boreholes at different time scales and soil properties.

Finally, Chapter 8 presents a summary of the main findings of this research as well as the contributions to knowledge and potential areas of future research.

Note: Matlab codes developed in this Ph.D. research can be found here or in the following web address:
https://data.mendeley.com/datasets/gc4wf4dg8t/draft?a=2554b852-cfc9-4152-ac9f-0572fb677f95.

2. Literature Review

In this chapter, the literature that is most relevant to the research aim is reviewed. The review starts with an overview of the more generic themes and gradually moves towards the specific. This is necessary to determine in detail the gap in knowledge and the potential ways to cover this gap. The literature in this chapter is divided into three main themes. The first covers seasonal storage, its importance and the most common methods. The second part focuses on solar-assisted ground source heat pumps (SAGSHP); their operating principles, configurations and relevant examples are shown. Finally, the third part deals with the main methods for modelling vertical geothermal (borehole) heat exchangers and the superposition technique for modelling heat transfer in complex multidimensional systems.

2.1 Seasonal thermal storage

It is well known that the buildings sector is one of the primary consumers of global energy, being responsible for 40% of the total global energy consumption [20]. For this reason, in recent decades, standards have been implemented for more efficient construction in order to avoid excessive growth in the energy demand of buildings [21]. Likewise, there has been great support for the implementation of renewable energy technologies in the building sector [22]. Within these, both thermal and photovoltaic solar energy have been the most widely developed technologies in recent years, which has had the effect of reducing prices. For example, the price of photovoltaic panels have decreased by 70% between 2010 and 2016 [22]. This, undoubtedly, sets an encouraging scenario for years to come. However, one of the significant challenges that has not been completely resolved is the mismatch between the availability/generation of energy through renewable sources and the use of it [23]. When talking only about thermal systems, solar energy is the most common form of renewable energy to contribute

to the heat demand of modern buildings [24]. However, the highest production of solar energy occurs during summer and in the daytime when the heat demand is lowest. For this reason, heat storage both in the long term (seasonal) and in the short term (diurnal) is the best option to deal with the mismatch between heating production and consumption [25]. Of these two, short-time heat storage has been widely studied for several decades, is efficient and is relatively affordable. However, in locations with very cold winters and/or low availability of solar energy during the winter, its contribution to heating is very limited [26].

For this reason, seasonal heat storage systems have generated more interest. Although its initial cost is higher and the heat losses throughout the year are more significant, it has been shown that the overall efficiency of the seasonal storage heating system is higher, and this translates into long-term savings [27]. In fact, it has been shown, through experimental storage systems implemented in Europe, that the benefit/cost is higher for seasonal storage than short-term storage. It is anticipated that seasonal storage could typically cover up to 70% of annual heat demands compared to 20% if short-term storage is used [25]. In the following sections, the advantages of seasonal heat storage are described in greater detail, as well as the main storage methods.

2.1.1 Principles and importance of thermal storage

The principle of heat storage is to deal with the mismatch between heat production and use. For example, Figure 2.1 shows the typical distribution between annual solar heat production and heat demand in buildings in locations in the northern hemisphere. The principle of seasonal heat storage is to temporarily store the excess heat generated during summer, to distribute it or use it to meet the heating needs during the winter. In an ideal system that has seasonal heat storage, the advantages are not only about overcoming the mismatch, but also that the overall efficiency of the system is higher, there is a reduction in CO_2 emissions, and the sustainability of the system is greater [28].

Heat can be stored in three different ways: sensible, latent or thermochemical [29]. Sensible heat storage is the most common form of heat storage. In this type of storage, when the heat is injected into or extracted from a medium,

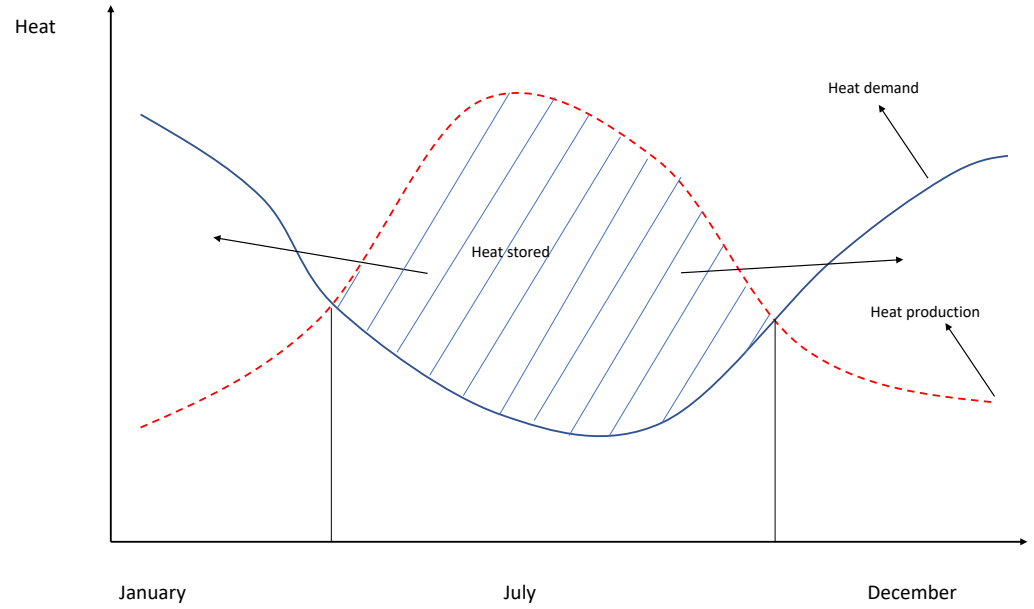

Figure 2.1: Typical heating production/demand distribution

only the temperature of that medium is affected (water, soil, rock, oil, among others). This is the simplest form of heat storage and the amount of heat stored is proportional to the mass of the medium, the specific heat and the temperature gradient between the initial and final state of the storage medium, as expressed in Equation 2.1:

$$q_{st} = mc_p\Delta T \tag{2.1}$$

where: q_{st} is the heat stored in J, m is the mass of the medium where heat is stored (water, soil rocks, etc.) in kg, c_p is the specific heat of the storage medium J/kgK and ΔT is the temperature difference in K.

Since in sensible heat storage there is a change in the temperature of the medium, the heat losses are typically greater. Therefore, greater efforts are made in the use of insulation and in determining optimal ways to improve the compactness of practical storage units to reduce the heat exchange with the surroundings [27].

The latent heat storage occurs when material stores or releases heat during the phase change transition and ideally is an isothermal process (although in practice there is small temperature gradient from the beginning to the end of the phase change). The phase change can occur during boiling or condensation (gas and liquid phases) or melting and solidification (solid and liquid phases).

In latent heat storage for building heating applications, the process is usually done in liquid-solid phases due to the high energy density (enthalpy) and to avoid problems related to pressure changes [28]. When heat is being stored, the material melts at constant temperature. The amount of heat stored by the material can be expressed according to Equation 2.2:

$$q_{st} = m\Delta h \tag{2.2}$$

where: Δh is the phase change enthalpy or the fusion enthalpy in J/kg.

Latent heat storage has a higher energy density compared to sensible heat storage and has several advantages such as lower heat losses and a lower material mass requirement [29]. However, it still has the barrier that the technologies have not been highly developed, so their implementation has a high cost mainly for seasonal storage due to the large volumes of material needed [30].

Thermochemical heat storage involves the use of materials that store and release heat by chemical reactions to certain conditions. The energy density of thermochemical reactions is very high compared to that of sensible and latent storage [28]. One of the most common examples in thermochemical storage is by using salt hydrate reactions. This type of storage is still in the initial research stage, and an ideal form of thermochemical reaction for seasonal storage has not been identified [31]. Table 2.1 shows a summary of the main characteristics of the different types of heat storage (data adapted from [28] and [30]).

Due to the scope of this research, which is based on sensible heat storage, the literature review focuses on technologies and research conducted on sensible seasonal storage. The following sections show in greater detail the different methods of sensible seasonal storage, as well as relevant examples in building applications.

2.1.2 Seasonal thermal storage methods

Within seasonal heat storage there are mainly two types of storage medium: solid (e.g. rocks, ground, sand, etc.) and liquid (e.g. water). The heat storage capacity, as well as the ease of absorbing and releasing heat, depends on the thermal conductivity and the specific heat in solids and the convection heat

Table 2.1: Comparison of different thermal storage methods

Storage type	**Energy density kWh/m^3**	**Conditions**	**Cost £/m^3**
		Sensible	
Granite	14	ΔT= 20°C	50-150
Water	23	ΔT= 20°C	30-500
		Latent (melting)	
Water	85	T_{melt}= 0°C	50-500
Paraffins	50	T_{melt}= 5-130°C	
Salts	167-417	T_{melt}=300-800°C	
		Thermochemical	
Salt hydrates	>556	T=65°C	2-5000

transfer and specific heat in liquids [27]. The difference between using a solid or liquid medium depends on availability. Water has a higher specific heat capacity than solids and transfers heat more easily. However, common solids used in seasonal heat storage can tolerate higher temperature ranges without undergoing phase change. Also, solids do not present problems related to leaks as water does [32]. The most common forms of seasonal heat storage were defined in the EU-funded project (FP7 EINSTEIN) on "Effective Integration of Seasonal Thermal Energy Storage (STES) in Existing Buildings" [1, 33] where four methods of seasonal heat storage were distinguished:

Tank Thermal Energy Storage (TTES)

It consists of a large water tank connected to the charging/discharging heating circuit. Heating charging can be direct (when the storage water circulates through the solar system) or indirect (when the heat is transferred to the water through a heat exchanger). This tank is usually placed underground to reduce heat losses, it is insulated, and the housing is usually made of concrete or steel. To improve heat transfer, the tank is normally stratified. These types of tanks allow storage temperatures of up to 95°C when not pressurized. Figure 2.2 shows

a schematic of a TTES [1]. According to the EINSTEIN project report [1], in order to be feasible, a TTES must have a storage volume greater than 1000 m^3. At a volume below these dimensions the heat losses are very high. The heat storage density of TTES is in the range of 60-80 kWh/m^3. This type of system can be installed in any location if the soil where it is installed is stable. It is typically installed at depths between 5 and 15 metres and has the advantage of not contaminating the environment since it is not in direct contact with underground water flows.

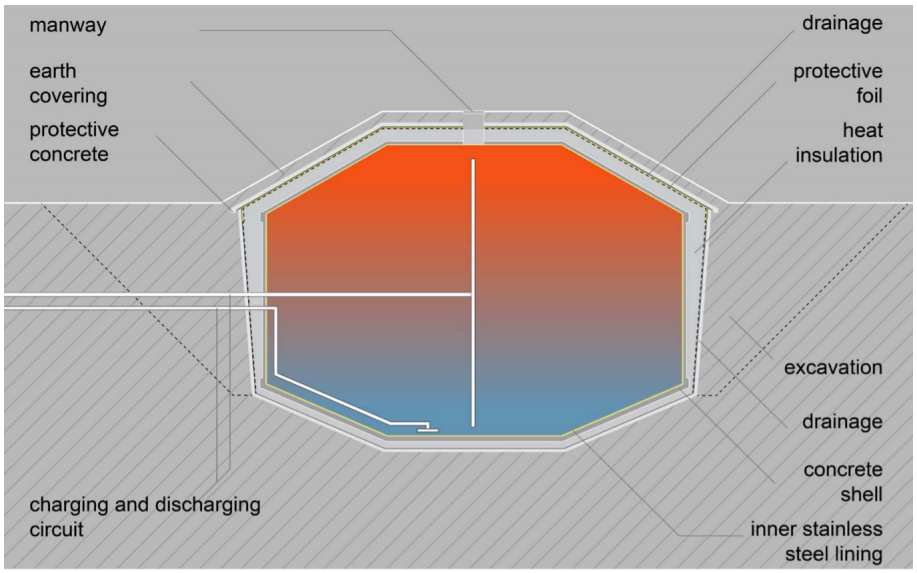

Figure 2.2: Schematic of a TTES: from [1]

Pit Thermal Energy Storage (PTES)

It consists of an underground excavation typically between 5 to 15 metres deep. The side walls are supported by shotcrete. The walls and floor of the pit may or may not be insulated, while the covering is always insulated to avoid heat loss with the surface. Pits are usually filled with water or a mixture of water and gravel. The combination of these two materials means that this type of storage has a lower capacity than a TTES, so the PTES require a greater storage volume than the TTES. Normally, as the gravel has greater thermal conductivity, there is less water stratification. The heat storage density of the PTES is in the range of 30-50 kWh/m^3. Charging and discharging can be done by direct or indirect heat exchange, the latter being the most desirable in order to prevent

solid materials from obstructing the passage of the fluid [1]. The construction of PTES is simpler than of TTES since they do not require concrete supports. PTES are usually constructed using naturally inclined pit walls. Figure 2.3 shows a typical scheme of a PTES.

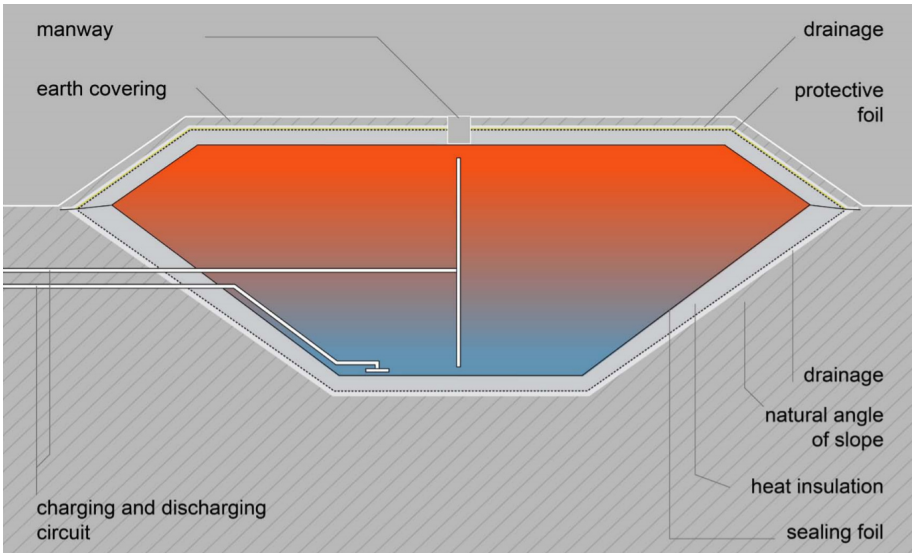

Figure 2.3: Schematic of a PTES: from [1]

Aquifer Thermal Energy Storage (ATES)

This type of storage takes advantage of self-contained natural underground aquifers as a heat storage medium. ATES work by the use of two wells, one for injection (hot well) and one for extraction (cold well). Water is pumped into the solar system from the cold well and is injected back into the aquifer through the hot well. Then, when the stored heat is needed, the system is reversed, and the heat is extracted from the water through the hot well indirectly and it is reinjected into the aquifer through the cold well. This type of system is much less expensive since natural underground aquifers are used. However, heat losses are greater since no insulation is used. Wells are normally constructed by drilling the ground. One of the fundamental requirements in the ATES is that the aquifers are confined in natural geological formations, hence, there are no natural water flows [1]. One of the main limitations of the ATES is the difficulty to accurately estimate the storage volume and therefore the energy capacity of the ATES. Figure 2.4 shows a typical scheme of an ATES.

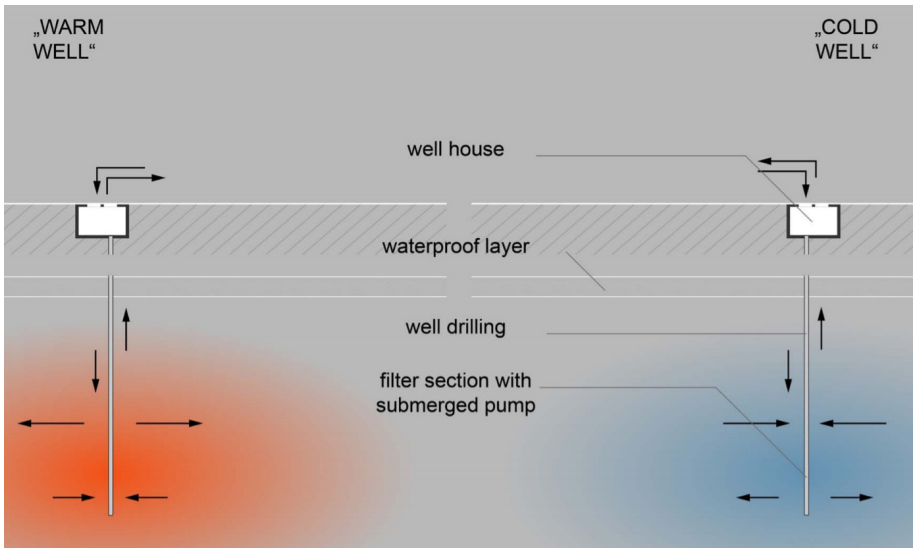

Figure 2.4: Schematic of an ATES: from [1]

Borehole Thermal Energy Storage (BTES)

This type of system stores heat in the subsurface ground. Vertical or inclined boreholes are used to indirectly inject heat into the ground through a working fluid (typically water). Vertical boreholes are installed at depths of up to 100 metres. When heat is required, it can be extracted for direct heating (in case of high-temperature storage) or through a heat pump when the storage temperature is low. For the installation of vertical boreholes, the ground is drilled, and heat exchangers are installed, which can be single or double U-tube or coaxial tubes. Finally, the boreholes are filled with grouting material that serves as a stabilizer and is also a non-permeable material. The grouting material must have a thermal conductivity close to the ground thermal conductivity (typically from 0.8 to 3 W/mK) to avoid a high thermal resistance between the ground and the fluid. This type of system is usually only insulated at the top. Moreover, it is not desirable to install BTES in sites with large groundwater flows [1]. Likewise, due to the lower specific heat of the ground compared to water and because the heat transfer is only conductive, the ground has greater thermal inertia. Therefore, these systems are not suitable to meet peak heat demands and require a backup system or a heat pump. The heat storage density of the BTES is in the range of 15-30 kWh/m^3. Figure 2.5 shows a diagram of the typical configuration of a BTES.

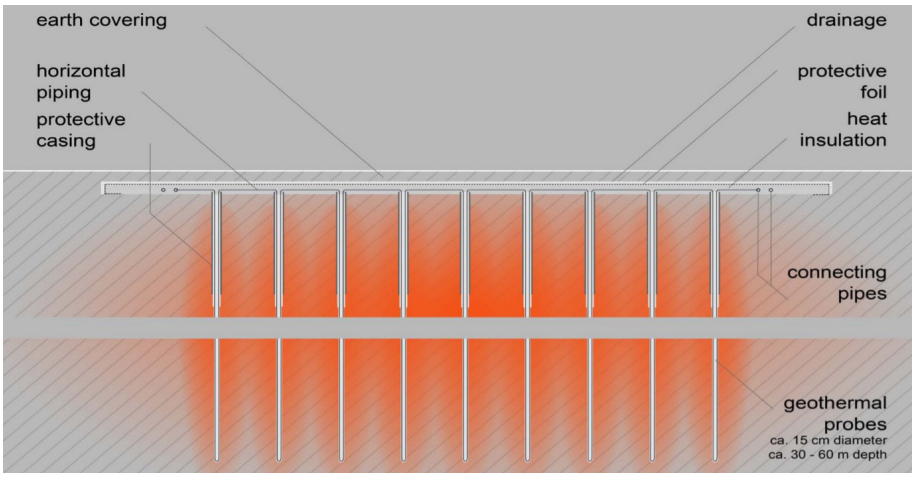

Figure 2.5: Schematic of a BTES: from [1]

Each of the four forms of seasonal sensible heat storage has advantages and disadvantages over others. For example, TTES can be installed at any location and are independent of the type of ground. In addition, water has greater heat capacity than ground, so they require a smaller volume. However, this type of system is very expensive (up to 500 £/m^3 [30]) because it requires the construction of a large insulated water tank and needs appropriate supporting elements. On the other hand, PTES are less expensive than TTES and have adequate thermal properties (storage density of up to 50 kWh/m^3 [30]). However, this type of system cannot be installed in any location since it requires not only a large surface but also a stable soil. ATES have advantages since the storage medium is water, but its use is very limited since there must be unique geological conditions for its proper performance. Finally, the BTES are more accessible (up to 150 £/m3 [30]) than the TTES and the PTES, and do not require installations or insulation since the ground is a slow heat diffuser. On the other hand, due to the low thermal capacity of the ground, BTES require very large volumes which can make the system more expensive. However, this type of system has a lot of potential in new building constructions since already scheduled soil removal can be increased to install vertical boreholes more affordably. In addition, given today's emphasis on building efficiency (e.g. greater use of insulation, greater air tightness, passive designs, etc.), the heating loads of buildings are lower in new constructions. This makes the necessary volume of heat storage smaller. Consequently, very shallow vertical boreholes can be considered.

This research focuses on this last point. That is, in the use of BTES as a heat storage system. The study focuses on using the soil as a medium for seasonal storage of low-temperature heat (less than 30°C) with solar energy injection. When the soil stores heat at a low-temperature, that heat cannot be used for direct heating, and a heat pump is required to increase the temperature for space heating. Storing heat at low-temperature has several advantages. For example, heat losses are lower since there is a lower thermal gradient with the surroundings. In addition, a heat pump that operates in soil at a temperature higher than the natural one has greater efficiency. The following section shows relevant examples of the use of BTES to cover building thermal loads.

2.1.3 Relevant studies using large-scale BTES

BTES can be used to store heat both in the short-term and in the long-term and can also work for heating and cooling [34]. The most common way to store heat is by using vertical boreholes (single or double U-tube), although there are also horizontal subsurface systems. However, the latter is not desirable for seasonal storage because of the greater area of contact with the environment that increases heat losses [35]. Regarding heat sources, BTES are commonly coupled to solar systems, although in case of availability, they can also be recharged by heat rejected from industrial processes [34]. Several examples of BTES recharged by rejected heat from air conditioning systems or industrial processes can be found in [36–41]. This review summarises the most relevant examples of BTES recharged by solar energy for district heating or large-scale systems.

Undoubtedly one of the most relevant examples of district heating using BTES is the case of Drake Landing Solar Community (DLSC) in Okotoks, Alberta (Canada). This system uses BTES to store heat seasonally, through 2293 m^2 of flat plate solar collectors. This heat serves to supply up to 90% of the heating demands of 52 homes. The BTES consists of 144 vertical boreholes of 35 metres deep. Additionally, the system has a 240 m^3 water tank for short-term heat storage, which serves to meet peak heat demands. The storage temperature in the centre of the BTES ranges between 40 and 70°C throughout the year. The heating system operates by prioritising the use of the short-term storage tank.

If the heat in the tank is insufficient, then heat stored in the BTES is sent to the water tank via a heat exchanger. Finally, if the demand cannot be satisfied, natural gas boilers are used as a backup [42]. This system is one of the best known since it is the only large-scale system that has been able to reach a solar fraction of 90% for more than 5 years of operation. Also, this system has the peculiarity that it does not use a heat pump to extract heat from the ground due to the high heat storage temperature. Another interesting example is the Braedstrup District Heating (Denmark) that supplies heat to 1500 homes. Part of this heat is supplied by a BTES system that can supply up to 20% of the total heating load. The BTES consists of 48 vertical boreholes (single U-tube) of 45 metres depth. The heat that is stored in the ground comes from 18600 m^2 of flat plate solar collectors. The difference with the DLSC system is that in Braedstrup the heat is extracted by a 1.2 MW ground source heat pump. Simulation studies of this system have shown that the storage temperature in the centre of the BTES would reach 40°C [43]. Another district heating system was built in Anneberg (Sweden). The BTES system consists of 100 vertical boreholes of 65 metres deep heated from 2400 m^2 of flat plate solar collectors. In this system the heat is not extracted through a heat pump, but directly from the ground and is heated to the desired temperature by electric heaters. After a two-year experimental evaluation, it was determined that the contribution of heat stored in the ground is minimal since more than 40% of heat is lost annually [44]. Another important example is that of Neckarsulm (Germany) where a BTES system for domestic heating of 300 apartments was built. The BTES is charged by heat from 5670 m^2 of flat plate solar collectors. The BTES consists of 528 vertical boreholes (single U-tube) of 35 metres deep. The centre of the BTES reaches a temperature of up to 70°C and heat extraction does not require a heat pump. The design solar fraction of the system was 50% and after two years of monitoring, it was shown that the system reached a solar fraction of 44% which is very promising [45]. Undoubtedly, there are more district heating systems using BTES, however, the core of this research focuses on small-scale systems which are reviewed in greater detail in section 2.2.

2.1.4 Barriers and challenges in seasonal thermal storage

Based on the literature review conducted, different types of barriers to the implementation of seasonal heat storage systems can be identified. One of the greatest barriers is the cost of such systems and the large initial investment required to install a seasonal storage system. Even in the case of the BTES that are the most economical, the initial costs for drilling the ground are usually the main barrier for their implementation [46]. On the other hand, technical and geological barriers limit the large-scale application of seasonal storage systems. As previously seen, PTES, ATES or BTES systems require certain geological conditions for installation. This implies that geological surveys are required to assess the feasibility of implementing these systems, which implies an additional cost [47]. Finally, the lack of trained personnel to create this type of system (both for design and for implementation) makes the application of seasonal thermal storage limited [48]. However, the scenario is not entirely pessimistic. The number of projects implemented using BTES has increased in recent years [49] and there are increasingly more successful and economically viable examples. Hence, research in this field is very important in order to overcome the challenges in seasonal heat storage systems.

2.2 Small-scale solar-assisted ground source heat pump systems

In section 2.1.3, large-scale or district heating systems using BTES were reviewed. This section focuses on the core of this research, which is the use of solar-assisted ground source heat pumps (SAGSHP) to meet the energy demands of small buildings. This would be a specific application of small-scale BTES which have not been widely studied. This section shows the operating principles of SAGSHP systems, starting with the basic principles.

2.2.1 Basic concepts in ground source heat pump systems

Before going into the details of the operation of ground source heat pumps (GSHP) it is important to describe the working principle and the main components of a heat pump (HP). A HP is a device capable of transferring heat from an energy source to a higher temperature energy sink. In order to move heat against a thermal gradient, a HP must perform work to transfer the heat. A common example of a heat pump is a home refrigerator, which is capable of transferring heat from a low-temperature energy source (inside the fridge) to a higher temperature energy sink (outside fridge) by work input (electricity).

A HP ideally operates under the refrigeration cycle or inverted Rankine cycle. Therefore, it has four key elements: compressor, condenser, expansion valve and evaporator. The working fluid is a refrigerant selected according to the type of HP and the operating conditions [50], but in most cases, it is a hydrofluorocarbon fluid (HFC) or hydrocarbon fluid (HC) [51]. Figure 2.6 shows the operation of a HP. In state 1, the fluid is in the vapour state at low pressure and then passes through a compressor where it reaches state 2 of superheated vapour at high pressure. Then, the fluid is condensed and gives up its heat to another medium (the energy sink) through a heat exchanger reaching state 3 as a saturated liquid at high pressure. The fluid in this state passes through an expansion valve in an isenthalpic process in which the fluid expands, and its temperature decreases significantly (state 4). Finally, the fluid at low pressure and temperature is evaporated in a heat exchanger taking heat from a heat source until it reaches state 1 again and the cycle is repeated.

The main advantage of HPs is low electricity consumption. The average Coefficient of Performance (COP) of a HP is in the range of 3 to 5, this indicates that for each unit of energy input to the compressor, the HP delivers 3 to 5 units of energy as heat into the condenser. Thus, the COP is defined as Equation 2.3 indicates.

$$COP = \frac{Q_{out}}{W_{in}} \tag{2.3}$$

The amount of heat delivered in the condenser as well as the required work to operate a HP depend on several factors such as the temperatures of the source

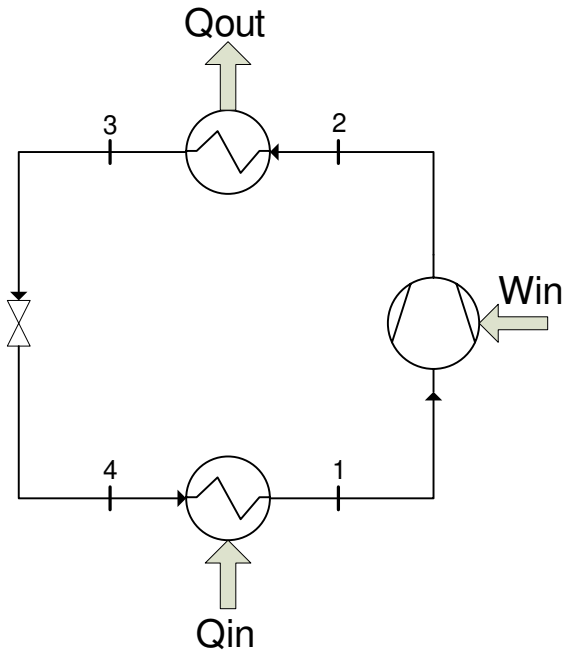

Figure 2.6: Heat Pump operation cycle

and sink, the working fluid and the components of the HP [52]. The higher the COP the greater the energy savings. However, some authors have shown a slow payback in HP systems compared to conventional systems because of the high initial investment [52]. On the other hand, several studies [51,53,54] have shown successful economical results. Therefore, the feasibility of such a system should be based on an case by case analysis since it depends on the local market and electricity costs.

The classic configuration of a HP uses ambient air as the low-temperature energy source and is known as an air source heat pump (ASHP). This technology has been commercially available since the 50s but with a higher market penetration since the 70s due to the oil crisis [52]. An advantage of this configuration is the low cost. However, the ambient air has several seasonal and even daily fluctuations, which makes an unstable HP operation and therefore its average COP is usually lower than that for other sources, particularly in coldest weathers where the demand is highest. Additionally, defrost processes must be considered at very low ambient temperatures [54] due to ice generation in the condenser. Due to this problem, a few years later, in the 80s, the first commercial geothermal heat pumps appeared (although several non commercial units

were already developed since the 40s [55]). This technology, better known as Ground Source Heat Pump (GSHP), has a better average performance than the ASHP. The soil is a heat source (or sink in cooling applications) and hourly and seasonal variations are much smaller than that for air [5]. Indeed, according to Emmi et al. [56], the soil temperature is affected by the air temperature only in the first few meters. This is shown as well by Ozgener and Hepbasli [57] who indicate that below 10 meters depth there is little or no seasonal variation in the ground temperature. The author clearly shows the advantages of GSHP compared to ASHP mainly because a supplementary heat source is not required in times of cold temperature extremes, the thermal stability of the ground and the lower energy consumption. In fact, a GSHP can easily achieve a COP between 5 to 6 compared to an ASHP which usually ranges from 3 to 4 [58]. The main disadvantage of GSHP is the initial cost which can be between 20% to 30% greater than an ASHP [57].

According to the ASHRAE Handbook of Applications [59], three types of GSHP systems can be distinguished: a) ground-coupled heat pumps (GCHP); b) groundwater heat pumps (GWHP) and c) surface water heat pumps (e.g. ponds) (SWHP). GCHPs are characterised by being closed-loop systems where subsurface ground serves as a heat source (in heating mode) or a heat sink (in cooling mode) through a ground heat exchanger (GHE). GWHPs are typically open-loop systems characterised by the use of groundwater extracted from wells as heat sources or sinks. However, sediments in the water can damage pumps and other components, hence, closed-loop systems are more used [60]. SWHPs are closed-loop systems which use surface waters such as ponds or reservoirs as heat sources or sinks [61]. The present research focuses on closed-loop systems connected to subsurface ground (GCHP), which is the most commonly used configuration in the UK. However, the terminology GSHP will be used when referring to this type of system since this is commonly used and accepted.

In a GSHP the low-temperature energy source is the ground (Figure 2.7), i.e. the evaporator is connected to the ground either directly or indirectly (through a heat exchanger). Within the configurations of the ground heat exchangers (GHE), two main groups can be found. On one side, there are the horizontal

ground heat exchangers (HGHE) placed typically at depths of up to 2 m and their applications are mostly for residential buildings. On the other hand, there are the vertical ground heat exchangers (VGHE) or boreholes placed typically at depths between 40 and 300 m. From these two groups, the vertical configuration is mostly used since the temperature of the ground at greater depths is more stable, requires less land surface, does not require excavation, etc. [62].

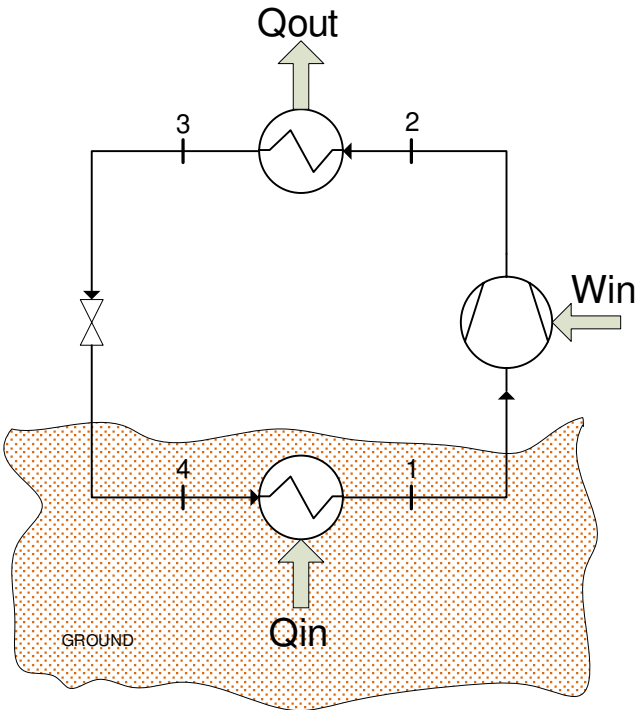

Figure 2.7: Ground Source Heat Pump

Despite the advantage of GSHP systems over ASHP systems, it is important to mention that during prolonged operation of the former, the ground which serves as a source or sink of heat is affected. If a GSHP operates in heating mode, the ground will lose heat and thus its temperature will decrease. On the other hand, if a GSHP operates in cooling mode, the ground will serve as a heat sink and its temperature will tend to increase. This behaviour is unimportant when the thermal loads are balanced, i.e. when heating and cooling needs are similar throughout the year. In this case, the heat extracted in heating mode is then compensated in cooling mode hence, the ground temperature will not be affected on a yearly basis [56]. However, there are very few cases where thermal loads are balanced throughout the year, so it is very common that thermal imbalance of the ground, known as 'thermal drift', occurs in the long term.

The main problem of this phenomenon is the decrease in HP efficiency in the long-term [56]. Particularly, in climates dominated by heating loads, the use of GSHP will cause a decrease in the ground temperature in the long-term. In fact, Zhu et al. [63] show in their study that the continued use of a GSHP decreased ground temperature by 0.185°C per year. Increasing the length of the pipes in the borehole is an option to deal with the thermal imbalance, but the cost implied limits this practice [5]. To minimise this problem, the idea of injecting heat into the ground from another energy source appears, the most common practice being the injection of solar thermal energy [64, 65]. This is also the principle of seasonal thermal storage. This technology, known as Solar Assisted GSHP (SAGSHP) uses solar energy as a heat source for space or DHW heating, as a heat source for increasing the evaporator temperature, as a heat source for recharging the ground (storage) or as a combination of all these [66].

2.2.2 Principles of solar-assisted ground source heat pump systems

It is noteworthy that a SAGSHP could also be considered a GSHP whose electrical power supply comes from solar energy through photovoltaic panels (PV-SAGSHP). An example of this is the study by Franco and Fantozzi [58], in which the photovoltaic system reached an efficiency between 12% and 16%. However, the authors could not make clear conclusions on the whole system's energy balance as the heat pump was oversized and had no prolonged periods of operation. On the other hand, Thygesen and Karlsson [67] conducted a comparative techno-economic study of three different configurations of SAGSHP, one PV assisted in which the electricity was used for running the HP, another solar thermal assisted and a third PV and solar thermal assisted. The authors concluded that the first configuration is the most profitable because it does not require thermal storage. However, the authors did not consider the energy imbalance of the ground nor the savings energy costs caused by the use of shorter boreholes when the system is solar thermal assisted. Likewise, Cao et al. [23] evaluated by energy simulation two buildings in Helsinki and Shanghai comparing the use of GSHP assisted by PV and solar thermal. The authors concluded that the thermal

system is preferable, in a global energy balance, due to the increase in the HP efficiency. The present research will focus on solar thermal assisted technologies as a suitable solution for heating-dominated sites. For this reason, hereinafter, the term SAGSHP will refer to solar thermal assisted GSHP.

The principle of operation of a SAGSHP is to use the solar thermal energy gained through solar collectors to assist in meeting the heating loads of a building either directly or indirectly. When solar energy is delivered at a high enough temperature to meet heat demands directly, the solar system and the ground are considered to work in parallel (Figure 2.8). On the other hand, when solar energy is only used to store (or recover) heat in the ground, it is a series system (Figure 2.9) [19]. In the latter case, the geothermal heat pump is responsible for extracting heat from the ground and is the only one that covers the heating loads.

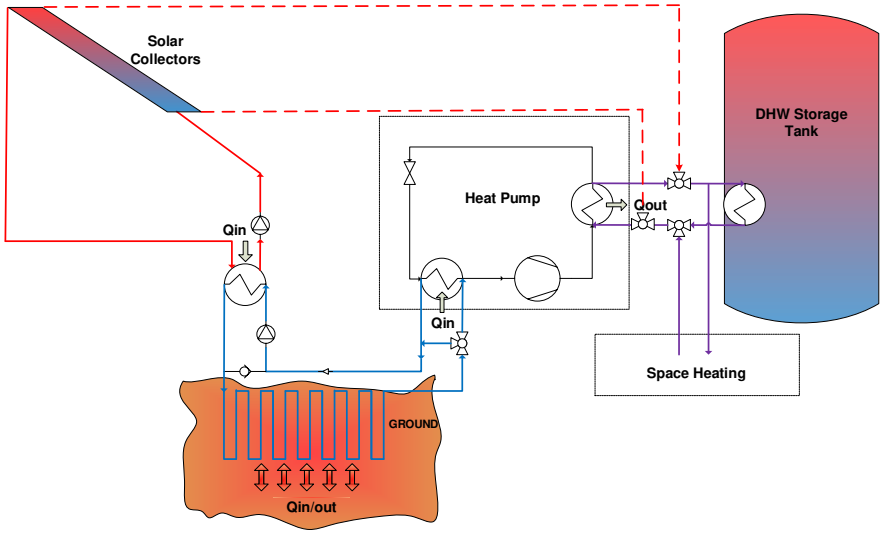

Figure 2.8: Parallel configuration of SAGSHP

When the system operates in parallel, typically if there is a demand for heat and there is solar availability, the demand is covered by the solar system. In case there is no available solar resource, the heat demand is covered by the GSHP. In summer months when there is solar availability and there is not a high demand for heating, excess heat is used to recharge or store heat in the ground. On the other hand, when the system operates in series, the heating loads are always covered by the GSHP and the solar resource is only used to recharge or

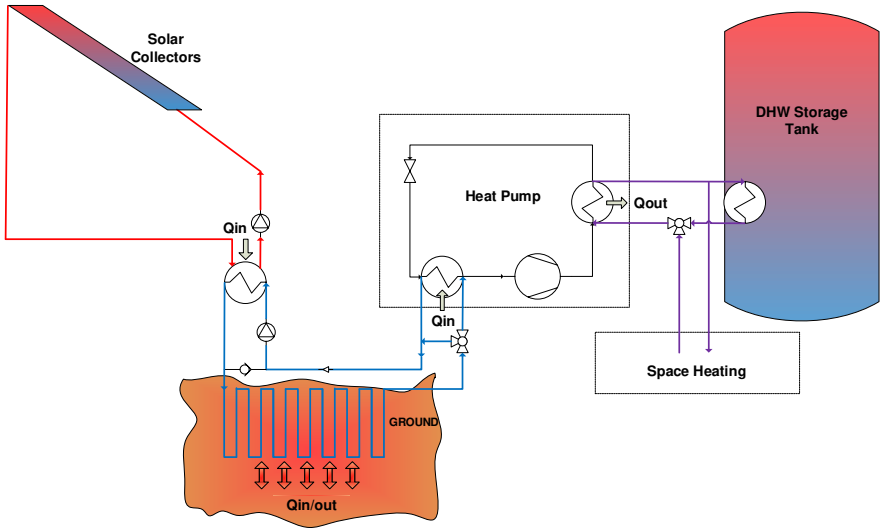

Figure 2.9: Series configuration of SAGSHP

store heat in the ground. There is no consensus in the literature on the optimal configuration of SAGSHP. The following section shows a summary of relevant studies of SAGSHP systems.

2.2.3 Relevant studies of SAGSHP

Various researchers have studied SAGSHP with different system configurations, operation modes and control strategies. Numerical and experimental studies, as well as optimisation studies, have also been performed. However, as there is no consensus on an optimal design configuration, it is important to mention the positive and negative points of the most relevant research in this field.

Numerical studies

Several numerical studies have been conducted on the performance of SAGSHP systems. Eslami-Nejad and Bernier [68] conducted a numerical study in which a model of SAGSHP with double U-tube in the borehole was developed and compared with the behaviour of a SAGSHP system with a simple U-tube and with a conventional GSHP system. The solar energy was used to recharge the ground. The authors performed a 20-year simulation and concluded that despite the heat recharge of the ground, the power consumption of the heat pump is not reduced. However, the authors also emphasise that the solar recharge benefits in

reducing the length of boreholes which reduces the cost of installation. Similarly, Kjellsson et al. [69] studied by simulation, different configurations of SAGSHP systems. The authors show that the performance of such systems depends on the system design and the rate of heat extraction from the ground. Based on this, the authors concluded that the desired configuration is a system in which solar energy is used to produce DHW in summer and recharge the ground in winter. Other numerical studies include the use of phase change materials (PCM) for storing solar energy. For example, Han et al. [70] conducted a study of a SAGSHP system with latent energy storage by using calcium chloride (CaCl2 6H2O) as PCM. In their study, the heat source of the heat pump was alternated between the ground and latent storage. This configuration helped in the increase of the overall system COP throughout the year.

Banjac [64] conducted a numerical study in order to size the required solar collectors to ensure the annual thermal balance in a SAGSHP system in Belgrade, Serbia. The particularity of this study was the use of seasonal heat storage in a buried water tank. The author found that with a slight oversizing, the system was able to achieve an annual thermal balance. Regarding the thermal storage, the author concluded that there is a lot of temperature variation in the water temperature throughout the year. However, it is reduced with an increase in the volume of the water tank. Finally, the author mentioned that the burial depth of the water tank has little effect on the water temperature.

Emmi et al. [56] conducted a TRNSYS simulation to assess the main factors affecting the performance of SAGSHP systems. The study was conducted for six different climates (Poland, Italy, China, Lithuania, Canada and Sweden). The authors recommend the use of TRNSYS as the software can analyse each subsystem and different control strategies step by step. The authors concluded that without the use of solar energy, GSHP seasonal efficiency decreases by 10% for all locations. Finally, the authors highlighted in their study that by using solar energy injection, it is possible to reduce the length of the boreholes without compromising the seasonal efficiency of the system. This would help in reducing the initial investment of such systems.

Chiasson and Yavuzturk [71] simulated a SAGSHP system in a school build-

ing of 4924 m^2 for six different cities in the USA. The authors concluded that for all locations the system is economically viable. Likewise, the authors highlight that the use of solar energy to recharge the ground allows a reduction in the length of the boreholes between 16 and 33%. Likewise, Nord et al. [72] conducted a numerical study to evaluate the behaviour of a SAGSHP system for a 202 m^2 family house in Larvik, Norway. The authors concluded that although the recharge of ground with solar energy is beneficial to prevent it for overcooling, a higher solar fraction of the system can be achieved if the solar heat is used directly for domestic or water heating. The authors attribute this performance due to the fast ground natural recharge.

Reda [73] studied in TRNSYS different control strategies for a SAGSHP system for an 880 m^2 residential building in Helsinki, Finland. The author compared three configurations of SAGSHP systems to a GSHP reference system. One of the most important findings of the author was that unglazed solar collectors (UC) are more efficient than flat plates collectors (FPC) and evacuated tubes collectors (ETC) at lower ambient temperatures. The author also recommends using FPC with small systems and short boreholes depths, while the use of ETC is recommended in larger systems with greater boreholes depths. Finally, the author emphasises that the control strategy to inject heat into the ground should be set based on the depth of the boreholes and the type of collectors. In a subsequent study, Reda et al. [74] analysed by TRNSYS simulation the performance of different configurations of SAGSHP systems for different locations in Italy (Milan, Palermo and Rome). The authors suggest that the heat injection to the ground is only recommended for cold locations like Milan due to its cold ground temperature. In warmer locations (Palermo and Rome), the ground has already a warm temperature which is enough for a good performance of the GSHP. They point out that the use of solar energy helps to improve the overall efficiency of the system, but the energy must be used directly for heating. However, the locations used in this research did not include regions dominated by heating loads.

Experimental studies

Xi et al. [75] conducted an experimental study in Shijiazhuang, China. In their study, the authors compared the behaviour of a GSHP system and a SAGSHP in continuous and intermittent operation mode. Continuous mode refers to the heating system working during 48 hours where the ground is the only heat source. Intermittent operation refers to a heating system enabled only during 9 hours per day (from 08h30 to 17h30). The authors show that both GSHP and SAGSHP works better in intermittent mode since this allows the ground temperature to recover following periods of heat extraction. The GSHP system in intermittent mode does not cause a significant ground temperature decrease. By the end of the heating season, the ground temperature had decreased by 0.9°C. On the other hand, the GSHP system in continuous operation causes a rapid decrease in the borehole temperature (up to 10 K) in the first 10 hours of operation at a depth of 10 metres reaching a value of 6.39°C. However, once the heating season has finished, the borehole temperature is restored to 14°C in just 16 hours. The authors point out that this behaviour is due to the high heat gains from the surroundings. The authors demonstrated a significant increase in the whole system efficiency by the use of SAGSHP systems compared with GSHP systems. They noted a decrease in the HP electricity consumption due to the increase in the evaporator operating temperature. However, the authors concluded that it is not ideal to use solar energy for storage in the ground due to the high thermal capacitance of the earth. They recommend that once the ground reaches its natural temperature, instead of storing heat in the ground, it should be used for direct heating or DHW.

Wang et al. [76] studied various configurations of a SAGSHP system in heating and cooling mode. The authors emphasise the importance of thermal storage in the summer months. In contrast, during the winter months, solar energy should be used as a priority for direct heating instead of storing it in the ground. In their study, the authors indicate that after a year of operation, the solar energy injected into the ground exceeded the heat removed, which will improve the HP efficiency on its next operation.

Stojanovic and Akander [77] conducted an experimental study of a SAGSHP

system in Sandviken, Sweden using a horizontal heat exchanger buried at 1.5 metres. The authors performed the build-up and a performance study of the system for two years in a residential application. This system has two noticeable features, the first is that the solar collectors are unglazed and the second is that the solar energy is only used to recharge the ground (through a heat exchanger) and not for water heating or preheating. The authors justify this configuration highlighting that the heat gain for water heating is minimal compared to the reduction in the HP utilisation and the cost involved in installing a more complex configuration. The results show that the system performs better in spring and autumn than in winter. The authors concluded that despite the unfavourable northern conditions, the system was able to meet the requirements continuously for two years. However, it was not possible to demonstrate seasonal heat storage due to the intermittent recharging/discharging of the ground.

Another interesting study was by Zhu et al. [63] who conducted an experimental study of a SAGSHP system installed in a group of buildings on a campus of Tianjin University in China. The system consists of 1500 m^2 of FPC and 580 sets of underground heat exchangers at 120 m intended to store heat seasonally. The study was compared with experimental data obtained from the same system that operated as a GSHP for 4 years. The results show that before the seasonal storage, the average ground temperature decreased by 0.185°C per year. Also, the system with no seasonal storage has a COP 2.3% lower than the COP of the system with storage. In contrast, when the system was configured to work with seasonal storage, the system COP increased by 3.4% and the average ground temperature increased by 0.21°C. The authors conclude that economically, this system is promising when considering the long-term operation of such systems.

Dai et al. [78] conducted an experimental study of a SAGSHP system in cold conditions in Dailan, China. In this research, a hot water storage tank from solar collectors was used. The authors evaluated different operating modes of the whole system. The results indicate that the ground recharge is beneficial but should be optimised according to the water temperature in the tank to prevent unnecessary use of pumps mainly at night. The authors concluded that the serial operation of the storage tank with the underground heat exchanger is the

optimal configuration for the coldest months.

2.2.4 Challenges and opportunities of SAGSHP

As seen above, there is a wide variety in the type of studies conducted and in the configurations of SAGSHP. This shows that there is much interest in this subject and that research is very active in this field. From the previous overview, it can also be seen that further research into this type of system is needed, especially considering that in Europe the annual growth rate of GSHP systems installed is 10% [73]. However, some discrepancies between research results are also shown, demonstrating the need for future work. For example, it is known that most research conducted is numerical. Some of these studies discourage the use of SAGSHP technology. However, experimental studies produce more encouraging results and indicate that this technology may be economically viable in the longer term. For this reason, it is important to conduct more experimental research [63]. Fantozzi and Franco [58] point out the lack of long-term dynamic studies of such systems.

It is important to mention that the long-term efficiency of SAGSHP systems depends on the ability to avoid the thermal imbalance of the ground so that heat injected into the ground compensates for heat extraction. A system that works in heating mode and does not compensate the heat extracted from the ground will lose efficiency in the first years of operation. While it is true that the use of solar energy for seasonal storage helps in reducing the effects of thermal imbalance, their evaluation using modelling is still a challenge. In order to minimise heat losses in seasonal storage, conventional boreholes (more than 30-metre depth) are used, as the ground temperature at that depth is constant and higher than the ambient temperature in wintertime. This type of configuration is expensive mainly because of the cost of the drilling process.

In this context, the use of very shallow boreholes (less than 3-metre depth) would represent a considerable saving in the installation of SAGSHP systems. However, the effect of seasonal storage can be compromised due to the greater heat losses to the environment due to the lower thermal stability of the very shallow soil. It is worthwhile to research deeper into the behaviour of very shallow

boreholes because of the economic advantages that can be obtained. Unfortunately, the lack of a practical and accurate model for this type of configuration has made studies of very shallow boreholes scarce. Alternatively, conventional borehole models could be employed, and their results might be extrapolated for very shallow configurations. However, this approach might lead to an increase in the uncertainty between numerical and experimental results. For these reasons, the need for a practical, simple and accurate model that considers the most important variables (location, soil properties, GHE depth, etc.) to evaluate GSHP configurations with very shallow boreholes is evident.

The core of this research is to help in overcoming this research gap and develop a simple and practical model that allows the study of very shallow borehole heat exchangers in the short and long term. However, to achieve this aim, a deeper understanding of the currently available models for assessing boreholes is needed. Likewise, an appropriate understanding of heat transfer methods for analysing complex systems with variable boundary conditions is also required.

2.3 Modelling of vertical ground heat exchangers

This section covers a review of the most relevant conventional models (analytical and numerical) to study the performance of boreholes and on the potential heat transfer approaches to deal with the study of very shallow boreholes. However, it is first necessary to understand the thermal behaviour of the very shallow natural soils as this is the region where a very shallow ground heat exchanger will be placed.

2.3.1 Thermal performance of very shallow natural soil

The behaviour of natural soil is relevant in the study of any type of ground heat exchangers. As mentioned in section 2.2.4, conventional boreholes are installed typically at depths ranging from 40 to 300 metres. At such depths, it is normal to consider the natural soil as a medium with constant temperature all over the year. However, if a borehole is installed in the very shallow soil (up to 5-metre depth), the natural soil temperature is variable in time. This part of the

soil is mainly affected by the heat balance in the soil surface. More details on such balance can be found in Appendix C. Below, different models (analytical, numerical and empirical) to analyse the natural temperature variation of the very shallow soil are briefly described.

Analytical models

Several studies using analytical models have considered the soil temperature to have a harmonic (sinusoidal) variation over time [79]. For instance, one of the most accepted sinusoidal models is that of Kusuda and Achenbach [80]. This approach is most accurate at depths where short-term (hourly and daily) changes in the soil's thermal behaviour can be neglected, which is generally at depths greater than 1 m. Likewise, the semi-infinite solid model [81] can be used to study transient phenomena in solids where the heat diffusion is predominantly one dimensional. This model is accurate to study short-term variations in the soil temperature but only at very shallow depths (no more than a few centimetres).

Some studies have proposed different models to estimate the variation of soil temperature. For example, Charpin et al. [82] performed an analytical study using a sinusoidal harmonic model of the heat transfer in a concrete block exposed to the environment. In their study, the authors used the soil surface exposed to a heat flux that includes solar radiation and convection, as a boundary condition. They used the harmonic model to define the variation of ambient air temperature. The authors report that, for a one-day period, the concrete block shows variations in its temperature up to a depth of 20 cm (thermal penetration depth). The model did not allow accurate predictions of the hourly temperature variation but was suitable for a first estimation although the results of the model were not experimentally validated. Likewise, Cleall et al. [83] proposed an analytical model to estimate the soil temperature based on harmonic variations of global solar radiation and ambient temperature. The resolution of the analytical model was compared with a numerical model showing an acceptable match. Although obtaining the analytical solution is complex, the implementation of the final model is simple, and its calculation is fast. This model serves to accu-

rately estimate the thermal behaviour of the soil, although short-term variations cannot be estimated given the harmonic principle of the model. The harmonic model correlated well (R^2 = 0.96) with the experimental data at a depth of 1 m however the correlation was poor (R^2 = 0.63) at a depth of 0.025 m since short-term variations are not represented well by a harmonic function. In another study, Badache et al. [84] propose an analytical model, based on the Kusuda and Achenbach model, in which the boundary condition is a surface temperature value determined by an empirical model. This method reduces the complexity in obtaining the analytical solution. The model was validated with monthly experimental data from three different locations at depths between 0.1 and 4 metres. The validation shows a good correlation with a root mean square error ($RMSE$) of 2.5 K in the worst case at 1 m depth. However, a limitation of this model is its inability to represent the shallow soil behaviour in the short-term (hourly or daily variations). Due to the complexity of the actual interaction between the soil and the environment, analytical models only deal with the heat transfer phenomenon and neglect the moisture transport process. Appendix A shows in more detail the development of the Kusuda and Achenbach model [80] as well as the semi-infinite model [81] to estimate the temperature of the shallow soil.

Numerical models

Numerical models are known to be more accurate and robust for the study of different soil typologies and boundary conditions (BC). However, numerical methods are more complex to implement and take longer to solve [85]. Usually, constant surface temperature or constant heat flux [83] are applied as boundary conditions at the soil surface level. For either of these, it is necessary to determine the soil surface temperature which is normally a parameter that cannot be easily determined since conventional meteorological stations do not measure it [86]. To deal with this problem, in some cases, the soil surface temperature can be approximated as the air temperature [82]. As numerical models are able to represent periodic boundary conditions as well as a more realistic approach to the interaction between soil and environment (including heat and moisture

transfer), numerical studies have demonstrated greater accuracy than analytical models for the study of the thermal behaviour of soil. In fact, Yilmaz et al. [87] concluded in their study that analytical models are generally unrealistic for soil temperature prediction. They compared a harmonic model with a numerical model using the finite difference method (FDM) with heat flux at the surface as a boundary condition. This numerical model allowed short-term fluctuations to be estimated. However, the model was not validated with experimental data. Wullschleger et al. [88] developed a computational tool that numerically predicts the soil temperature variation. They included heat and moisture transfer phenomena in the model, which required the precipitation or water irrigation in the soil as input data. The model is able to predict hourly temperature variations on a daily basis. However, it lacks experimental validation and requires a large number of input parameters.

In the same way, Chalhoub et al. [89] performed a numerical study to estimate the soil temperature using the FDM. In order to improve accuracy, they considered not only the heat diffusion, convection and radiation but also evaporation. They included in their model an approach to calculate the water content in the soil which is variable according to the rainfall rate. In addition, the authors modelled the variable thermal conductivity and thermal capacitance as a function of the soil moisture content. The results of the numerical model were validated experimentally with data monitored at depths from 0.06 m to 1.5 m. The authors defined the efficiency of the model as the ratio between the residual variance of the model and the variance of the data set, and it ranges from 0.87 to 0.98. This numerical model is very accurate and can be implemented in numerical simulation programs. However, as the model requires a large number of input parameters, its implementation is impractical when insufficient data are available. Section 5.4 shows in more detail the development of a numerical model using the finite difference method (FDM) to study the temperature variation of the shallow soil.

Empirical and semi-empirical models

Empirical models have been developed through correlations or more complex statistical methods, by using time series input parameters based on experimental data. For example, Kenan Tezcan [90] developed an equation to determine the ground temperature at 1-metre depth in the soil of Turkey. His equation was based on measurements taken at 193 meteorological stations. Nevertheless, his model is only valid to estimate the average annual temperature. In another empirical study, Chow et al. [79] conducted a non-linear multivariate regression to create an empirical model for estimating the soil temperature at different depths in Hong Kong. In their study, the authors emphasize that at depths of up to 3 metres, air temperature is the variable that most affects the thermal behaviour of the soil, whereas variables such as solar radiation, rainfall, relative humidity or wind speed have little or no influence on the soil. Finally, their empirical model was validated with experimental data from two different meteorological stations showing an $RMSE$ from 0.61 K to 1.55 K. This empirical model requires only time, depth and ambient temperature as input parameters, but it is only valid for the soil and ambient conditions of Hong Kong. Droulia et al. [85] compared an analytical model based on daily and annual harmonic variations of the air temperature with two semi-empirical models in which they used average values of air temperature and soil surface temperature. The results show that the analytical model is adequate to estimate the average monthly soil thermal behaviour, but it does not represent the short-term variations well.

In contrast, semi-empirical models show a greater correlation to the shallow soil variation in the short term compared to purely empirical models. However, in both the analytical and the semi-empirical models, the determination of certain input parameters requires complex statistical functions. In a study, Hu et al. [91] developed a semi-empirical model to determine the shallow soil temperature. In their study, the input parameters included are air temperature, rainfall, vegetation cover, solar radiation, and water flux density. The results were compared with experimental data monitored from two different locations at three different depths (5 cm, 10 cm and 20 cm) showing a good correlation at all depths studied (R^2 between 0.82 and 0.97). However, the use of many

variables as input parameters makes this model very complex for a practical application.

Most of the empirical and semi-empirical models have been developed using time series as input data in the same way as most forecasting models. The development of time series models requires a very large set of input data mainly of daily average ambient temperature [92] but some of them also require the use of a data set of daily average soil temperature [93, 94]. These models have been demonstrated to be very accurate and useful in forecasting. However, most of them are not designed to predict sub-daily temperature fluctuations and their application to different locations would require at least some snapshot measurements of the soil temperature, as stated by Dolschak et al. [93].

As mentioned before, the study of the natural temperature variation of the very shallow soil is crucial for assessing the performance of very shallow borehole heat exchangers. It is important to combine the natural temperature variation with any conventional model to evaluate the thermal response of boreholes. The next sections show a review of the conventional models to evaluate boreholes as well as the potential heat transfer techniques to study very shallow boreholes.

2.3.2 Analytical models to evaluate borehole heat exchangers

For the design of a borehole heat exchanger (see Appendix B), it is necessary to ensure that the soil can be used as a source (or sink) of heat to meet heating (or cooling) loads at peak periods [48]. These can be estimated quickly by Equation 2.4.

$$Q_{gr} = \frac{Q_{build} - W_{comp}}{\varepsilon_{HX}} \tag{2.4}$$

In Equation 2.4, Q_{gr} is the energy extracted (positive) or injected (negative) in the soil per unit time [W], Q_{build} is the heating (positive) or cooling (negative) load [W], W_{comp} is the compressor work [W] and ε_{HX} is the efficiency of the ground-water heat exchanger in the heat pump.

Through simple analysis, considering a constant compressor work, it can be seen that if the required heat cannot be extracted (injected) from (to) the soil, the heating (cooling) demand is not satisfied. For this reason, a correct design must

be able to extract (dissipate) the required Q_{gr} from (in) the soil throughout the useful life including periods of peak demand.

To meet this need, it is necessary to study the heat transfer process in the soil through the borehole heat exchanger. Heat can be transferred into the soil by conduction, convection (when there is a considerable movement of underground water), evaporation (in highly porous media) and radiation (with the exterior). However, according to several studies [55, 59, 95], the conduction heat transfer is dominant and purely conductive models are widely accepted and used for the design and analysis of boreholes. Heat transfer by conduction occurs between the soil and the heat exchanger piping. Usually, boreholes are composed of the pipe (coaxial, single U-tube or double U-tube) through which the working fluid circulates, and the borehole-filling which is typically composed of high heat capacity materials like bentonite, concrete, sand, etc. Figure 2.10 shows the typical configuration of a single borehole.

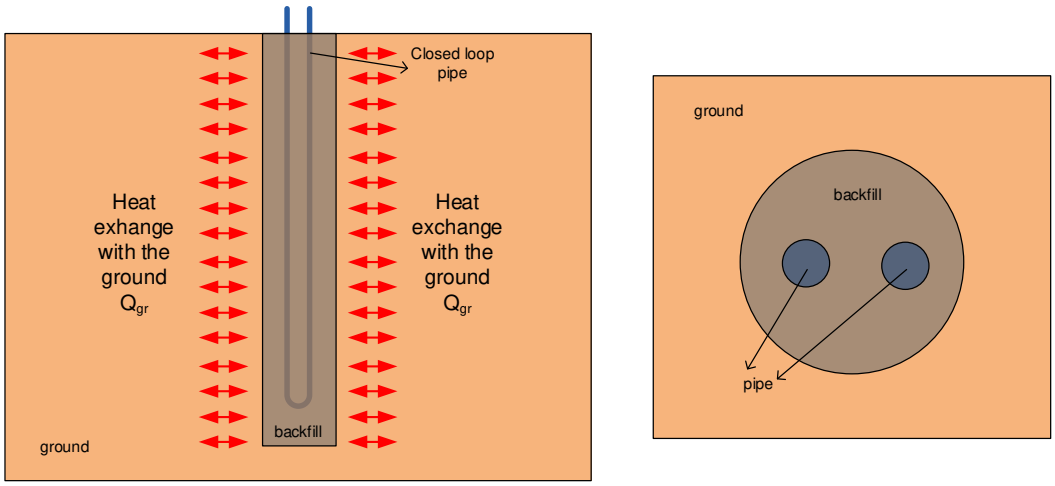

Figure 2.10: Vertical and horizontal cross-sections of a single U-tube borehole

As seen in Figure 2.10, boreholes usually have a cylindrical shape. For this reason, the study of heat transfer is typically done in cylindrical coordinates where the equation of the bidimensional heat diffusion can be written as stated in Equation 2.5 [81].

$$\frac{1}{r}\frac{\partial}{\partial r}\left(kr\frac{\partial T}{\partial r}\right)+\frac{\partial}{\partial z}\left(k\frac{\partial T}{\partial z}\right)=\rho\, c_p\frac{\partial T}{\partial t} \tag{2.5}$$

where: r represents the radial direction of analysis; z represents the axial direction of analysis; k, ρ and c_p represent the thermal conductivity, density and specific heat of the heat diffusion medium and t represents the time.

The resolution of this equation is complex since it is bidimensional and transient. Several authors have made numerous simplifications that have been proven experimentally to be accurate in certain ranges. For example, according to Li and Lai [95], the most common simplifications are usually: a) assuming the soil as an infinite or semi-infinite medium; b) the initial temperature of the soil approaches the undisturbed soil temperature (temperature typically below 10 meters depth); c) the boundary condition for the borehole wall is commonly treated as a constant heat flux condition and d) although the soil is composed of layers of different thermal properties, it is usually considered that the effective thermal properties of the soil are uniform around the borehole.

By assuming the borehole wall as the boundary, it can be deduced that heat diffusion is mainly studied in two control volumes: the space outside the wall (soil/ground) and the space inside the wall (filling and piping) [55]. Also, the study timescales depend directly on the analysed space. In this context, Li et al. [96] have proposed dividing the timescale of study according to the study space as shown in Table 2.2.

Table 2.2: Space and time scales for the study of heat transfer in VGHE

Space scale	**Timescale**
Space inside the piping (fluid)	$t_r \sim \frac{H}{u}$ order of minutes
Inside the borehole $r < r_b$	$t_b \sim \frac{{r_b}^2}{\alpha_b}$ order of 1 h
Space between adjacent boreholes $r_b < \frac{B}{2}$	$t_B \sim \frac{B^2}{4\alpha_s}$ order of 1 month
Diffusion space in the soil $\frac{B}{2} < r < \frac{H}{2}$	$t_H \sim \frac{H^2}{4\alpha_s}$ order of years

In Table 2.2, r_b represents the radius of the borehole; α_b and α_s are the thermal diffusivity of the filling and soil respectively; B is the distance between adjacent boreholes; H is the borehole length and u is the velocity of the fluid inside the pipe.

It is worth noting that, according to several authors [55, 96, 97], the transient

analysis inside the borehole loses importance when the analysis time is greater than $5t_b$. From that time, the phenomenon of heat transfer within the borehole can be considered as a steady-state heat flux, where the temperature difference between the borehole wall and the working fluid remains constant over time. From this time, the space between the borehole wall and the fluid (pipe and filling) can be considered as a constant thermal resistance called borehole thermal resistance R_b. The majority of analytical models in the literature consider this type of analysis. However, this assumption of R_b is only valid for long-term analysis (in the order of days up to years).

As mentioned above, one of the most common assumptions for the study of heat transfer between working fluid and soil is to assume that the borehole wall is a boundary with constant heat flux. This can be expressed as in Equation 2.6 [95].

$$q_b = \frac{T_f(t) - T_o}{R(t)} \tag{2.6}$$

where: q_b is the heat flux between the fluid temperature, $T_f(t)$ and the undisturbed soil temperature T_o along a total resistance $R(t)$ between the fluid and the soil. The total resistance is variable over time. The determination of this variable resistance is an implicit part of the analytical problem of heat transfer along with the soil. On the other hand, q_b represents the heat that is extracted or injected into the soil per unit length of borehole (Q_{gr}/H). The temperature at any point $T(r,t)$ can also be determined by applying a suitable total resistance to the point of analysis.

It is important to mention that in order to make long-term estimations, the heat flux can be approximated to the average heat flux (monthly, annual or seasonal) that is determined by the demand of the heat pump. Long-term results would give a good estimate of the fluid or soil temperature. However, in real applications, the heat transfer between the fluid and the soil varies in short periods depending on the variation in the heat pump operation [95]. This causes fluctuations in the order of minutes of the heat flux. To deal with such a phenomenon, several authors refer to the application of the superposition theorem [96,98–101]. By this theorem, the variable loads can be solved by summing the responses of

each load. That is an overlap of transient responses as a function of a variable load. It can be expressed as shown in Equation 2.7.

$$T_i(r,t) = T_o + \sum_{j=0}^{N-1} \Delta q_{b,j} R(r, t - j\Delta t) \tag{2.7}$$

Where $\Delta q_{b,j}$ represents the change in q_b at the beginning of the interval j and N is the number of interval loads. Thus, for example, if the heat flux varies from one hour to another, that will cause the response of the current analysis interval to change from the response of the previous analysis interval. It is thus possible to analyse the fluctuations in the heat flux. Also, the superposition theorem is valid to estimate the thermal response of a given point when there exists interaction between adjacent boreholes. In this case, the responses of different boreholes are overlapped at the same point [102]. The superposition method is very important for the short-term analysis and for the integration in building energy simulation software, as the latter usually deals with variable loads in hourly or sub-hourly periods.

Analytical methods of ground thermal response have been implemented for three main purposes which are the design of borehole heat exchangers (see Appendix B), in-situ ground thermal conductivity tests and the integration of models into building energy simulation (BES) software [102]. Many of them prioritise the thermal response of the soil because of the heat extraction or injection in the long-term (from a few hours to years). Also, most of these methods simplify the transfer of heat inside the borehole (filling, pipe and fluid), hence they cannot be used for short-term analysis (the first minutes and hours of operation).

Long-term models

Infinite line source (ILS) model: The first analytical solutions for borehole analysis were proposed by Ingersoll [103] based on the Kelvin linear source theory [104]. In this model, the borehole is considered as an infinite line from which constant heat flux is emitted. In this model, also, the existence of the borehole (filling, pipe and fluid) is neglected by assuming that the infinite line is surrounded directly by the soil (which has constant and homogeneous properties). Through this method, the soil temperature can be determined at any

radius and at any time by the resolution of Equation 2.8 proposed by Carslaw and Jaeger [105].

$$T - T_o = \frac{q_b}{4\pi k_{gr}} \int_{\frac{r^2}{4\alpha_{gr}t}}^{\infty} \frac{e^{-u}}{u} du = \frac{q_b}{4\pi k_{gr}} \times E_1 \left(\frac{r^2}{4\alpha_{gr}t} \right) \tag{2.8}$$

where: q_b is the heat flux (W/m) of the linear source, E_1 represents the solution of the exponential integral and T_o is the initial temperature of the soil (undisturbed ground temperature).

The exponential integral can be approximated to a sum as shown in Equation 2.9.

$$E_1(x) = -\gamma - \ln(x) - \sum_{n=1}^{\infty} \frac{(-1)^n x^n}{n \times n!} \tag{2.9}$$

where: γ is the Euler constant and is equal to 0.5772.

For long timescales ($t > \frac{5r^2}{\alpha_{gr}}$) the solution can be simplified (Equation 2.10). This approximation is valid (errors less than 2%) for times between 3 to 10 hours.

$$T - T_o \cong \frac{q_b}{4\pi k_{gr}} \left[\ln \left(\frac{4\alpha_{gr}t}{r^2} \right) - \gamma \right] \tag{2.10}$$

Equation 2.10 is valid to determine the temperature in the borehole wall (T_b if $r = r_b$). From this temperature, the average fluid temperature T_f can be determined by the borehole thermal resistance R_b assuming that the borehole has reached a steady-state (Equation 2.11) [102].

$$T_f = T_b + q_b \times R_b \tag{2.11}$$

Despite its limitations, this model has been widely used in the design of boreholes and in the analysis of the in-situ ground thermal response.

Infinite cylindrical source (ICS) model: Carslaw and Jaeger [105] proposed a model of conduction heat transfer in the radial direction as a solution to Equation 2.5. In this case, it is assumed that a cylinder ($r = r_b$) has a constant heat flux emitted from its wall in the radial direction. The solution can be expressed as (Equation 2.12):

$$T - T_o = \frac{q_b}{\pi^2 k_{gr}} \int_0^\infty (e^{-u^2 Fo} - 1) \frac{J_0(u)\, Y_1(u) - Y_0(u)\, J_1(u)}{u^2 (J_1{}^2(u) + Y_1{}^2(u))} du \tag{2.12}$$

where: J_0, Y_0, J_1 and Y_1 are the zero-order and first-order Bessel functions.

For long scale values ($t > \frac{5r^2}{\alpha_{gr}}$) the solution can be simplified (Equation 2.13).

$$T - T_o \cong \frac{q_b}{4\pi k_{gr}} \left[\ln\left(\frac{4\alpha_{gr} t}{r^2}\right) - \gamma + \frac{r^2}{2\alpha_{gr} t} \left(\ln\left(\frac{4\alpha_{gr} t}{r^2}\right) - \gamma + 1 \right) \right] \tag{2.13}$$

Equation 2.13 is valid to determine the temperature of the borehole wall (T_b if $r = r_b$). From this, the average fluid temperature T_f can be determined from the borehole thermal resistance R_b by Equation 2.11 as in the ILS method.

As can be seen, the ICS model is quite similar to ILS and both are considered to be simple models. However, as mentioned by Li and Lai [95], these models are not appropriate for short-term analysis since the filling material is not considered. Besides, these models are also not suitable for very long-term analysis (over 20 years) since the influence of the ground surface and the heat diffusion in the axial direction at the bottom of the borehole (end effect) is ignored [102]. In the long-term, the ground surface temperature variation has an impact on the variation of the ground temperature mainly when the loads are unbalanced. This causes the soil temperature to gradually increase or decrease [95]. Also, in the long-term, the end effect (heat transfer at the borehole bottom) is important and should not be ignored [102]. For this reason, bidimensional models such as finite line source (FLS) or g functions are recommended for the long-term analysis.

Finite line source (FLS) model: The finite line source model (FLS) allows determining the soil temperature at any point (*r*,*z*) as a function of time. The model is based on a constant heat flux q_b along a line of length H located at a distance D below the ground surface. The model was initially proposed by Eskilson [106] and adapted several years later by Zeng [107]. The solution can be applied for a constant temperature boundary condition at the ground surface (equal to the undisturbed soil temperature) or for an adiabatic surface. The FLS

model is shown in Equation 2.14. In order to have the constant surface temperature boundary condition, the Kelvin theory of heat sources and the method of images are combined in a reflective plane. In this way, a mirror image is obtained and the symmetry causes the reflection line to become a constant surface temperature boundary condition.

$$T(r,t) = T_o + \frac{q_b}{4\pi k_{gr}} \int_0^H \left(\frac{\operatorname{erfc}\left(\sqrt{\frac{r^2+(z-h)^2}{2\sqrt{\alpha_{gr}t}}}\right)}{\sqrt{r^2+(z-h)^2}} - \frac{\operatorname{erfc}\left(\sqrt{\frac{r^2+(z+h)^2}{2\sqrt{\alpha_{gr}t}}}\right)}{\sqrt{r^2+(z+h)^2}} \right) dh \tag{2.14}$$

where: erfc is the complementary error function. For the adiabatic boundary condition, the negative sign between the two complementary error functions must be replaced by a positive sign.

Through this model, the average response of the borehole can be estimated by evaluating the midpoint ($z = H/2$). There is better accuracy in evaluating the average temperature along a line (H_2) at a depth D_2. However, this raised the need to solve a double integral increasing the computational cost [95]. A contribution was proposed by Lamarche and Beauchamp [99] in which the double integral is eliminated without sacrificing accuracy. Equation 2.15 is the basis for the development of the g functions of Cimmino and Bernier [108]. It is also possible to evaluate the borehole wall temperature when $r = r_b$ and estimate the average fluid temperature by Equation 2.11.

$$T(r,z,t) = T_o + \frac{\frac{q_b}{4\pi k_{gr}} \int_{D_2}^{D_2+H_2} \int_D^{D+H} \left(\frac{\operatorname{erfc}\left(\sqrt{\frac{r^2+(z-h)^2}{2\sqrt{\alpha_{gr}t}}}\right)}{\sqrt{r^2+(z-h)^2}} - \frac{\operatorname{erfc}\left(\sqrt{\frac{r^2+(z+h)^2}{2\sqrt{\alpha_{gr}t}}}\right)}{\sqrt{r^2+(z+h)^2}} \right) dh dz}{H_2} \tag{2.15}$$

G-Functions method: G-functions, initially proposed by Eskilson [106], have been used, from the superposition theorem, to analyse the thermal response of borehole heat exchangers. The idea of the G-functions is to simplify the complex analytical methods and to evaluate graphically what would be the typical response of a borehole heat exchanger according to its arrangement and the geometry in a determined time. Typically, the G-functions depend on: a) t/t_s; b)

B/H, c) r_b/H and d) D/H, where t_s is a characteristic time ($\frac{H^2}{9\alpha_s}$). Thus, the G-functions allow the analyst to determine the temperature of the borehole wall by Equation 2.16.

$$T_b = T_o + \frac{q_b}{2\pi k_{gr}} \times g\left(\frac{t}{t_s}, \frac{B}{H}, \frac{r_b}{H}, \frac{D}{H}\right) \tag{2.16}$$

The G-functions are based on the numerical or analytical resolution of bidimensional models and the response of a unit step function of heat q is studied. Through the theory of superposition, the influence of adjacent boreholes is also analysed. Finally, the results are presented graphically in terms of the previously mentioned dimensionless terms. Figure 2.11 shows a representation of some of the G-functions developed by Eskilson and compiled by Yavuzturk [2].

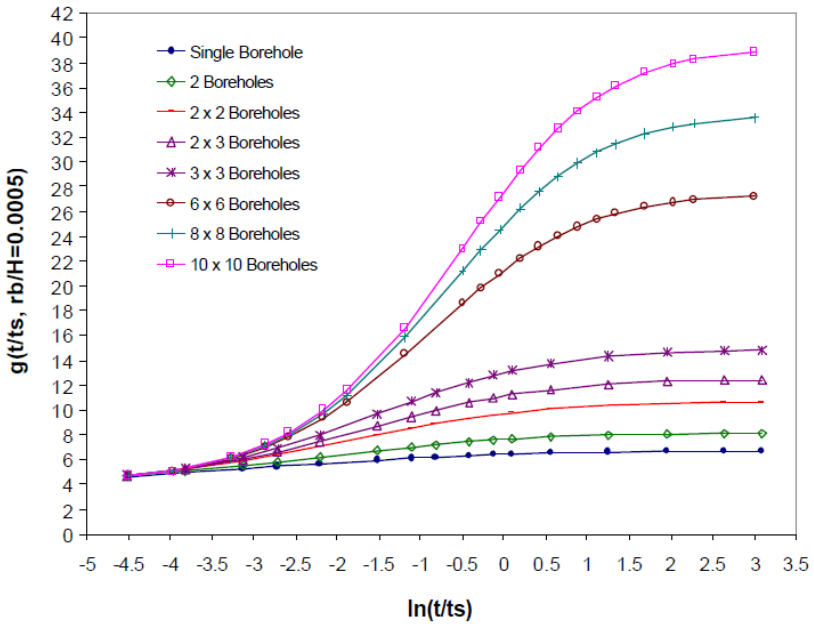

Figure 2.11: G-functions for multiple boreholes arrangements Source: Yavuzturk 1999 [2]

When a variable loads analysis is required, the superposition theorem can be used in conjunction with the G-functions and very accurate results can be obtained (Equation 2.17) [55]. Several authors have developed new G-functions or correlations for their simple application. However, the principle is still based on bidimensional heat transfer analysis. The G-functions are ideal for analysing the ground thermal response in the medium and long-term. However, they are

not suitable for thermal response in the short-term (from minutes to hours) since the filling material of the borehole is not considered.

$$T_b = T_o + \sum_{i=1}^{n} \frac{q_i - q_{i-1}}{2\pi k_{gr}} \times g\left(\frac{t_n - t_{i-1}}{t_s}, \frac{B}{H}, \frac{r_b}{H}, \frac{D}{H}\right) \tag{2.17}$$

The superposition method is very useful for the analysis in hourly simulation software. However, it can be very time consuming when analysing the thermal response for an entire year (or longer times). For these cases, it is recommended to use aggregation methods. For example, if an annual simulation (8760 hours) is required, the analysis can be divided into an average heat flux for the first 8000 hours, then an average heat flux for the next 730 hours and finally 30 hourly heat flows for the last 30 hours. Thus instead of doing 8760 times the analysis, it is reduced to 32 times. The absolute error of using this aggregation method is less than 0.5 K in the final temperature value calculated [59].

It is important to mention that also, through the G-functions, the temperature in the borehole wall can be determined and the average fluid temperature can be estimated by Equation 2.11. One of the limitations of the G-functions is that through them the temperature can be determined in the borehole wall but not at a different radial point. When analysis at different points is required, alternative methods should be used.

Short-term models

As noted earlier, one of the main limitations of medium and long-term analysis methods is the omission the filling material and pipe inside the borehole or the treatment of them as a constant thermal resistance. This procedure is not the most appropriate since it is assumed that as soon as heat flux touches the pipe the temperature of the borehole wall is modified. In other words, the transient effect inside the borehole is not considered. This effect is very important in the first minutes and hours of operation and when highly fluctuating thermal loads are imposed. In order to address this problem, different analytical models have been proposed for short-term analysis. These models are characterised by considering the thermal capacity of the filling material and the fluid inside the pipe and are suitable for analysis at times scales of minutes up to a few hours

($t_b < \frac{{r_b}^2}{\alpha_b}$) [99].

Short-term G-function model: Yavuzturk and Spitler [109] were the first to propose a model of analysis in the short-term. The authors, by numerical methods, determined the thermal response of the filling material and expressed it in the form of G-functions from Eskilson [106]. From that, they adapted the solution of Equation 2.16 including a total thermal resistance for the filling, pipe and fluid (Equation 2.18).

$$T_b = T_o + \frac{q_b}{2\pi k_{gr}} \times g\left(\frac{t}{t_s}, \frac{B}{H}, \frac{r_b}{H}, \frac{D}{H}\right) + R_{tot} q_b \tag{2.18}$$

where: R_{tot} is the total resistance including the filling, the pipe and the fluid (Equation 2.19).

$$R_{tot} = R_b + R_p + R_{conv} \tag{2.19}$$

The resistance of the filling R_b can be determined using Paul's model [110] (Equation 2.20) as a function of the conductivity of the filling material k_b, the borehole diameter D_b, the pipe diameter D_p and the shape coefficients β_o, β_1 suggested by the author (Table B.1).

$$R_b = \frac{1}{k_b \beta_o \left(\frac{D_b}{D_p}\right)^{\beta_1}} \tag{2.20}$$

On the other hand, the resistances of the pipe and the fluid can be determined by Equations 2.21 and 2.22 respectively.

$$R_p = \frac{\ln\left(\frac{D_{out}}{D_{in}}\right)}{4\pi k_p} \tag{2.21}$$

$$R_{conv} = \frac{1}{2\pi D_{in} h_{in}} \tag{2.22}$$

where: D_{out} and D_{in} represent the outer and inner pipe diameter, k_p the conductivity of the pipe and h_{in} the coefficient of convection between the fluid and the inner pipe.

Yavuzturk and Spitler [109] suggest that this method is valid for time intervals between 2.5 minutes up to 200 hours and for analysis from the 200 hours they suggest to use the G-functions proposed by Eskilson [106].

Short-term Infinite cylindrical source model: This method was proposed by Lamarche and Beauchamp [99] and is based on applying the heat diffusion equation to two different media (filling and soil). The method is inspired by previous methods such as Sutton et al. [111] and Young's buried cable method [112]. This model simplifies the configuration of the U-tube by an approximation of a single tube of equivalent radius r_{eq} that can be calculated by Equation 2.23 [111].

$$\frac{\log\left(\frac{r_b}{r_{eq}}\right)}{2\pi k_b} = R_b \tag{2.23}$$

Lamarche and Beauchamp proposed the solution for the filling domain $r_{eq} < r < r_b$ for two scenarios. The first is considering a constant heat flux q_b as the boundary condition, and the second is considering convection heat transfer inside the pipe as boundary condition. The analytical solution for these scenarios can be found in detail in [99].

The analytical solutions, according to the authors, have very accurate results when compared with numerical models (finite elements). However, in order to enhance practicality, G-functions could be developed based on the proposed analytical resolution. In short-term analyses, there is no relevant interference with adjacent boreholes since the timescale of study is very short.

Other authors have focused on the study of the thermal response in the short-term with very accurate results. The use of the equivalent radius has been widely accepted by researchers to avoid problems of U-tube analysis. These models can be seen in more detail in [113–118]. However, Li and Lai [95] emphasise that this simplification can lead to problems in matching short-term models to medium and long-term models. The same authors in another study developed a model for the short-term analysis based on Jaeger's infinite composite medium. By this methodology, it can be assumed that the legs of the U-tubes are linear sources of heat [113].

2.3.3 Numerical models to evaluate borehole heat exchangers

Numerical models to evaluate borehole heat exchangers have been widely used. With advances in computational power, nowadays almost any heat transfer problem can be evaluated using numerical approaches. Powerful software tools like ANSYS and OpenFoam have been used to evaluate borehole heat exchangers [102, 119–121]. However, this type of study has been focused on the the short-term response of borehole heat exchangers.

Due to the complexity of these numerical models and the computational cost, these models are not appropriate for long-term analysis. However, simpler numerical models in one or two dimensions have the potential to solve more quickly the thermal response of borehole heat exchangers. For instance, Fine et al. [122] developed a simple numerical model based on the finite difference method (FDM) in cartesian coordinates, to evaluate the long-term behaviour of a SAGSHP.

Based on a similar approach, Chapter 6 shows the development of a numerical model based on the FDM in radial coordinates and the superposition technique to evaluate the thermal response of arrays of very shallow boreholes.

2.3.4 Superposition technique to solve complex heat transfer problems

The principle of the superposition technique is to treat a complex heat transfer problem as the sum of the results of simpler problems. For example, in bidimensional or tridimensional heat transfer problems, with the superposition technique, the problem can be approached by solving two or three one dimensional problems and summing the results. Likewise, superposition techniques can be used to treat problems with different boundary conditions which can be treated separately, and their results summed. Superposition techniques in heat transfer have been successfully used in both, numerical and analytical problems [18].

For example, Figure 2.12 shows a one-dimensional problem with two different boundary conditions (BC) at $X = 0m$ and $X = L(L = 2m)$. The problem has

been solved numerically considering the two different BC and then by summing up the results of two more simple problems with as shown in Figure 2.13. The thermal properties for the solid material are: k_s= 1.3 W/mK, C_s=1140 J/kgK and ρ_s= 1500 kg/m^3.

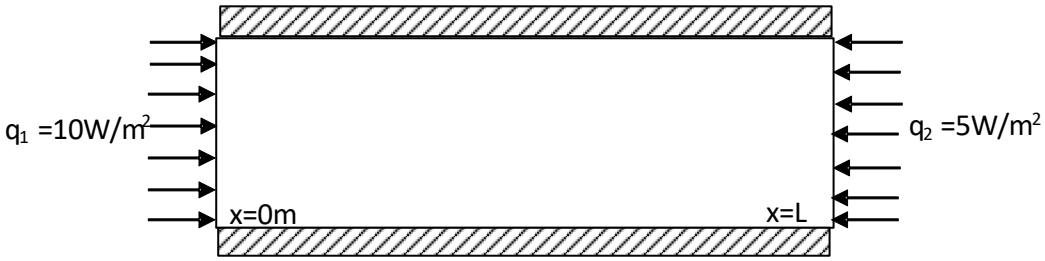

Figure 2.12: Complex one-dimensional heat transfer problem with 2 different boundary conditions

Figure 2.14 shows the results for the temperature variation (ΔT) with reference to the initial temperature (T_o) for the problem shown in Figure 2.12 while Figure 2.15a and 2.15b shows the temperature variation of the two simple problems of Figure 2.13 and Figure 2.15c shows the results of the sum of the two simple problems. The results shown in the figures are for a time (t) equal to 13.5 hours. It can be seen that the superposition technique match perfectly in this case as the results of in Figure 2.15c are exactly the same results showed in Figure 2.14.

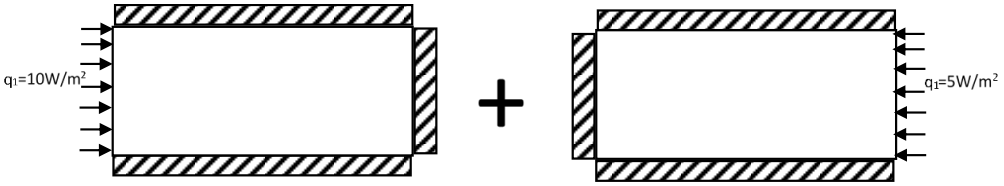

Figure 2.13: Sum of two simple one-dimensional heat transfer problems

The superposition technique can be used to superimpose thermal responses from different dimensions as well. In this case, a bidimensional problem can be solved as the superposition of the responses of two one-dimensional problems.

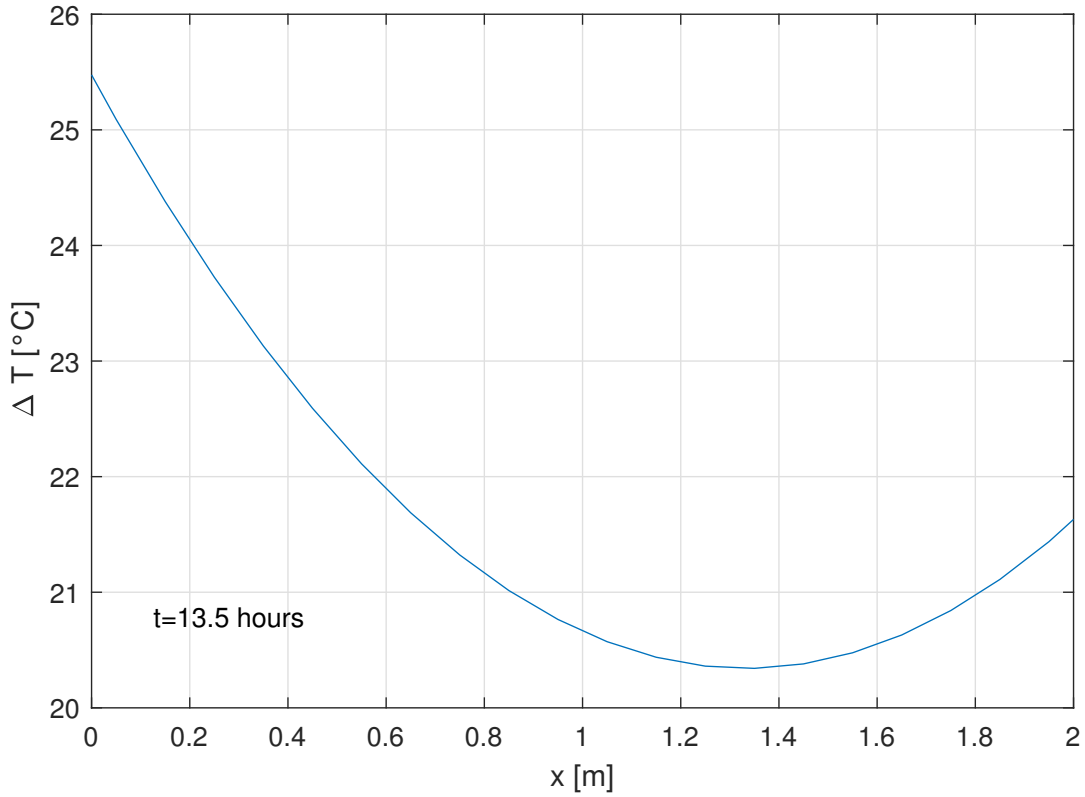

Figure 2.14: Results of the complex problem on Fig. 2.12

2.4 Summary of the chapter

This chapter reviewed key literature needed to carry out the appropriate development of the thesis. It starts by showing the potential of seasonal heat storage through different technologies. It also highlighted the lack of small-scale systems for seasonal heat storage. It is evident that BTES systems have a lot of potential for small-scale buildings since they require less land area and are more affordable than TTES, PTES and ATES. A review of SAGSHP systems and their typical configurations was also carried out. It is highlighted that there are no studies where very shallow vertical boreholes are used, despite their potential for reducing costs. In addition, this type of very shallow system is ideal for new and efficient small-scale buildings where thermal loads have been reduced by improvements in building design. However, as no models have been developed to analyse the performance of very shallow ground heat exchangers, their actual potential has not been fully analysed. Therefore, a model must be created

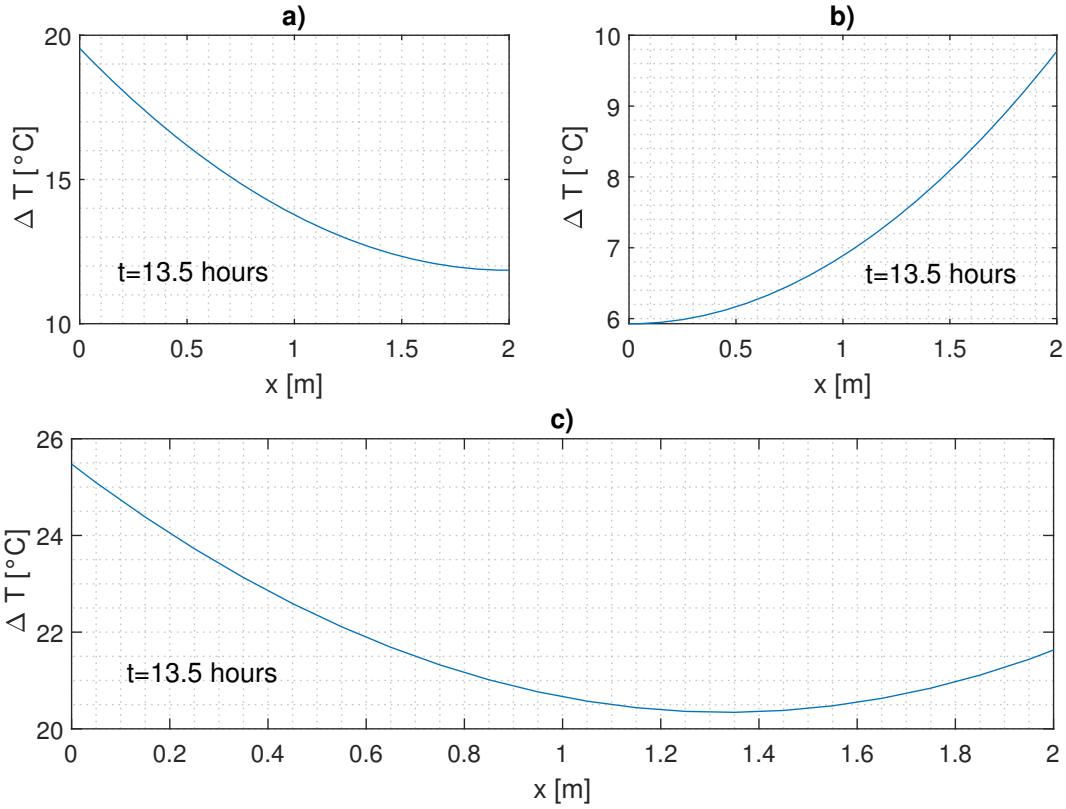

Figure 2.15: a) Results of the left side of the problem in Fig. 2.13 b) Results of the right side of the problem in Fig. 2.13 c) Results of the superposition of the two simple problems in Fig. 2.13

that integrates the thermal response of conventional models, with the natural thermal response of the very shallow soil. For this reason, a review of this type of model was conducted, which serves as the basis for the development of the model proposed in this thesis. That is, in the development of a model to study the behaviour of very shallow vertical boreholes applying the technique of superposition in a multidimensional heat transfer problem. The following chapter shows a brief description of the proposed methodology to reach the main aim of the investigation.

3. Methodology

This chapter describes the methodology adopted to address the aim of this research and achieve the objectives. The methodology is based on the concepts, theories, experiences and models that were described in the literature review of Chapter 2.

3.1 Hypothesis

As described in Chapter 1, the aim of this research is to develop a model that is accurate and simple enough to evaluate the thermal response of very shallow geothermal boreholes.

Section 2.1 described a range of seasonal heat storage methods and justified the storage of heat in the soil using geothermal boreholes. This is the most economical approach for seasonal storage, where heat can be extracted by a geothermal heat pump. Then, section 2.2 described the significant amount of research activity into small-scale solar-assisted ground source heat pumps (SAGSHP). However, there is a lack of research into this type of system combined with very shallow geothermal boreholes, so the potential advantages that these systems have due to their low installation cost were highlighted. While the use of very shallow boreholes limits the actual amount of heat stored and extracted from the ground, the developments in energy-efficient or low energy consumption buildings have opened a door to the use of smaller heating systems where the use of very shallow boreholes has high potential. Finally, section 2.3 reviewed the models that can be used to study the natural variation of shallow soil temperature, the thermal response of geothermal boreholes, and the superposition technique to study the thermal response of complex multidimensional heat transfer problems.

Based on this review, the following hypothesis is proposed, to be tested through the research described in this thesis:

The use of the finite difference method together with the superposition technique of thermal responses is adequate to develop a thermal response model of arrays of very shallow geothermal boreholes fast and accurately.

To test the hypothesis proposed, it is necessary to develop different heat transfer models, investigate whether the finite difference method (FDM) is more practical than conventional analytical models and finally prove that the superposition technique is adequate to determine the thermal response of arrays of very shallow geothermal boreholes. These types of proposed models, given their innovative nature, require validation by comparison with experimental data of a pilot system of these characteristics.

3.2 Ideal methodology

An ideal methodology to test the hypothesis would focus on trying to reduce the uncertainty of the experimental data to validate the models. This starts by using the latest generation equipment for monitoring and data collection that can show missing data in real-time to correct any errors that may arise in data collection. It would also be necessary to have a testing system that is very flexible in order to allow the experimental study of different system parameters. For example, the variation of soil materials and borehole grouting material, spacing between geothermal boreholes, types of boreholes arrangements (series and parallel), depths of geothermal boreholes, different boundary conditions and control strategies for heat injection and extraction. Finally, the ideal methodology would require a longitudinal study of the experimental system over the medium to long term (for more than 10 years) to assess the validity of the models.

Unfortunately, this methodology is impractical within the scope of the present project because of the high costs that would be involved. In addition, a greater number of people would be required to carry out the different types of experiments given the complexity and time that this methodology would require. Also, given the duration of this investigation, it is impractical to conduct a long-term experimental study as the subject of a Ph.D.

3.3 Chosen methodology

For the reasons stated above, a more pragmatic methodology is proposed, but one that will nevertheless test the hypothesis. This methodology is suitable for doctoral research work and focuses first on an experimental study of a specific design of an array of very shallow boreholes. Then a numerical study is proposed where models are developed to estimate the thermal response of arrays of very shallow boreholes. These models must be validated with the experimental data collected. Finally, an application of the validated model is proposed to study the thermal response of very shallow geothermal boreholes in the long term and under different thermal properties. This methodology is summarised in graphical form in Figure 3.1.

3.4 Experimental investigation

The experimental part will be based on the Grasmere Street Project, an experimental project carried out by De Montfort University, which has the necessary inputs and monitors the essential parameters to validate theoretical models. This project consists of a very shallow SAGSHP that is being monitored for research purposes. It aims to evaluate the seasonal heating storage for small domestic heating applications.

The experimental approach for this stage of the research includes the identification of the most important variables of the system and how these impact on the system's overall performance. The use of the monitored data will be the first step of this approach in order to determine the soil temperature profiles (over space and time) as well as the underground storage or earth energy bank (EEB) temperature profiles. Additionally, the experimental energy balance of the whole system will be determined. Through this, a general idea of the whole system performance can be obtained. The general energy balance equation to be used for this purpose includes all the energy fluxes coming in and out the EEB (Equation 3.1).

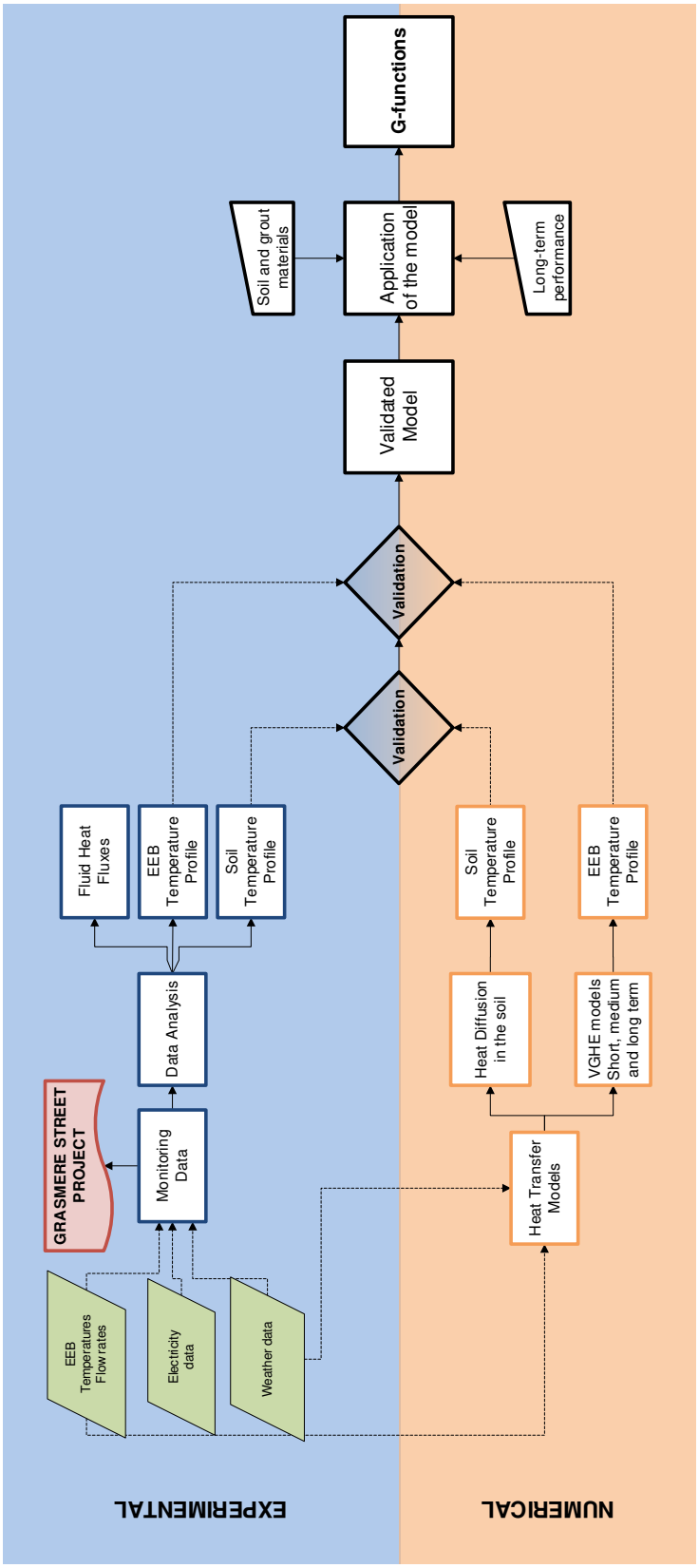

Figure 3.1: Proposed research methodology

$$Q_{solar} + Q_{geo} - Q_{eva} - Q_{loss} = Q_{EEB} \tag{3.1}$$

where: Q_{solar} is the solar thermal energy gained from the PVT, Q_{geo} is the geothermal heat gained from the surrounding soil, Q_{eva} is the energy demanded by the evaporator of the GSHP, Q_{loss} are the total heat losses and Q_{EEB} is the heat stored in the ground.

The approach for the experimental investigation has four main steps:

- *Data monitoring and selection of data set:* This part consists in the analysis of the variables that are monitored in order be able to analyse the thermal performance of the SAGSHP and the EEB. Likewise, this also includes the timestep or frequency of recording of the measured variables. The selection of dataset refers to the amount of monitored data to be used to determine the performance of the SAGSHP. In this case, at least one year of data collection is needed in order to study the effects of seasonal thermal storage.

- *Pre-treatment of collected data:* In this part, the data collected and selected for the experimental investigation will be treated to reduce the bias due to outliers and missing data. Hence, simple statistical analysis will identify the outliers to be removed and then all the missing data (including the removed outliers) will be filled by linear interpolation. As the data are monitored on an hourly basis (high frequency for a yearly analysis), linear interpolation is a reliable approach to fill in missing data.

- *Uncertainty analysis:* Before conducting the experimental investigation, an uncertainty analysis will be conducted in order to estimate the errors in the monitored and calculated variables. This will be based on the accuracy of the sensors used and the precision obtained from calibration. Calibration data will be taken from the sensor manufacturers and the accumulative error approach [123] will be used to calculate the error in calculated values.

- *Data analysis and output variables:* This will be the core of the experimental investigation. Here, all the calculations, data analysis, coding, and derivation of results will be done. The inputs will be previously validated and

treated data. As seasonal thermal energy storage is related to heat fluxes and temperature variations, heat transfer equations will be used to calculate the net energy balance of the system. The output variables will be the net energy inputs and outputs of the whole system over the whole period of analysis. Moreover, the temperature profiles of the EEB will be analysed and compared to the natural soil temperature profile to understand the potential of seasonal storage in the very shallow soil.

The experimental investigation is presented in Chapter 4 and will indicate relevant conclusions on the thermal behaviour of a SAGSHP with very shallow boreholes and seasonal energy storage in the soil. Likewise, the experimental data will be used as input data and to validate the models developed in the numerical investigation.

3.5 Numerical investigation

The theoretical study will be based on the development of heat transfer models using experimental data to assist the development of the models. This will be the core of the research and where the hypothesis will be tested. To test the hypothesis, several steps must be carried out as part of the numerical investigation, and they are summarised below:

- *Models to study the natural temperature variation of the very shallow soil:* This part will focus on the analysis of common models to estimate the natural soil temperature variation at different depths in the very shallow soil. The existing models are very accurate for large depths. However, they do not reflect the dynamic behaviour of the soil temperature in the first centimetres of depth. Hence, a numerical model to study the natural soil temperature variation based on the finite difference method (FDM) will be developed. The main idea is to create a simple model that is accurate and fast to simulate which will be a valuable contribution to the research in this field. The output variables for the validation of the model developed will be the natural soil temperature profile at different depths.

- *Models to study the thermal response of geothermal boreholes:* This part will focus on the development of a model to study the thermal response of the very shallow boreholes at different time and space scales. According to the literature, current models have shown good accuracy in predicting the behaviour of conventional boreholes that are usually very deep (30 to 150 metres). However, these models might not be appropriate for the study of very shallow boreholes since the soil is less stable at shallower depths where boundary conditions are more dynamic. First, analytical models like the Infinite Line and Cylindrical Source (ILS and ICS) model will be evaluated. Then, a numerical model based on the FDM will be created and compared in terms of accuracy and simulation time with the analytical models.

- *Superposition technique to study arrays of very shallow boreholes:* This is a key part to test the hypothesis proposed. Both the analytical and numerical (FDM) models, developed in the previous stage, will be used with the superposition technique to superimpose the thermal response of adjacent boreholes (in an array) and the natural temperature variation of the very shallow soil. This will create the main model proposed in the hypothesis and as a reference, the thermal response will be compared with the thermal response of analytical models. If the model proposed is accurate and fast for simulation, then the hypothesis can be supported. The output variables for the validation of the model will be the EEB temperature variation profiles and fluid outlet temperature from the ground heat exchanger (GHE).

3.6 Validation of models developed

The accuracy and simulation time of both numerical and analytical models will be compared with the results of the experimental data analysis. In the case of no validation, modifications will be made to the models, mainly focused on the potential uncertainties. The models will be validated using three different metrics:

- *Coefficient of determination (R^2):* This is an output from regression analysis and is an interpretation of the correlation between the predicted (calculated) variable and the actual (experimental) variable. It is important to note that the R^2 only shows if there is a correlation between the two sets of data, but it is not a measure of the accuracy of the model. Hence, more metrics are needed to demonstrate the accuracy of a model to predict the output data. The R^2 can be determined using Equation 3.2:

$$R^2 = \left[\left(\frac{1}{n} \right) \sum_{i=1}^{n} \frac{(s_i - \bar{s})(m_i - \bar{m})}{\sigma_s \sigma_m} \right]^2 \tag{3.2}$$

  where: n is the size of the sample, s_i the simulated data, $\bar{s}$ the mean of the whole simulated dataset, m_i the measured data, $\bar{m}$ the mean of the measured dataset, σ_s the standard deviation of the simulated dataset and σ_m the standard deviation of the measured dataset.

- *Root mean square error (RMSE):* This parameter represents the standard deviation of the residuals, which means how the data deviate from a line of best fit. This indicator is usually used along with the R^2 to see the potential error of simulated data. The $RMSE$ can be determined by using Equation 3.3:

$$RMSE = \sqrt{\frac{\sum_{i=1}^{n} (s_i - m_i)^2}{n}} \tag{3.3}$$

  The relative value of the $RMSE$ is the normalised root mean square error ($NRMSE$), which is simply the $RMSE$ divided by the overall range of the set of experimental data ($m_{max} - m_{min}$).

- *The efficiency of the model (EF):* This parameter represents the residual variance of the simulations compared to the variance of the measured data [89]. Hence, this parameter evaluates the accuracy of a model when used to predict reliable results. An EF closer to 1 indicates accurate predictions from the models. The EF is the most meaningful of the three parameters and can be determined by using Equation 3.4:

$$EF = 1 - \frac{\sum_{i=1}^{n} (s_i - m_i)^2}{\sum_{i=1}^{n} (m_i - \bar{m})^2} \tag{3.4}$$

The output of the validation is support or disproof of the hypothesis. If the hypothesis is supported, then the model will be applied to study different parameters. Otherwise, if the hypothesis is disproved then another approach might be proposed for further research.

3.7 Application of models developed

Finally, from the validated models, different variables such as soil properties, grout thermal conductivities, borehole spacing, and long-term effects will be evaluated parametrically. From these results, improvements in the configuration of the system or the configuration of an optimal system are expected to be obtained as output. Likewise, from the validated model G-functions can be developed. These are graphical representations of the thermal response of very shallow boreholes. G-functions for this kind of system will be a valuable contribution to knowledge as different configurations of this type of system could be evaluated. This will be one of the main outputs of the model developed.

3.8 Summary of the chapter

In this chapter, the main hypothesis and the methodology to test the hypothesis are presented. An ideal methodology is shown and reasons suggested as to why the ideal methodology is inappropriate. The main methodology is based on an experimental and numerical investigation and is divided in four main steps which are:

1. An experimental investigation of a SAGSHP with very shallow geothermal boreholes;

2. A numerical investigation in which the model proposed in the hypothesis is developed;

3. A validation of the model in which the hypothesis will be proved true or false and

4. An application of the model developed.

Chapter 4 shows the experimental investigation proposed in this methodology, while Chapters 5 and 6 deal with the model development and validation. Finally, Chapter 7 shows the application of the model developed.

4. Experimental system development and analysis

As mentioned in the methodology chapter, the current research includes an experimental approach and a modelling approach. The experimental approach of the research helps not only to get accurate and precise data to validate the modelling work but also to become familiar with the actual operation of a very shallow solar assisted ground source heat pump system. A systemic experimental analysis can lead to identifying general trends regarding the system performance, to find failures in the design and operation of the system, to analyse the impact and the correlation between the most relevant monitored parameters, among others. Through experimental data analysis, the main parameters affecting the performance of the system can be also identified, which will help in defining the most relevant parameter for the modelling.

The experimental system was installed under the supervision of the researchers of the Institute of Energy and Sustainable Development (IESD) at De Montfort University and the private company Caplin Homes. The latter is responsible for the design of the whole solar-assisted ground source heat pump system. This installation is intended to be used as a laboratory to test the system performance and study ways to improve its performance and design.

This chapter provides a description of the experimental system set-up for the current research, the monitoring equipment used, and the calculation of the main heat fluxes of the energy system that were determined from the experimental data. An uncertainty analysis is also presented in order to quantify the maximal error between the measured and calculated data.

4.1 Physical installation of the system

4.1.1 Building description

The experimental system used to carry out the research is based on a domestic building owned by De Montfort University and used as a lab for crime scene mocks-ups by forensic science students. The building is a two-storey 19th-century Victorian house. The house is located in Leicester (UK) next to the building of the School of Engineering and Sustainable Development (52.63° N, 1.14° W). The building is a terrace house adjacent on both sides to similar houses as shown in Figure 4.1. The house was retrofitted in the year 2015 with loft insulation and double-glazed windows. However, it has no insulation in the external solid brick walls. The pitched roof is covered in slate tiles.

Figure 4.1: House of the current study

The main heating system of the house is the underfloor heating system installed in the two main rooms within the slab of the ground floor. During the system installation, the timber floor was replaced with a solid concrete floor. The previously installed gas-fired combination boiler with radiators is still available as a back-up. Even though the house was retrofitted, the fact of not having insulation in the external walls leads to much higher thermal loads than those of modern low-energy houses, which are the main target market for the very shallow SAGSHP system under investigation. The heating system also includes

a storage tank (120 litres) for domestic hot water (DHW), although since the house is unoccupied, the hot water consumption is negligible. Figure 4.2 shows the plan of the house. A room on the second floor was used as the control room. Here all the data collection equipment, heat pump unit and water storage tank were installed (Figure 4.3).

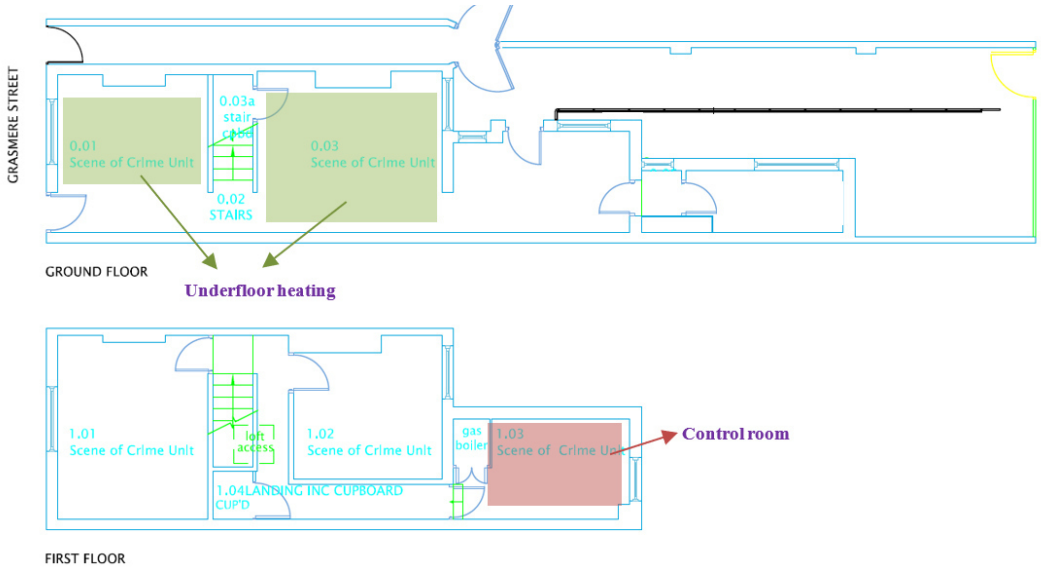

Figure 4.2: Plan of the house of study

4.1.2 SAGSHP system description

The very shallow SAGSHP system is configured as illustrated in Figure 4.4. The system has eight solar panels of which seven are photovoltaic-thermal (PVT) panels. The manufacturer of the PVTs is Solar Angel [124] and the technical specifications are shown in Table 4.1 at standard testing conditions (STC). According to the manufacturer, the test conditions for the specifications followed the standard EN 12975 [125] for the thermal side, and IEC 61215 [126] and IEC 61730 [127] for the electrical side. Hence, test conditions were conducted at an insolation of 1000 W/m^2, fluid temperature difference of 2 K and wind speed of 0 m/s. The PVTs are installed parallel to the roof of the house at an inclination of 40° facing south-west (azimuth of 60°). Ideally, the azimuth of the PVTs should be facing south (0°). Nevertheless, this was not possible as the roof orientation dictated the PVTs orientation.

The heat gained through the solar collectors is transferred to an underground

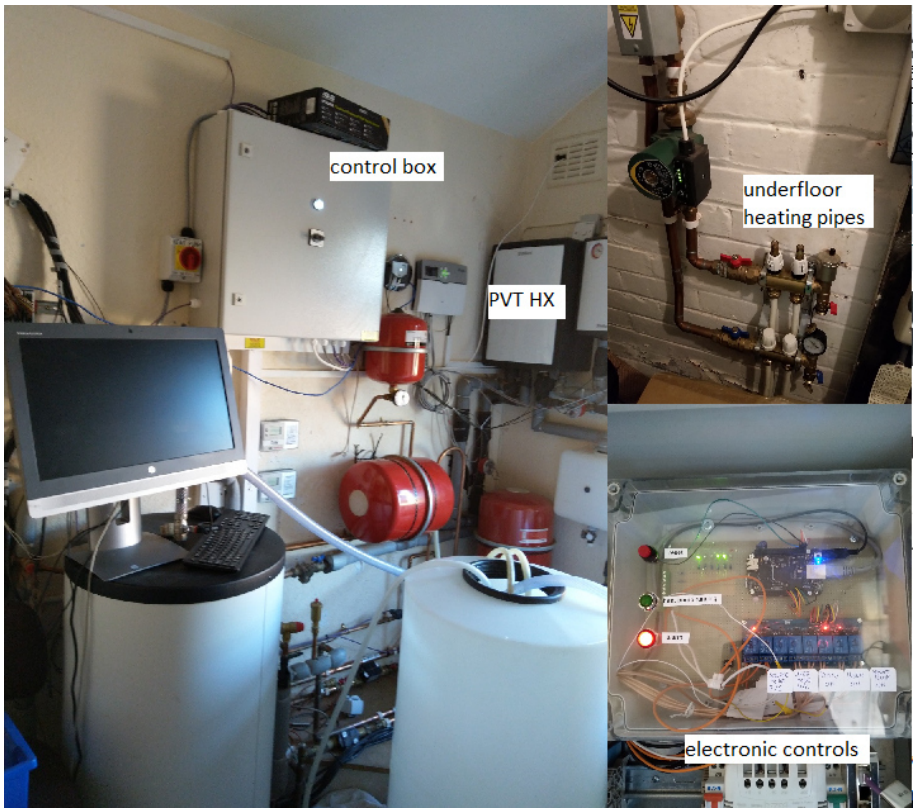

Figure 4.3: Control room

thermal energy store known as an Earth Energy Bank (EEB) via a ground heat exchanger (GHE). The EEB is then used as a low-temperature heat source for a ground source heat pump (GSHP) unit, which delivers the heat to the house, covering the thermal loads.

As seen in Figure 4.4, the SAGSHP can be seen as a system comprising three sub-system or three different loops, the solar loop (yellow lines), the ground loop (green lines) and the heating loop (orange and blue lines). The system can be regarded as a hybrid heating system, since both solar and geothermal energy are involved, and its operation is seasonal. In summer, as the heating load is low and the solar radiation is high, the heat collected by the PVT panels is mainly stored in the EEB. On the other hand, in winter, when the solar availability is low, and the heating loads are higher, the heat pump extracts the heat stored from the EEB in order to cover the heating loads. According to this principle, the control strategy of the SAGSHP is set in accordance with the temperatures measured at the outlet of the PVT and the middle of the EEB.

Whenever the outlet temperature of the PVT panels is 7 K higher than the

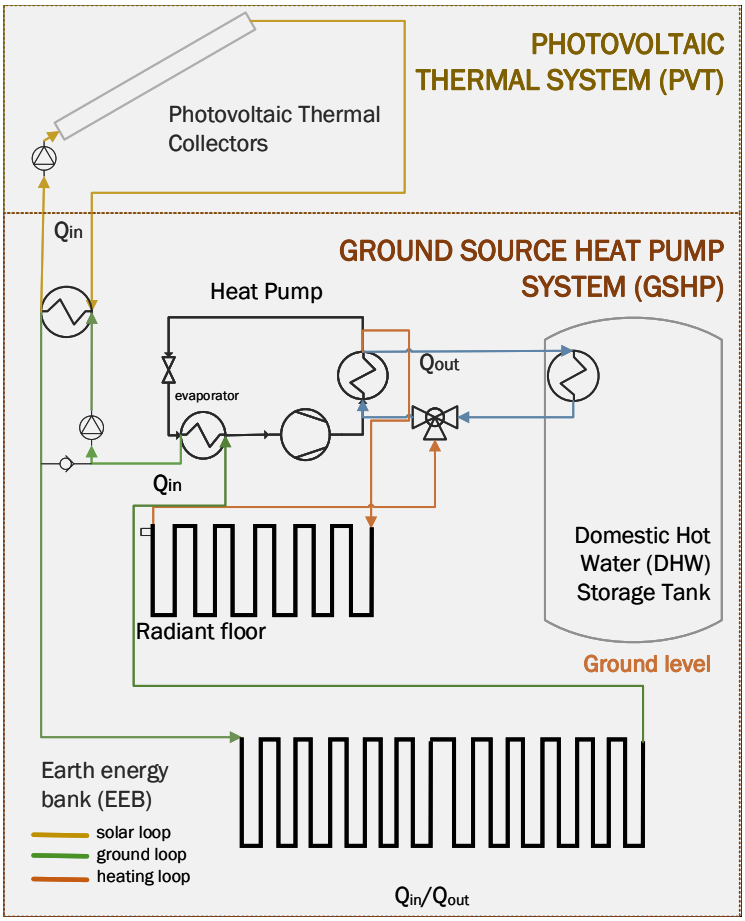

Figure 4.4: SAGSHP configuration

EEB temperature, the solar loop pump is activated. Then, the heat gained through the PVT panels is transferred to the EEB using the GHE (described later in this chapter). If the heat pump is off (no heating load), then the fluid in the ground loop recirculates keeping the soil recharging from the solar subsystem until the temperature difference between the EEB and the outlet of the PVT panels is lower than 4 K. Therefore, the control hysteresis is 3 K.

On the other hand, whenever the PVT temperature is lower than the EEB temperature, the solar loop pump is turned off. If the heat pump is turned on (heating demanded by the building), a pump, controlled by the heat pump in the evaporator side, is activated. Therefore, the heat is transferred from the EEB to the evaporator discharging the heat stored in the EEB which will be replaced when solar energy is available again, or by natural recovery.

As stated previously, the heat pump covers the demand for both space heating and DHW, although there is no DHW demand. The heat pump has a heating

Table 4.1: PVT technical specifications at STC

PV output (peak)	250 W
Electrical efficiency	15.6%
Thermal output (peak)	648 W
Gross collector area	1.6 m^2
Thermal efficiency	42%
Aperture area	1.5 m^2
Stagnation temperature	78.9°C
Inclination/Azimuth	40°/60°
Operating fluid	Glycol (30%)

capacity of 3 kW which is enough to cover the heating demands from a well-insulated small dwelling in the UK [128] which is the target of the system of this study. The technical specifications of the heat pump are shown in Table 4.2.

Table 4.2: Heat Pump technical specifications

Manufacturer	Vaillant UK
Heating capacity	3 kW
Max. power input	1.1 kW
Source inlet temperature range	-10 to 20°C
Source circuit fluid	Ethylene glycol 30%
Source flow rate	620 l/h
Heating circuit output temperature range	20 to 55°C
Heating circuit flow rate	250 to 465 l/h
Refrigerant	R410A
Nominal COP	4.5

4.1.3 Earth Energy Bank and Ground Heat Exchanger description

The Earth Energy Bank (EEB) consists of a volume of soil, as shown in Figure 4.5. The EEB was originally conceived to be placed within the foundations of the house as is being constructed, which is how all commercial units have been

installed in new homes. However, in the case of this research, since the SAGSHP system was installed after the house was built, another approach was used. In this case, the EEB was installed in an adjacent grass verge, next to the building, under a surface of the same footprint of the house which is 10 m by 4 m (40 m^2). With the idea to replicate an actual installation, the EEB was insulated with polyisocyanurate (Celotex) on the top (20 cm thick) and sides (10 cm thick). This insulation has a thermal conductivity of 0.021 W/mK, which makes it one of the best insulation materials for buildings available in the market. To protect the insulation from rainwater and avoid the decrease of its thermal properties, a 0.3 mm polyethylene sheet was used as a protective layer for all the insulation. This approach is similar to the one used for a new building, in which the EEB would be placed beneath the insulated soil ground floor. Additionally, the EEB has concrete sides (10 cm thick) between the insulation and the surrounding soil. This concrete represents the foundations in a real installation, which also helps in avoiding heat losses due to groundwater flows.

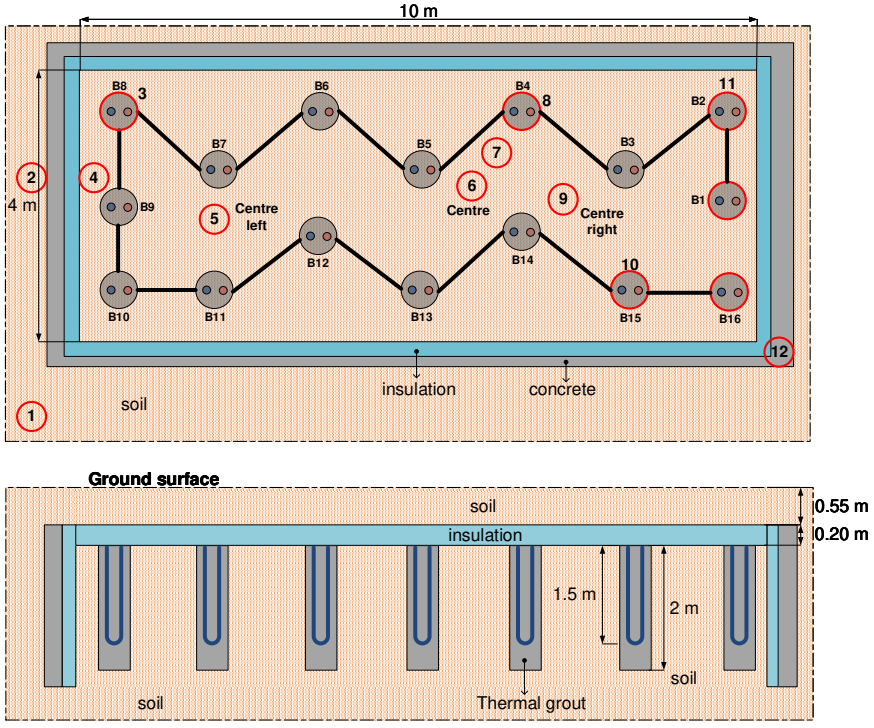

Figure 4.5: Earth Energy Bank configuration and sensors location

The ground heat exchanger (GHE) is composed of 16 very shallow boreholes connected in series. The distance between adjacent boreholes is 1.5 m except for

the distances between boreholes B1-B2, B10-B11 and B15-B16 (Figure 4.5) which are spaced 1 m apart. The GHE specifications are shown in Table 4.3.

Table 4.3: Ground heat exchanger specifications

Depth of boreholes	1.5 m
Borehole diameter	0.15 m
Pipe outer diameter	4.0 cm
Pipe inner diameter	3.4 cm
Pipe material	HDPE
Pipe connection	In series
Grouting material	Bentonite
Operating fluid	Glycol (30%)

Thermal properties of the soil were obtained through a thermal response test conducted in the site before the SAGSHP system was installed. The detailed results of the soil survey are shown in the Annexe AA and are summarised in Table 4.4 along with the thermal properties of the working fluid and the grout material. It is important to mention that the thermal response test was conducted to evaluate the thermal conductivity and the type of soil, hence other properties like density and specific heat were obtained through the look-up tables from the microgeneration installation standard MCS 022 [129].

Table 4.4: Soil, grouting and working fluid thermal properties

Type of solid/fluid	Wet clay	Bentonite	Glycol (30%)
Thermal conductivity	1.5 W/mK	0.8 W/mK	0.45 W/mK
Density	1800 kg/m^3	2500 kg/m^3	1070 kg/m^3
Specific Heat	1200 J/kgK	1250 J/kgK	3768 J/kgK
Thermal diffusivity	6.94 x10^{-7} m^2/s	2.72 x10^{-7} m^2/s	1.11 x10^{-7} m^2/s

4.2 Monitoring equipment

For the current research, four different sets of monitoring equipment were used to provide robust information for the operation of the whole system and to determine the main parameters affecting its performance. The experimental data collected through the monitoring equipment are crucial to develop accurate thermal energy models, to study the energy balance of the system and to determine the system's current efficiency.

4.2.1 Earth energy bank temperature data

The monitoring of the EEB thermal performance is very important not only to study the applicability and potential of very shallow boreholes but also to validate the models developed for further research of this technology. In this context, temperatures of the EEB were measured at several locations and depths using PT1000 resistance temperature detector (RTD) sensors. PT1000 were chosen over PT100 to minimise errors as the length of the wires from the monitoring point and the data logger are in the range of several metres. As PT1000 sensors have lower resistance wires, the errors can be minimised. In total, 48 RTD sensors were installed at different locations of interest within the EEB. Figure 4.5 shows the location of the sensors (1 to 12) while Table 4.5 describes the location and depths of monitoring for each sensor.

Table 4.5: Sensors location and depth of measurement for the EEB

Sensors point	**Location**	**Depth [m]**
1	9 m away from the EEB wall	0.75, 1.25, 1.75, 2.75
2	Just Outside EEB	0.75, 1.25, 1.75, 2.75
4	Just Inside EEB	0.75, 1.25, 1.75, 2.75
3, 8, 10, 11	Borehole wall (B8, B4, B15, B2)	0.75, 1.25, 1.75, 2.75
5, 6, 7, 9	Centre of the EEB	0.75, 1.25, 1.75, 2.75
12	Inside and outside the insulation	1.75 (two sensors)

All the PT1000 sensors were connected through a NI9226 interface module to

a temperature data logger NI cDAQ 9133 23-bit from National Instruments. The data were recorded at 15 minutes time steps using Labview [130]. Data were recorded from 10th February 2016 to 31st December 2017.

4.2.2 Whole thermal system data

The whole thermal system refers to the data needed to calculate the heat fluxes and the energy balance of the whole system. It includes inlet and outlet fluid temperature sensors in each of the thermal loops as well as the volume flow rates for the fluids in the loops. For this, a monitoring system called RESOL VBus was installed. For this system, data were recorded at a time step of 5 minutes and stored online. The data stored were emailed on a weekly basis.

Likewise, it was possible to get real-time access to the monitored variables and evaluate the current system behaviour. The temperature sensors for the RESOL unit are also PT1000 while pulse flow meters were installed to monitor the flow rate of the solar and ground loop. All these variables were recorded from the 4th June 2016 until the 31st December 2017. By analysing these variables, it is possible to calculate the heat fluxes of the whole system. Additionally, a half-hourly electricity sensor was used to monitor the electricity consumption of the heat pump. Figure 4.6 shows a schematic of the monitored parameters and sensors position in the system as displayed on the portal *VBUS.net*.

4.2.3 PV and PVT panels electricity data

Although the current research is focused on the study of the thermal behaviour of the SAGSHP system, electricity data were also monitored for further research (out of scope) of the performance of PVT panels and their advantages (if any) over PV panels. For this, SMA's Sunny Portal application was used. Each solar panel (either PV or PVT) has its own micro inverter and Sunny Portal collects electricity generation data at 15 minutes intervals. Data is stored online and can be also displayed in real-time. Figure 4.7 shows a screenshot of the display in *sunnyportal.com*.

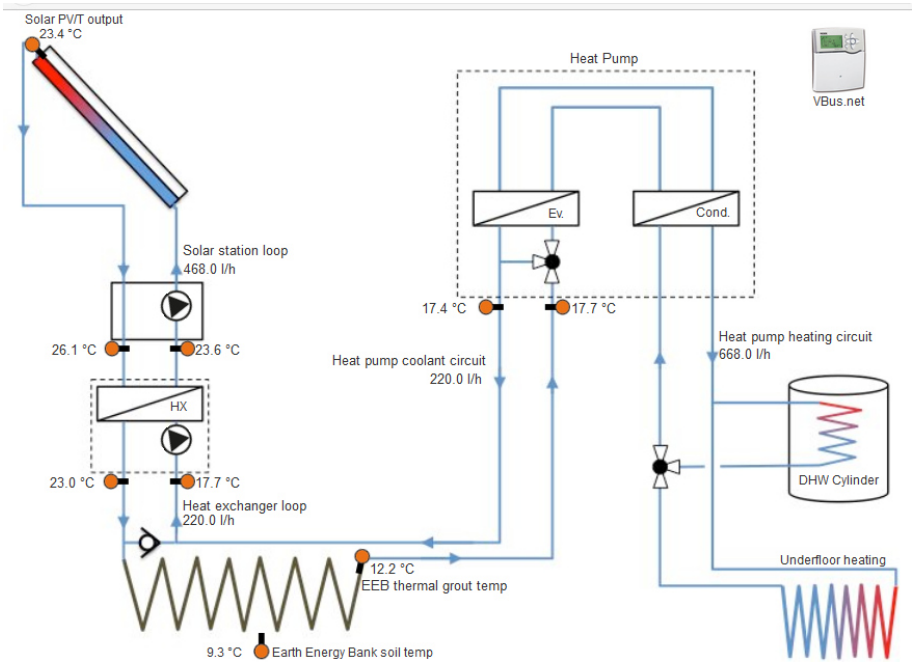

Figure 4.6: VBUS monitoring system and sensors location

4.2.4 Weather data

Weather data are essential for the current research, as many input parameters for the system modelling come from the ambient conditions. Likewise, weather data is crucial to determine the current efficiency of the PVT panels, and the thermal performance of the natural shallow soil. A weather station is installed on the roof of The Gateway House building on De Montfort University campus. This station is located 250 metres far from the SAGSHP system. Data from the weather station can be downloaded on-site at hourly time steps. The main parameters measured include the dry bulb temperature, relative humidity, wind speed and direction, solar radiation (global and diffuse) and precipitation. Figure 4.8 shows the monthly solar insolation in MWh/m^2 and the mean, minimum and maximum monthly ambient temperature. Data from the weather station were used from June 2016 to December 2017. The figure shows that even in summer months the mean ambient temperature is relatively low (below 20°C) while the minimum temperature in summer months can be easily lower than 10°C. Therefore, it is expected to have space heating loads even during summer.

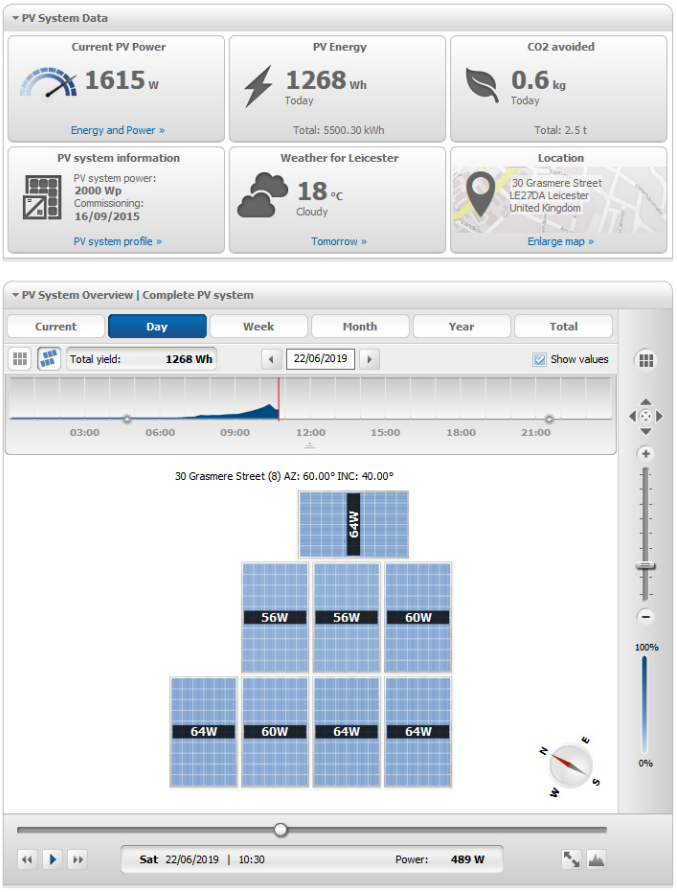

Figure 4.7: Display of the data monitored by Sunny Portal

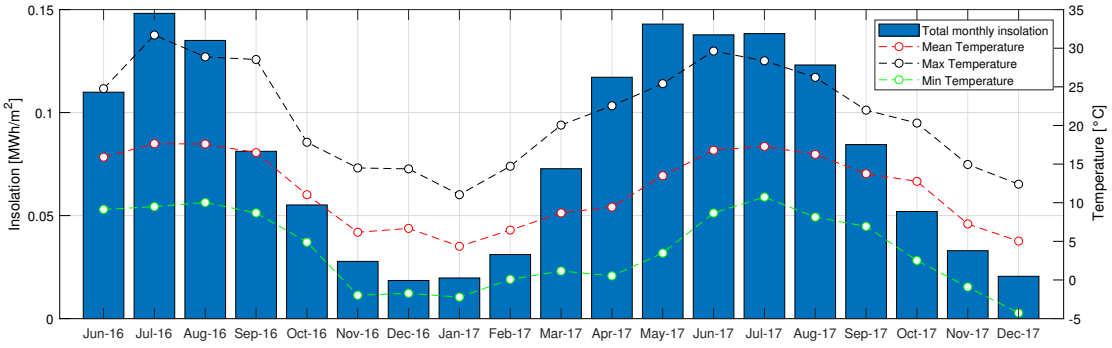

Figure 4.8: Monthly average ambient temperature and solar insolation from the monitored data

4.3 Pre-treatment of data and uncertainty analysis

As different sets of data and monitoring equipment were used, a standardisation and treatment of the data collected were needed. Firstly, a general analysis of the time series data was conducted. In this way, missing data, as well as

obvious outliers, were found. Any outlier was removed from the set of data and then linear interpolation was used to fill any missing data. As the time step of the raw data is sub-hourly and missing data appear sporadically, linear interpolation is a valid method to fill in missing data [131]. Secondly, as the data were monitored at different time steps and data from different sources are needed to perform calculations, all the sets of data were arranged on an hourly basis like the weather data. For this, all temperature and flow rate data were hourly averaged. Finally, all sets of data were merged into a single set. Since flow rate data, which is essential to calculate the system energy fluxes, were monitored from the 4th June 2016, the whole set of data was filtered from the 4th June 2016 until the 31st December 2017.

In order to determine the uncertainty (error) of the measured and calculated parameters, it is important to analyse the sensor accuracy and the measurement error. All the PT1000 RTD sensors were calibrated before the installation by the seller, and calibration results were provided along with the accuracy error. These results allow getting the function of the temperature in terms of the resistance. The mathematical functions were set in both, the NI cDAQ unit and the RESOL unit to compensate for any inaccuracy. Likewise, a precision test was conducted by immersing the RTD sensors in thermal baths at 0°C and 100°C to verify the readings and the uncertainty. The accuracy of pulse flow meters connected to the RESOL unit was verified by checking that every voltage pulse recorder matches with the display in the flowmeter. The thermal conductivity of the soil was obtained from thermal response tests during a soil survey in which 54 samples of soil from different layers were analysed. The observed maximum deviations were used to estimate the uncertainty of the calculated parameters using Equation 4.1 [123, 132], where R is the calculated parameter, ω is the uncertainty, x is the measured value of the primary variable i, and a is the exponent of the primary variable in the function of the calculated parameter. More details on the process to conduct uncertainty analysis can be found in [123]. Table 4.6 shows the details of the uncertainty of the primary (measured) variables and the

main calculated parameters.

$$\frac{\omega_R}{R} = \left[\sum_i \left(\frac{a_i \omega_{xi}}{x_i}\right)^2\right]^{1/2} \tag{4.1}$$

Table 4.6: Uncertainty in measured and calculated data

	Parameter	Range	Max. Uncertainty
Measured parameters	Fluid inlet and outlet temperature	-3 to 45 °C	0.23°C
	Soil temperatures	0 to 20 °C	0.2°C
	Volumetric flow rate	100 to 500 l/h	7.5 l/h
	Thermal conductivity	1.44 to 1.64 W/mK	0.04 W/mK
Calculated parameters	Heat flow in the GHE	-2000 to 2000 W	30 W
	Heat flow by conduction in the ground	-100 to 180 W	4.93 W

4.4 Calculations from measured data

To understand clearly the system performance, it is important to first clarify how the sub-systems work within the whole system. For this, the EEB (ground loop) is the sub-system that directly interacts with the solar sub-system and the heating (heat pump evaporator) sub-system. As a consequence, the performance of the whole SAGSHP system can be assessed through the EEB. Figure 4.9 shows the thermal boundaries of the EEB as well as the input and output energy fluxes interacting in it. The actual EEB is insulated at the top and sides. A heat transfer analysis using the Fourier law found that the heat transfer from the insulated surfaces is negligible (average of -0.17 ±0.22 W/m^2 for the top and -0.24 ±0.18 W/m^2 for the sides). Therefore, these surfaces were assumed to be adiabatic. Nevertheless, at the bottom of the EEB, as there is no insulation, heat can be

exchanged by conduction with the surrounding soil. Whenever the temperature in the EEB is higher than the surrounding heat is lost from the EEB, otherwise the EEB gains heat. Equation 4.2 shows the general energy balance equation of the EEB.

$$Q_{solar} + Q_{geo} - Q_{eva} - Q_{loss} = Q_{EEB} \tag{4.2}$$

The heat from the PVT (Q_{solar}) is injected to the EEB while heat demanded by the heat pump evaporator (Q_{eva}) is extracted from the EEB. When solar heat is injected, the ground temperature in the EEB increases and consequently heat may be lost through the bottom of the EEB (Q_{loss}) if EEB temperature rises sufficiently. On the other hand, when heat is extracted from the EEB and the ground temperature decreases, heat may be gained from the surrounding ground through the bottom of the EEB (Q_{geo}). The remaining heat (Q_{EEB}) is the net heat stored (positive)/ extracted (negative) in/from the EEB.

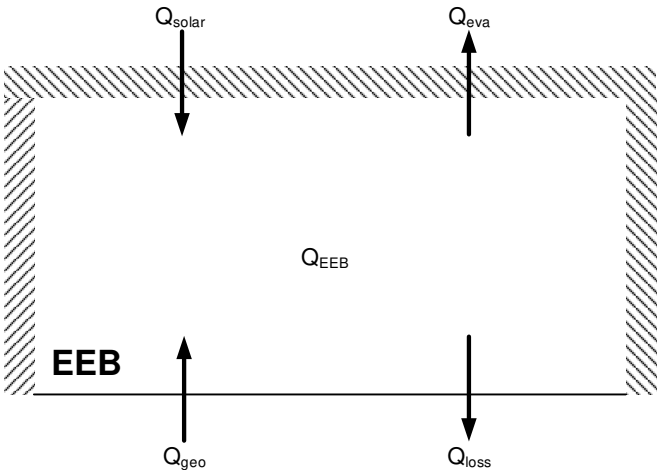

Figure 4.9: EEB system boundaries (vertical section, insulated hatched areas assumed adiabatic)

Solar heat gains (Q_{solar}) and the heat extracted from the evaporator heat pump (Q_{eva}) are calculated using Equation 4.3 and 4.4 respectively.

$$Q_{solar} = \dot{m}_{ghe} \times \ c_p \times \left(T_{in_{solar}} - T_{out_{solar}}\right) \tag{4.3}$$

$$Q_{eva} = \dot{m}_{ghe} \times \ c_p \times \left(T_{in_{eva}} - T_{out_{eva}}\right) \tag{4.4}$$

In Equations 4.3 and 4.4, $\dot{m}_{ghe}$ is the mass flow rate of the glycol in the ground heat exchanger and c_p is its specific heat. The mass flow rate is determined from the measured volumetric flow rate, $\dot{V}_{ghe}$, data multiplied by the density of glycol ρ_f (Equation 4.5). While it is true that the physical properties of fluids vary with temperature, from a practical and engineering point of view this variation can be neglected since it is less than 1.8% in the temperature ranges from 5°C to 50°C [133]. Thermal properties corresponding to a glycol average temperature of 26.7°C were used in this study. Similarly, inlet and outlet fluid temperatures are the ones from experimental data monitored by the RESOL unit.

$$\dot{m}_{ghe} = \dot{V}_{ghe} \times \rho_f \tag{4.5}$$

In order to calculate the heat exchanged with the surroundings from the bottom of the EEB (Q_{surr}), it is important to first determine up to which depth below the EEB the soil temperature is affected by the heat injection or extraction. For this, the average temperature measured at the deepest part of the EEB (2.75 m) was compared with the far field soil temperature at the same depth as seen in Figure 4.10. Even though, the bottom of the GHE in the EEB is at 2.25 metres below the surface, at a depth of 2.75 metres, the soil below the EEB is still assumed to be affected by the GHE.

To determine the depth at which the soil below the EEB is not any more affected by the GHE, a numerical model developed to calculate the very shallow soil temperature variation [12] was used to compare the temperature profile below the EEB with the far-field temperature, at similar depths. It was observed that the temperature profile was similar in both cases at 3.75 m depth. This implies that the heat transfer from the borehole heat exchanger had no effect at 1.5 m from the bottom boundary of the EEB (which is 2.25 m deep) and that below 3.75 m the soil temperature is that of the natural soil.

In order to quantify the heat loss from the bottom of the EEB (Q_{surr}), heat conduction analysis was carried out on the volume of soil in the 1.5 m region (i.e. between 2.25 m and 3.75 m) below the EEB. For the boundary conditions, the temperature at 2.25 m (the bottom boundary of the EEB) was obtained from experimental measurements, while temperatures at 3.75 m were determined from

Figure 4.10: Comparison of the measured temperature at 2.75 m below the EEB and in the far-field

the numerical model in [12]. Fourier's law (Equation 4.6) was then used to calculate the heat transfer between the bottom of the earth energy bank and the natural soil temperature at 3.75 m ($Q_{EEB-Nat}$)

Due to the temperature gradient in the natural soil, heat transfer usually occurs in the vertical direction (Q_{Nat}). This was estimated using Equation 4.7 and temperatures from the far field soil. The temperature at 2.25 m (in the natural soil) was obtained from experimental measurements. Finally, in order to determine the actual heat transfer at the bottom of the EEB (Q_{surr}), solely resulting from the system, the natural heat transfer Q_{Nat} was subtracted from the total heat transfer ($Q_{EEB-Nat}$) as illustrated in Equation 4.8.

$$Q_{EEB-Nat} = k_{soil} \frac{A_{EEB} \left(T_{EEB_{2.25}} - T_{Nat_{3.75}}\right)}{1.5\ m} \tag{4.6}$$

$$Q_{Nat} = k_{soil} \frac{A_{EEB} \left(T_{Nat_{2.25}} - T_{Nat_{3.75}}\right)}{1.5\ m} \tag{4.7}$$

$$Q_{surr} = Q_{EEB-Nat} - Q_{Nat} \tag{4.8}$$

From the heat exchanged with the surroundings (Q_{surr}), negative values represent heating losses (Q_{loss}) while positive values represent heating gains (Q_{geo}).

4.5 Modes of operation

From the experimental data analysis, four different modes of operation of the system were identified and summarised in Table 4.7. As mentioned before in

section 4.1.2, the solar thermal pump is activated whenever the difference between the outlet temperature of the PVT panels is at least 7 K higher than the EEB temperature. Likewise, the heat pump (evaporator) is on whenever a space heating requirement exists. It is important to mention that since the house is unoccupied, the indoor temperature set point of the house is 18°C and the heating system operates full time (24/7) for research purposes. Therefore, the heat delivered to the house will be considerably higher than the actual heat delivered by a commercial unit with a heating system controlled by occupancy schedules.

Table 4.7: System operation modes

	Solar thermal pump	**Heat Pump**	**Condition**	**Consequence**
Mode 1	ON	OFF	N/A	Solar energy flows into the EEB
Mode 2	ON	ON	Solar energy >evaporator demand	Solar energy covers evaporator demand, and the surplus flows into the EEB
Mode 3	ON	ON	Solar energy <evaporator demand	Solar energy partially covers evaporator demand, and the EEB supplies the rest
Mode 4	OFF	ON	N/A	EEB supplies all the evaporator demand

In Mode 1, the solar sub-system is operating, but the heat pump is turned off due to the lack of heating demand. Hence, in this mode, the heat gained from the sun through the PVT panels is mainly stored in the EEB. In this operation mode, as the average EEB temperature increases, the heat losses through the bottom of the EEB also increase. This operation mode is expected to occur mainly in summer when the solar availability is high, and the house does not require any heating. In Mode 2, the heat pump and the pump of the solar sub-system are

turned on but the solar heat gained is higher than the heat demand on the evaporator $Q_{solar} > Q_{eva}$. Therefore, the heat gained through the PVT panels can directly satisfy all the heat demanded by the evaporator (Q_{eva}) while the remaining heat is injected into the EEB. This mode of operation is expected to occur on a sunny day at the beginning or the end of summer. Likewise, in a real application of this system, this behaviour might occur on a summer day when heating is required to supply DHW. In Mode 3, the heat pump and the pump of the solar sub-system are turned on but the solar heat gained is lower than the heat demand at the evaporator $Q_{solar} < Q_{eva}$. Hence, the heat supplied by the PVT panels cannot satisfy the heat demanded by the evaporator. Therefore, the heat is partially covered by the solar heat gained while the remaining heat demand is extracted from the EEB. This behaviour can occur on a sunny winter day when despite having solar availability, this is not enough to cover the heating requirements. Finally, in Mode 4, the heat pump is operating, and the solar sub-system is not operating (no solar heat gain). As a result, the heat demanded by the evaporator is entirely satisfied by the heat stored in the EEB which may be replaced to some extent by heat from the surrounding soil through the bottom of the EEB. This mode of operation will occur mainly in winter and during cold nights, when heating is demanded.

4.6 Results from calculations and discussions

This section discusses the main results and findings from the experimental data analysis and calculations. A general overview of how the system performs is discussed, and highlights from the main findings are shown. The results suggest that the PVT panels are oversized compared to the size of the GHE. Hence an improved configuration might be the use of an intermediate storage medium for the short-term. Likewise, results show that the use of insulation in the sides can be avoided for the storage temperatures of this study. In fact, the use of insulation at the sides reduces the EEB's heat gain from the surroundings during winter. Finally, the potential of using another type of solar collector technology is considered. A solar energy technology with a higher outlet temperature will

have a higher rate of heat transfer and therefore a higher storage temperature, which could significantly increase the whole system efficiency.

As mentioned in section 4.3, the set of data selected for the experimental analysis and calculations corresponds to the period from the 4th June 2016 to the 31st December 2017.

4.6.1 Energy balance of the earth energy bank

First, a general view of the GHE behaviour is shown. Figure 4.11 shows the averaged hourly values of the GHE inlet and outlet fluid temperature. The figure shows that the system works as expected in terms of heat storage and extraction. During summertime, from June to September, it is seen that, in general, the inlet temperature is higher than the outlet temperature, thus heat is being transferred to the EEB. By contrast, in wintertime, from November to February, the outlet fluid temperature is higher than the inlet temperature, which means that heat is being extracted from the EEB. It can be noted that the temperature difference (either in injection or extraction mode) between the inlet and outlet temperature is variable. This may be due to the variation of the mass flow rate but is more likely to be due to the variation of the EEB temperature. However, it can be noticed that this temperature difference, for the highest injection rate, is typically not higher than 6 K (Figure 4.12). This small temperature difference is common in GSHP systems where the temperature difference in mainly driven by the mass flow rate.

Figure 4.12 also shows the dynamic operation of the GHE. The variation in average hourly GHE temperature difference shows that the SAGSHP system can dynamically switch from injection to extraction mode in the same season, month, or even day. This behaviour depends on the heating demand and the solar outlet and EEB temperature. It is also important to mention that on occasion during cold winter nights, due to heat extraction from the EEB the average EEB temperature reaches values considerably lower than the ambient air temperature. At such times, as long as the temperature difference between the EEB and the outlet of the PVT panels (ambient temperature) is higher than 7 K, the solar pump is activated and the EEB is recharged by the natural ambient temperature through

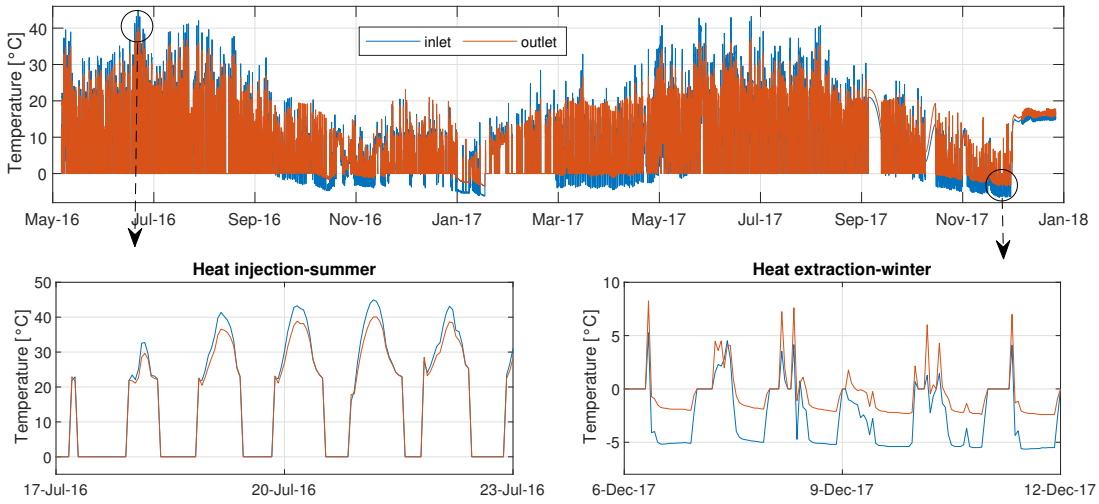

Figure 4.11: Inlet and Outlet fluid temperatures in the EEB

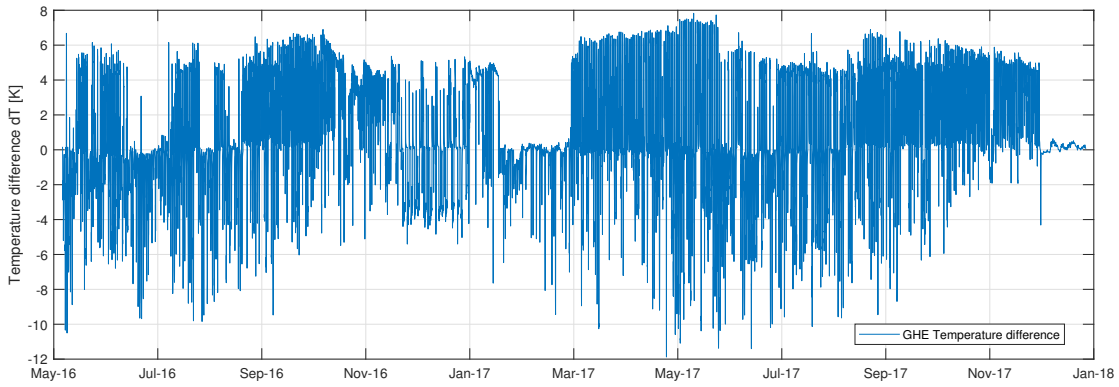

Figure 4.12: GHE temperature difference, positive is heat extraction, and negative is heat injection

the solar loop. Once again, this indicates that the heat extracted from the EEB by the GHE can quickly affect the EEB temperature, and it is important to keep recharging the EEB.

Before analysing the heating fluxes in the different operation modes, it is important to analyse how the PVT panels perform according to solar availability. For this, the incident solar radiation on the PVT panels' surface was determined. The global and diffuse horizontal radiation data are collected from the weather station. However, in order to calculate the solar radiation incident on the PVT panels, the solar radiation at the tilted surface must be calculated. The inclination of the PVT panels is 40° and the radiation at the tilted surface was

calculated by using Perez's model [134] in TRNSYS software [135]. The results were integrated on a monthly basis in order to derive the insolation (heat per square metre). Then, the useful solar heat gains (Q_u) were determined from the experimental data using the temperature difference between the inlet and outlet temperature of the PVT panels (ΔT_{PVT}), the mass flow rate in the solar loop ($\dot{m}_{sol}$) and the specific heat (c_p). Similarly, the results were integrated into monthly basis to get the monthly useful solar heat gains (Equation 4.9). The results are shown in Figure 4.13.

$$Q_u = \int_{t_o}^{t_f} \dot{m}_{sol} \times c_p \times (\Delta T_{PVT})\, dt \tag{4.9}$$

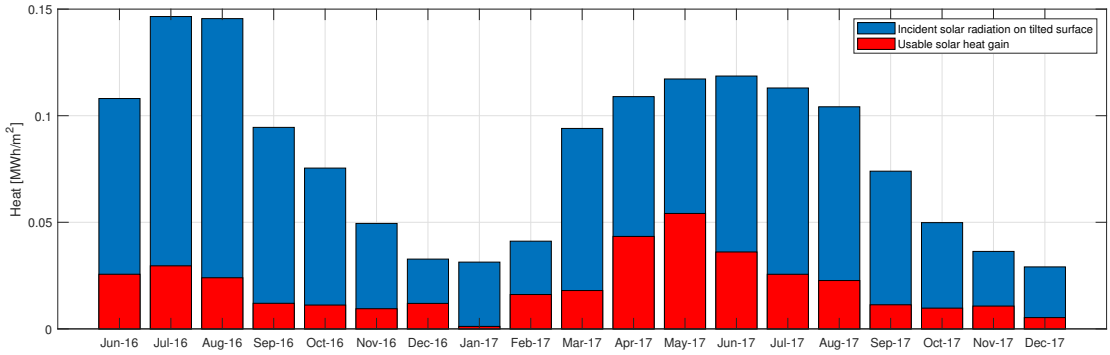

Figure 4.13: Incident solar radiation on the PVT and actual heat gain

It can easily be noted that the average solar utilisation ratio of the PVT panels is around 20%, which compares poorly with PVT test data. Nevertheless, considering that the useful solar heat gains are limited by the actual heat injection rate to the EEB, and consequently by the size of the GHE, it is not possible to conclude that the thermal efficiency of the PVT panels is as low as 20%. In fact, a normal PVT panel, tested at standard conditions (insolation of 1000 W/m^2) has a maximal thermal efficiency (η_o) between 40% and 60% [136, 137]. Therefore, the seven PVT panels have more solar thermal potential that cannot be captured or stored. This leads to the suggestion of using a buffer tank or some other intermediary energy store between the solar collectors and the EEB in order to exploit the full potential of the installed PVT panels. Another suggestion might be the use of another type of solar energy technology that can supply heat at higher temperatures.

The whole set of data analysed to study the heat fluxes in the EEB corresponds to a total of 13820 hours (from the 4th June 2016 to the 31st December 2017). From these hours, the system was in operation either in injection or extraction mode (GHE pump ON) for 8605 hours. Table 4.8 shows the number of hours when the SAGHSP system was working in the different modes of operation.

Table 4.8: Hours of operation of the system in each mode

Operation mode	**Hours of operation**
Mode 1	2246 (26%)
Mode 2	915 (11%)
Mode 3	455 (5%)
Mode 4	4989 (58%)

The main mode of operation of the system is Mode 4, in this mode, the system is extracting heat from the EEB to cover the heating loads. More than 50% of the time the system operates in this mode. On the other hand, in heating injection mode (Mode 1), it is seen that the system operates more than 26% on the total hours. However, the total heat injected or extracted not only depends on the number of hours (time) but also on the fluid inlet and outlet temperature difference. As seen in Figure 4.12, the GHE inlet and outlet temperature difference are typically higher during heating injection mode, this suggests that the hourly amount of heat that is injected is higher than the one that is extracted and this can be verified in Figure 4.14. The system also works a considerable number of hours in Mode 2. This mode might cause some issues as the PVT panels are directly covering the evaporator demand and the fluid entering temperature (FET) in the evaporator might occasionally rise to more than the maximum tolerated by the heat pump. During this research, the PVT panels normally have a low outlet temperature when heating is required. However, in commercial units this might not always be the case, for example if DHW is required during Mode 2 operation. This situation must be avoided.

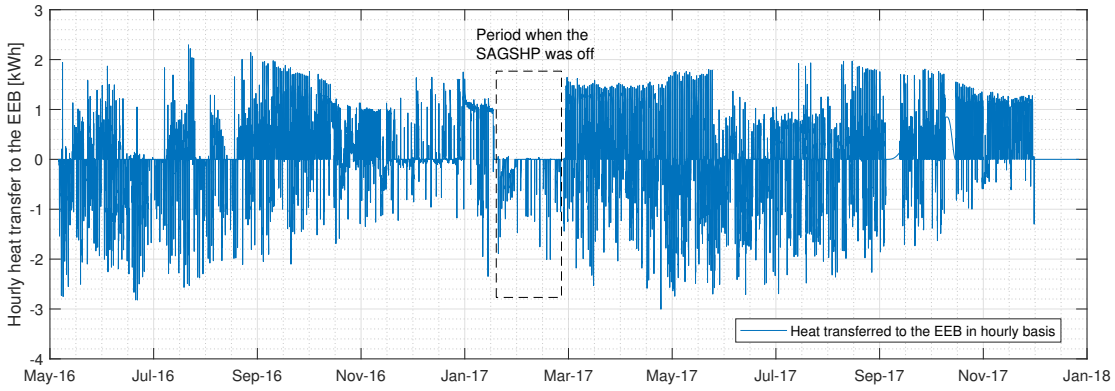

Figure 4.14: Hourly heat transferred to the EEB, positive is heat extraction, negative is heat injection

All modes of operation

The calculations of the energy fluxes under all modes of operation are shown in Figure 4.15. In general terms, during summer the system mostly injects heat in the EEB while during winter, the system mainly extracts heat from the EEB. Some evaporator heat demands exist during summertime (from June to August). This occurs mainly in colds nights of summer when heating is required as the indoor temperature set point remained active at 18°C. From October to January, solar availability is very low, and the heat demanded by the evaporator is relatively high. Hence, the heat is supplied mainly from the heat stored in the EEB. However, it is noticed that a considerable amount of heat is also supplied from the geothermal energy coming from the bottom of the EEB. This is because as the heat is being extracted from the EEB, its temperature decreases and the temperature difference with the surrounding soil allows the EEB to gain some heat naturally. From February to May, most of the heat is supplied directly by solar energy through the EEB. This is something unusual for those months of operation. As seen in the figure, between December 2016 and March 2017, there is a very low heat demand from the evaporator, even though those very cold months.

After investigating this issue, it was noticed that the back-up boiler-radiator system was enabled during those months. Hence, the SAGSHP system was working to only cover partially the heat demanded by the house.

This might have affected the entire project, as a considerable amount of heat was not extracted from the EEB during those months. However, for this research, the experimental set-up was configured in a way that the heating system was enabled 24 hours (always ON). Therefore, the extracted heat from the EEB is also higher than in a real system where heating is controlled by schedules either automatically or manually. Likewise, as mentioned previously in section 4.1.1, the house of this study has much lower thermal efficiency than a modern low-energy house, which would be the target for this kind of technology. Hence, the amount of heat extracted from the EEB in the current research is almost definitely higher than would be the case in a commercial application.

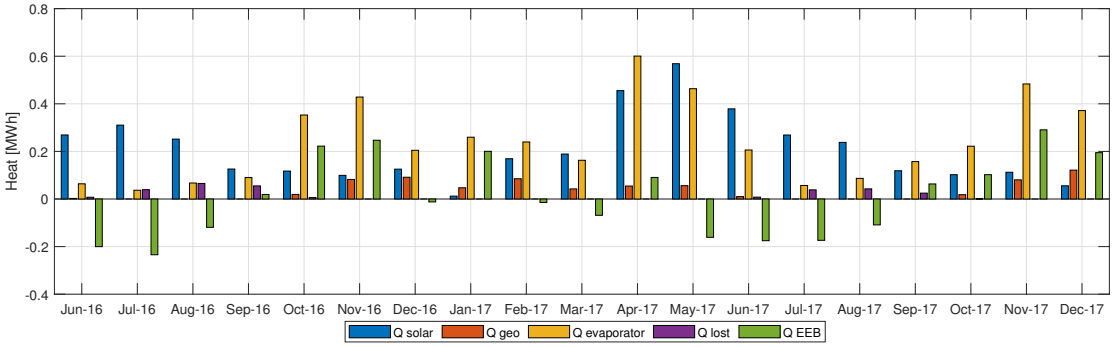

Figure 4.15: Monthly heat fluxes: All modes

Regarding the total energy balance during the whole period of analysis, it is worth mentioning that about 18% (0.87 MWh) of the input energy comes from geothermal energy and 82% (3.97 MWh) from solar energy. Likewise, the heat pump directly uses about 54% (2.6 MWh) of the input energy while 46% (2.24 MWh) is stored in the EEB. The total heat losses during the whole period of the analysis are 6% (0.29 MWh). Figure 4.16 shows the Sankey diagram, where the use of the total amount of energy during the whole period of analysis can be appreciated.

Mode 1

This mode of operation is purely injection of heat from the PVT panels. Hence, as the evaporator demands no heat most of it is stored in the EEB. Some heat losses are also noticeable mainly in late summer as the average temperature

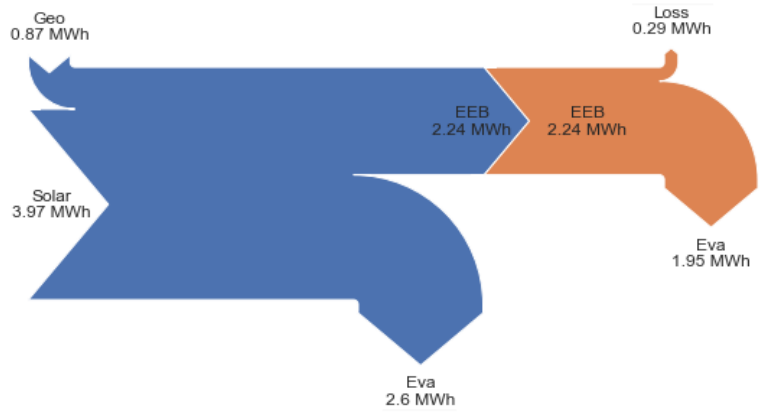

Figure 4.16: Sankey diagram of the total data analysed

in the EEB becomes higher than that of the surrounding soil. It can be noted that, in February 2017, some heat is also gained from the bottom of the EEB (geothermal heat gain). This is mainly after a heating extraction period, where the EEB temperature is lower than that of the surrounding soil and relatively little heat was demanded by the evaporator (due to the accidental activation of the backup heating system). Hence, the EEB is naturally gaining heat from the surroundings, while the PVT panels are also providing heat to be stored (Figure 4.17). The solar potential of the PVT panel, as seen in Figure 4.13, is higher than what is actually stored. On average during summer months, between 230 and 280 kWh of heat is monthly stored in the EEB.

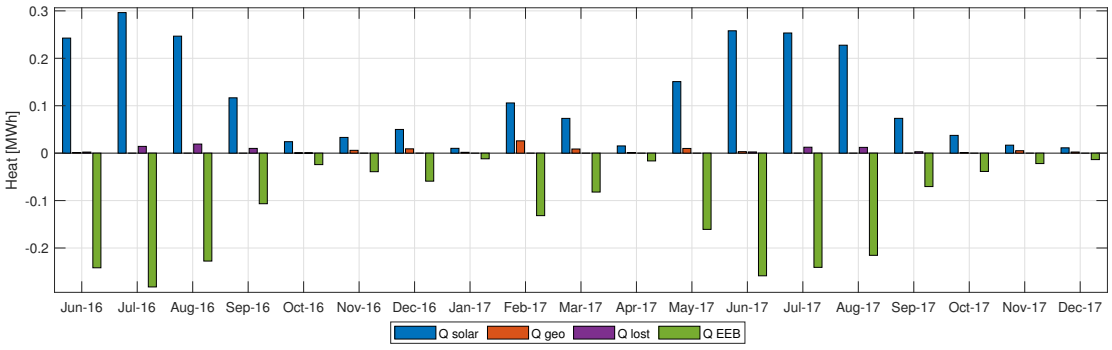

Figure 4.17: Monthly heat fluxes: Mode 1

Mode 2

Figure 4.18 shows the energy balance of the system when working in Mode 2. This mode occurs rarely and is focused during the transition period, which is the

beginning and end of summer. This mode happens, whenever the heat pump is ON, and the solar energy gained through the PVT panels is higher than the heat demanded by the evaporator. For example, during a cold morning on a sunny day. Typically, in the first hours of the morning, the heating loads of houses are higher than in the afternoon. However, solar radiation can be high enough to cover these thermal loads and provide surplus heat for storage in the EEB. In an occupied house, this mode of operation can also occur when DHW is required on a sunny day. In real applications, the designers must be careful with this mode of operation as there is a risk of having too high an inlet fluid temperature at the evaporator when the heat pump compressor is running. Normally, heat pumps are designed to trip out when a fluid with excessive temperature is supplied to the evaporator, in order to avoid damage to the heat pump. However, this will also prevent heat from being delivered when a requirement exists. One potential solution to this problem is the use of a three-way valve to keep recirculating the fluid through the solar loop while heat is extracted from the EEB to supply the evaporator demand.

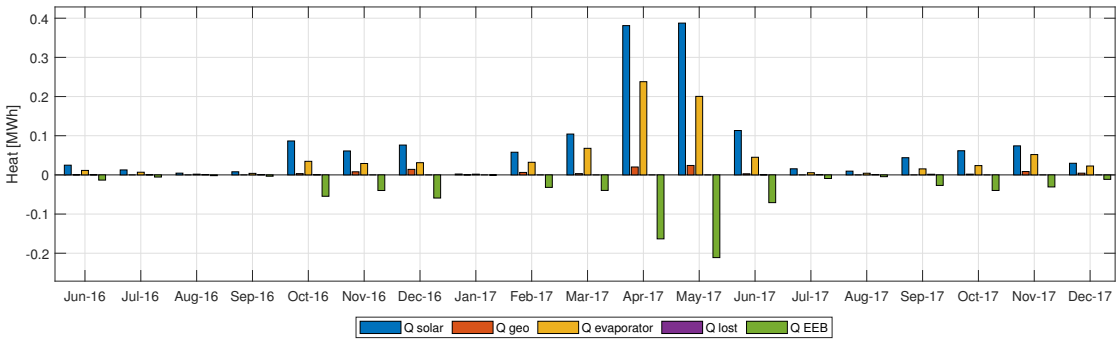

Figure 4.18: Monthly heat fluxes: Mode 2

Mode 3

Mode 3 of operation is also an unusual mode of operation like Mode 2. The few cases in which this mode occurs are mainly in the transition periods (Figure 4.19). This happens when there are heating requirements, and low solar energy is available. Hence, the heating demands are covered by both the solar gains and the heat extracted from the EEB. It is noted that during this operation mode,

minimal heat losses occur since in this mode the EEB is generally colder than the surrounding soil and therefore heat is transferred from the surrounding soil to the EEB through the bottom.

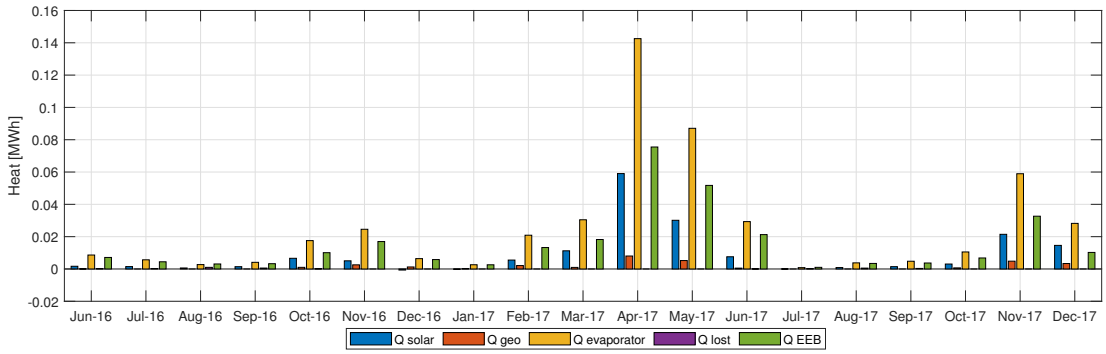

Figure 4.19: Monthly heat fluxes: Mode 3

Mode 4

This mode of operation occurs mainly in winter and during cold nights where solar energy is not available, and the house requires heating. Thus, heating is covered by the heat in the EEB, which is not only the stored heat but also the heat gained from the surrounding soil. This mode of operation is the most common of the system. Figure 4.20 shows that under this mode of operation, during winter months, from 150 to 340 kWh of heat are monthly extracted from the EEB. As noted, very few heat losses exist as the average temperature in the EEB is lower than that of the surrounding soil. The few losses existing under this mode of operation are in summer months.

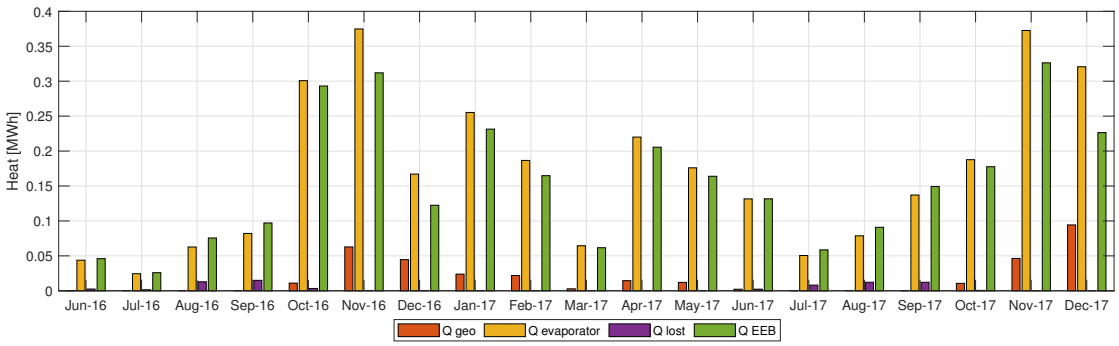

Figure 4.20: Monthly heat fluxes: Mode 4

Seasonal Performance Factor

In order to evaluate the performance of the heat pump unit of the system, the seasonal performance factor SPF was calculated. The SPF is the ratio of the energy output and the electricity input. For this calculation, the electricity used for running the heat pump and the pumps for the GHE and the radiant floor was used. As the actual variables to determine the heat output were not monitored, the SPF was calculated based on the heat extracted from the ground (Q_{eva}) as shown in Equation 4.10. This is what some authors call the SPF-H3 [55], which is based on the energy output from the condenser divided by the electricity input to run the compressor and complementary pumps.

$$SPF = \int_{t_o}^{t_f} \frac{Q_{eva} + W_{ele}}{W_{ele}} dt \tag{4.10}$$

Figure 4.21 shows the monthly seasonal performance factor (SPF). An average monthly SPF of 2.51 was calculated for the whole period of analysis. This value is quite low when compared with conventional GHSP systems in which SPF-1 higher than 3.5 is common [55]. The lower efficiency was expected due to the use of very shallow boreholes which reduce the temperature of the EEB quickly, decreasing the whole system efficiency. However, considering the low cost of installation of the GHE and by having in mind that a SPF of 2.51 is higher than conventional air-source heat pumps (typically from 2 to 2.5 [65]), the system performance is encouraging. It is important to mention that the consumption of DHW will have an impact on the SPF as well.

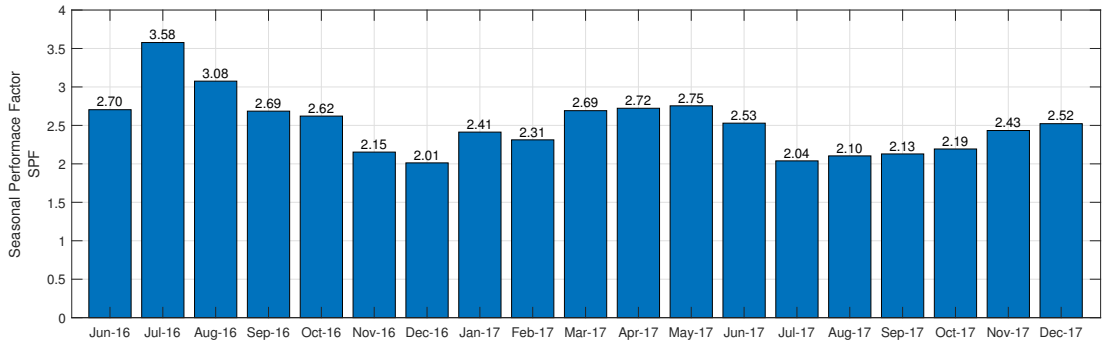

Figure 4.21: Monthly Seasonal Performance Factor (SPF) of the heat pump unit

Figure 4.21 also shows the difference in the SPF in wintertime and summer-

time. In summer, SPFs higher than three can be obtained. This is mainly related to the average temperature of the source (EEB). The higher the source temperature of a heat pump, the higher the heat pump COP.

4.6.2 Earth energy bank thermal performance

In this section, an analysis of the thermal performance of the earth energy bank (EEB) is presented. First, it is important to understand how shallow soil behaves thermally. For this, an analysis using experimental data from the far-field soil temperature (sensor 1 in Figure 4.5) is done. Figure 4.22 shows the temperature variation of the natural soil at depths of 0.75 m, 1.25 m, 1.75 m and 2.75 m. According to the data measured, the natural heat recharging of the EEB occurs from mid-March to mid-September, where the maximum temperature of the soil at 2.75 m is slightly higher than 15°C. On the other hand, the natural discharging of the EEB occurs from mid-September to mid-March, and the minimum soil temperature is below 10°C at 2.75 m. Hence, although the installation of the ground heat exchanger is at a maximum depth of 2.75 m, the natural annual temperature oscillation is around 5 K, which is small enough to not seriously reduce the performance of the heat pump. Also noticeable is the shift in the maximum and minimum soil temperatures at different depths. As the soil has a high heat capacity, the peaks (highest and lowest) temperature conditions affect more quickly the layers of soil closer to the surface. Likewise, it is noted that the average annual temperature for all the different depths is very similar (around 12.5°C). This annual average temperature is normally considered as the undisturbed ground temperature for that location.

The heat stored or extracted in the EEB, and therefore, the temperature variation in the soil of the EEB and the thermal grout (bentonite) are directly related to the GHE inlet temperature. Figure 4.23 shows the temperature variation of the soil in the centre of the EEB at 1.25-metre deep, the temperature of the 16th borehole wall and the GHE inlet temperature. The figure shows that from March to the beginning of July, the temperature of the EEB mainly increases as heat is being stored. From September to December the EEB mainly discharges heat and its temperature decreases. Transition periods occur from July to September and

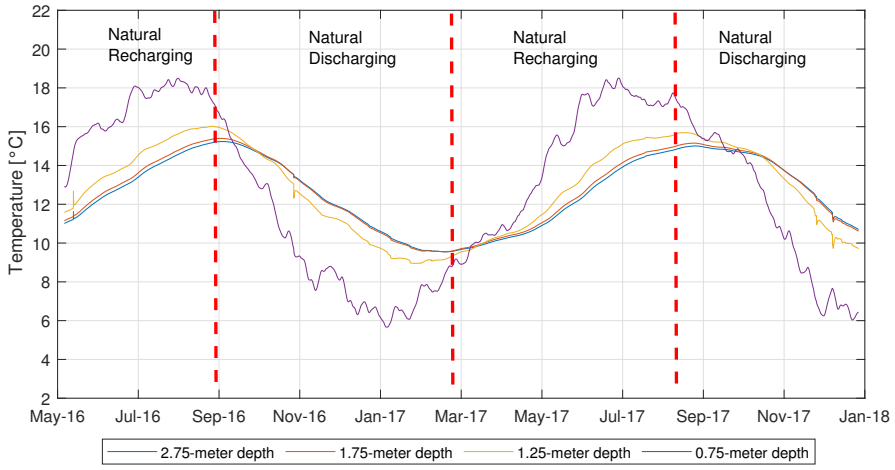

Figure 4.22: Natural soil temperature variation, sensor 1

from December to March. These periods might vary from one year to another, as they will depend on the seasonal conditions as well as the thermal loads of the building. During transition periods, the temperature of the EEB remains relatively constant as there is a balance between the heat injected and extracted.

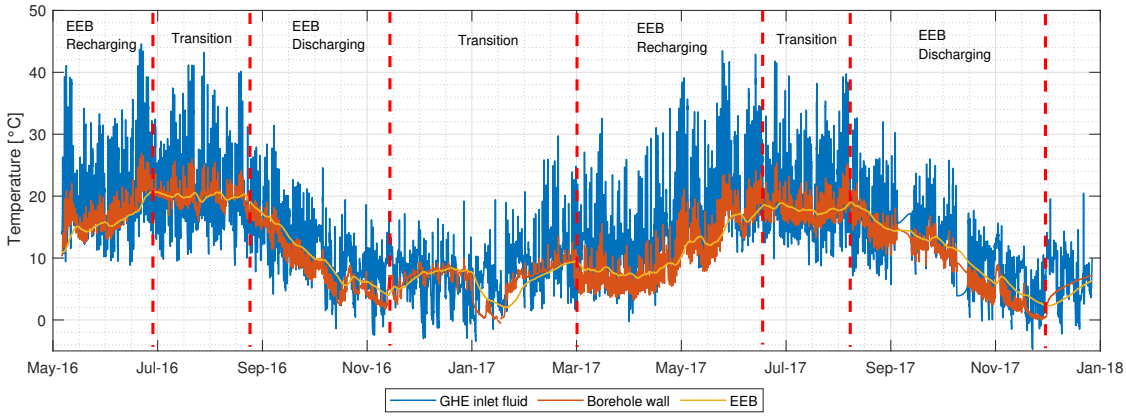

Figure 4.23: Main temperature variations of the SAGSHP system

Regarding the heat stored or extracted from the EEB, Figure 4.24 shows the temperature variation of the EEB centre temperature (sensors 5, 6, 7 and 9 in Figure 4.5) compared to the far-field temperature variation (sensor 1) at different depths. When the temperature in the EEB is higher than the far-field temperature, it is considered that there is net heat stored in the EEB. Likewise, when the EEB temperature is lower than the far-field temperature, it is considered

that there has been a net heat loss. These cases are highlighted in the figure. For example, at a depth of 1.25 m, the EEB reaches a maximum temperature of 19°C, which is about 4 K higher than the natural soil temperature at the same depth. In contrast, the lowest temperature of the EEB at the same depth is close to 2°C, which is around 8 K lower than the natural soil at the same depth. It is worth mentioning that at higher heat extraction rates, the soil in the centre of the EEB might reach temperatures below 0°C. This phenomenon could lead to 'soil heave' and should be avoided, but it is out of scope in this research. As the GHE for commercial installations is located within the foundations of a building, the freezing of the water content in the soil (which can cause a volume expansion of up to 9%) might compromise the foundations [138].

The experimental data show greater storage effects (ΔT) at mid-range depths, as expected. This kind of storage system creates a 'heat bubble' which increases the storage efficiency as less surface is exposed to the surroundings. No conclusions about the long-term energy balance can be drawn yet, as this analysis should be performed using data collected over several years.

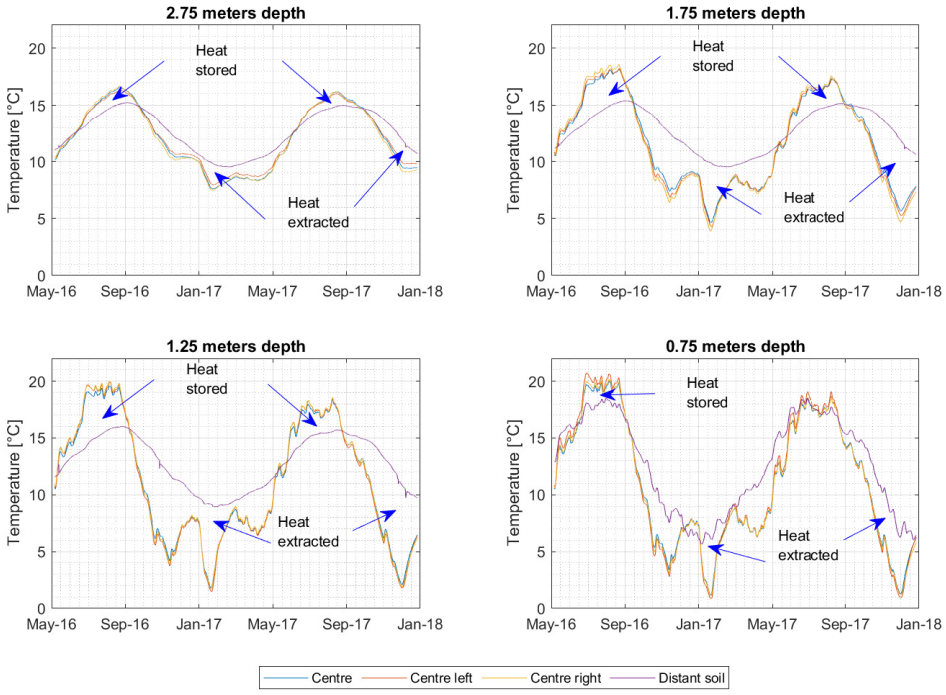

Figure 4.24: EEB and natural soil temperature variation

Figure 4.25 compares the temperature measurements at both sides of the EEB

insulation with the distant soil temperature (sensor 1) as a reference. This is done to study the utility of the insulation in the sides. The insulation was installed with the intention to retain the heat stored during summer by reducing the heat losses to the surrounding soil. However, at the relatively low EEB soil temperatures experienced during summer and considering the high heat capacity (low heat diffusion) of the soil, the conduction of heat through the sides of the EEB might actually be very low. From the experimental results, it can be seen that in summer 2016, there was about 1 K temperature difference across the insulation (higher inside the EEB), while in summer 2017, the temperature inside the insulation remains very close to the temperature outside the insulation. In contrast, in winter months the inside temperature is lower (up to 3 K) than the outside temperature. This implies that the insulation might actually reduce system performance since it prevents the EEB from gaining heat from the surrounding soil at the sides during the colder months. In this research and experimental set-up, the insulation does not make a big contribution. However, no strong conclusions on the use of insulation can be obtained from this. For instance, the layer of insulation on the sides might have been in contact with rainwater over the months, losing its thermal properties (though the insulation used in the EEB is supposed to be hydrophobic). Likewise, if the project had used a solar technology with a higher outlet temperature (e.g. evacuated tube collectors or flat plate collectors), the average EEB temperature might be significantly higher, and consequently the use of insulation in the sides might be beneficial. This would require further research, but it was evident that for this particular installation the use of insulation on the sides of the EEB could have been avoided, with no significant impact on the thermal performance of the EEB.

Finally, it is important to highlight some points regarding the performance of the thermal energy store with shallow boreholes. The thermal storage capacity of the EEB depends on the volumetric heat capacity of the soil, the volume of the EEB and the temperature difference between the beginning and the end of heat injection/extraction periods. The volumetric heat capacity of the soil of study (wet clay) has a value of 2.16 MJ/m^3K, and the volume of the EEB is 80 m^3. Considering an annual temperature variation, at the centre of the EEB,

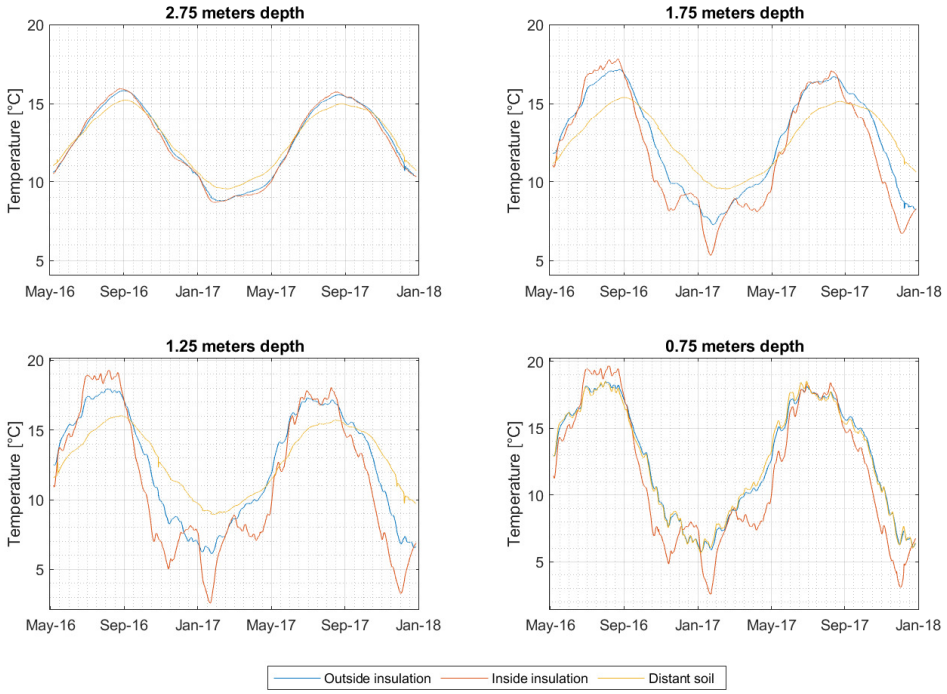

Figure 4.25: Soil temperature variation inside and outside the insulation

of 15 K (as shown experimentally in this study), the heat capacity of the EEB would reach a value of 720 kWh. As noticed, with a heat pump with an average SPF of 2.51, the EEB would not be enough to cover the annual winter heating demand. However, an analysis of this type is not suitable for this study. Firstly, 57% of the heat demanded by the evaporator is covered directly by the heat gained through the solar collectors, as shown in the Sankey diagram in Figure 4.16. The study has shown that this system can be considered as a hybrid solar-ground source system, which is partially covered by solar energy and partially by the heat gained from the surrounding soil. Moreover, it is very important to highlight that the operation of the system is very dynamic regarding the heat injection and extraction (i.e. significant heat can be injected and extracted on the same day or month). This behaviour allows the EEB to store and release a much higher quantity (as shown in Figure 4.16) of heat during the year. As seen in Figure 4.12, the change in temperature in the EEB and the borehole wall is very dynamic. So, it cannot be compared to a system that has a linear increase or reduction in the temperature of the ground.

4.7 Summary of the chapter

In this chapter, the performance of an experimental installation of a shallow SAGSHP system for residential heating applications has been analysed. The system performance was studied from data collected over 19 months. During the time of operation, the system was able to inject 2.24 MWh from the solar energy into the ground to help not only in covering the evaporator demand in winter but also to prevent/recover the ground from any thermal imbalance over the year. The experimental data also showed that the system exchanges heat with the surroundings. In the cold months, the soil in the EEB gains heat from the surrounding soil underneath it, while in summer, heat loss from the bottom was also observed, although the heat gains are higher than the heat losses. This is mainly because the yearly heating extraction is higher than the heating injection. In fact, with the current system, the heat injection can be only done when solar energy is available, which is mainly on sunny days. On the other hand, heat extraction occurs in winter at any time of the day. Hence, during the total hours of operation, the system works much more in heating extraction mode, than in heating injection mode. During the transition periods (from summer to winter and vice versa) most of the evaporator demand was directly supplied from the usable solar energy gained through the PVT collectors. This operation mode must be analysed in detail, and a solution should be investigated that avoids fluid with excessive temperature from entering the evaporator of the heat pump. For instance, the use of a three-way valve that allows the fluid from the solar loop to keep recirculating without going to the evaporator, while the heat demanded by the evaporator is extracted from the EEB. Another option could be to use a secondary heat store (such as a water cylinder) inserted between the PVT and the EEB to buffer the solar heat on a daily basis. This solution might also help in maintaining heat injection to the EEB long after PVT temperature has peaked such as during night time after a hot day.

The EEB soil temperature, at a depth of 1.25 m, was observed to be up to 4 K higher than the natural soil temperature at the same depth. Also, during the heat extraction period the EEB soil temperature can drop to just 2°C. Without so-

lar recharging, the temperature in the soil might reach temperatures below 0°C, freezing the soil and affecting the overall system efficiency as well as causing volume expansion issues. Conclusions obtained from this study are not discouraging as the system has proved to perform relatively well even though the use of shallow boreholes limits the actual amount of heat that can be stored or extracted. With these first findings it has been shown that this system configuration is worthy of further study as the use of shallow boreholes implies considerably reduced cost of installation compared to other SAGSHP systems. The main results from the experimental data analysis show that, despite the use of shallow boreholes, the system was able to operate at an SPF comparable to conventional GSHP systems (typically from 2 to 3.5). Indubitably, shallow boreholes would not be a good choice for large buildings. However, for the low-energy domestic sector, where the peak heating loads are typically below 20 W/m^2, shallow boreholes seem to be an affordable and feasible solution to cover heating demand. That is why the target market for this kind of system is the low-energy small domestic sector.

The experimental data analysis has also indicated some key areas for further study. For example, it was noted that the rate of heat output from the PVT collectors is often much higher than the capacity of the GHE to transfer it to the EEB, causing a low heat transfer from the solar system. As seen in the results, the actual solar output is not only limited by the efficiency of the PVT but also by the transfer of heat into the EEB. The results also indicated that the vertical insulation around the EEB helps in reducing heat losses during the charging period, but also prevents the natural recharging from the surrounding soil in winter months. However, in general terms, for this particular research, the use of insulated sides could have been avoided. Further research is needed to determine under which circumstances insulation around the EEB is beneficial.

With this first experimental analysis, some research questions have been raised, but without doubt the shallow SAGSHP is a system with a high potential for the low-energy small domestic sector and is worthy of further study. As the main innovation of this system is the use of shallow boreholes, the real challenge of this research is to be able to model and predict the behaviour of

shallow boreholes. With an accurate model to estimate the thermal performance of arrays of shallow boreholes, a valuable contribution to knowledge can be made. Enough experimental data have been generated to validate any analytical or numerical model applied to shallow boreholes. However, something else that has also been demonstrated is the high degree of influence of the natural soil temperature variation upon the thermal performance of the EEB. For this reason, it is important to first determine an appropriate model to estimate the natural temperature variation of the shallow soil. This will be the main focus of the next chapter.

5. Modelling of the shallow soil temperature

As mentioned in the Methodology (Chapter 3), an approach based on experiments and modelling is proposed to achieve the aim of this research. Chapter 4 provides a detailed explanation of the experimental approach. It provides all the information regarding the experimental set-up and the analysis of the data collected. It also shows the general characteristics in the performance of shallow geothermal systems and how the particular system under investigation has operated for almost two years. The second part of the methodology is related to the modelling approach used to study the performance of shallow vertical ground heat exchangers. To deal with the modelling of shallow boreholes in locations close to the surface, it is crucial to first understand the thermal performance of the natural soil near the surface. As the vertical boreholes will be installed into soil that is affected by the ambient conditions, the modelling of the natural temperature variation of the soil must be analysed. Then, further analysis can be carried out to investigate the extent to which the natural ambient conditions might affect the performance of shallow ground heat exchangers.

In this context, the objective of this chapter is to study the performance and accuracy of different analytical and numerical models to predict the natural temperature variation over time of the shallow soil. The modelling results are compared with experimental results from the data monitored in the far field soil of the experimental installation of the Earth Energy Bank (EEB).

5.1 Experimental data of the natural soil

Before studying the application and accuracy of different analytical and numerical models to predict the temporal variation of the soil temperature, it is important to show the experimental data that will be used for the validation of

the different models. This provides a clear idea of the variation of the temperature in the shallow soil and demonstrates why its study is important. The soil studied is the same as that in which the experimental EEB was installed (see Chapter 3). The far field measurement point is five metres from the side wall in the installation of the EEB (Figure 5.1). Table 5.1 shows the soil type and its thermal properties. The classification of the soil and the thermal conductivity was obtained through a soil test carried out prior to the installation of the shallow geothermal system, while the other thermal properties were estimated from the MSC 022 tables for installations of GSHP systems [129]. The sensors used for monitoring the soil are PT1000 resistance temperature detector (RTD) sensors. All sensors were calibrated by the manufacturer and have an accuracy of ± 0.2°C as previously mentioned in section 4.3.

Figure 5.1: Far-field monitoring point location

Figure 5.2 shows the experimental data used in this chapter for the validation of the models studied. The data correspond to average hourly measurements of soil temperature at depths of 0.75 m, 1.25 m, 1.75 m and 2.75 m. The data correspond to the period between February 10, 2016 and February 24, 2017.

The figure also shows the temporal variation of the air temperature. These data relate to the weather station described in Chapter 3. The figure shows that the ambient temperature has a direct impact on the variation of the soil temper-

Table 5.1: EEB soil thermal properties

Type of soil	Wet clay
Thermal conductivity	1.5 W/mK
Density	1800 kg/m^3
Specific Heat	1200 J/kgK
Thermal diffusivity	6.94 x10^{-7} m^2/s

ature. Likewise, it is observed that the oscillations of the ambient temperature have a greater influence on the temperature of the layers of soil closest to the surface. As the depth increases, oscillations in the short term have less influence. It is also seen that even at a depth of 2.75 m, the soil presents a seasonal variation with an oscillation amplitude of approximately 5 K. This demonstrates that, at the depth of installation of the shallow geothermal system, the soil cannot be considered to be undisturbed, and for this reason the natural variation in soil temperature will be expected to have an important influence on the thermal behaviour of the shallow geothermal heat exchanger.

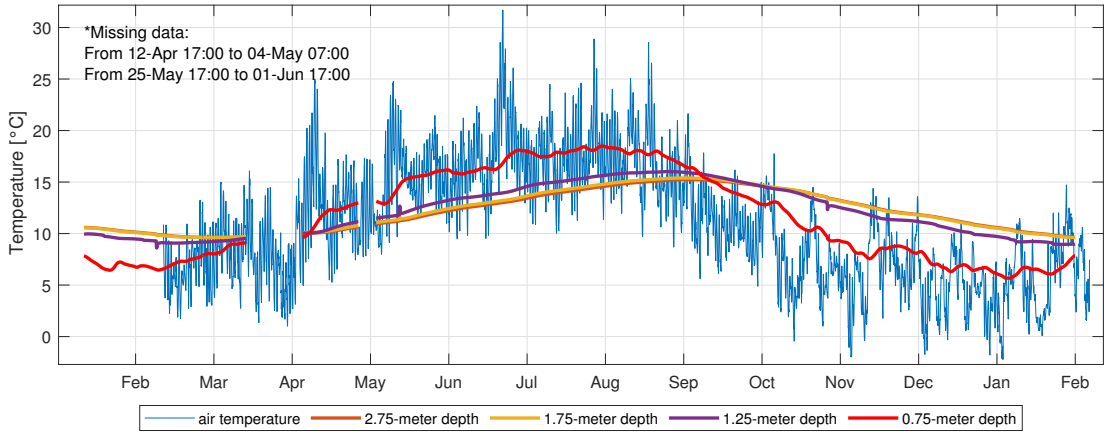

Figure 5.2: Experimental data of the far-field soil and ambient temperature

5.2 Undisturbed ground temperature

The undisturbed ground temperature is the temperature of the soil at depths where the seasonal variations have no influence. This temperature is very important as is a crucial input parameter for both analytical and numerical models. The values of this temperature vary according to the location and the most accurate way to determine this is through experimental measurements of the deep ground. In reality, such experimental measurements can be difficult, so the value of undisturbed temperature may be estimated by different methods. The simplest is to assume that the value of the annual average air temperature matches the undisturbed ground temperature. However, in very variable climates, this assumption may be erroneous [139]. Hence for greater accuracy, the average temperature of the soil surface may be used in place of the average air temperature. The average temperature of the soil surface is not easily available, as conventional weather stations do not usually monitor this parameter. This research uses the correlation model proposed by Badache et al. [84] which allows the undisturbed ground temperature (T_{gr} in K) to be estimated from the average ambient temperature using Equation 5.1:

$$T_{gr} = 17.898 + 0.951 T_a \tag{5.1}$$

where T_a is the average annual air temperature in K.

This model has a coefficient of determination (R^2) of 0.995 verified with experimental values from seventeen different locations around the world. In the case of the soil in Leicester, UK, the undisturbed ground temperature is 14.87°C based on an average annual ambient temperature of 10.88°C.

5.3 Conventional analytical models to study the temperature variation of the shallow soil

As mentioned in the literature review (section 2.3.1), there are different analytical and empirical models to estimate the natural soil temperature over time at different depths. The analytical models that were used in this study correspond to

the sinusoidal model of Kusuda and Achenbach [80] and the analytical model of heat diffusion in a semi-infinite solid medium [81]. The Kusuda and Achenbach sinusoidal model has been the most used to estimate the temporal variation of the soil at different depths. This model is more accurate at greater depths since it has the limitation of not considering temperature variations in the short term. On the other hand, the semi-infinite model is more accurate at shallower depths since the depth of influence depends on the time the soil is subjected to a temperature. That is, at shorter time intervals, the variation of the temperature in the shallow soil can be studied. Equation 5.2 shows the analytical solution of the Kusuda and Achenbanch model. More information about this model can be found in Appendix A.

$$T(z,t) = (T_s - \Delta T)\, e^{-z\sqrt{\frac{\omega}{2\alpha}}} \cos\left(\omega t - \varphi_s - \left(\sqrt{\frac{\omega}{2\alpha}}\right) z\right) \tag{5.2}$$

where:

z= depth of analysis; $\omega = \frac{2\pi}{t}$; α= soil thermal diffusivity φ_s= time of year of minimum surface soil temperature in rad and T_s= undisturbed soil temperature in °C.

On the other hand, Equation 5.3 shows the analytical solution of the semi-infinite model considering constant surface temperature in the soil (but variable in hourly intervals). More information about the semi-infinite model can be found in Appendix A or in [81].

$$T(z,t) = \left[\text{erf}\left(\frac{z}{2\sqrt{\alpha t}}\right)(T_o - T_s)\right] + T_s \tag{5.3}$$

where:

T_o= initial soil temperature and erf= error function.

5.3.1 Sinusoidal model

This section assesses whether the sinusoidal model of Kusuda and Achenbanch [80] is sufficiently accurate to estimate the temporal variation of the shallow soil temperature. For this, Equation 5.2 was used and the values shown in Table 5.2 were used as input data. The results calculated using the sinusoidal model were compared with the experimental data described in section 5.1. As shown

in the input data, φ_s is the time in radians when the soil surface temperature is minimal considering that 2π rad equals 365 days. Based on the measured experimental data, the minimum daily average temperature occurs on January 31.

Table 5.2: Input data for the sinusoidal model

T_s= 14.87°C
ΔT= 8°C
α_s= 6.95 x10^{-7} m^2/s
φ_s= $\frac{2\pi}{365}\frac{31}{}$ rad

The sinusoidal model is supposed to be an accurate model for predicting the temperature of deep soil. However, when compared with experimental data, this model was found to be impractical and highly dependent on the value of the undisturbed ground temperature. In fact, with the calculated value of the undisturbed ground temperature (14.87°C), the model did not match the experimental data as seen in Figure 5.3. It is noted that the model overestimates the ground temperature at all the assessed depths. This might be due to the uncertainty in the calculated value of the undisturbed ground temperature. Unfortunately, this value is rarely measured by weather stations, and estimations must be made. It is clear to see that the current undisturbed ground temperature may be lower that the predicted by Badache et al. [84] model. However, when no experimental data are available, this value must be determined by means of the ambient air temperature and consequently the uncertainty of the application of this model increases. For this reason, the sinusoidal model should be used carefully as this it is very sensitive to small differences in the input values.

In order to increase the accuracy of the sinusoidal model, the input value of the average surface temperature was adjusted until find a better fit. Figure 5.4 shows the results of the exact same sinusoidal model but using an average surface temperature of 12.5°C. As seen in the figure, the accuracy increases noticeably. However, the aim of this exercise is merely to show how sensitive is the sinusoidal model to a small difference in the average surface temperature.

As mentioned before, experimental values of the undisturbed ground temperature are not usually available in common weather stations, hence this method, despite its simplicity, has a high uncertainty (see section 5.5) and should be carefully used.

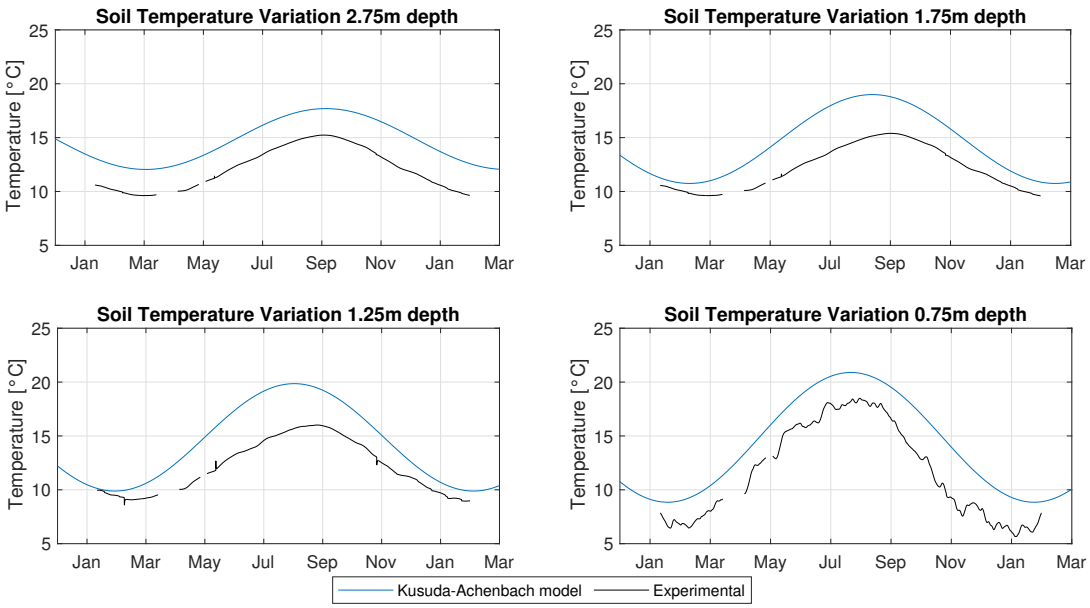

Figure 5.3: Comparison between the sinusoidal model and experimental

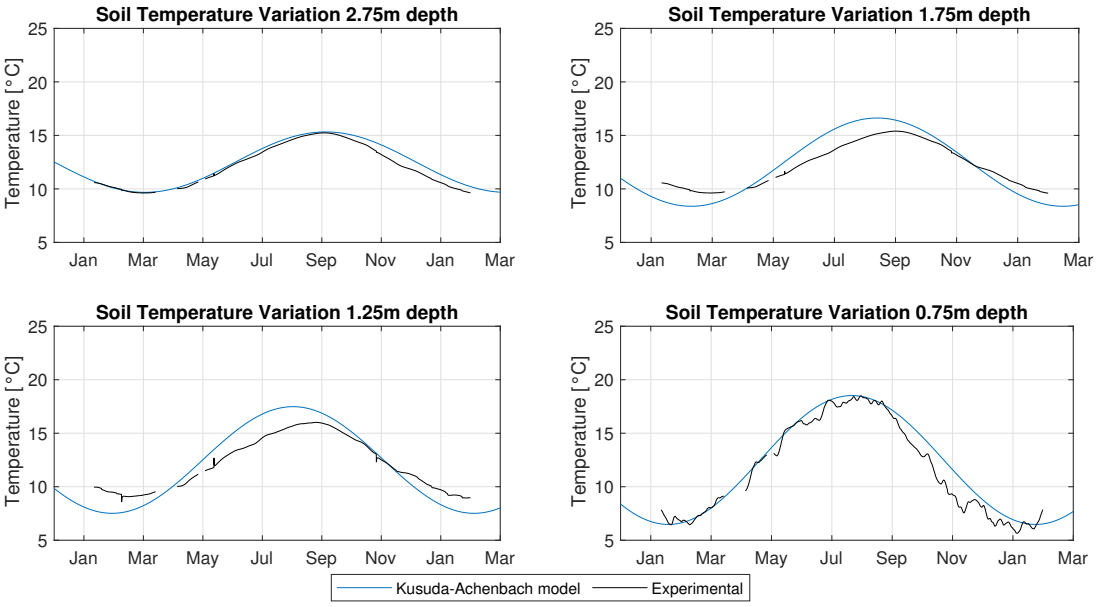

Figure 5.4: Comparison between the sinusoidal model and experimental with adjusted surface temperature

5.3.2 Semi-infinite model

This section assesses whether the semi-infinite solid sinusoidal model [81] is accurate to estimate the temporal variation of shallow soil temperature. For this, Equation 5.3 was used, and the values shown in Table 5.3 were used as input data. As with the sinusoidal model, the results calculated using the semi-infinite solid model were compared with the experimental data described in section 5.1.

Table 5.3: Input data for the sinusoidal model

T_o= mean air temperature °C
T_s= air temperature °C
α_s= 6.95 x10^{-7} m^2/s

In the semi-infinite model, as the depth of analysis increases the accuracy of the model is reduced due to the thermal penetration depth (see Appendix A). Hence, the model is more accurate at shallower depths, as previously explained. To increase the accuracy and applicability of this model, the analysis was considered at variable time steps according to the depth as shown in Table 5.4. In this case, for the soil of the EEB with thermal diffusivity α=6.95 x10^{-7} m^2/s, more exposure time of a boundary condition at the surface soil is needed to have a higher thermal penetration depth. Hence, to be able to compare the modelled temperature with the experimental data, for 0.75 metres, the minimum analysis time is 89 hours. Therefore, the average value of the air temperature was obtained every 89 hours and that value was imposed as a boundary condition for 89 hours. For the analysis at depths of 1.25, 1.75 and 2.75 metres, the minimum times of analysis are 246, 482 and 1188 hours respectively. As can be noted, for larger depths, the minimum analysis time was increased to very high values and consequently the correlation against experimental data is reduced.

From Table 5.4, it is seen that this model is accurate enough to predict the temperature of very shallow soil (depths less than 1 m) but loses accuracy at greater depths. Figure 5.5 shows the comparison between the experimental data and the predictions of the semi-infinite solid model considering constant surface temperature as a boundary condition (but variable at hourly time intervals).

Table 5.4: Thermal penetration depth at different analysis time

t (hours)	δ_p **(metres)**
0	0
1	0.05
15	0.3
40	0.5
89	0.75
246	1.25
482	1.75
1188	2.75
1413	3

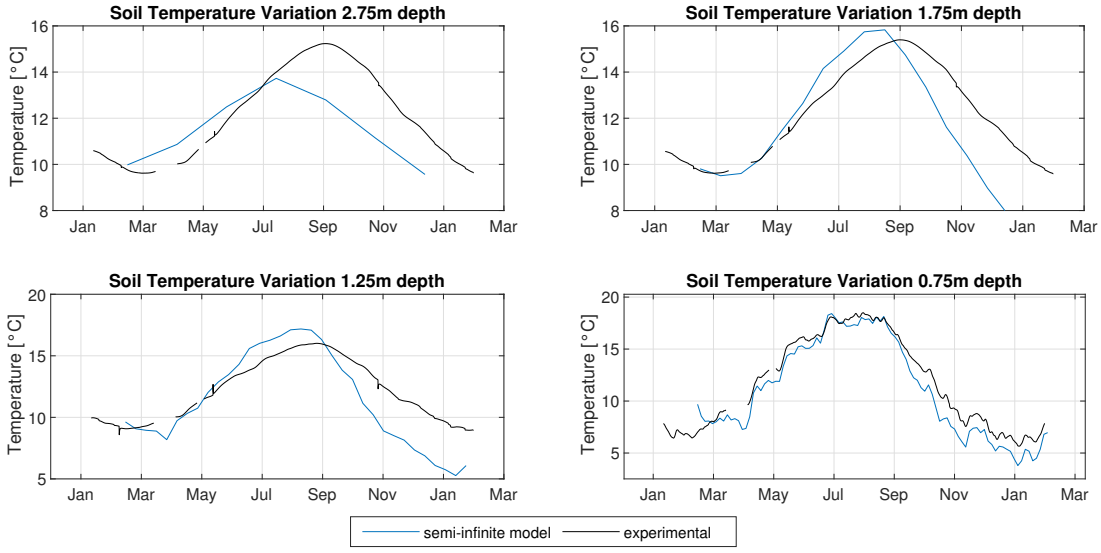

Figure 5.5: Comparison between the semi-infinite solid model and the experimental data

As seen in Equation 5.3, the semi-infinite model does not need the undisturbed ground temperature as an input parameter. For this reason, this model is more accurate at depths closer to the surface. This also indicates that the layers of soil that are closer to the surface are much more influenced by the heat fluxes coming from the ambient rather that the underground. The error increases with soil depth (see section 5.5) because the semi-infinite model is not appropriate to study the impact of very variable thermal loads in the soil deeper than a few

centimetres.

5.4 Finite difference method models to model the shallow soil

As previously seen, the sinusoidal model lacks accuracy to represent the thermal behaviour of the very shallow and for short-term thermal responses. On the other hand, the semi-infinite solid model is more accurate to dynamically analyse the temperature of shallow soil (of the order of a few centimetres) but lacks precision for deep soil. In this sense, to increase the range of analysis and accuracy, the soil can be modelled by the numerical method of the finite differences (FDM). This method is widely used for the analysis of complex geometries, as well as for the analysis of variable boundary conditions. The principle of the method is to numerically solve the Fourier heat equation in one dimension (Equation 5.4) by dividing the analysis system into a large but finite number of elements or nodes. Then each element is analysed independently in space and time. This method allows for accumulating previous results so is robust for modelling. Each node or element has its own boundary conditions and its thermal response affects its adjacent nodes.

$$\frac{\partial T}{\partial t} = \alpha \frac{\partial^2 T}{\partial z^2} \tag{5.4}$$

5.4.1 Equation discretisation

In order to discretise Equation 5.4, the explicit method was used [81]. In this method, the temperature of a node is evaluated from the knowledge of the temperatures of the previous time steps. Explicit method was preferred over implicit method as it was simpler to formulate and quick enough to compute. Figure 5.6 shows a schematic of the studied soil divided by n elements of thickness Δz along the z-direction. The temperature is evaluated in the centre of each node m.

Equation 5.5 represents the discretisation of Equation 5.4 by the explicit form of the FDM considering one-dimensional heat transfer, m is each space element

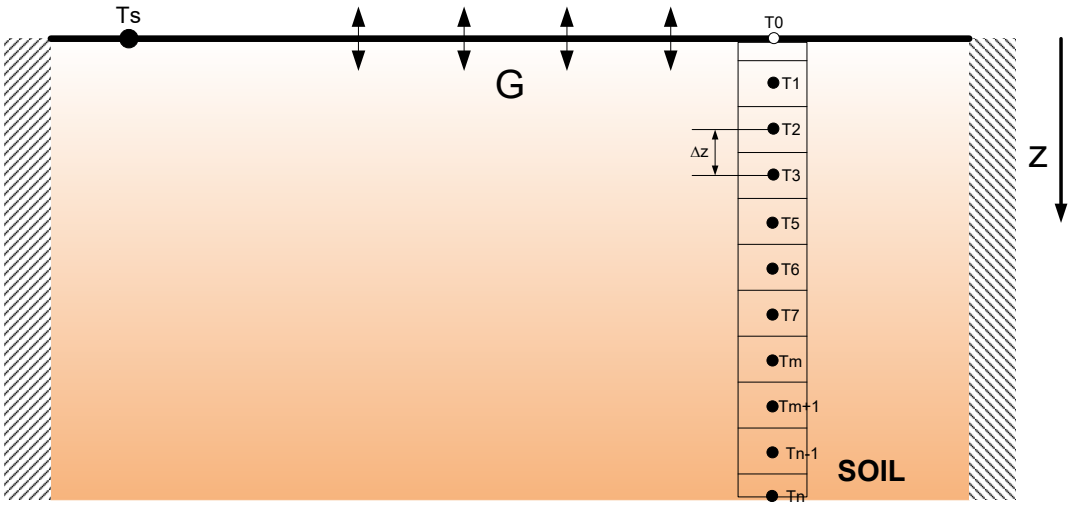

Figure 5.6: Finite difference representation of the soil

or node; p is each temporal element, Δt is the differential time step where $t = p\Delta t$ and Δz is the length of each differential element.

$$\frac{1}{\alpha_s}\frac{T_m^{p+1} - T_m^p}{\Delta t} = \frac{T_{m+1}^p + T_{m-1}^p - 2T_m^p}{\Delta z^2} \tag{5.5}$$

Through some simplifications like $Fo = \frac{\alpha_s \Delta_t}{\Delta_z^2}$, where Fo is the Fourier number which represents the dimensionless time, the expression is reduced to (Equation 5.6):

$$T_m^{p+1} = Fo\left(T_{m+1}^p + T_{m-1}^p\right) + (1 - 2Fo)T_m^p \tag{5.6}$$

To solve this equation correctly by the explicit method, it is important to consider the stability criterion that is related to the minimum value of Δt for the equation to be solved. Thus, the stability criterion of Equation 5.6 is $(1 - 2Fo) > 0$.

Equation 5.6 is valid for any interior node that does not have internal heat generation. However, for the external nodes, the discretisation must be done by an energy balance considering the boundary conditions to which the external nodes are exposed.

5.4.2 Soil surface temperature as boundary condition FDM-T

Figure 5.6 shows the heat transfer problem to solve by the finite difference method of the soil exposed to a constant surface temperature as boundary condition (FDM-T).

Hence, for node o (Figure 5.7), Equation 5.7 is used to to evaluate the surface temperature ($m = 1$).

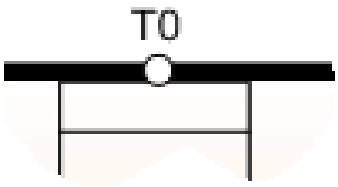

Figure 5.7: FDM-T representation, node 0

$$T_0 = T_s \tag{5.7}$$

To evaluate the temperature of the internal nodes ($m = 2$ to $n - 1$), the energy balance method (Equation 5.8) [81] was conducted (Figure 5.8).

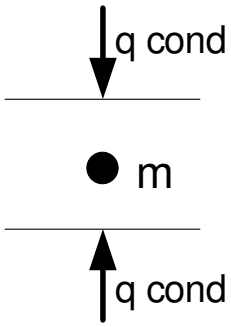

Figure 5.8: FDM-T representation, node m

$$\frac{k_s}{\Delta z}\left(T_{m+1}^{p} - T_{m}^{p}\right) + \frac{k}{\Delta z}\left(T_{m-1}^{p} - T_{m}^{p}\right) = \frac{\rho_s C p_s \Delta z}{\Delta t\left(T_{m}^{p+1} - T_{m}^{p}\right)} \tag{5.8}$$

By solving this energy balance, the result is simplified to the same results as Equation 5.6.

To evaluate the temperature of the last node ($m = n$) the energy balance method (Figure 5.9) was also conducted (Equation 5.9):

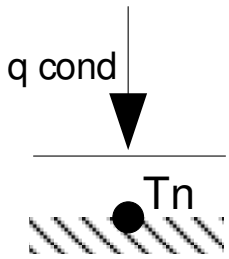

Figure 5.9: FDM-T representation, node n

$$\frac{k}{\Delta z}\left(T_{m-1}^{p} - T_{m}^{p}\right) = \frac{\rho_s C p_s \Delta z}{\Delta t}(T_{m}^{p+1} - T_{m}^{p}) \tag{5.9}$$

By solving this energy balance, the temperature of the node n can be evaluated by using Equation 5.10.

$$T_{m}^{p+1} = Fo T_{m-1}^{p} + (1 - 2Fo) T_{m}^{p} \tag{5.10}$$

The resolution of Equations 5.6 and 5.10 implies the use of numerical methods and will be more accurate for a greater number of elements m and a lower time interval Δt. However, this would imply a higher computational cost (depending on the processing capacity of the computer). To consider the periodic variation of the boundary condition, it is assumed that every hour, the surface temperature (T_s) is modified and therefore the temperature of node 1 (T_0). Table 5.5 shows the input parameter used for modelling the shallow soil by the finite difference method with temperature as boundary condition (FDM-T).

Figure 5.10 shows the comparison of the results of the FDM-T and the actual variation of the soil temperature at different depths. The air temperature was approximated as the temperature of the soil surface. For ground covered with vegetation or grass this approach is justified. However, the energy balance at the soil surface (Appendix C) must be solved to determine this temperature for other surfaces conditions. As shown in Figure 5.10, by this method the accuracy increases markedly, and the model is able to show the short-term thermal oscillations at shallow depths (0.75 metres). However, at depths of 1.25 and 1.75

Table 5.5: Input data for the FDM-T model

Δz= 0.075 m
Δt= 3600 s
α_s= 6.95 x10^{-7} m^2/s
k_s= 1.5 W/mK
T_s= air temperature °C
ρ_s= 1800 kg/m^3
Cp_s= 1200 J/kgK

metres the margin of discrepancy increases, especially in the cold months. This may occur due to the uncertainty in the consideration of the soil physical properties such as thermal diffusivity or the variation of the thermal conductivity as a function of temperature and water content, which might be more influential near the surface [140].

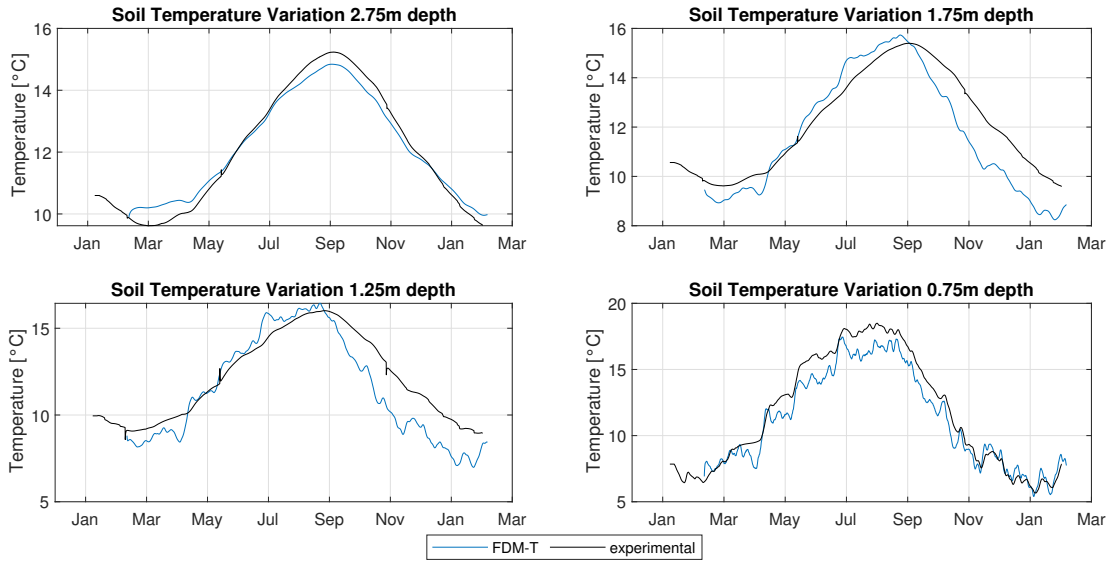

Figure 5.10: Comparison between the FDM-T and the experimental data

5.4.3 Soil surface heat flux as boundary condition FDM-HF

Figure 5.6 shows the heat transfer problem to solve by the finite difference method of the soil exposed to a constant heat flux G as boundary condition

(FDM-HF). Hence, for node 0 ($m = 1$) an energy balance is conducted (Figure 5.11) as shown in Equation 5.11.

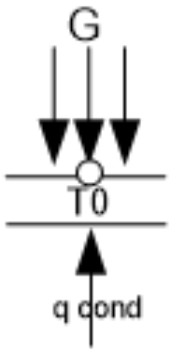

Figure 5.11: FDM-T representation, node n

$$G + \frac{k_s}{\Delta z}\left(T_{m+1}^{p} - T_{m}^{p}\right) = \frac{\rho_s C p_s \Delta z}{\Delta t}\left(T_{m}^{p+1} - T_{m}^{p}\right) \tag{5.11}$$

By solving this energy balance, the result is simplified as shown in Equation 5.12.

$$T_{m}^{p+1} = \frac{Fo \Delta z G}{k_s} + Fo T_{m+1}^{p} + (1 - Fo) T_{m}^{p} \tag{5.12}$$

In order to evaluate the temperature for the internal nodes ($m = 1$ to $n - 1$) and for the last node ($m = n$) Equation 5.6 and 5.10 should be used respectively.

To calculate the heat flux G, an energy balance in the soil surface must be conducted considering the heat transfer by conduction, convection, radiation and evaporation. The Appendix C shows a methodology for the energy balance at the soil surface.

The FDM-HF is more complex to solve than the FDM-T, this is mainly due to the iterative process to calculate the soil surface heat flux (G) considering the energy balance for node 1. Hence, the computational cost increases. To consider the periodic variation of the boundary condition, it is assumed that every hour, the heat flux on the surface (G) changes. Table 5.6 shows the input parameter used for modelling the shallow soil by the finite difference method with heat flux in the soil surface as boundary condition (FDM-HF).

Figure 5.12 shows a comparison between experimental data and the predicted soil temperature variation at different depths using the FDM with constant heat

Table 5.6: Input data for the FDM-HF model

Δz= 0.075 m
Δt= 360 s
α_s= 6.95 x10^{-7} m^2/s
k_s= 1.5 W/mK
T_s= air temperature °C
ρ_s= 1800 kg/m^3
Cp_s= 1200 J/kgK
G= calculated as shown in Appendix C

flux (periodically variable) as a boundary condition (FDM-HF). This approach is more complex than the FDM-T as a larger number of inputs is required (solar radiation, air temperature, rainfall, wind speed, soil porosity, relative humidity, etc.) but it should be more accurate for soil that is covered with vegetation. However, Figure 5.12 shows that using this approach reduced accuracy compared to FDM-T. This is probably due to the consideration of heat transfer by evaporation and radiation, which increases uncertainty due to the inclusion of more input parameters. Some of these parameters such as the rainfall, solar radiation, wind speed and relative humidity were measured from the weather station (see Chapter 4). However, others such as soil porosity, soil emissivity, soil absorptivity, convection coefficient and sky temperature were estimated or calculated. For all the depths considered the model underestimates the soil temperature variation.

5.5 Error analysis of the different models

In order to evaluate the accuracy of the different models using statistical indicators, the coefficient of determination (R^2), the root mean square error ($RMSE$) and the normalised root mean square error ($NRMSE$) were determined (see section 3.6 for details of these indicators) and are shown in Table 5.7.

The four models show a high R^2 at depths of 0.75 and 1.25 meters ranging from 0.74 to 0.98. This means that the experimental values have a correlation with the model predictions. The lowest R^2 values corresponds to the semi-

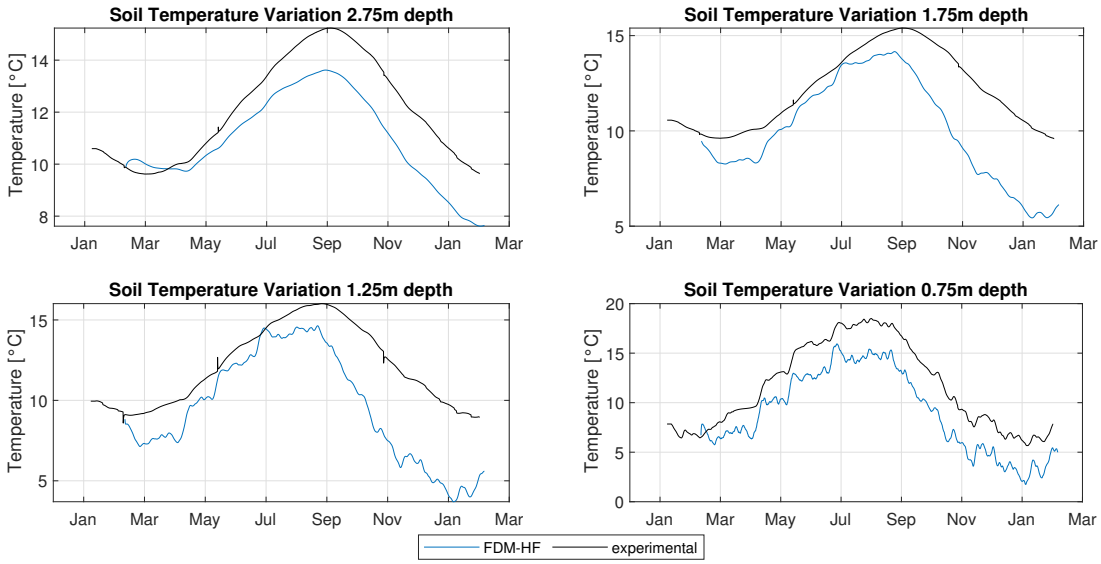

Figure 5.12: Comparison between the FDM-HF and the experimental data

infinite model at depths of 1.75 m (R^2= 0.55) and 2.75 m (R^2= 0.36) while the highest correspond to the FDM-T at depths of 0.75m (R^2= 0.98) and 2.75m (R^2= 0.99). However, it is worth noting that the coefficient of determination is not the best indicator to show how good a model fits experimental data as this only show the existent correlation of two variables. For this reason, it is also important to determine the error between the model predictions and the experimental data (see section 3.6). In this context, Table 5.7 shows that even if a model has a high coefficient of determination, the error may still be significant. For instance, for the sinusoidal model at a depth of 2.75 m, the coefficient of determination is 0.97. However, the $NRMSE$ is 49.19%, which is high enough to make a model unacceptable. This error is mainly due to an overestimation of the undisturbed ground temperature, as seen in Figure 5.3. Regarding the semi-infinite model, the $NRMSE$ at 0.75 m and 1.25 m are 9.77% and 15.23% respectively which is low enough to estimate the temperature variation of the shallow soil. Nevertheless, at greater depths, the error increases significantly up to 46.66% at a depth of 2.75 m. This confirms the previous findings that the semi-infinite model lacks accuracy for deeper soil due to the low thermal penetration depth.

With respect to the FDM-HF, it shows a very high error at all the evaluated depths even though the R^2 is not particularly low. Indeed, the $NRMSE$ for the FDM-HF ranges from 24.49% to 48.14%. This is mainly due to the large number

of uncertainties in the input variables for this model such as soil emissivity, sky temperature, soil porosity, etc. On the other hand, the FDM-T model shows the best fit at the closest depth to the surface (0.7 5m) of all the studied models ($NRMSE$= 8.48%). Hence, this model is a good approach for evaluating the short-term soil temperature behaviour and it can predict hourly temperature fluctuations, as shown in Figure 5.10. Nonetheless, the FDM-T model has not been tested under high vegetated soils or concrete or asphalt-covered soil. In these cases, the model might not be applicable because the surface temperature will be significantly different compared to the air temperature. As can be noted, all the models show less accuracy for medium depths (1.25 m and 1.75 m). This may be due to a variation in the soil properties with depth. It is common to find that real soil has a different composition at different depths, causing a variation in the thermal properties. Likewise, it is worth considering in future research that the thermal conductivity and specific heat may vary over time due to the changing water content of the soil.

Finally, it is important to note that the computational time to solve the model for one year using hourly time steps by the numerical explicit method is 5 seconds for the FDM-T and 9 seconds for the FDM-HF on a 1.8 GHz 8-core processors (Intel Core i7 of eighth generation) personal computer. Hence, the use of the explicit method has a low computational cost for an annual simulation, and it is suitable for integration into building simulation software.

5.6 Summary of the chapter

In this chapter, a comparison is made between different analytical and numerical models to predict the temporal variation of the soil temperature at different depths. Two analytical models and two numerical models were studied to evaluate the soil temperature and the results were compared with one year of hourly experimental data from the location where the EEB is installed. The analytical sinusoidal model, despite its high coefficient of determination (more than 0.93 in average), has one of the highest errors due to the uncertainty on the actual value of the undisturbed ground temperature. Moreover, this model is not able

Table 5.7: Statistical parameters of the different models

Model	Depth m	R^2	RMSE °C	NRMSE %
Sinusoidal	0.75	0.97	3.12	24.34
	1.25	0.94	2.95	39.69
	1.75	0.93	2.87	49.49
	2.75	0.97	2.76	49.19
Semi-infinite	0.75	0.97	1.24	9.77
	1.25	0.96	1.71	15.23
	1.75	0.55	2.22	16.99
	2.75	0.36	2.24	46.66
FDM-T	0.75	0.98	1.09	8.48
	1.25	0.87	1.41	19.96
	1.75	0.87	1.08	18.57
	2.75	0.99	0.32	5.7
FDM-HF	0.75	0.95	3.14	24.49
	1.25	0.74	3.4	48.14
	1.75	0.68	2.78	47.87
	2.75	0.83	1.55	27.65

to determine accurately the short-term temperature variations in shallow spoil (less than 2 m). This error can be reduced easily with a modification on the input value of the undisturbed ground temperature. However, this parameter is commonly not measured by weather stations and models must be applied. The analytical semi-infinite model accurately determines the soil temperature variation at very shallow depths (a few centimetres) and it also predicts short-term fluctuations with low error and independently of the value of the undisturbed ground temperature. However, it lacks applicability for analysis at depths greater than one metre. Numerical models, despite their higher complexity in model developing and coding, are able to predict both short and long-term soil temperature variations. The FDM-T had the lowest error and has the benefit that in addition to soil properties, it only requires air temperature as an input parameter.

However, the consideration of the air temperature as the surface soil boundary condition is only valid for grass or soil covered grounds. For other types of ground surfaces such us concrete, asphalt or dense vegetation, other approaches must be considered to determine the temperature at the surface. The FDM-HF did not show a very high accuracy, which can be attributed to the uncertainty of the large number of input parameters required, such as rainfall, solar radiation, sky temperature, relative humidity, etc. However, if more certitude of the input data can be achieved, the accuracy of this model will increase as shown in the study of Chalhoub et al. [89] where the error of the predictions is lower than 7%. Likewise, this model could be used to study soil temperature beneath all kinds of ground surfaces and vegetations.

The FDM-T is therefore chosen for this study due to its high accuracy and relative simplicity. This model is able to support rapid computation, which is desired for multi-year simulations. Additionally, unlike the sinusoidal model, the FDM-T does not have a high dependence on the value of the undisturbed ground temperature but on the ambient air temperature which reduces the uncertainty of the shallow soil temperature prediction. These findings are relevant for different research fields such as the study of shallow geothermal systems such as horizontal ground source heat pumps, mainly related to the short-term prediction of a geothermal system performance. The findings are also relevant for the study of the natural soil temperature variation which is a key topic in agriculture and climate analysis. As noted, the accuracy of the FDM-T can be improved by adding extra considerations such as variable thermal conductivity as a function of time and depth. This opens the door to future research.

As seen in this chapter, there are different approaches that can be used to estimate the natural temperature variation of the shallow soil which is particularly important when there are not experimental measurements of the shallow soil. The natural soil temperature is very important when analysing shallow geothermal systems. The next chapter will show the integration of the natural soil temperature variation with the thermal response of geothermal systems in the shallow soil by using the superposition technique for heat transfer models.

6. Modelling shallow boreholes in vertical ground heat exchangers

The objective of this chapter is to develop a model that is appropriate for studying the ground heat exchanger (GHE) of the Earth Energy Bank (EEB), in the short and long term. Conventional models may not be appropriate for studying the particular configuration of the GHE in the EEB of the current research. One of the main reasons is that the borehole heat exchanger is very shallow (1.5-metre depth). For this reason, the ground cannot be considered as undisturbed. The natural variation of the shallow soil temperature throughout the year has an evident impact on the behaviour of the heat exchanger and the effective heat storage temperature. Likewise, the distribution of the boreholes within the EEB is not symmetrical. Consequently, the simplifications of heat transfer models for symmetric systems cannot be used. These peculiarities make the development of an accurate, fast and simple model for this type of system challenging.

6.1 Description of the very shallow ground heat exchanger

The ground heat exchanger of the present study is the one previously described in section 4.1.3 of Chapter 3. The scheme in Figure 6.1 shows the configuration of the heat exchanger. As seen in the figure, the system has the characteristic of being shallow and asymmetrical. The spacing between the boreholes is 1.5 m, except for the spacing between boreholes B1-B2, B10-B11 and B15-B16 that are 1 m apart. The boreholes are of the single U-tube type and are filled with bentonite to give a total bore diameter of 0.15 m. Table 6.1 shows the main characteristics of the GHE and Table 4.4 the thermal properties of the soil, backfill and working fluid.

According to several authors [99, 114, 141–143], the analysis of both single

and double U-tubes can be simplified by the concept of using a single tube of an equivalent radius (Figure 6.2). For this, several equivalent radius correlations have been defined with different level of complexity. The selection of the appropriate correlation is particularly important when studying the thermal behaviour of a GHE in the short term [55]. That is when one wants to evaluate the borehole backfill, the temperature of the borehole wall, or the temperature of the working fluid. In the present study, considering that it is intended to contribute practically to development of the GHE model, the concept from Claesson and Dunand [144] of the equivalent radius will be used as this is one of the most commonly used correlations and its application is simple. Equation 6.1 indicates the method of calculation of the equivalent radius [55]. Considering that the outer radius of the pipe (r_{po}) of the GHE is 0.0208 m, then the equivalent radius (r_{eq}) would be 0.0295 m.

$$r_{eq} = \sqrt{2}\, r_{po} \tag{6.1}$$

Table 6.1: Parameters of the GHE

Type of GHE	Single U-Tube
Depth of the boreholes	1.5 m
Number of boreholes	16
Borehole radius	0.15 m
Pipes connexion	In series
Pipe material	HDPE SDR 11
Outer radius pipe (r_{po})	0.0208 m
Pipe thickness	3.7 mm

6.2 Ground thermal load and fluid inlet temperature

The parameters described in section 6.1 are essential to evaluate or develop heat transfer models for the GHE of the EEB. However, it is also very important to determine the input parameters of any model. Typically, the conventional ana-

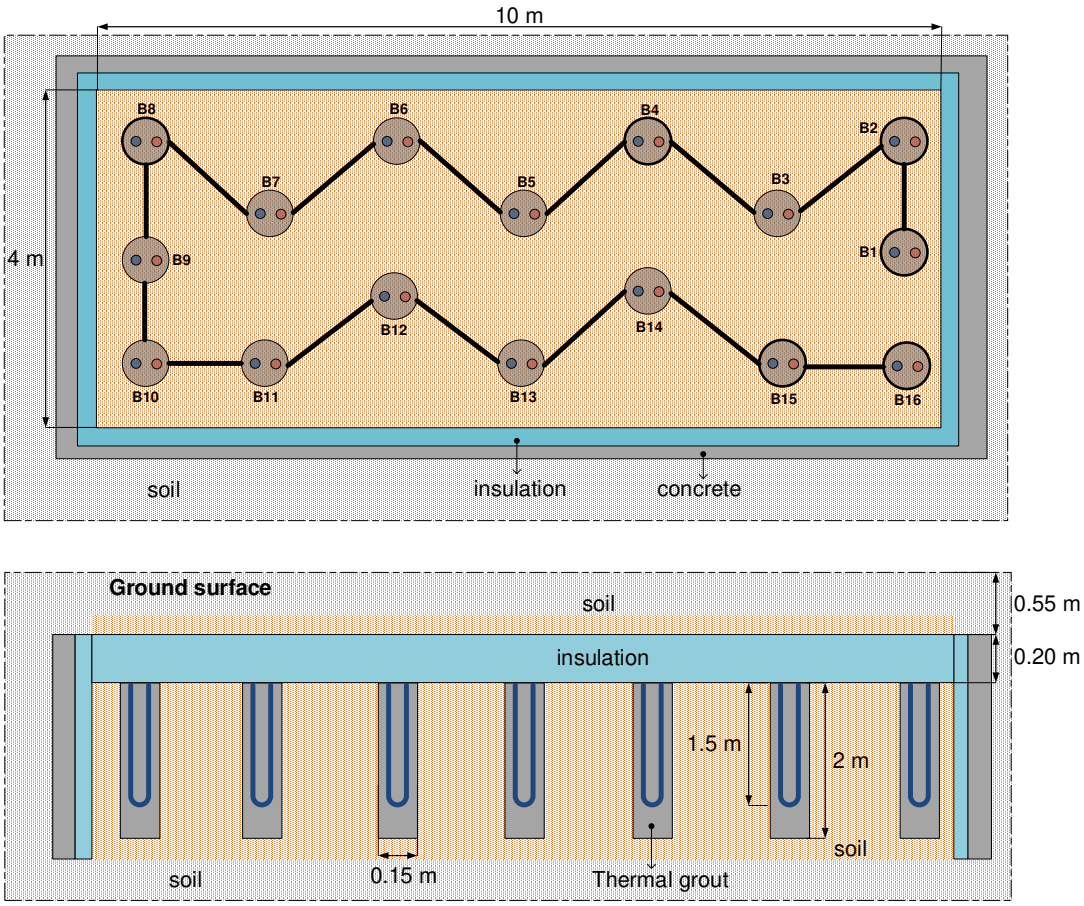

Figure 6.1: GHE configuration, top and side view

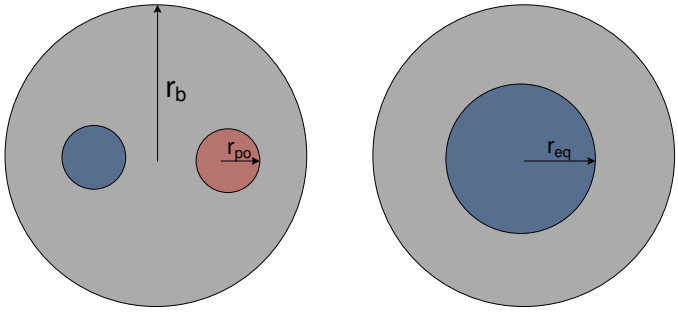

Figure 6.2: Equivalent diameter criteria

lytical models described in section 2.3.2 use the thermal load per metre during injection or extraction of heat (q_r in W/m) as an input parameter to estimate the thermal response of the soil, and in that way to predict the average temperature of the working fluid in the heat exchanger. On the other hand, the more complex numerical models use the temperature of the fluid at the inlet of the ground heat exchanger (T_{fi}) as an input parameter to predict the outlet fluid

Table 6.2: Soil, backfill and fluid thermal properties

	Soil	**Backfill**	**Fluid**
Type of solid/fluid	Wet clay	Bentonite	Glycol (30%)
Thermal conductivity	1.5 W/mK	0.8 W/mK	0.45 W/mK
Density	1800 kg/m^3	2500 kg/m^3	1070 kg/m^3
Specific Heat	1200 J/kgK	1250 J/kgK	3768 J/kgK
Thermal diffusivity	6.94 x10^{-7} m^2/s	2.72 x10^{-7} m^2/s	1.11 x10^{-7} m^2/s

temperature (T_{fo}) and from this, the actual heat flow applied to the ground (q_r).

Both methods have particular applications. For example, typically using the heat flow to the ground (q_r) as an input parameter can predict the impact of such a heat flow on the ground in the short and long term. This heat flow (q_r) can be estimated from the thermal demand of the building and may include the heat gained from solar collectors. In contrast, by using the fluid inlet temperature (T_{fi}) as the input parameter, the impact of the fluid inlet temperature on the ground surrounding the GHE can be estimated. In turn, this temperature can be correlated with the thermal behaviour of the heat pump or solar collectors. For this reason, the models that use the fluid temperature as an input parameter tend to be more complex but allow for a more detailed evaluation of the thermal performance of ground heat exchangers.

For the evaluation, development and validation of models in this study, experimental measurements of the heat flow (q_r) and fluid inlet temperature (T_{fi}) will be used. The experimental data used are recorded on an hourly basis and correspond to the period from 06/04/2016 to 12/31/2017, with a total of 14169 hours.

6.2.1 Heat flow data

The heat flow data for the GHE was determined experimentally from measurements of the fluid inlet and outlet temperatures, the specific heat of the fluid and the mass flow rate as indicated in Equation 6.2.

$$Q_{gr} = \dot{m}_{ghe} \times \ c_p \times \left(T_{fi} - T_{fo}\right) \tag{6.2}$$

The analytical and numerical models use the heat flow per metre of borehole depth as the input parameter. Since the boreholes of the GHE are connected in series, the total heat must be divided for the total depth plus the equivalent of the length of the pipe representing the separation distance between each borehole. In this way, the heat flow per metre was determined according to Equation 6.3.

$$q_r = \frac{Q_{gr}}{(N1.5) + 11} \tag{6.3}$$

In Equation 6.3, N represents the number of boreholes, 1.5 m is the depth of each borehole and 11 m is the total length of the connecting pipes between each borehole divided by 2. This division is made since the boreholes are of single U-tube type, so each metre of borehole depth is twice the length of pipe. In this way, the total equivalent length is 35 metres.

Figure 6.3 shows the actual heat flow per metre (q_r) that is applied to the boreholes. It is important to mention that the actual load is variable at each borehole due to the variation of the fluid temperature. However, due to the small size of the heat exchanger and since the difference in fluid temperature at the inlet and outlet of the GHE is very low (see Section 4.6.1), it can be assumed that the radial load per metre unit is the same in all boreholes. On the other hand, Figure 6.3 (bottom) shows the heat flow per metre in a week dominated by heat injection and in a week dominated by heat extraction respectively.

As seen in Figure 6.3, the heat flow per metre is very dynamic and varies between heat injection and heat extraction. As the operation of the system depends not only on the thermal demand of the building but also on the availability of solar energy, the system can change rapidly between injection and heat extraction in the short term, for example in the same month, week or even on the same day. For this reason, the heat transfer model has some peculiarities that make it complex. Firstly, we cannot assume a constant thermal load on the GHE as analytical models do, and secondly, the principle of superposition of loads to deal with dynamic loads makes the application of a dynamic model computationally expensive compared to a constant heat flow as input parameter.

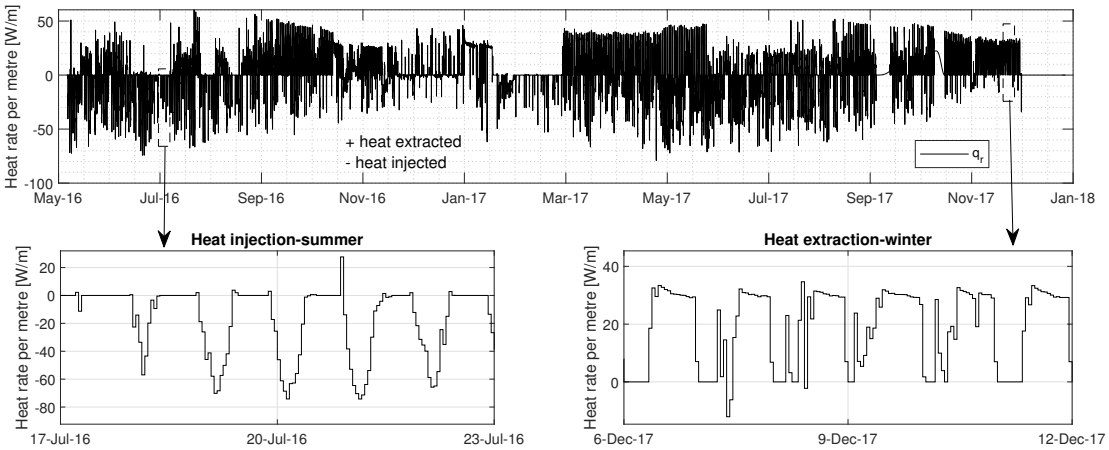

Figure 6.3: Heat Flow per metre in the GHE

6.2.2 Fluid inlet temperature data

The fluid inlet temperature in the GHE was experimentally obtained as explained in Chapter 4. This fluid inlet temperature (T_{fi}) was used as an input parameter to model and validate the thermal performance of the GHE and estimate the GHE fluid outlet temperature (T_{fo}).

Figure 6.4 shows the actual GHE fluid inlet temperature over time. This temperature is highly variable and depends on several factors. For example, during heat injection into the EEB, the fluid inlet temperature depends on the outlet temperature of the PVT as well as on the EEB temperature. In summer this temperature can exceed 40°C. On the other hand, in the periods of heat extraction, the temperature entering the GHE will depend on the thermal demand to be covered in the house, the operation of the heat pump and also on the EEB temperature itself. It can be observed in the moments of the highest heat extraction in winter, the fluid inlet temperature can fall down to 5°C below zero.

It is important to note that when the temperature of the fluid seems to be zero in the graphs, it is not necessarily the case that the temperature of the fluid is zero at the inlet of the GHE, but merely that the system does not pump fluid at those times. A filter was used to give a zero value to the temperature data when the system's pumps were off to be better able to visualize the data when the fluid is flowing. This does not generate errors in the models since the heat

flow calculations depend on both temperature data and mass flow data. When the mass flow is zero (system off) the heat flow out of the pipe is obviously zero too.

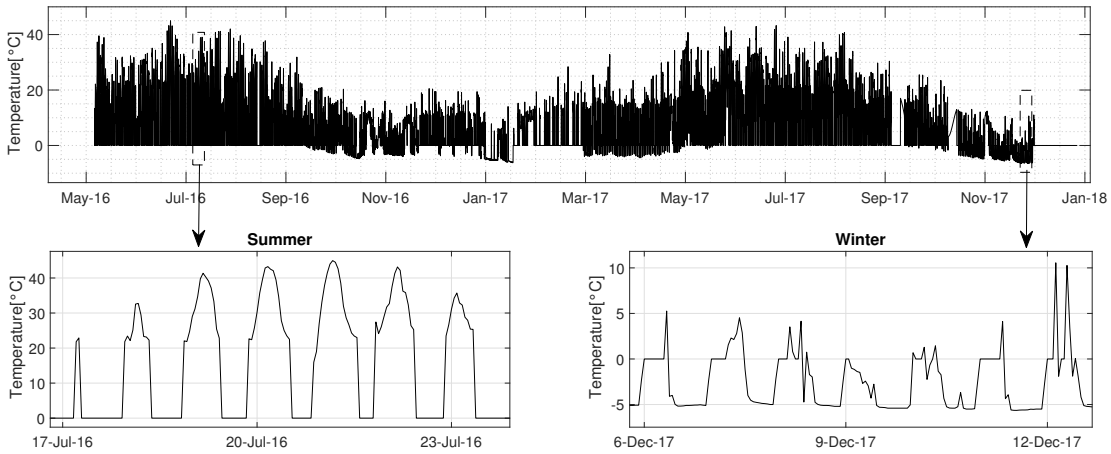

Figure 6.4: GHE inlet fluid temperature (summer and winter)

6.3 Conventional analytical models to estimate the thermal response of the EEB

As described in the literature review (section 2.3.2), there are different types of analytical model that can be used to evaluate borehole heat exchangers. Depending on the time scale of the analysis, different types of more or less accurate and complex models can be used.

The most common analytical models for studying such systems are the Infinite Line Source (ILS) model, Infinite Cylindrical Source (ICS) and the Finite Line Source (FLS) model. These models were already described in section 2.3.2 in the literature review. In this section, an adaptation with the dimensionless temperature (Θ_s) as done in [16] is done.

First, the ILS (Equation 6.4) or ICS (Equation 6.5) models can be used in a similar way without necessarily having a great discrepancy between the two when used to analyse the response in the long term or at distances greater than the borehole radius [16].

$$\Theta_s(Fo_r) = \frac{1}{4\pi}\int_{\frac{r^2}{4\alpha_s t}}^{\infty}\frac{e^{-u}}{u}du = \frac{1}{4\pi}\times\ E_1\left(\frac{1}{4Fo_r}\right) \tag{6.4}$$

$$\Theta_s\left(Fo_b, \frac{r}{r_b}\right) = \frac{1}{\pi^2}\int_0^{\infty}(e^{-u^2 Fo_b}-1)\frac{J_0\left(\frac{r}{r_b}u\right)Y_1(u) - Y_0\left(\frac{r}{r_b}u\right)J_1(u)}{u^2\left({J_1}^2(u)+{Y_1}^2(u)\right)}du \tag{6.5}$$

where: $\Theta_s = \frac{(T(t)-T_o)k_s}{q_r}$; $Fo_r = \frac{\alpha_s t}{r^2}$ and $Fo_b = \frac{\alpha_s t}{r_b^2}$.

In Equations 6.4 and 6.5, Θ_s represents the solution of the dimensionless temperature. These models are applicable when there is a constant thermal load over time. However, in the case of the GHE of the EEB, the thermal load is very dynamic on an hourly basis and also varies between injection and extraction. There are also multiple boreholes whereas the simplest ILS and ICS models are intended to represent the performance of single boreholes. To deal with variable thermal loads, the total load can be averaged over time and used as a constant. This method could be useful to evaluate the long-term response of a single borehole, but it would not be useful to evaluate the short-term response. On the other hand, the concept of temporal superposition can be used to deal with time-varying thermal loads and spatial superposition to deal with multiple boreholes. Equations 6.6 and 6.7 [16] show the application of the superposition technique, previously explained in Section 2.3.4.

$$T(x,t) - T_o = \sum_{i=0}^{n-1}\frac{\Theta_s(x, t-i\Delta t)(\Delta q_r^i)}{k_s} \tag{6.6}$$

where: $\Delta q_r^i = q_r^{i+1} - q_r^i$; Δt= time step; q_r^0= 0; N= number of steps and x= spatial coordinate from the borehole.

$$T(x,t) - T_o = \sum_{j=1}^{N_b}\frac{\Theta_s(x^j, t)\,q_r}{k_s} \tag{6.7}$$

where: N_b= number of borehole and x^j= spatial coordinate from the j^{th} borehole.

In Equations 6.6 and 6.7, Θ_s represents the solution of the dimensionless thermal response of any model used (e.g. ILS, ICS, FLS, etc.). Taking into account the heat flow as an input parameter in the radial direction (described in section 6.2.1), the most common analytical models (ILS and ICS) and the superposition

technique, the accuracy of these models to evaluate the thermal performance of the GHE in the EEB was analysed.

6.3.1 Application of the ILS model and superposition techniques

This section evaluates whether the combination of the ILS model and the superposition technique is valid to accurately study the performance of EEB over time. For this, it is proposed to use temporal and spatial superposition. In the case of temporal superposition, the hourly thermal loads (q_r) obtained from the experimental data shown in section 6.2.1 and Equation 6.6 were used. Regarding spatial superposition, Equation 6.7 was used and as comparison points for the analysis between simulated and experimental data, sensors A and B were used (Figure 6.5). Sensor A corresponds to a point in the centre of the EEB at 1.75 m depth, while sensor B corresponds to a point in the borehole wall at 1.75 m depth. Using these two points, one can have a clear idea about the accuracy of the different models to evaluate the temporal thermal response in the short term (in the borehole wall) and in the long term (centre of the EEB).

For the spatial superposition, the influence of all the boreholes of the GHE on points A and B was analysed initially. That is, the thermal response of each borehole was superimposed. Boreholes that are furthest from measuring points A and B might have a low or no impact. For this reason, the influence of each borehole was analysed one by one and boreholes whose influence on the thermal response on points A and B was less than 1% on the total response were discarded. Consequently, only the boreholes shown in Figures 6.6a and 6.6b were used to study the thermal response on measuring points A and B respectively. It is important to mention that, to treat the boreholes closest to the insulation, symmetry theory was considered. That is, instead of considering an adiabatic wall at a radial distance r from the centre of the borehole, a similar borehole was considered at a distance $2r$. Table 6.3 shows the distances between the boreholes considered in the spatial superposition and the sensors A and B. Finally, the natural heat gains through the bottom of the EEB at a depth of 1.75 m from the surface were superimposed. Typically, models for studying vertical boreholes do not consider the natural heat gains of the soil. However, in the case of the

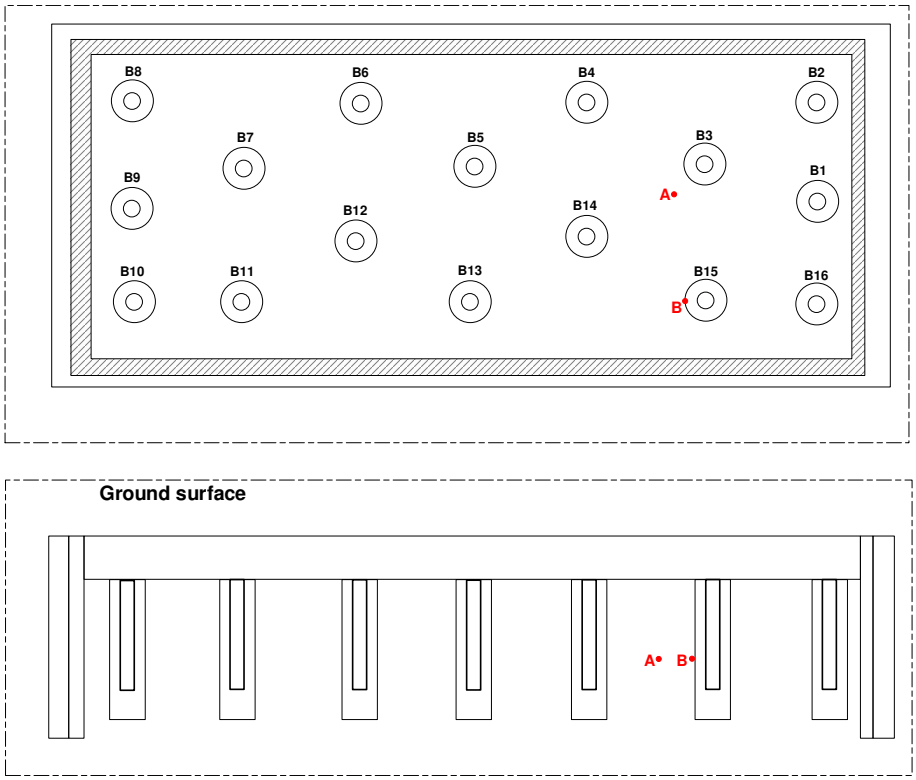

Figure 6.5: Location of sensors A and B used for validation of the thermal response models

EEB, due to its proximity to the surface, the influence of the natural variation in soil temperature cannot be neglected.

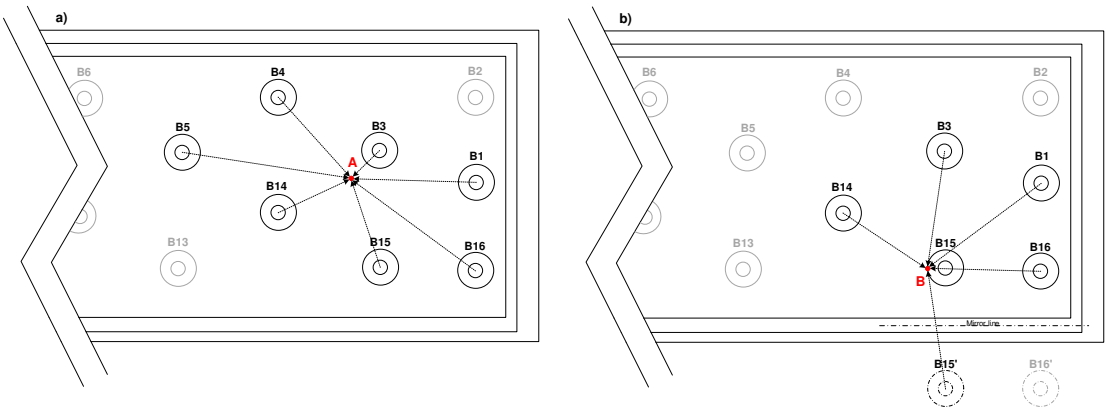

Figure 6.6: Boreholes affecting the thermal response at the location of: a) Sensor A and b) Sensor B

Figure 6.7 shows a comparison between the temporal variations of the experimental and simulated temperature of sensor A. Simulated temperatures were generated by using the ILS model with spatial and temporal superposition in-

Table 6.3: Distance from neighbour boreholes to sensors

Borehole	**Distance to Sensor A**	**Borehole**	**Distance to Sensor B**
B3	0.675 m	B15	0.075 m
B14	1 m	B16	1 m
B4	1.25 m	B14	1.25 m
B15	1.25 m	B1	1.5 m
B1	1.5 m	B3	1.5 m
B5	2.25 m	B15′	1.5 m
B16	2.25 m		

cluding the variation of the natural soil temperature. The figure shows an acceptable accuracy in which the efficiency of the model (EF), the root mean square error ($RMSE$) and the adjusted coefficient of determination (R^2) (see Section 3.6) are equal to 0.9564, 0.559 K and 0.983 respectively. Figure 6.8 shows the scatter plot that correlates the experimental data of sensor A with the data estimated using the ILS model.

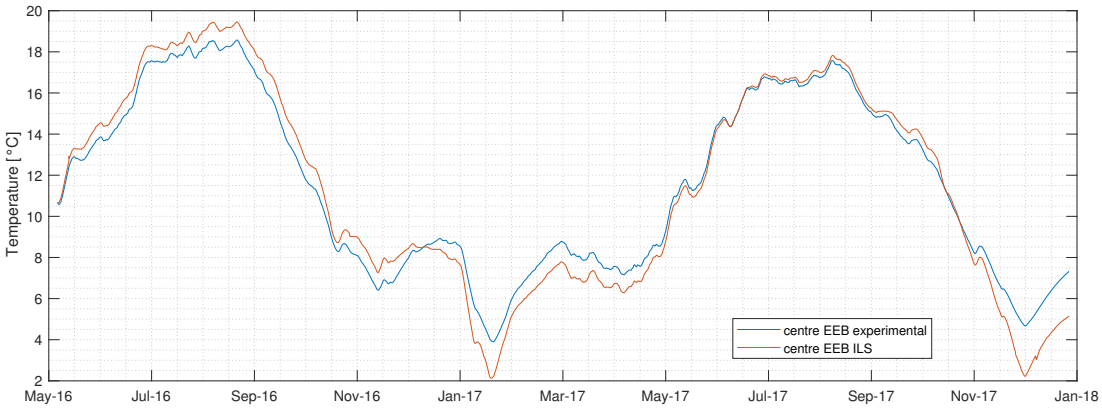

Figure 6.7: Sensor A temperature variation experimental vs ILS model prediction

Figure 6.9 shows the comparison of the temporal variation of the experimental temperature data and the data calculated using the ILS of sensor B (borehole wall). In this case, the model also presents acceptable accuracy in which the EF, $RMSE$ and R^2 are equal to 0.8991, 1.59 K and 0.933 respectively. However, it is

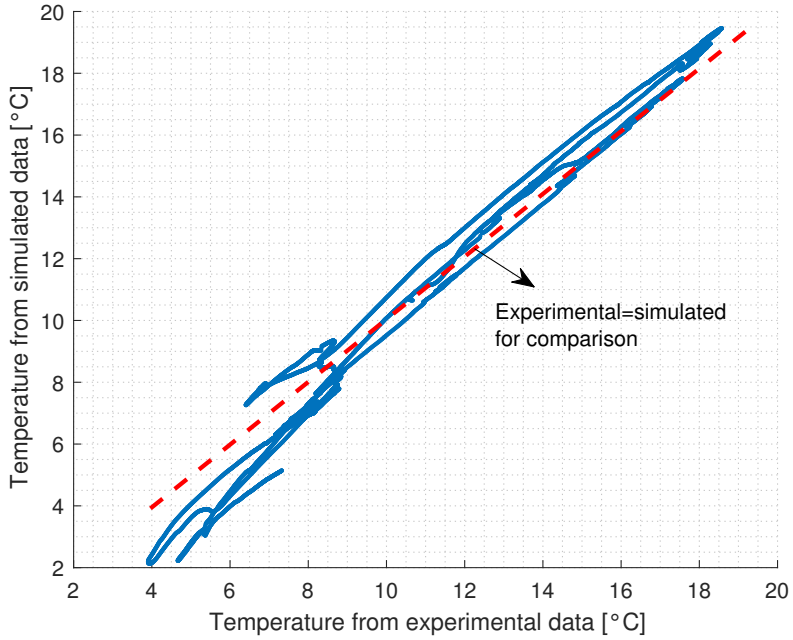

Figure 6.8: Scatter plot Sensor A experimental vs ILS model prediction

important to mention that the ILS model has a limitation in that it does not consider the backfill material. Likewise, Figure 6.10 shows the scatter that correlates the experimental data of sensor B with the data estimated using the ILS model, showing a clear correlation.

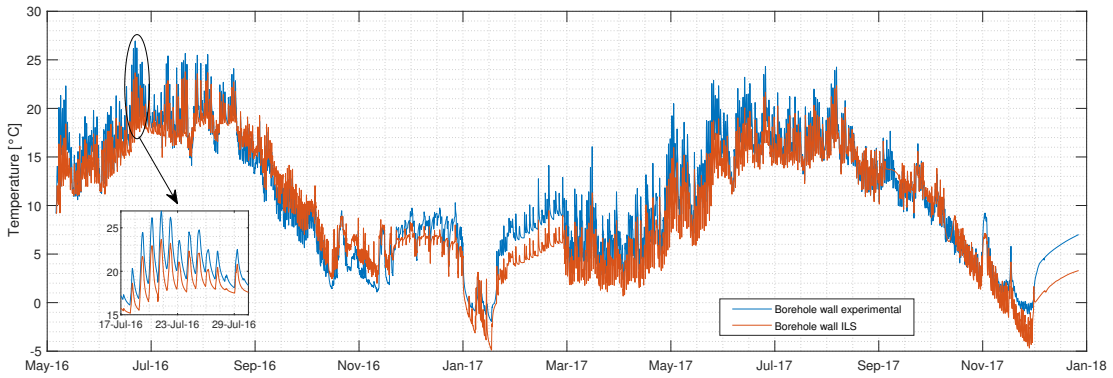

Figure 6.9: Sensor B temperature variation experimental vs ILS model prediction

Although the data calculated using the ILS model show good accuracy and a low error in determining the thermal response, it is important to mention that this model is more accurate for analysing the thermal response at a point far

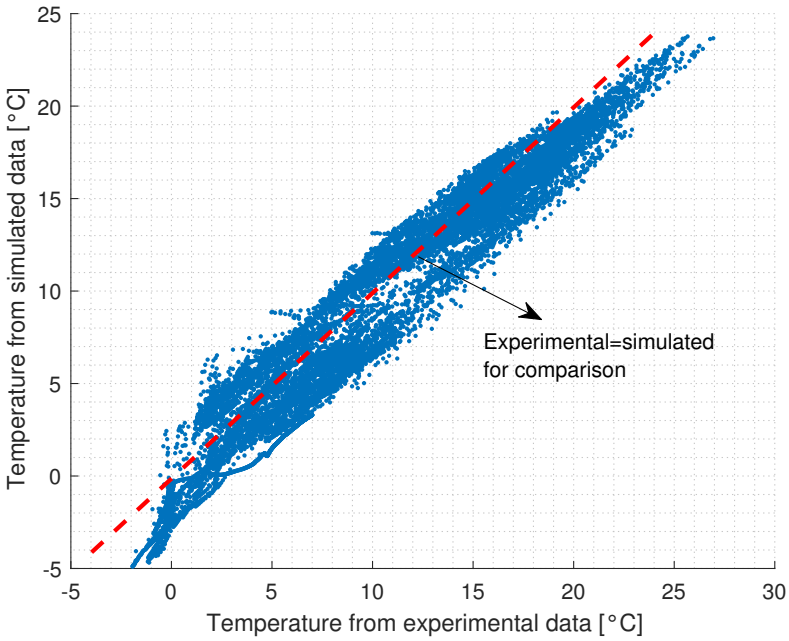

Figure 6.10: Scatter plot Sensor B experimental vs ILS model prediction

from the borehole wall ($r \geq 2r_b$).

6.3.2 Application of the ICS model and superposition techniques

As in section 6.3.1, this section evaluates the accuracy and complexity of the analytical method using the ICS model (Equation 6.5) to evaluate the thermal behaviour of the EEB subject to a variable heat flux (q_r) at the borehole wall ($r = r_b$). As in the previous section, the measuring points of sensors A and B at 1-metre depth were used for the evaluation. The variable loads and the presence of multiple boreholes were represented by the methods of temporal and spatial superposition respectively (Equations 6.6 and 6.7).

The entire calculation procedure was similar to that of section 6.3.1 with the difference of the model used (ICS model) and the time step of the analysis. Initially, the hourly time step (14169-time intervals) was considered for the analysis to be able to compare the data with the previous model. However, this was found to be impossible due to the long simulation time required, which made this approach impractical for the present study. After 36 hours of simulation, less than 5% of the final temperature data had been calculated. Besides, since the ICS model has a definite integral as a function of time (Equation 6.5), the

computation time increases exponentially as the analysis progresses. For this reason, the calculation was simplified by using daily average data instead of hourly data to reduce the number of time steps from 14169 to 590.

Figure 6.11 shows the temporal variation of the experimental and simulated temperature data of sensor A calculated using the ICS model. The results include the superposition of the thermal response of the neighbouring boreholes (Figure 6.6a) and the natural variation of the soil temperature. As shown in the figure, the accuracy is acceptable. The efficiency of the model (EF), the $RMSE$ and R^2 are 0.9558, 0.56 K and 0.983 respectively. This accuracy is similar to that of the ILS model but with a higher computational cost. Figure 6.12 shows the scatter plot which correlates the experimental data with the data calculated using the ICS model. The smaller number of points is due to the use of daily data instead of hourly data.

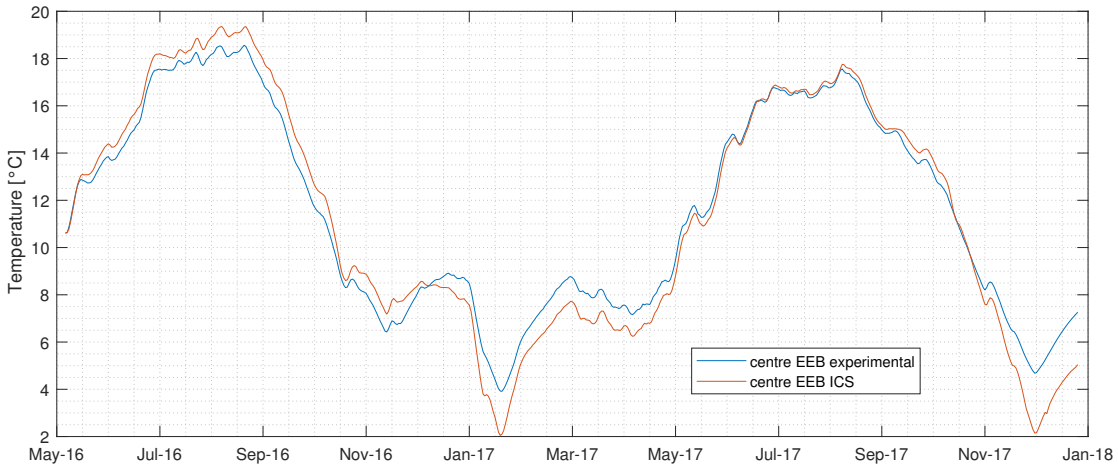

Figure 6.11: Sensor A temperature variation experimental vs ICS model prediction

Figure 6.13 shows a comparison between the experimental and simulated data (using the ICS model) of the temporal temperature variation of sensor B (borehole wall). As with the ILS model, the spatial superposition of contributions from neighbouring boreholes (Figure 6.6b) and the natural variation of soil temperature was applied. This model, like the ILS, also presents acceptable accuracy in which the EF, $RMSE$ and R^2 are equal to 0.8585, 1.78 K and 0.913 respectively. However, the accuracy is lower than that achieved using the ILS

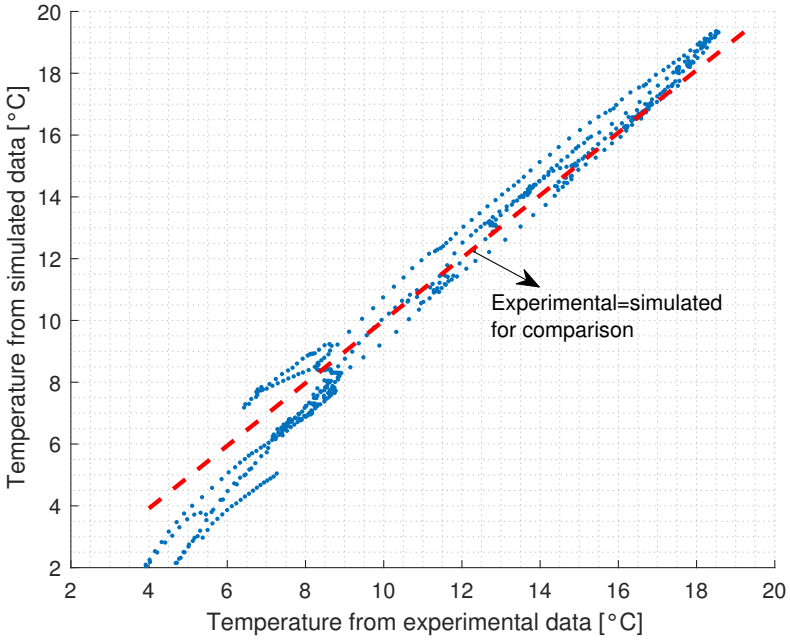

Figure 6.12: Scatter plot Sensor A experimental vs ICS model prediction

model. This is mainly due to two factors. The first is that in this model, it is estimated that the heat flow is imposed on the borehole wall, for this reason, the heat that actually flows through the borehole backfill is ignored which will increase the simulated borehole wall temperature compared to the experimental one. The second is that, like the ILS model, the ICS model does not consider the backfill material as mentioned in section 2.3.2. Figure 6.14 shows the scatter plot that correlates the experimental data of sensor B with the data estimated by the ICS model, showing less correlation than that of the ILS model.

Note that the application of the ICS model showed a similar accuracy to that of the ILS model. However, the application of the ICS model is much more computationally intensive than the ILS model (as can be seen in Equations 6.4 and 6.5). Implementing the code for Equation 6.5 including temporal and spatial superposition is very complex and has a very high computational cost which limits its practical application. This model is inappropriate for long-term analysis of variable loads at short time intervals.

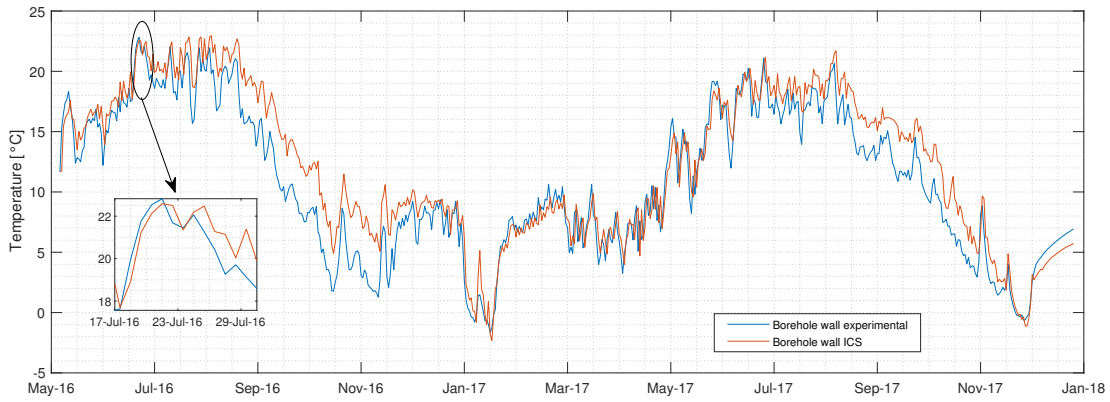

Figure 6.13: Sensor B temperature variation experimental vs ICS model prediction

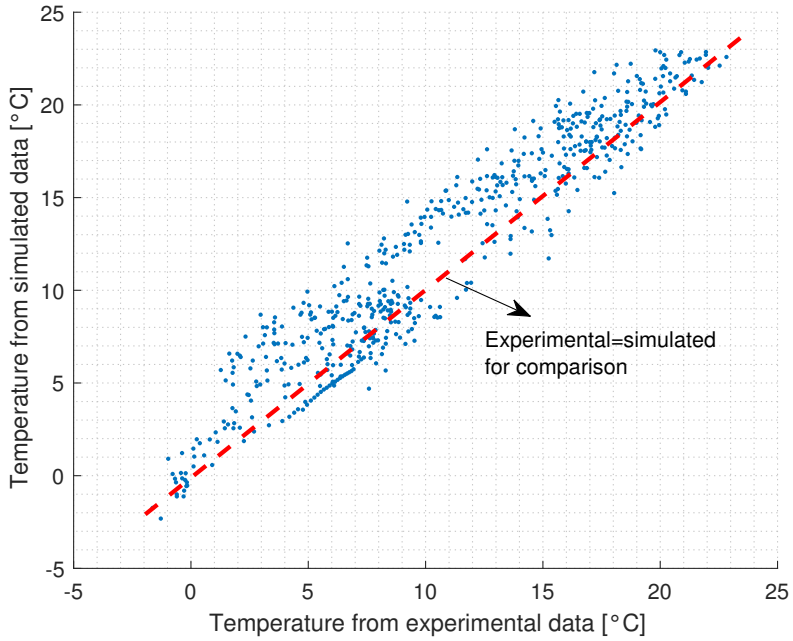

Figure 6.14: Scatter plot Sensor B experimental vs ICS model prediction

6.4 Superposition technique and numerical FDM

This section shows the development and application of the numerical method of Finite Differences (FDM) to estimate the thermal behaviour of the GHE of the EEB. Because analytical methods, despite being reliable and accurate (see section 6.3), have a high computational cost to model variable thermal loads (e.g. hourly loads), it is proposed to use simple numerical methods to deal with

this problem. In this context, a system based on the FDM was modelled using radial coordinates. As before the concept of the equivalent radius (see section 6.1) was used to model the pipe wall. The backfill material of the borehole was also considered in the model. On the other hand, the soil was treated as a semi-infinite medium. The radial size of the element used (dr) was set to 0.015 m. For calculation purposes, the analysis radius was 3 metres from the centre of the borehole pipe, giving a total of 199 nodes. From preliminary simulations, it was determined that at a distance of 3 metres the impact of the heat flow of the borehole on the soil temperature is less than 0.7%, being almost negligible.

Figure 6.15 shows a schematic of the heat transfer problem in radial coordinates using the FDM. As seen in the figure, it is a one-dimensional problem in the radial direction. However, the superposition technique was used to include the natural variation of the soil temperature in the axial direction. In this way, a two-dimensional problem is treated in a simpler way.

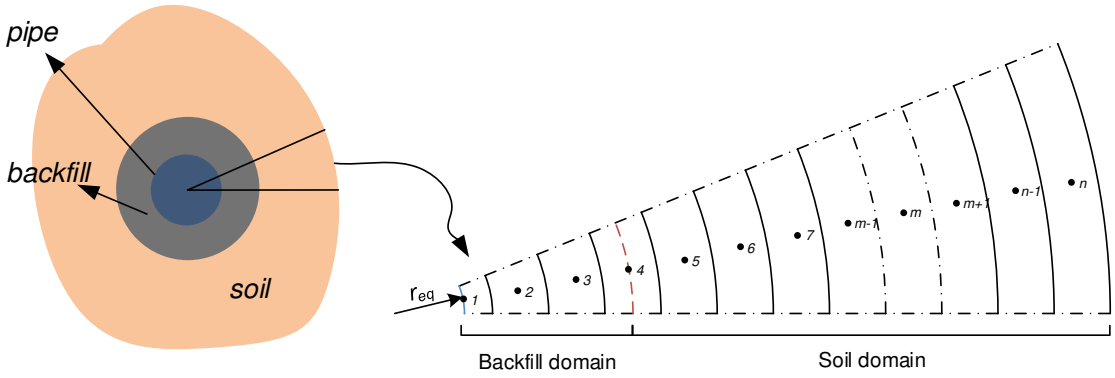

Figure 6.15: A simple schematic of the FDM in radial coordinates

The boundary conditions studied in the FDM were: a) Heat flow (time-variable) at the pipe wall (q_r) and b) internal convection in the pipe with time-variable fluid inlet temperature (T_{fi}).

6.4.1 Heat flux as boundary condition

Figure 6.16 shows a schematic of the heat transfer problem solved by the FDM with heat flow in the pipe wall as boundary condition (the model will be known as FDM-HF). The heat flow data are the experimental data shown in section 6.2.1.

As described previously, this model allows both the borehole backfill material and the soil to be taken into account. For simplicity, and since the simulation time is fast, the explicit method was used to solve the heat transfer problem.

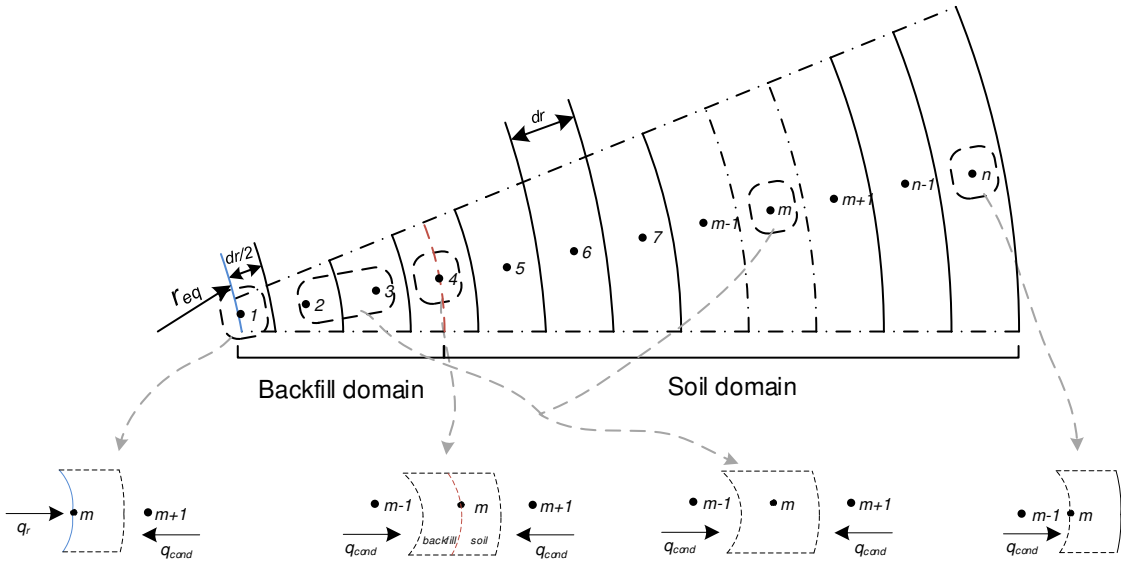

Figure 6.16: Schematic of the heat transfer problem for the FDM-HF

To numerically discretise the problem equations, the energy balance method (Equation 6.8) was used for each node using a spatial element size (dr) of 0.015 m. In this method, it is assumed that all heat flows to the node under analysis. In this way, the energy balance for node 1 ($m = 1$) is shown in Equation 6.9.

$$q_{in} + q_{gen} = q_{st} \tag{6.8}$$

where: q_{in}= heat flow into the node m (W/m); q_{gen}= heat generated in the node m (W/m) and q_{st}= heat stored in the node m (W/m).

$$\begin{aligned} q_r^p + 2\pi \left(r_{eq} + \frac{dr}{2}\right) \frac{k_b}{dr} \left(T_{m+1}^p - T_m^p\right) \quad = \\ \frac{\rho_b c_{p_b}}{\Delta t} 2\pi \frac{dr}{2} \left(r_{eq} + \frac{dr}{4}\right) \left(T_m^{p+1} - T_m^p\right) \end{aligned} \tag{6.9}$$

For the inner nodes of the backfill borehole ($m = 2$ and $m = 3$), the energy balance is shown in Equation 6.10.

$$
\begin{aligned}
2\pi\left(r_{eq}+(m-1)\,dr-\frac{dr}{2}\right)\frac{k_b}{dr}\;\left(T^p_{m-1}-T^p_m\right)\;+\\
2\pi\left(r_{eq}+(m-1)\,dr+\frac{dr}{2}\right)\frac{k_b}{dr}\;\left(T^p_{m+1}-T^p_m\right)\;=\\
\frac{\rho_b c_{p_b}}{\Delta t}2\pi\,dr\,\left(r_{eq}+(m-1)\,dr\right)\left(T^{p+1}_m-T^p_m\right)
\end{aligned}
\tag{6.10}
$$

For the node of the interphase backfill-soil ($m = 4$), the energy balance is shown in Equation 6.11.

$$
\begin{aligned}
2\pi\left(r_{eq}+(m-1)\,dr-\frac{dr}{2}\right)\frac{k_b}{dr}\;\left(T^p_{m-1}-T^p_m\right)\;+\\
2\pi\left(r_{eq}+(m-1)\,dr+\frac{dr}{2}\right)\frac{k_s}{dr}\;\left(T^p_{m+1}-T^p_m\right)\;=\\
\left(T^{p+1}_m-T^p_m\right)\frac{\rho_b c_{p_b}}{\Delta t}2\pi\frac{dr}{2}\;\left(r_{eq}+(m-1)\,dr-\frac{dr}{4}\right)+\\
\left(T^{p+1}_m-T^p_m\right)\frac{\rho_s c_{p_s}}{\Delta t}2\pi\frac{dr}{2}\;\left(r_{eq}+(m-1)\,dr+\frac{dr}{4}\right)
\end{aligned}
\tag{6.11}
$$

For the inner nodes in the soil domain ($m = 5$ to $m = n-1$), the energy balance is shown in Equation 6.12.

$$
\begin{aligned}
2\pi\left(r_{eq}+(m-1)\,dr-\frac{dr}{2}\right)\frac{k_s}{dr}\;\left(T^p_{m-1}-T^p_m\right)\;+\\
2\pi\left(r_{eq}+(m-1)\,dr+\frac{dr}{2}\right)\frac{k_s}{dr}\;\left(T^p_{m+1}-T^p_m\right)\;=\\
\frac{\rho_s c_{p_s}}{\Delta t}2\pi\,dr\,\left(r_{eq}+(m-1)\,dr\right)\left(T^{p+1}_m-T^p_m\right)
\end{aligned}
\tag{6.12}
$$

Finally, for the last node ($m = n$), the energy balance is shown in Equation 6.13. The value of n depends on the size of the soil domain and dr. In this case, n takes a value of 199. To treat the soil as a semi-infinite solid, the last node (3 metres from the centre of the pipe) has no boundary condition at the outer radius.

$$
\begin{aligned}
2\pi\left(r_{eq}+(m-1)\,dr-\frac{dr}{2}\right)\frac{k_s}{dr}\;\left(T^p_{m-1}-T^p_m\right)=\\
\frac{\rho_s c_{p_s}}{\Delta t}2\pi\,dr\,\left(r_{eq}+(m-1)\,dr\right)\left(T^{p+1}_m-T^p_m\right)
\end{aligned}
\tag{6.13}
$$

Equations 6.9, 6.10, 6.11, 6.12 and 6.13 were simplified for numerical resolution as shown in Equations 6.14, 6.15, 6.16, 6.17 and 6.18.

$$
T^{p+1}_m=\left(1-2Fo_b A\right)T^p_m+2Fo\left(AT^p_m+\frac{q^p_r dr}{2\pi k_b\left(r_{eq}+\frac{dr}{4}\right)}\right)
\tag{6.14}
$$

$$T_m^{p+1} = (1 - 2Fo_b)\, T_m^p + Fo_b \left(1 - \frac{dr}{2B}\right) T_{m-1}^p + Fo_b \left(1 + \frac{dr}{2B}\right) T_{m+1}^p \tag{6.15}$$

$$T_m^{p+1} = DT_{m-1}^p + ET_{m+1}^p + (1 - D - E)\, T_m^p \tag{6.16}$$

$$T_m^{p+1} = (1 - 2Fo_s)\, T_m^p + Fo_s \left(1 - \frac{dr}{2B}\right) T_{m-1}^p + Fo_s \left(1 + \frac{dr}{2B}\right) T_{m+1}^p \tag{6.17}$$

$$T_m^{p+1} = (1 - 2Fo_s)\, T_m^p + Fo_s \left(1 - \frac{dr}{2B}\right) T_{m-1}^p \tag{6.18}$$

where:

$$Fo_b = \frac{k_b}{\rho_b c_{p_b}} \frac{dt}{dr^2};\quad Fo_s = \frac{k_s}{\rho_s c_{p_s}} \frac{dt}{dr^2};\quad A = \frac{4r_{eq} + 2dr}{4r_{eq} + dr};\quad B = r_{eq} + (m-1)\, dr;$$

$$C = \left[\frac{B - \frac{dr}{4}}{2Fo_b k_s} + \frac{B + \frac{dr}{4}}{2Fo_s k_b}\right];\quad D = \frac{B - \frac{dr}{2}}{Ck_s} \text{ and } \quad E = \frac{B + \frac{dr}{2}}{Ck_b}$$

In the explicit method, to determine the value of the temporal element (Δt) the condition of Equation 6.19 must be satisfied, so the temporal element Δt must be less than 162 s.

$$\min\left(Fo_b \leq \frac{1}{2} \; or \; Fo_s \leq \frac{1}{2}\right) \tag{6.19}$$

Finally, Table 6.4 shows all the input parameters used to solve the heat transfer problem using the finite difference method with heat flow as boundary condition (FDM-HF).

As in Section 6.3, sensors A and B were used to validate the FDM-HF. To deal with the impact of the multiple boreholes, spatial superposition was also applied. That is, the thermal response of the most influential boreholes in sensors A and B was superimposed, being the same as in Figures 6.6a and 6.6b. Although the numerical method is more complex to develop and code than analytical models, it has the advantage that it is fast to simulate. It allows, without major computational cost, the rapid simulation of the temporal response in

Table 6.4: Distance from neighbour boreholes to sensors

q_r= from experimental data in W/m	ρ_s= 1800 kg/m^3
dr= 0.015 m	c_{p_b}= 1250 J/kgK
r_{eq}= 0.03 m	c_{p_s}= 1200 J/kgK
Δt= 36 s	m= spatial element(1 to n)
k_b= 0.85 W/mK	p= temporal element(1 to 14169)
k_s= 1.5 W/mK	n= number of nodes (199)
ρ_b = 2500 kg/m^3	

hourly time steps for 199 radial nodes. The flowchart in Figure 6.17 shows the simulation process of the FDM-HF.

Figure 6.18 shows a comparison of the experimental data for the temporal temperature variation at sensor A with the data simulated by using the FDM method with variable heat flow (q_r) as boundary condition (FDM-HF). As seen in the figure, the FDM-HF method is a very accurate way to evaluate the temporal response of the soil when it is subjected to variable heat fluxes in the short term. The EF, $RMSE$ and R^2 of this data are 0.9795, 0.606 K and 0.98 respectively. Figure 6.19 shows the scatter plot that correlates the experimental data of the sensor A with the data estimated using the FDM-HF method. It can be seen that there is a good correlation between the simulated data and the experimental data.

Figure 6.20 shows the comparison between the temporal temperature variation of the experimental data of sensor B (borehole wall) and the data calculated using the FDM-HF. As in the application of the ILS and ICS models, in this model, the spatial superposition of neighbouring boreholes (Figure 6.6b) and the natural variation of soil temperature was applied. Once again, this model has better accuracy than the analytical models. The EF, $RMSE$ and R^2 are equal to 0.9653, 0.949 K and 0.9976 respectively. As shown, this method is more accurate than ILS and ICS models. Although several authors claim that numerical methods are less precise than exact (analytical) solutions, it is important to mention that there are no complete analytical solutions for borehole arrangements

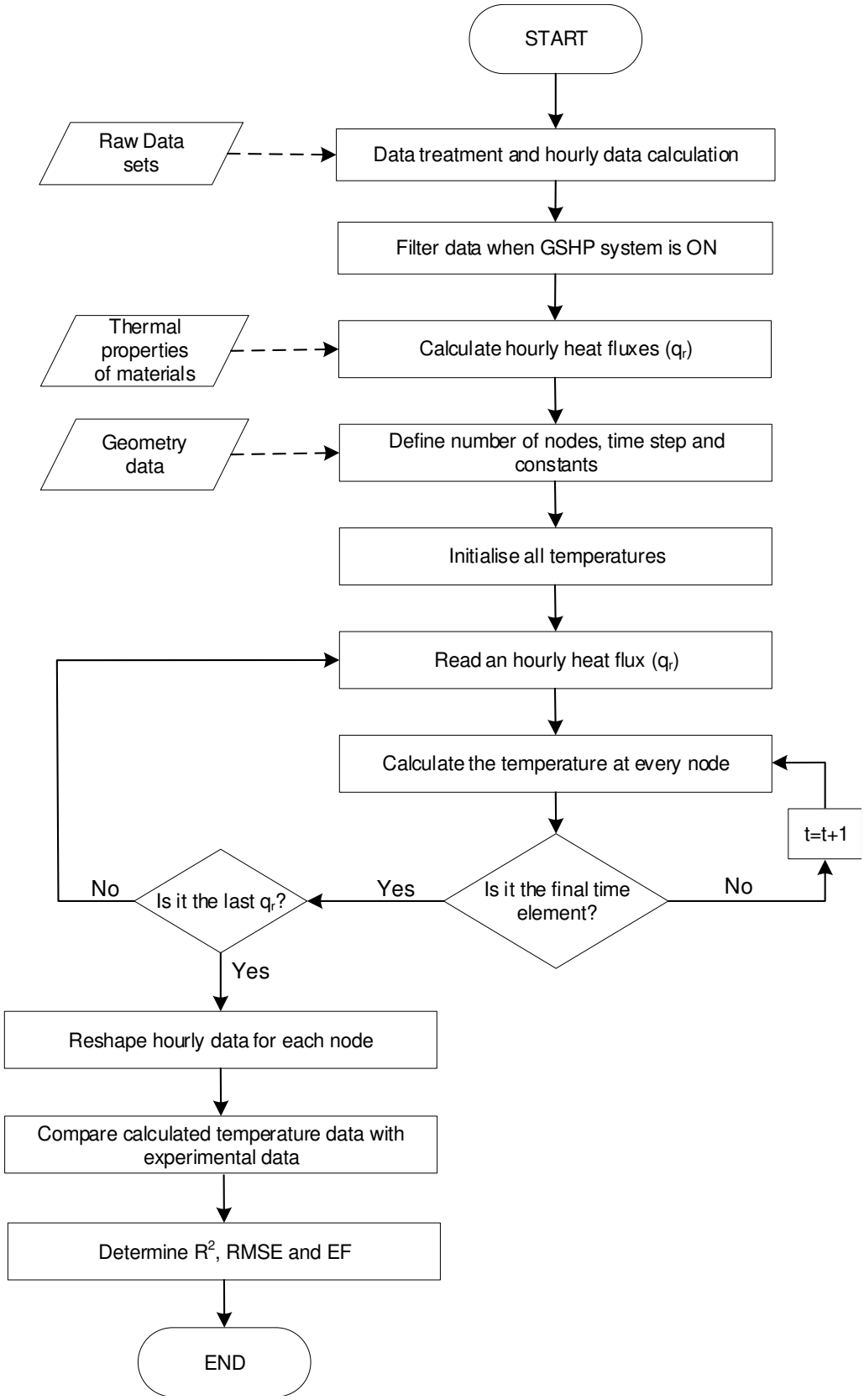

Figure 6.17: FDM-HF model flowchart

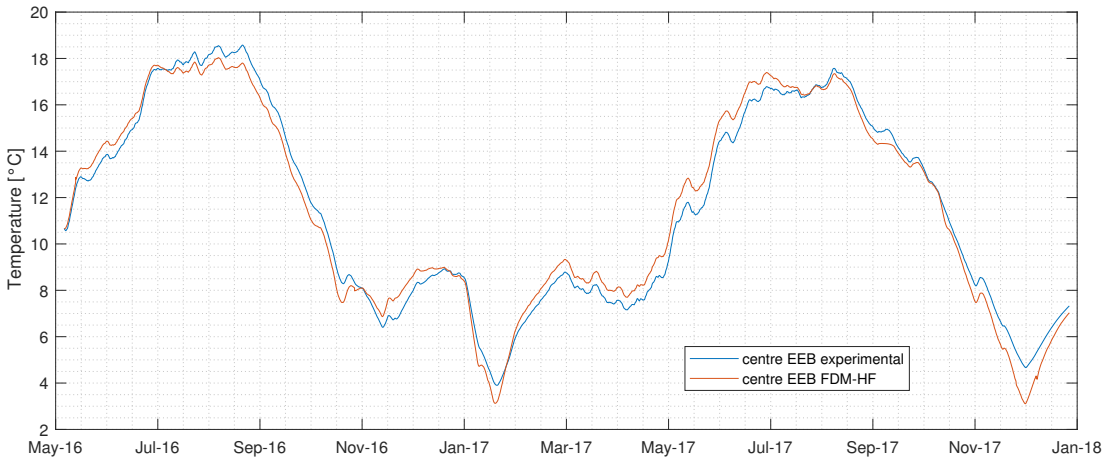

Figure 6.18: Sensor A temperature variation experimental vs FDM-HF model prediction

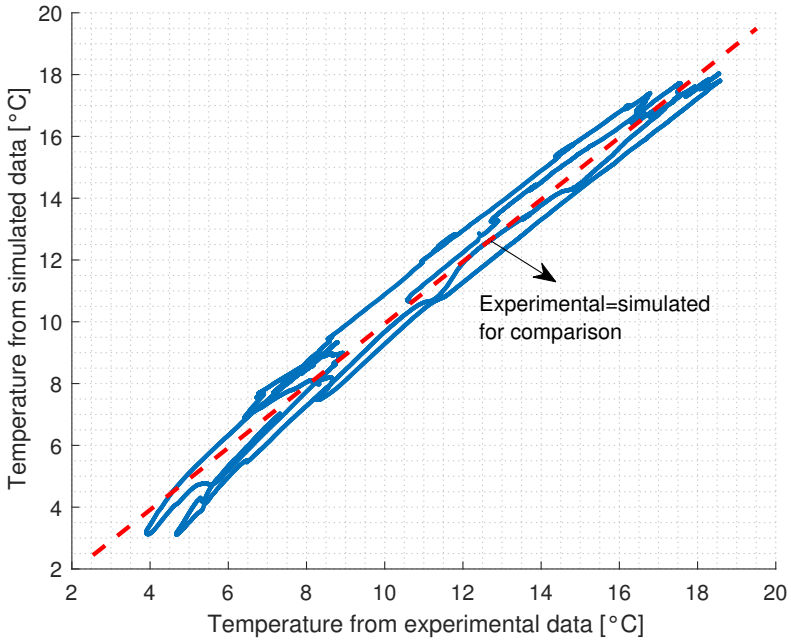

Figure 6.19: Scatter plot Sensor A experimental vs FDM-HF model prediction

that consider the backfill material and a temporal variation of heat flow. Therefore, numerical methods that consider these parameters may actually be more accurate than analytical methods for this type of analysis; and this is clearly demonstrated in the results obtained here. The superior accuracy is likely to be because the backfill material is considered here, although it is important to mention that consideration of the backfill material could also be a source of error if

there is uncertainty in the input data such as the thermal properties of the backfill material. Likewise, the consideration of the criterion of the equivalent radius and the application of the same heat flow to all the boreholes can introduce error. However, for the purpose of studying the temperature in the soil within EEB in the long term, these results are acceptable. Figure 6.21 shows the scatter plot that correlates the experimental data of sensor B with the data estimated by the FDM-HF, showing much better correlation than the analytical models.

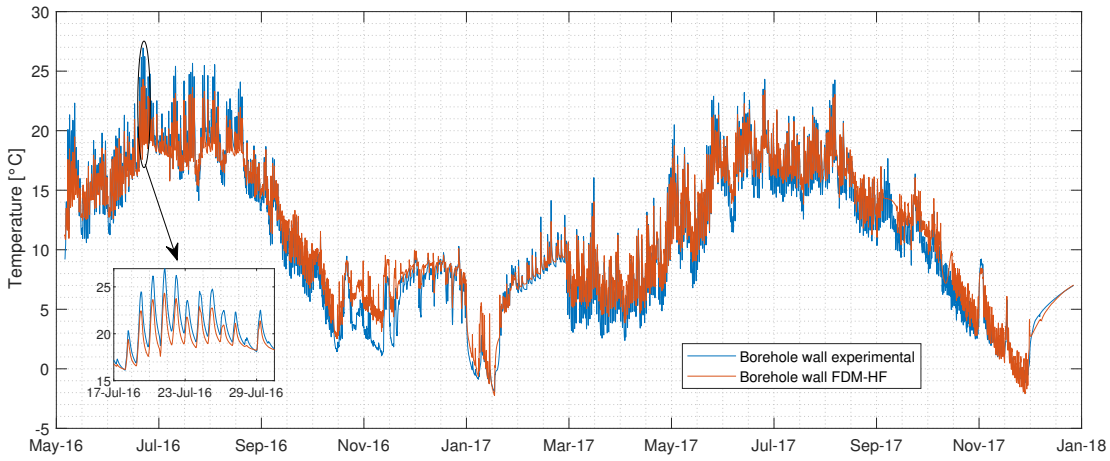

Figure 6.20: Sensor B temperature variation experimental vs FDM-HF model prediction

The FDM-HF is a comparable method with the ILS and ICS models since it has the same input parameters (heat flow) with the difference in the material of the backfill borehole. Undoubtedly, one of the limitations of the FDM-HF or any numerical model, in general, is the complex application and coding of the required equations (Equations 6.14 to 6.18). Being complex equations (discretisation of differential equations), coding errors and implementation are more difficult to identify. However, this method is also very advantageous compared to the analytical models. For instance, a greater number of radial analysis distances can be covered as well as the consideration of the backfill material in the simulation.

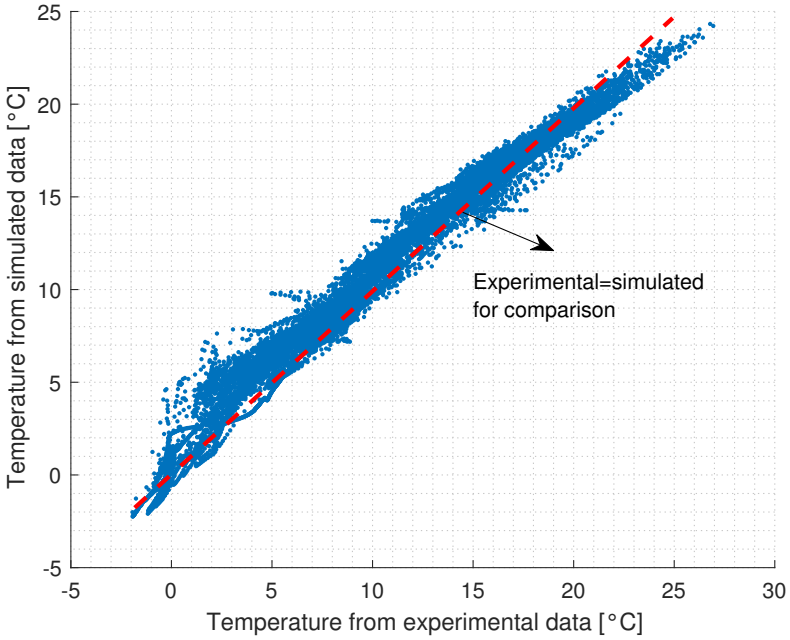

Figure 6.21: Scatter plot Sensor B experimental vs FDM-HF model prediction

6.4.2 Inlet fluid temperature as boundary condition

Figure 6.22 shows a scheme of heat transfer problem to be solved by the FDM with internal convection in the pipe with time-varying fluid inlet temperature (T_{fi}) as boundary condition (FDM-T). The fluid inlet temperature data are the experimental ones shown in section 6.2.2. As in the FDM-HF, this model also considers the backfill material and was solved by the explicit method. For the numerical resolution of the equations of the heat transfer problem, the same method of section 6.4.1 was used, and with similar input data. That is, Equations 6.14 to 6.18 were used. The heat flow in the pipe wall per metre (q_r) is equivalent to the heat flow by convection between the working fluid and the internal pipe wall per metre (q_{conv}). The main difference with the FDM-HF lies in the calculation of the fluid outlet temperature (T_{fo}) with which the heat flow in the pipe wall is determined (q_r). In this case, T_{fo} is calculated by studying the GHE as a heat exchanger subject to a constant surface temperature boundary condition (although variable in hourly time steps), as shown in Figure 6.23. The surface temperature (T_s) is the value taken by the temperature of node 1 and is equivalent to the wall temperature of the pipe of the equivalent radius (Equation

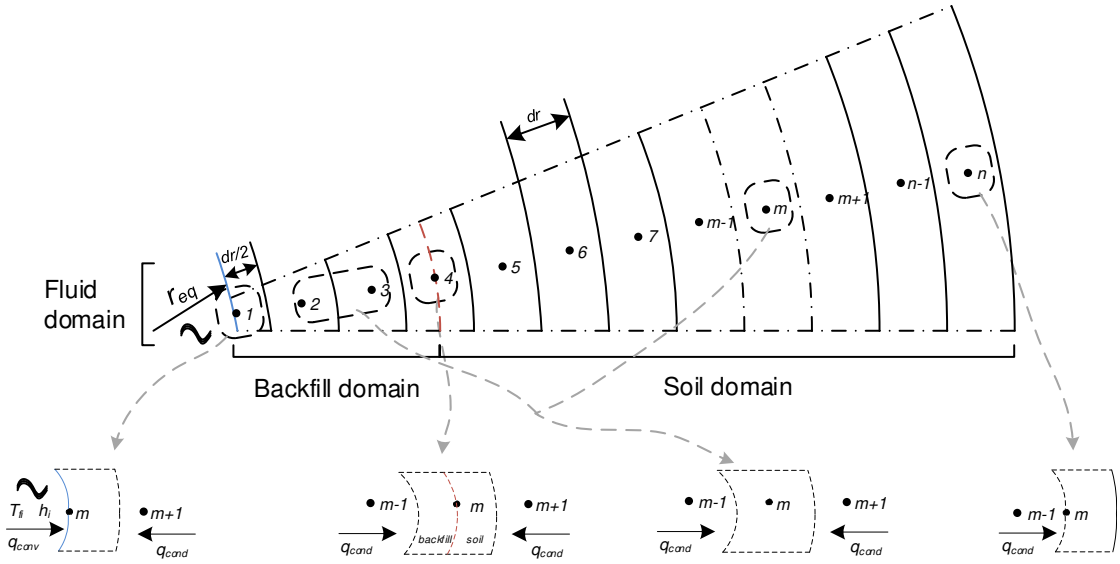

Figure 6.22: Schematic of the heat transfer problem for the FDM-T

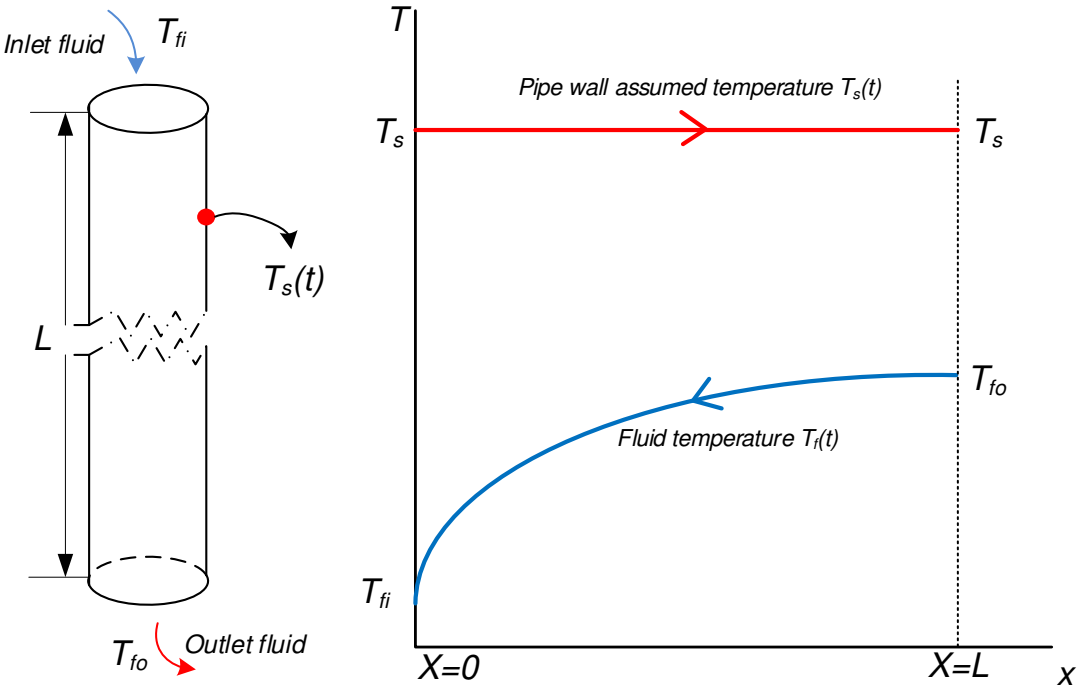

Figure 6.23: Schematic of the fluid temperature variation along the length of the GHE

6.14). T_s is calculated with the heat flux (q_r) of the previous time interval and is assumed to be constant during the time interval of analysis (1 hour). From this temperature, and knowing the fluid inlet temperature (T_{fi}), the fluid outlet temperature can be determined as indicated in Equation 6.20 [81]. Finally, the heat flux (q_r) of the next time interval is calculated using Equation 6.21.

$$T_{fo}^{p+1} = T_s^{p+1} - \left(T_s^{p+1} - T_{fi}^{p+1}\right) \exp\left(\frac{UA_T}{\dot{m}_{ghe}^{p+1} c_{p_f}}\right) \tag{6.20}$$

$$q_r^{p+1} = \dot{m}_{ghe}^{p+1} c_{p_f} \left(T_{fo}^{p+1} - T_{fi}^{p+1}\right) \tag{6.21}$$

In Equation 6.20, U represents the global heat transfer coefficient, which is the inverse of the total thermal resistance (R_{TOT}). For the present study, since the conduction resistance of the pipe wall is very small (0.000059 mK/W) compared to the convection resistance between the fluid and the internal pipe wall (0.11 mK/W in average), U is only equivalent to the convection heat transfer coefficient h_i (Equation 6.22) [81].

$$U = h_i = \frac{Nu_D k_f}{D_i} \tag{6.22}$$

In Equation 6.22, k_f is the thermal conductivity of the working fluid (glycol 30% by volume), D_i is the internal diameter of the pipe and Nu_D is the Nusselt number (Equation 6.23). More information on the process of calculating the heat transfer coefficient by convection can be found in [81].

$$Nu_D = \begin{cases} 3.66, & \text{for laminar flow} \\ 0.023 Re_D^{4/5} Pr^n, & \text{for turbulent flow} \end{cases} \tag{6.23}$$

where:

$$Re_D = \frac{4\dot{m}_{ghe}}{\pi D_i \mu}\ ; \quad n = \begin{cases} 0.4, & \text{for heating} \\ 0.3, & \text{for cooling} \end{cases}$$

Also, in Equation 6.20 A_T represents the area of contact of the fluid with the GHE along the internal pipe as shown in Equation 6.24, where L is the total length of the pipe and equal to 35 m (see section 6.2.1)

$$A_T = 2\pi\, r_{eq} L \tag{6.24}$$

Finally, Table 6.5 shows all the input parameters used to solve the heat transfer problem using the finite difference method with internal convection in the pipe as boundary condition (FDM-T).

Table 6.5: Input parameters for the FDM-T (Equations 6.14 to 6.24)

T_{fi}= from experimental data in °C	ρ_s= 1800 kg/m^3
dr= 0.015 m	c_{p_b}= 1250 J/kgK
r_{eq}= 0.03 m	c_{p_s}= 1200 J/kgK
Δt= 36 s	c_{p_f}= 3768.1 J/kgK
k_b= 0.85 W/mK	m= spatial element(1 to n)
k_s= 1.5 W/mK	p= temporal element(1 to 14169)
k_f= 0.485 W/mK (mean)	n= number of nodes (199)
ρ_b= 2500 kg/m^3	D_i= 0.06 m
L= 35 m	Pr= Prandlt number in data sets
$\dot{m}_{ghe}$= from experimental data in kg/s	μ= 0.0028 kg/ms (mean)

As for the previous models, sensors A and B were used to validate the FDM-T. To deal with the impact of multiple boreholes, spatial superposition technique was applied similar to the other studied models. The flowchart in Figure 6.24 shows the simulation process by using the FDM-T.

Figure 6.25 shows the temporal temperature variation of the experimental data of sensor A and the temperature calculated from the FDM with internal convection within the pipe as a boundary condition (FDM-T). The figure shows that the FDM-T overestimates the injection of heat into the soil and estimates higher temperatures in the soil during the heat injection period (summer). The EF, $RMSE$ and R^2 of these data are equal to 0.9319, 0.757 K and 0.969 respectively. As shown, this method is less accurate than ILS, ICS and FDM-HF to predict the temperature of the centre of the EEB. This discrepancy with the experimental data can be caused by the uncertainty that exists when using a greater number of input parameters in the FDM-T. Moreover, since it is a 16-borehole series configuration, the treatment of the fluid when connecting boreholes, generates a greater degree of uncertainty than when dealing with parallel configurations. This may be because, in the series configuration, the fluid has a longer residence time between the inlet and the outlet causing variation in the boundary conditions along the pipe which have a greater impact on the calculation of the fluid

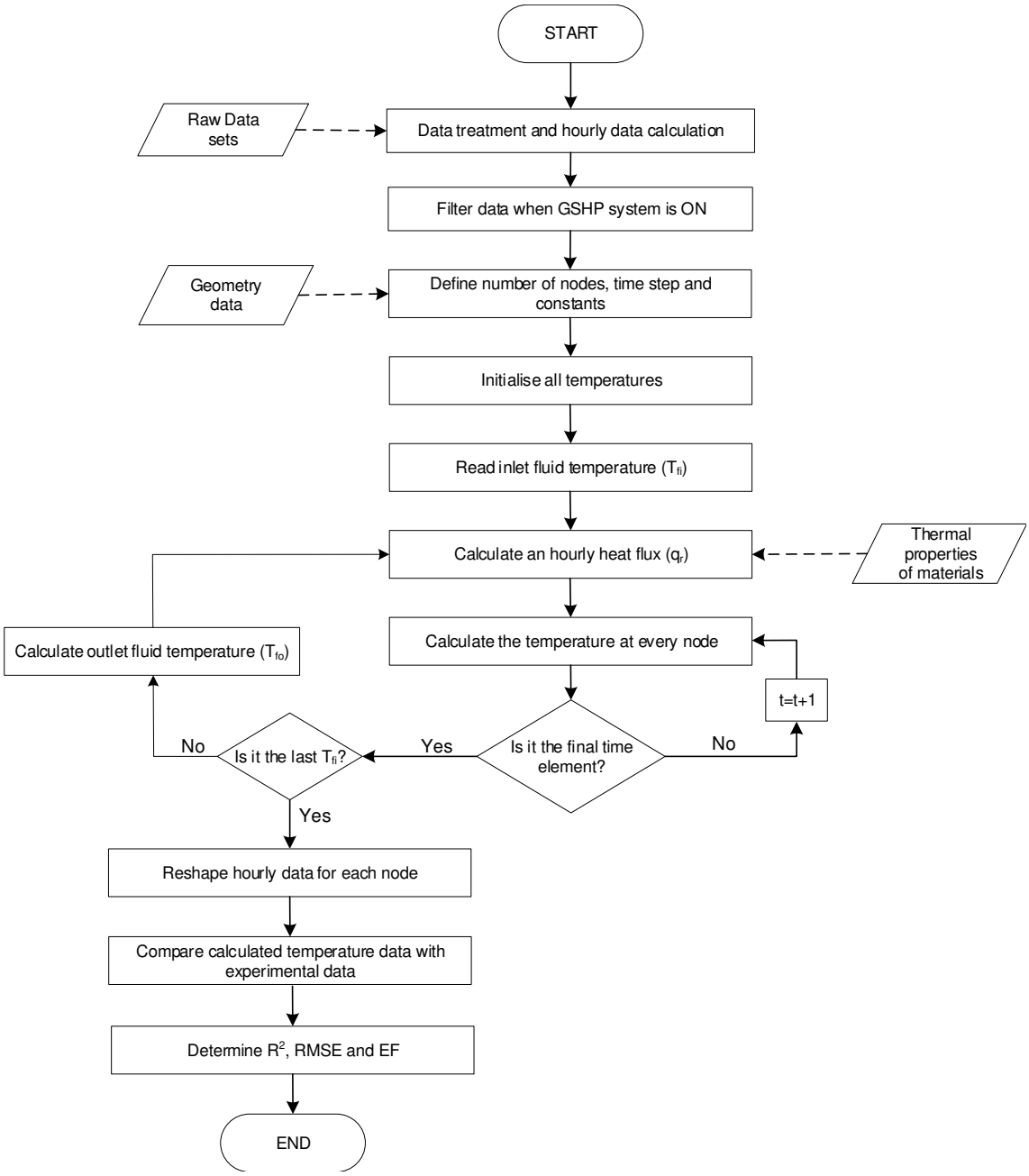

Figure 6.24: FDM-T model flowchart

outlet temperature. On the other hand, in parallel configurations, the inlet and outlet temperature are the same for all boreholes, so the residence time of the fluid is shorter, and this leads to fewer errors in the calculations. Figure 6.26 shows the scatter that correlates the experimental data of sensor A with the data estimated by the FDM-T.

Figure 6.27 shows the comparison of the temporal temperature variation of the sensor B (borehole wall) experimental data and the data calculated by the

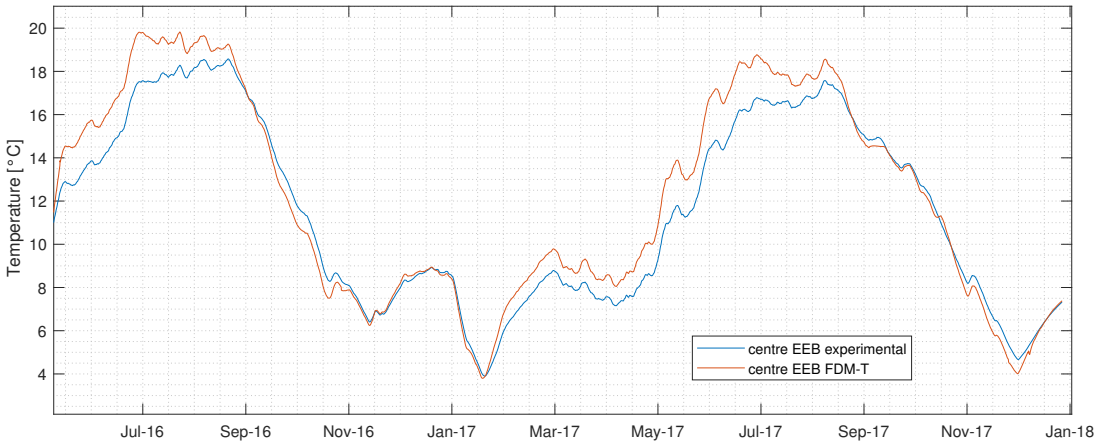

Figure 6.25: Sensor A temperature variation experimental vs FDM-T model prediction

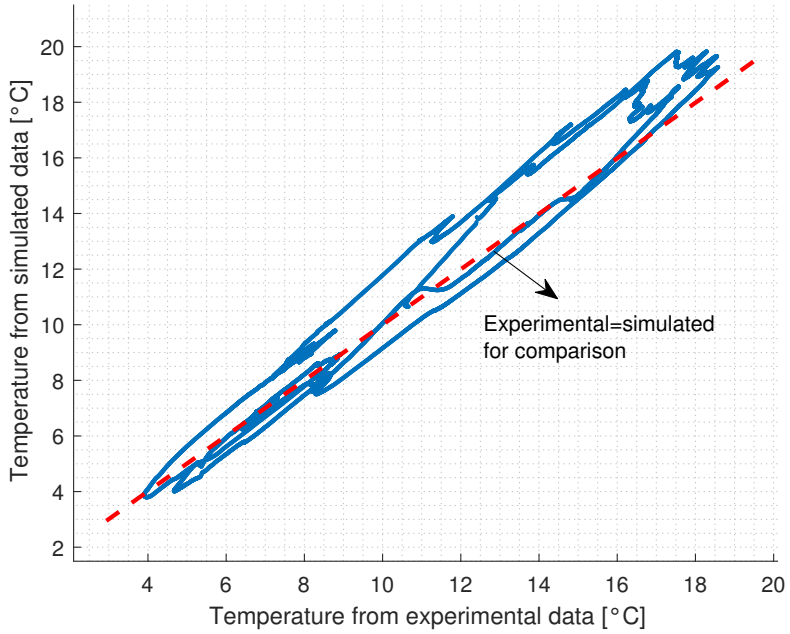

Figure 6.26: Scatter plot Sensor A experimental vs FDM-T model prediction

FDM-T. As for sensor A, this model has a greater error than the FDM-HF. However, it has better accuracy than the ILS and ICS models. The EF, $RMSE$ and $R2$ are equal to 0.9343, 0.84 K and 0.981 respectively. Again, the higher error when comparing with the FDM-HF is due to the greater uncertainty of the input data and the fact of the complexity of the serial model with variable boundary conditions. However, the smaller error when comparing it with the ILS and ICS

models is due to the fact that in the FDM-T the backfill material is considered, which best approximates reality when compared to the analytical models. Likewise, the consideration equivalent radius criterion leads to an increase in the error. Figure 6.28 shows the scatter plot that correlates the experimental data of sensor B with the data estimated by the FDM-T, showing a better correlation than the analytical models.

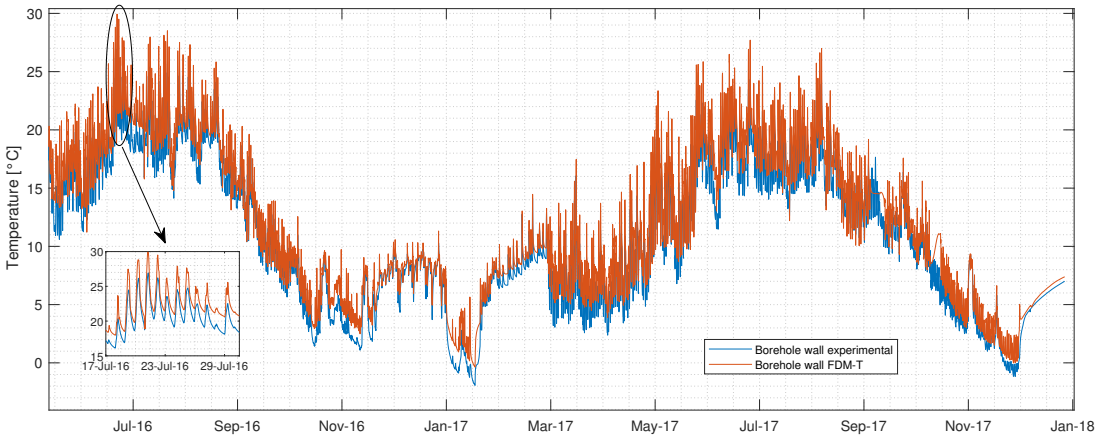

Figure 6.27: Sensor B temperature variation experimental vs FDM-T model prediction

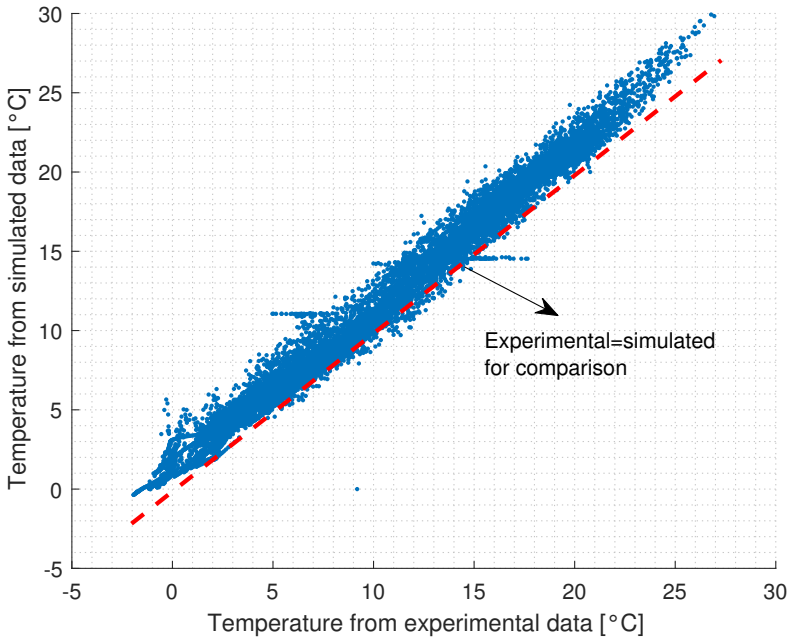

Figure 6.28: Scatter plot Sensor B experimental vs FDM-T model prediction

An important characteristic of the FDM-T model is that it is the only one of the models studied that allows an estimation of the fluid outlet temperature (T_{fo}) of the GHE, without knowledge of the heat flow (q_r). That is, this model only requires knowledge of the fluid inlet temperature (T_{fi}) and from this, the other parameters can be estimated.

In this context, the model was also validated with experimental data on the outlet fluid temperature of the GHE. Figure 6.29 shows the comparison of experimental outlet fluid temperature data and those calculated using the FDM-T model. The EF, $RMSE$ and R^2 are equal to 0.9593, 1.84 K and 0.96 respectively. The discrepancy increases in the shoulder months (spring and autumn). The intermittency between injection and heat extraction in the transition stages can affect the increase in error since such intermittences can occur at intervals shorter than one hour. Figure 6.30 shows the scatter plot that correlates the experimental data of the fluid outlet temperature with the data estimated by the FDM-T. It can be seen that there is a higher dispersion in temperature values between 10 and 20°C that are typical of the transition period.

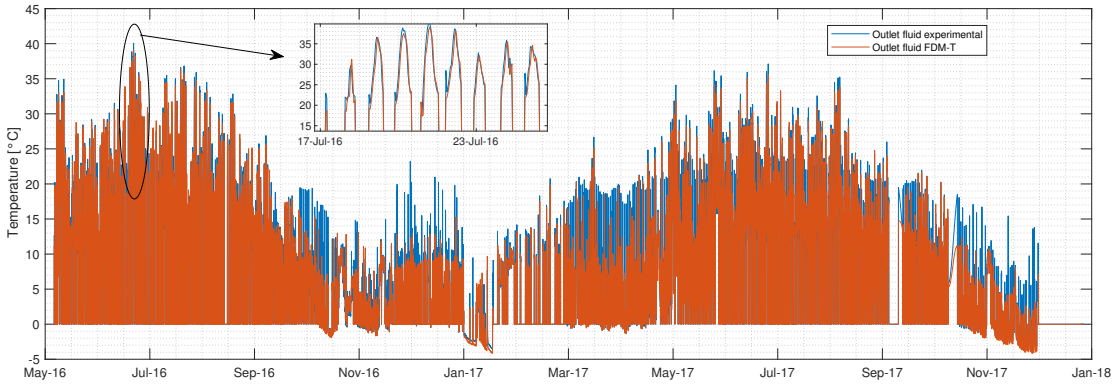

Figure 6.29: Outlet fluid temperature variation experimental vs FDM-T model prediction

Due to the increased intermittency in the transition periods, the fluid outlet temperature data were analysed on a daily time scale instead of hourly showing a significant improvement in the model accuracy. Figure 6.31 shows the comparison of the average daily data of the experimental GHE fluid outlet temperature and those calculated using the FDM-T. In this case, the EF, $RMSE$

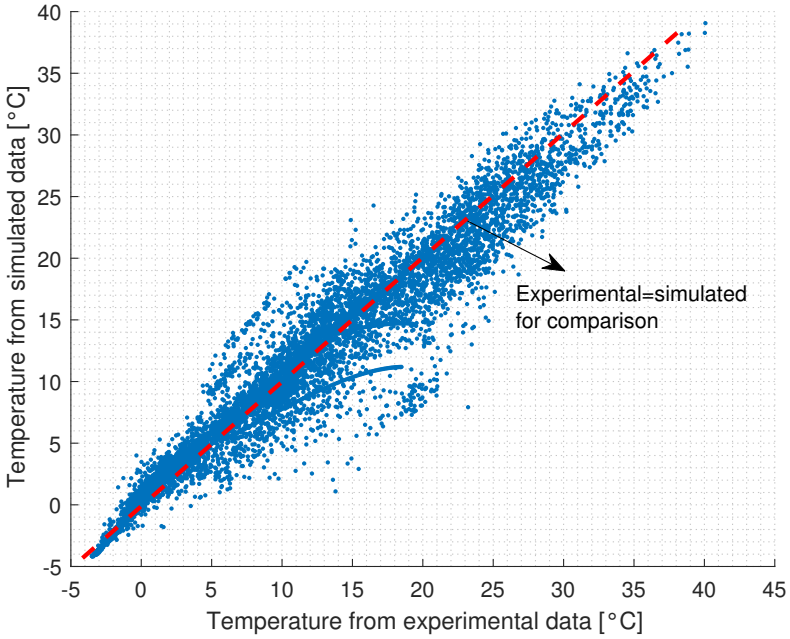

Figure 6.30: Scatter plot outlet fluid temperature experimental vs FDM-T model prediction

and R^2 are equal to 0.9905, 0.501 K and 0.992 respectively. This shows that the model presents a very good accuracy when increasing the study time interval as evidenced in the scatter plot of Figure 6.32.

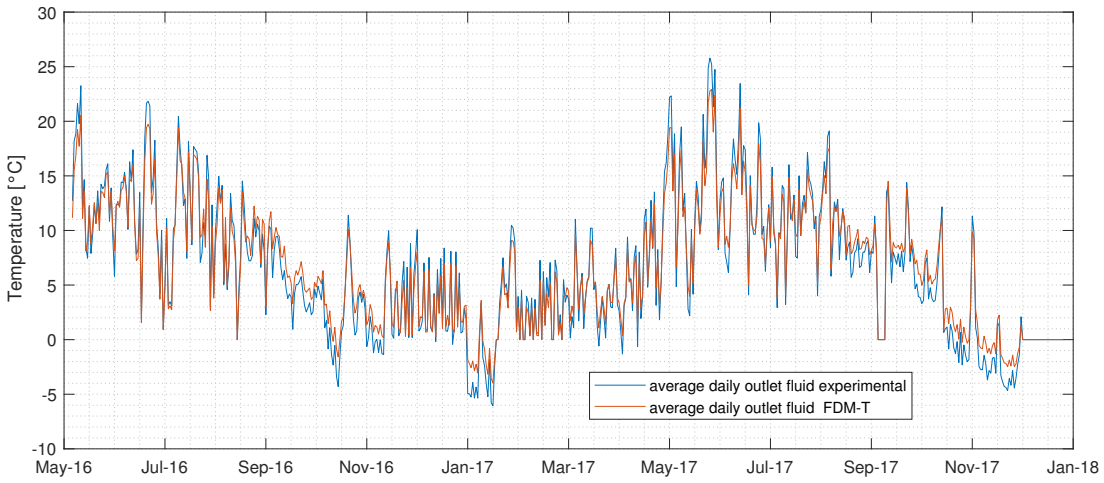

Figure 6.31: Daily average outlet fluid temperature variation experimental vs FDM-T model prediction

It has been demonstrated that the finite difference method using internal

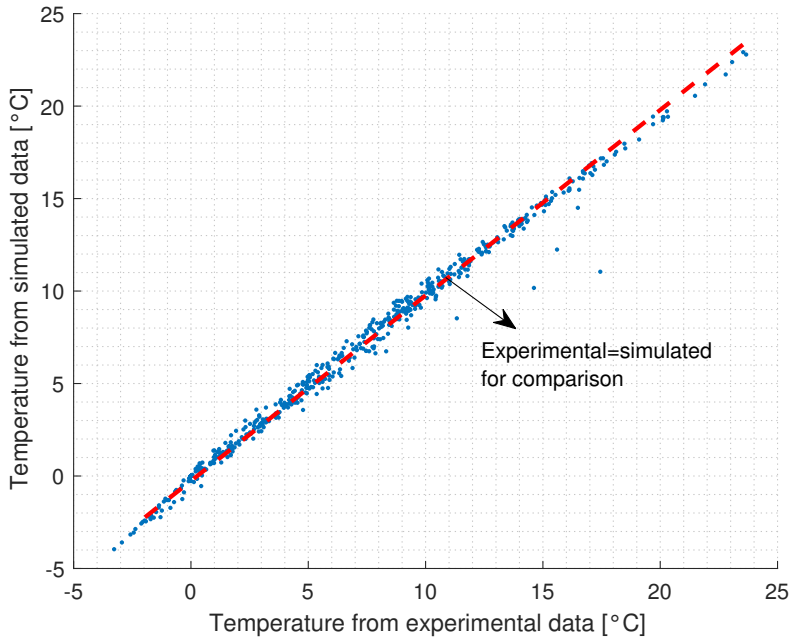

Figure 6.32: Scatter plot daily average outlet fluid temperature experimental vs FDM-T model prediction

convection in the pipe as a boundary condition has lower accuracy than the ILS and ICS analytical models and that the FDM-HF to determine the thermal response of the soil in the EEB centre. However, it has better accuracy than analytical models (ILS and ICS) to estimate the temperature at the borehole wall. Likewise, this model has the advantage of being able to estimate the fluid outlet temperature from the knowledge only of the fluid inlet temperature in the GHE. This gives an advantage in terms of the application of this model since it is not necessary to know in advance the heat extraction/injection rate from/to the soil. In fact, the heat flow can be calculated based on the total length of the GHE. For this reason, this model not only serves to study in greater detail the thermal performance of the GHE but also for its sizing the length of it which is a great plus in solar-assisted systems where the fluid inlet temperature depends on the solar thermal system.

In addition, this model would allow studying the application of different technologies of solar collectors and heat pumps since these components determine the inlet temperature of the fluid in the GHE. Undoubtedly, this opens the way to future research of shallow geothermal boreholes coupled to differ-

ent types of technologies for large-scale optimisation. The disadvantage or limitation of the FDM-T is the complex application and coding of the required equations that are even more complex than those required in the FDM-HF. This increases uncertainty as there is a higher number of input parameters, which increases the possibility of coding errors.

6.5 Comparison in the simulation time of the different models

Analytical models (ILS and ICS) are of simpler application and coding than numerical models. However, on of the most important limitations found on these models is not the error when used to estimate the temperature at the borehole wall, but the high computational cost. The application of the temporal superposition technique using hourly intervals and a variable thermal load means that the calculation of the temperature at a single point demand more simulation time compared to using constant heat flow. This highly increases the computational cost for a long-term analysis compared to the numerical methods (FDM-HF and FDM-T).

For this research, a personal computer with an eighth-generation Core i7 processor with 8 cores running at 1.8 GHz was used for all the simulations performed. Regarding the ILS model, to calculate the data shown in Figures 6.7 and 6.9, which used hourly thermal loads as input parameter, it was needed a computation time of 2 hours. For the ICS model, the computational cost was even higher, as mentioned above (section 6.3.2), due to the high computational cost the thermal loads had to be daily averaged in order to simulate the long-term performance. However, even with the reduction on the number of thermal loads, to obtain the data shown in Figures 6.11 and 6.13, the simulation time was of 4 hours. For this reason, analytical models are not suitable for long-term analysis of the thermal response of boreholes subjected to variable thermal loads in the short term.

On the other hand, by using the numerical models, the computation time was considerably reduced. In fact, to solve the FDM-HF and obtaining the results of

Figures 6.18 and 6.20, the computation time was less than 15 seconds. This time was enough to get the thermal response in a radius of 3 metres from the centre of the pipe in each of the 199 nodes (dr=0.015 m) subjected to hourly variable thermal load (14169 input data). Similarly, to solve the FDM-T and obtaining the hourly results of Figures 6.25 and 6.27, the computation time took less than 17 seconds. These findings, undoubtedly, make the use of numerical methods a good alternative to analytical models, mainly for long-term and parametric studies where different scenarios and multiple simulations must be carried out.

6.6 Summary of the chapter

In this chapter, which is the core of all the research, different models were studied to evaluate the thermal performance of the shallow borehole heat exchanger. The main idea of this chapter is to develop a model that is accurate enough from a practical approach to study the short- and long-term thermal response of vertical boreholes near the soil surface. The main challenge to achieve the objective is that the soil cannot be considered as undisturbed as seasonal variations cannot be neglected. On the other hand, the consideration of a multiple borehole system subjected to hourly variable thermal load (with injection and heat extraction) makes the development of the model even more challenging.

Initially, conventional analytical methods such as the ILS model and the ICS were modelled. To deal with multiple boreholes and hourly thermal loads, temporal and spatial superposition technique was used. Although these models are of a relatively simple application, the fact of using the temporal superposition considerably increased the simulation time, hence these models are inappropriate for long-term studies. In fact, the ICS model could not be simulated at an hourly time step due to the high computational cost and had to be simulated at a daily time step. In addition, since these models do not consider the borehole backfill material, they show a higher error to evaluate the temperature in the borehole wall as shown in Table 6.6.

On the other hand, the GHE modelling was also studied using the numerical method of finite differences (FDM) using heat flow in the radial direction in the

pipe wall (FDM-HF) and internal convection in the pipe (FDM-T) as boundary conditions. The results show that these methods, despite being more complex in their application, are more accurate and quicker to simulate. Therefore, they are more appropriate for the long-term study of these types of systems. Table 6.6 shows a comparison of the different analytical and numerical methods in terms of their accuracy, complexity and simulation time.

Table 6.6: Summary of the accuracy, complexity and simulation time of the different models

Model	**Point of calculation**	**EF**	**RMSE [K]**	**R^2**	**Complexity**	**Simulation time**
ILS	Sensor A	0.956	0.56	0.983	Low	2 hours (hourly)
	Sensor B	0.899	1.59	0.933		
ICS	Sensor A	0.956	0.56	0.983	Medium	4 hours (daily)
	Sensor B	0.859	1.78	0.913		
FDM-HF	Sensor A	0.98	0.61	0.98	High	15 seconds (hourly)
	Sensor B	0.965	0.95	0.998		
FDM-T	Sensor A	0.932	0.76	0.969	High	17 seconds (hourly)
	Sensor B	0.934	0.84	0.981		
	Outlet fluid temperature	0.959	1.84	0.96		

With these results, it can be shown that the main objective of this research is achieved since an accurate and efficient model has been developed that allows the study of shallow ground heat exchangers in both the short and long term. This opens many doors for future research by applying this model in different contexts. For example, the model can be used to design this type of system based on the thermal loads of a building. But one can also go further and evaluate different solar collector technologies to study their effect on seasonal storage. Also, this model could be included in transient simulation software such as TRNSYS or Modelica and coupled to other components like heat pumps, solar collectors to make a more complete optimisation study of different control

strategies.

7. Thermal performance of very shallow boreholes in vertical ground heat exchangers

In Chapter 6, two numerical models were developed using the finite difference method to model a very shallow geothermal heat exchanger more quickly and accurately. In this chapter, the previously developed models are applied and studied. First, the long-term thermal behaviour of the very shallow geothermal heat exchanger (GHE) is studied. Then the thermal response of the soil and the borehole wall is discussed under different values of thermal conductivity of the soil and grouting material. Finally, dimensionless temperature response graphs (G-functions) are proposed to study very shallow vertical boreholes in the short and long term. The graphical representations known as G-functions are widely used to study the thermal response of GSHP systems without the need for developing complex mathematical models.

7.1 Long-term analysis

In this section, the thermal behaviour of the EEB in the long term is studied. For this, the finite difference method (FDM-HF) was used with the heat flow rate in the pipe wall considered as a boundary condition, as described in section 6.4.1. The thermal properties of the soil and the grouting material, as well as the configuration of the ground heat exchanger (GHE) used in this study were the same as the experimental system described in Chapter 4 (Section 4.1.3). The thermal behaviour of the EEB was studied by considering a 16-year scenario that gives enough time to analyse the trend of the EEB thermal response. Three different scenarios were analysed. The first case considered both heat injection and extraction, that is, the EEB has solar heat injection (mainly in summer) and heat

extraction (in winter). The thermal load imposed was the experimental load of the year 2017 repeated for 16 consecutive years. The second case considered that the system only works in heat extraction mode and there is no heat injection from the solar system. This was conducted to study how the EEB would operate if the system does not have solar assistance. For this, the thermal load imposed was the experimental load of the year 2017 (repeated for 16 years) but only considering the heat extraction loads. Finally, in order to study the behaviour of EEB in terms of seasonal heat storage, the thermal response of the soil was studied in the long term when heat is only injected into the soil, and there is no heating extraction. For this, the experimental thermal load of the year 2017 (repeated for 16 years) was imposed considering only the heating injection loads. It is important to mention that, as the loads were repeated from experimental data, any data anomaly, like the period when the system was off, was also repeated.

7.1.1 Heat injection and extraction

Figure 7.1b shows the thermal load imposed for the long-term analysis of the EEB. The thermal load used in the simulation corresponds to the experimental heat flow per unit length (in metres - see section 6.2.1) for 2017 (Figure 7.1a) repeated for 16 years. As seen in the figure, there is heat injection from the solar PVT system (negative loads) and heat extraction through the geothermal heat pump (positive loads). The FDM-HF model (section 6.4.1) was used, and the thermal response was studied at the centre of the EEB and in the borehole wall at one-metre depth. These two points of analysis are enough to get a clear idea of the thermal behaviour of the EEB in the short and long term as mentioned in section 6.3.1. Moreover, the thermal response of the centre of the EEB indicates the average thermal response of the entire storage and heat extraction volume, while the thermal response of the borehole wall indicates the short-term variations that directly affect the performance of the heat pump [95].

Figure 7.2 shows the thermal response of the centre of the EEB in the long-term considering heat injection and extraction throughout each year. As seen in the figure, the centre of the EEB shows stable thermal behaviour in the long term where the highest and lowest temperatures are 18°C and 3°C respectively.

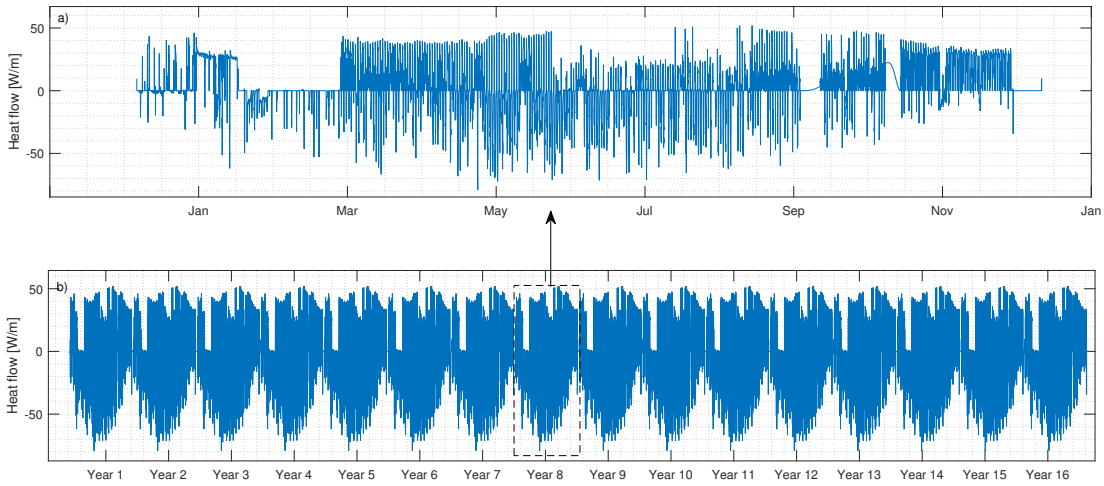

Figure 7.1: Long-term heat flow rate with heat injection and extraction

It is important to mention that over the whole year, there is a small annual imbalance between the net heat injected and extracted. In this case, there is more heat extraction than heat injection in the annual balance. Therefore, in the long term the average temperature of the centre of the EEB would be lower than the average temperature of the natural soil at the same depth. In fact, the average temperature of the centre of the EEB is 11.11°C while the average temperature of the natural soil at the same depth is 12.32°C. Due to this temperature difference, there is a higher gradient of temperature (more than natural) between the centre of the EEB and the surrounding soil. Consequently, there will be a higher heat transfer rate coming from the bottom of the EEB.

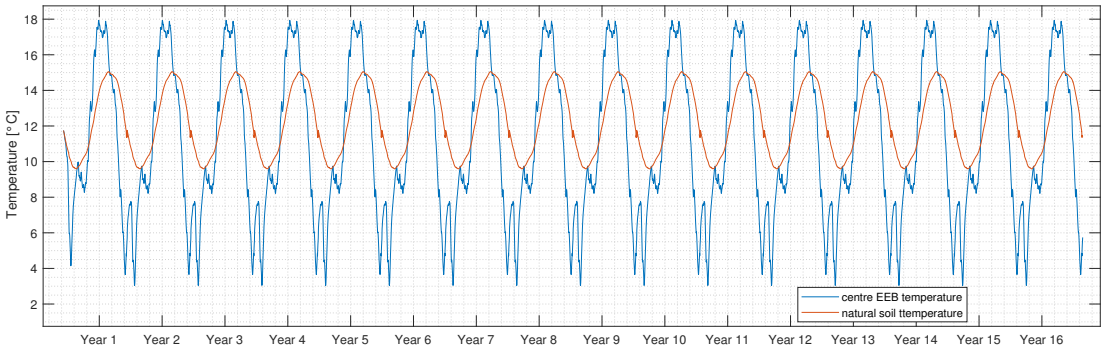

Figure 7.2: Long-term temperature variation at the centre of the EEB with heat injection and extraction

On the other hand, Figure 7.3 shows the variation of the temperature of the borehole wall in the long term when the GHE is subjected to heat injection and extraction loads. As in the centre of the EEB, it can be noted a stable thermal behaviour. However, due to the net heat imbalance, the average temperature of the long-term borehole wall temperature (10.63°C) is lower than the natural soil at the same depth (12.32°C). In this context, when the predominant load is that of extraction, the borehole wall might have low temperatures in winter which might affect the heat pump performance.

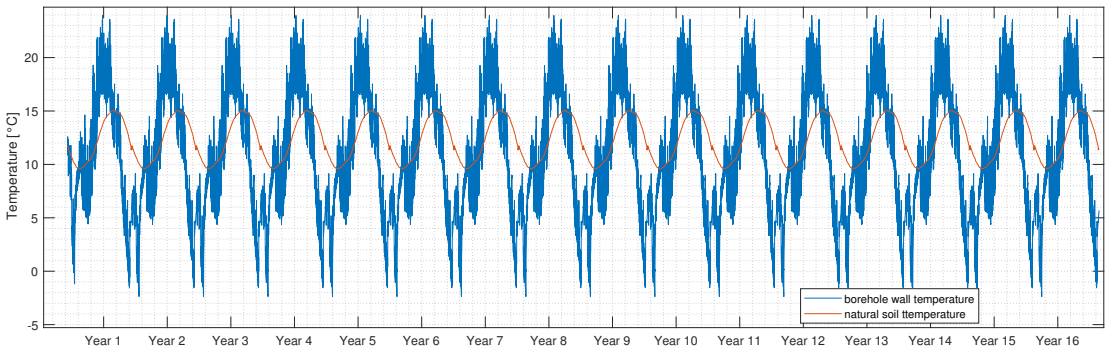

Figure 7.3: Long-term temperature variation at the borehole wall with heat injection and extraction

According to the results shown previously, one can question that, if the dominant load is heat extraction, it would be logical for the average temperature to decrease over the time in the long-term. This is particularly true during the transient period. However, as soon as the heat transfer medium reaches steady state conditions the temperature variation remain constant. This can be seen in Figure 7.4 which shows the thermal response of the EEB soil using the Finite Line Source (FLS) method [108] explained in section 2.3.2. The absolute temperature variation (dT) is negative when heat is extracted or positive when heat is injected. The figure shows the temperature change of the EEB at different radial distances when it is subjected to a constant heat rate of 2.1 W/m which is the annual net heat imbalance. For instance, in Figure 7.4 (in logarithmic scale), the temperature in the borehole wall (r= 0.075 m) stabilises before 3000 hours and that the decrease in temperature (with respect to the initial temperature) is 0.46 K. This shows that the EEB would reach its stable state in less than 3000 hours

or approximately 4 months (yellow zone in Figure 7.4).

However, the stabilisation temperature and time will depend not only on the total amount of heat extracted, but also in the length of the borehole. The shorter the borehole the lower the temperature change. Figure 7.5 (in logarithmic scale) shows, as an example, the temperature variation of the borehole wall for a 1.5-metre depth borehole by using the model developed in this research (FDM-HF). A constant heat extraction load of 2.1 W/m was simulated, and the variation in the borehole wall temperature was determined in the long term. It can be evidenced that initially the temperature of the borehole wall has a temperature drop of up to 0.5 K and reaches the maximum temperature difference (dT) in time lower than 3000 hours (yellow zone) and from that moment the temperature change (dT) stabilises in the long-term.

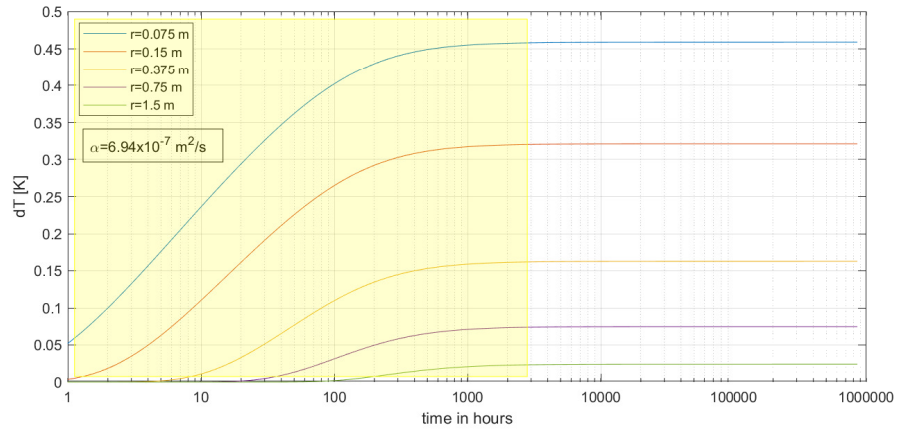

Figure 7.4: Long-term temperature variation at different radial coordinates by using the FLS model with a constant heat extraction rate

In the long-terms graphs (Figure 7.2 and Figure 7.3), the highest temperature change occurs during the first year (approximately four months) and from that moment steady state conditions are reached.

7.1.2 Heat extraction only

Figure 7.6b shows the thermal load imposed for running the model (FDM-HF) to study the thermal behaviour of EEB in the long term subjected to heat extraction only. The data used for the simulation of the model correspond to the experimental heat flow rate data for 2017 discarding the heat injection loads

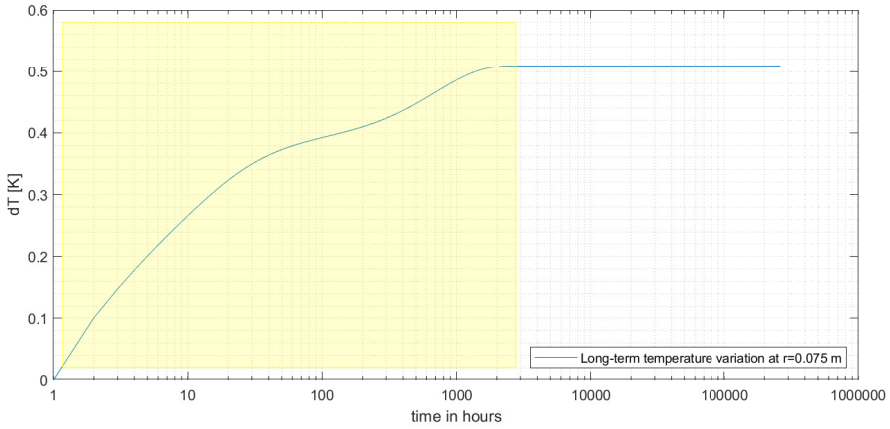

Figure 7.5: Long-term temperature variation at r=0.075 m by using the FDM-HF model with a constant heat extraction rate

(Figure 7.6a). This case is analysed to estimate the thermal behaviour of the EEB in a system that has no solar heat input or solar thermal storage, that is, for a conventional GSHP system. It is important to analyse this case to get insights of how a system with no storage or heat recovery performs.

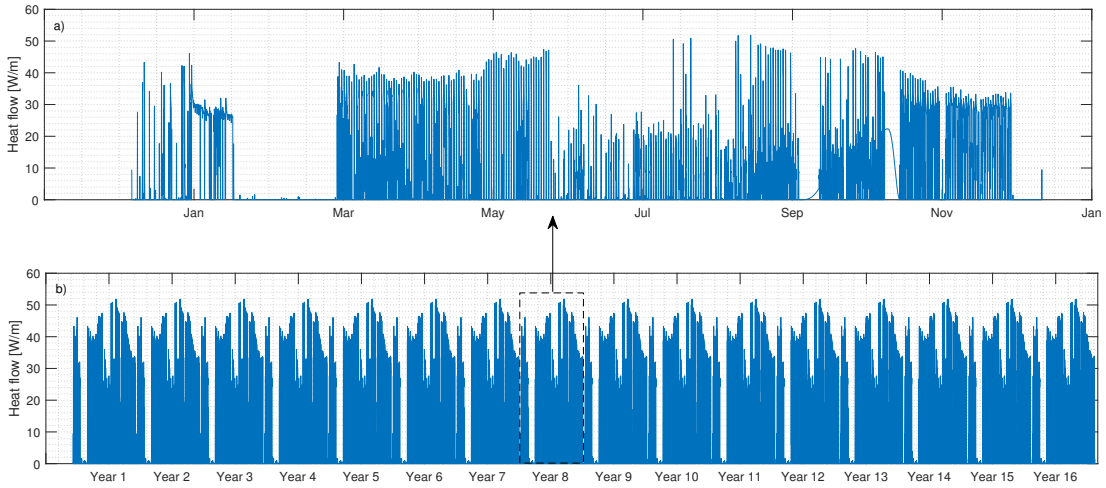

Figure 7.6: Long-term heat flow rate with heat extraction only

Figure 7.7 shows the thermal performance of the centre of the EEB when it is subjected to heat extraction for 16 years. The average long-term temperature of the centre of the EEB is 8.15°C which is 4.17 K lower than the average natural soil temperature at the same depth. This decrease in the average temperature cannot be recovered by the natural recovery during summertime. Hence, the

EEB might have a low temperature for an optimal heat pump operation during winter.

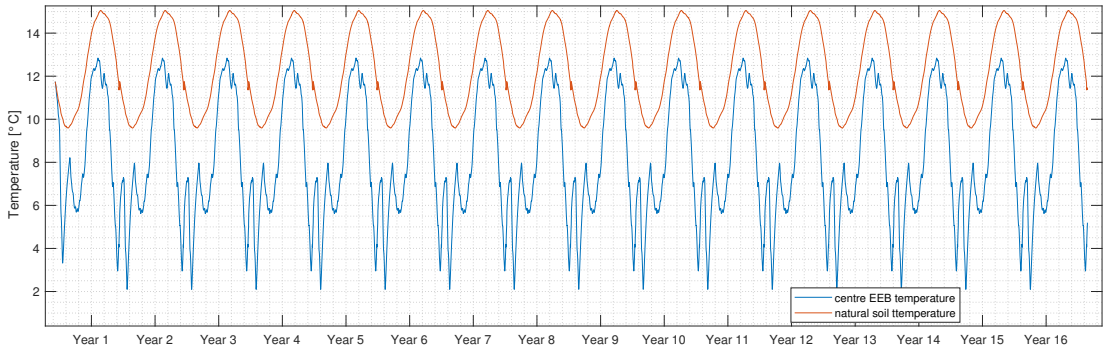

Figure 7.7: Long-term temperature variation at the centre of the EEB with heat extraction only

Similarly, Figure 7.8 shows the variation of the temperature in the borehole wall in the long term when the EEB is subjected to heat extraction only. During winter, the borehole wall temperature ranges between -4°C and 5°C. The average long-term temperature of the borehole wall is 6.52°C which is almost 6 K lower than the average natural soil temperature. The borehole wall temperature is critical in geothermal systems since it is this that directly affects the performance of the heat pump. For example, if the temperature in the borehole wall is 2°C and the system is extracting heat, then the temperature of the working fluid that exchanges heat with the evaporator of the heat pump should be considerably lower than the temperature of the borehole wall. Typically for adequate heat exchange between the EEB and the fluid, the fluid temperature must be between 6 K and 12 K less than the borehole wall temperature [145] so that there is greater potential for heat transfer. This makes the evaporator operate at very low fluid temperatures, and therefore its efficiency is very low [146]. Likewise, freezing in the borehole wall might happen affecting the physical properties of the soil near the borehole. The heat recovered during summertime is not enough to create annual thermal balance. This shows the importance of injecting and storing heat seasonally.

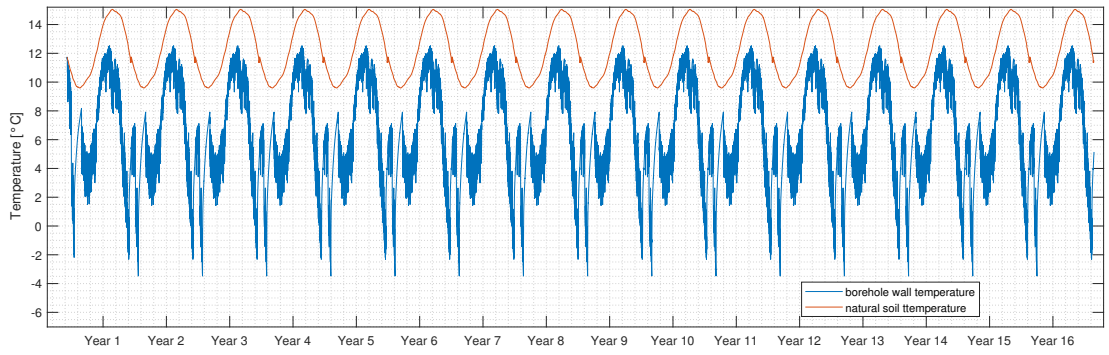

Figure 7.8: Long-term temperature variation at the borehole wall with heat extraction only

7.1.3 Heat injection only

This section shows a hypothetical case where there is only heat injection in the long term. This case is unlikely in a heating system since it would not make sense to inject or store solar heat without using it. However, this case was simulated to further explore the thermal response of the EEB by using the FDM-HF model. Note that for domestic systems where homes have only a cooling load, a geothermal system rejects heat into the ground, which would be similar to injecting heat into the ground without extracting heat from it [147]. Figure 7.9b shows the heat injection loads imposed for the simulation. The thermal loads considered are the experimental ones of 2017 discarding the heating extraction loads (Figure 7.9a). These data were repeated for 16 years for long-term simulation.

Figure 7.10 shows the temperature variation in the centre of the EEB when there is only heat injection. It can be clearly seen that EEB has a temperature higher than the natural temperature of the soil at the same depth, reaching a maximum of 20°C. The average long-term temperature of the centre of the EEB is 15.28°C which is 3 K higher than the natural temperature of the soil at the same depth. It can be also noticed that the lowest temperature reached in wintertime is higher than the natural soil temperature which mean that the heat stored is not totally lost during wintertime. However, it is clearly show that the temperature decreases considerably in winter which shows a poor performance for long-term storage.

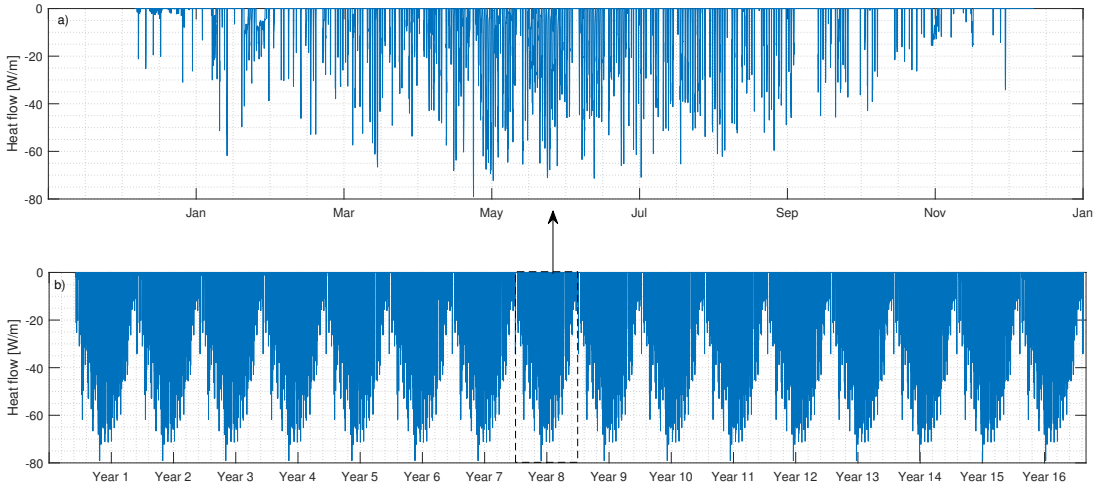

Figure 7.9: Long-term heat flow rate with heat injection only

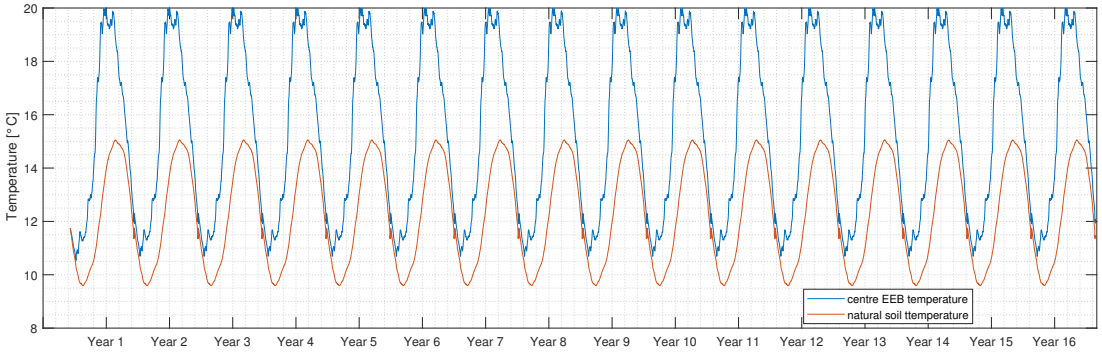

Figure 7.10: Long-term temperature variation at the centre of the EEB with heat injection only

On the other hand, Figure 7.11 shows the variation of the temperature of the borehole wall in the long term when the EEB is subjected to heat injection only. As in the centre of the EEB, the borehole wall temperature has a higher average long-term temperature than the natural soil temperature. Despite the temperature decrease in wintertime, the borehole wall temperature is always higher than the natural temperature of the soil at the same depth.

The results of the study of the behaviour of the system show that the use of a very shallow SAGSHP causes a relatively rapid thermal imbalance in the soil. For example, for the case studied, it was observed that in time lower than 5000 hours, the temperature of the EEB reaches its peak and from that moment the

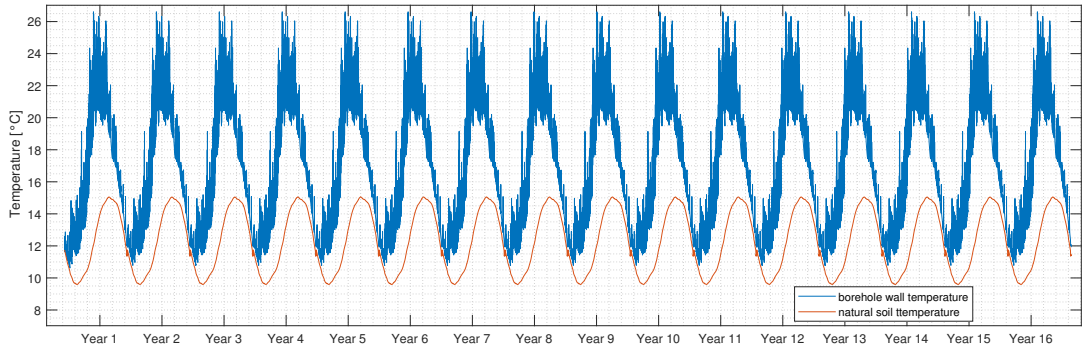

Figure 7.11: Long-term temperature variation at the borehole wall with heat extraction only

EEB tends to exchange heat slowly with the distant soil. Likewise, it could be evidenced that, if the system did not have solar heating injection, the initial temperature of the EEB could not be recovered and the efficiency of a GSHP system would be very low. Therefore, it is important that in shallow systems there is recovery or storage of heat during summer to maintain a stable operation of the system. The following sections show how the EEB would behave depending on the thermal conductivity of both the soil and thermal grout.

7.2 Variations in soil and grouting thermal conductivity

As mentioned in section 2.3.2, the performance of a geothermal system is different depending on the type of soil on which it is installed. In soils where there are no excessive underground water flows, the thermal conductivity of the soil is the most critical parameter in the performance of a GSHP system [10, 148]. The literature indicates that usually, a soil with higher thermal conductivity or a saturated soil has a better heat transfer rate and therefore the performance of a GSHP system is better in soil with higher thermal conductivity [46]. Naturally, in a real installation the type of existing soil or ground cannot be modified. However, it is essential to analyse the degree to which the thermal behaviour of very shallow geothermal systems depends on the type of soil. Similarly, the literature has indicated that the grouting material must have a high thermal con-

ductivity to reduce the thermal resistance between the fluid and the soil [149]. Nevertheless, it has also been shown that, in the long term, increasing the thermal conductivity of the grouting material is irrelevant [150]. For this reason, it is also important to evaluate the effect of the thermal conductivity of the borehole filling in very shallow borehole geothermal systems. In this section, a simulation study using the FDM-HF method (section 6.4.1) was performed using the experimental heat flow rate (considering injection and extraction) from May 2016 to April 2017 as input data. All the parameters described in Table 6.4 were maintained in the simulation, and only the values of the thermal conductivities of the soil and the grouting material were modified.

7.2.1 Soil thermal conductivity variation

Figure 7.12 shows the variation of the thermal response of the centre of the EEB to different values of soil thermal conductivity. Typically, the soil, depending on its mineral composition and the degree of water saturation, can have thermal conductivity values from 0.5 W/mK to 3 W/mK. In the case of the soil of the experimental system described in Chapter 4, the value of thermal conductivity is 1.5 W/mK. Therefore, thermal conductivity values of 0.5, 1.5 and 3 W/mK were used in the simulation. The value of the thermal conductivity of the grouting material was, in all cases, fixed and equal to 0.85 W/mK. In Figure 7.12 , it is shown that by increasing the thermal conductivity of the soil the thermal response of the soil increases due to the higher heat transfer rate. This means the surrounding soil temperature has a more significant impact on EEB when the thermal conductivity is higher. This behaviour is advantageous when the heat is extracted (during winter) as the temperature of the EEB has greater heat recovery due to its high heat diffusion. However, this behaviour is less desirable during the summer since the heat losses to the surroundings will be higher.

Figure 7.13 shows the temperature variation in the borehole wall for soils with different thermal conductivities. It can be seen in the figure that at lower thermal conductivity the borehole wall temperature variation has a higher amplitude. This behaviour is logical since the lower thermal conductivity decreases the heat diffusivity. For this reason, the layers of soil closer to the pipe wall are

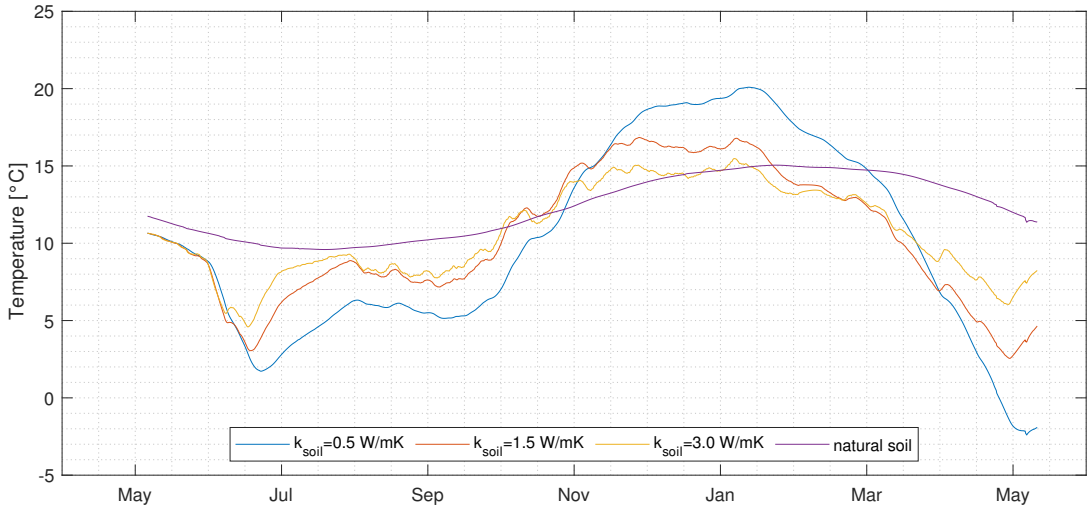

Figure 7.12: Temperature variation at the centre of the EEB for different soil thermal conductivities

the most affected by the heat flows. In general, a low thermal conductivity is not desirable in a GHSP because the heat pump would work at very low fluid temperatures during the heat extraction season. For example, according to Figure 7.13, for a soil thermal conductivity of 0.5 W/mK, the borehole wall reaches temperatures below -10°C in winter. These temperature ranges cause the heat pump to operate at very low efficiency (e.g. COP lower than 1.2 for the HP of the current study). Based on the data analysed in Figures 7.12 and 7.13, it is clear that, as mentioned in the literature, it is more desirable to work in soils with high thermal conductivity even when there is heat storage. Although lower thermal conductivity is favourable for heat storage, its negative impact on the heat pump operation is more relevant as its COP will be lower in winter due to the low borehole wall temperatures.

7.2.2 Grouting thermal conductivity variation

The backfilling of the boreholes is mainly used to provide rigidity and prevent the fracture of the pipes and to prevent the refrigerant from contaminating the soil in case of rupture since the backfilling is a material with low permeability. Typically, the thermal conductivity of the grouting material ranges between 0.5 and 1.5 W/mK. Therefore, using a material like this between the soil and the

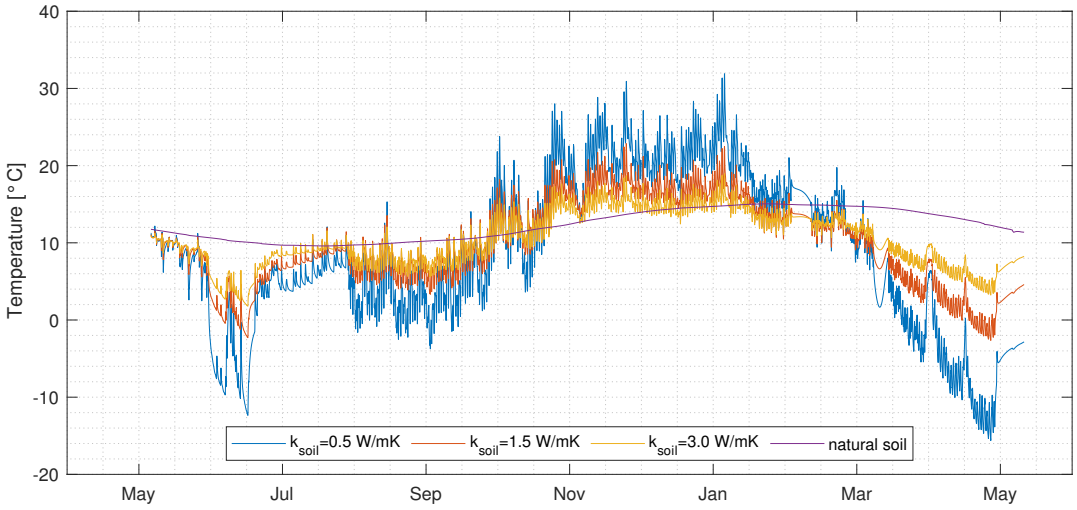

Figure 7.13: Temperature variation at the borehole wall for different soil thermal conductivities

pipe creates a thermal resistance that opposes the heat flow. For this reason, grouting materials with enhanced thermal properties have been developed in which thermal conductivities of up to 3 W/mK are achieved. However, this type of materials is more expensive, and some authors suggest that the grouting material does not have a significant impact on the long-term thermal response [150]. In this context, this section evaluates the influence of grout thermal conductivity on the short- and long-term thermal performance of the EEB. For this, the thermal response of the centre of the EEB and the borehole wall was simulated at grouting thermal conductivity values of 0.85, 1.5 and 3 W/mK. The thermal conductivity of the soil remained fixed at 1.5 W/mK.

Figure 7.14 shows the variation of the temperature in the centre of the EEB for different values of grout thermal conductivity. As seen, in the long term, the influence of the grouting material is practically negligible as the study of [150] states. This behaviour is because the size of the soil domain is considerable compared to the size of the grouting domain (range of metres vs range of few centimetres). This makes the value of the thermal resistance very low regardless of the type of material used. This behaviour is confirmed when the temperature variation in the borehole wall is studied, where it is also evident that the grouting material has little impact on the borehole wall temperature (Figure 7.15).

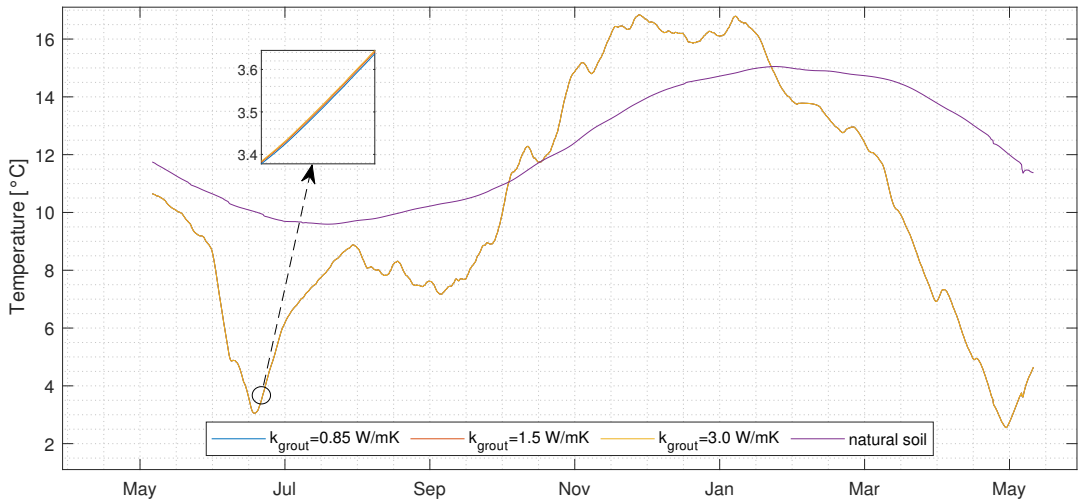

Figure 7.14: Temperature variation at the centre of the EEB for different grout thermal conductivities

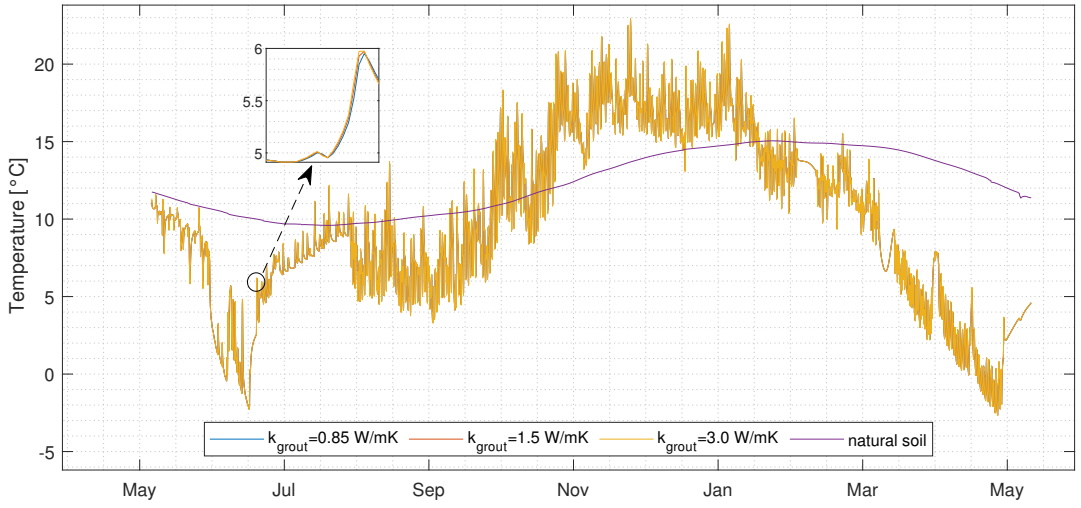

Figure 7.15: Temperature variation at the borehole wall for different grout thermal conductivities

The results shown in Figures 7.14 and 7.15, on the one hand, show that the grouting material is irrelevant in the long-term analysis. Likewise, it is shown that the consideration of the grouting material in the thermal models is irrelevant to determine the temperature in the borehole wall. Therefore, to study the behaviour of the borehole wall temperature one can use a simpler model and then treat the backfill as a thermal resistance to estimate the average tempera-

ture of the working fluid. This has been the most commonly used method when studying GSHP systems [151]. However, the model developed in the present investigation (FDM-HF) also allows evaluation of the temperature in the pipe wall of the vertical boreholes. In that context, Figure 7.16 shows the variation in the temperature of the pipe wall at different values of thermal conductivity in the grouting. This temperature value is crucial as it represents the thermal response of the system in the short term and is directly related to the operation of the heat pump. The figure shows that the pipe wall is more sensitive to the variation of the grouting material and shows that materials with higher conductivity are preferable since the amplitude of the temperature is lower. This result is significant since it is evident that, to optimise the seasonal storage (in the long term), the grouting material is irrelevant. However, for a better heat pump operation and maximizing its COP, it is desirable to use grouts with high thermal conductivity. This conclusion is also shown in the study of [150], in which it is mentioned that although the grouting material does not affect the long-term analysis, it is important for optimal heat pump performance.

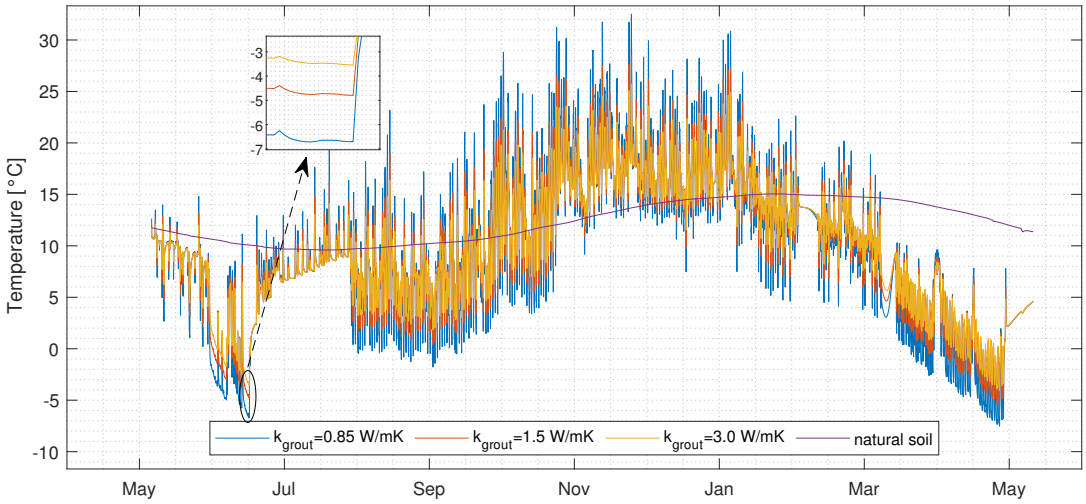

Figure 7.16: Temperature variation at the pipe wall for different grout thermal conductivities

The general conclusion of this section is that if one wants to maximise the heat pump efficiency and to operate the system optimally in the short term, a soil with high thermal conductivity is preferable, but if these conditions cannot

be achieved then this problem can be mitigated to some extent by using an enhanced grouting material. However, if one wants to maximise seasonal storage, soil with lower thermal conductivity is desirable. In any case, this opens a door for future research on optimisation and balance between heat storage and heat pump operation.

The following section shows the graphical representations also known as G-functions that are widely used to estimate the thermal response of the soil when it is subjected to heat flows from vertical boreholes. In this research, this type of representation is shown for very shallow geothermal systems.

7.3 G-functions for very shallow boreholes

As mentioned in section 2.3.2, G-functions are a graphic representation of the relationship between the rate of extraction or injection of heat from the geothermal borehole wall (qr) and its temperature (Tb) [152]. The G-functions come from Eskilson's work [106] to study the thermal response of the borehole wall in a simple way and without the need to solve complex models. In this investigation, Equation 7.1 is used to estimate the borehole wall temperature from the G-functions.

$$\Theta_s = G(Fo_b) \tag{7.1}$$

where:

$$\Theta_s = \frac{(T_b(t) - T_o)\, k_s}{q_r} \quad \text{and} \quad Fo_b = \frac{\alpha_s t}{r_b^2}$$

In Equation 7.1 , Θ_s is the dimensionless temperature, k_s is the soil thermal conductivity, q_r is the heat load in radial coordinates and Fo_b is the Fourier number at the borehole wall in function of the soil diffusivity (α_s), the time (t) and the borehole radius (r_b) (see section 2.3.2).

The G-functions of the current research are dimensionless so that they can be used for any type of soil, thermal load and duration (time) of analysis. The following sections show the G-functions obtained by applying the FDM-HF model for single and multiple shallow geothermal boreholes.

7.3.1 Single borehole G-functions

Figure 7.17 shows the G-function for a single borehole, that is the dimensionless profile of the temperature change (Θ_s) as a function of the Fourier number at the borehole wall (Fo_b) evaluated by the numerical model FDM-HF. The figure shows the thermal response for boreholes of different lengths. For low Fourier numbers ($Fo_b < 10^{-4}$), the thermal response is similar for any borehole length. This is normal since, in the first instants in which the borehole is subjected to heat flux, the axial effects are not present. The axial effects are evident al higher Fourier numbers and are different according to the length of the borehole. This is because the heat exchange with the surrounding soil (bottom of the EEB) takes more time as the length or depth of the borehole increases. It is important to mention that, in the case of very shallow geothermal boreholes (between 1 and 20 meters deep), the axial effects are more relevant and it is imperative to consider heat exchange with the distant soil.

Figure 7.17, being dimensionless, can be used to evaluate both heat extraction loads (Θ_s negative) or heat injection loads (Θ_s positive), any type of soil, different borehole diameters and different time scales. For this reason, the G-function graph is a useful tool to estimate the response in the medium and long term of very shallow GSHP systems.

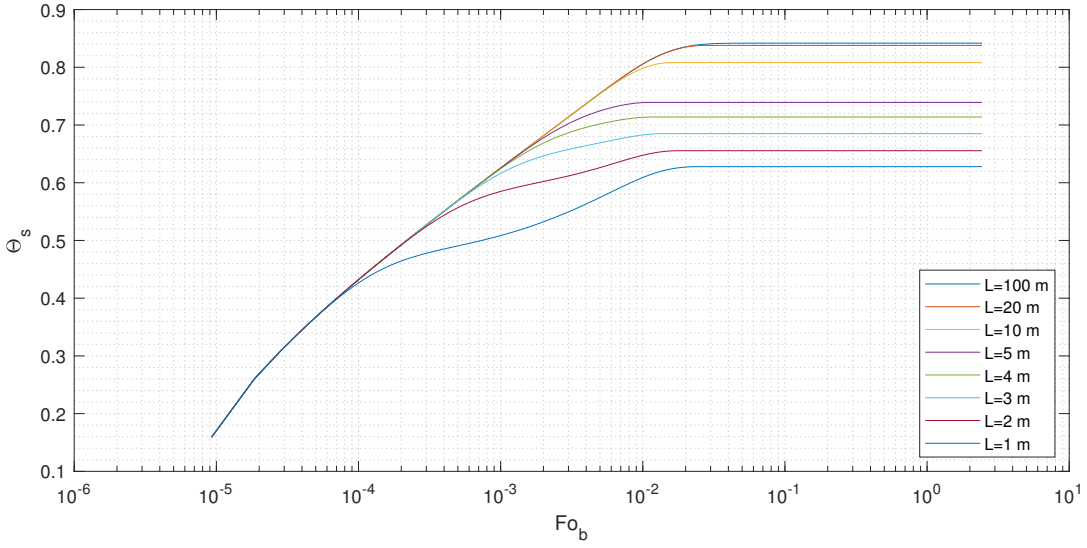

Figure 7.17: G-functions for a single borehole considering long-term axial effects

7.3.2 Multiple boreholes G-functions

The limitation of Figure 7.17 is that it is only applicable to single borehole systems. Therefore, one cannot study system with arrays of boreholes using this approach. In the case of vertical borehole arrays, G-functions were developed based on the FDM-HF to determine the borehole wall temperature when there is the influence of a neighbouring borehole located at a distance B. In that context, Figure 7.18 shows the profile of the dimensionless temperature (Θ_s) or G-functions for arrays of two vertical boreholes of different lengths, and with different separations (B) between them. If one wants to analyse the thermal response of arrays with more than two boreholes, the superposition technique can be applied and the change in the dimensionless temperature (Θ_s) of the different neighbouring boreholes within an array can be added to obtain the actual change in the dimensionless temperature.

As can be seen in the figure, in all cases, if the boreholes are separated by more than 2.5 m, the influence of the adjacent boreholes is very low. This indicates that if the boreholes are separated a distance greater than 2.5 m, they can be treated as single borehole systems. Hence, in the case where a GSHP system does not have solar heat injection or heat recovery, the neighbouring boreholes have a negative impact since they will affect the temperature change in the borehole wall making the heat pump operate less efficiently. On the other hand, if the system has storage and solar heat injection it is not advisable to install the boreholes at a separation greater than 2.5 m since the effect of storage would not be maximised.

7.4 Summary of the chapter

This chapter describes the application of the numerical model of finite differences (FDM-HF) that was developed in Chapter 6. To do this, a study of the long-term thermal behaviour of the EEB described in Chapter 4 was first conducted. In the annual heat balance, the dominant load is that of heat extraction. As the heat extraction loads are predominant, the average temperature of the EEB is lower than the natural temperature of the soil at the same depth.

On the other hand, it was observed that, if the EEB were only subjected to heat extraction loads, the average temperature of the EEB and the borehole wall would be very low, making it necessary to have very low working fluid temperatures to be able to extract heat from the soil. This performance negatively affects the operation of the heat pump. For this reason, in very shallow systems, it is necessary to have a means of heat regeneration to maintain proper operation of the heat pump.

Likewise, through the FDM-HF model, the temperature variation of the EEB, the borehole wall and the pipe wall at different values of thermal conductivity of the soil and the grouting material were studied. It was found that a soil with higher thermal conductivity is preferable since it diffuses heat more quickly allowing the average temperature of the EEB, during the heat extraction season, not to decrease dramatically. Moreover, it was evidenced that the thermal conductivity of the grouting material has no impact on the long-term thermal behaviour. However, it is more relevant in the short-term performance since it directly affects the efficiency of the heat pump. For this reason, in order to maximise the heat pump COP, it is desirable to use a grouting material with high thermal conductivity.

Finally, dimensionless graphs of the temperature profile as a function of time (G-functions) were developed to evaluate the thermal response in the medium and long term of different very shallow GSHP system configurations. These graphs consider the axial effects in the change of temperature in the long term. Through the developed G-functions, it was possible to evaluate that, for vertical boreholes arrays, at a spacing greater than 2.5 m, the neighbouring boreholes do not noticeably influence the temperature of the borehole wall. Therefore, in systems that do not have energy storage, it is preferable to have a spacing distance greater than 2.5 m to avoid the impact of neighbouring boreholes in the temperature of the borehole wall.

The following chapter shows the conclusions of the work of the current research, as well as the opportunities for future work to continue contributing with in-depth knowledge in the area of very shallow vertical geothermal systems.

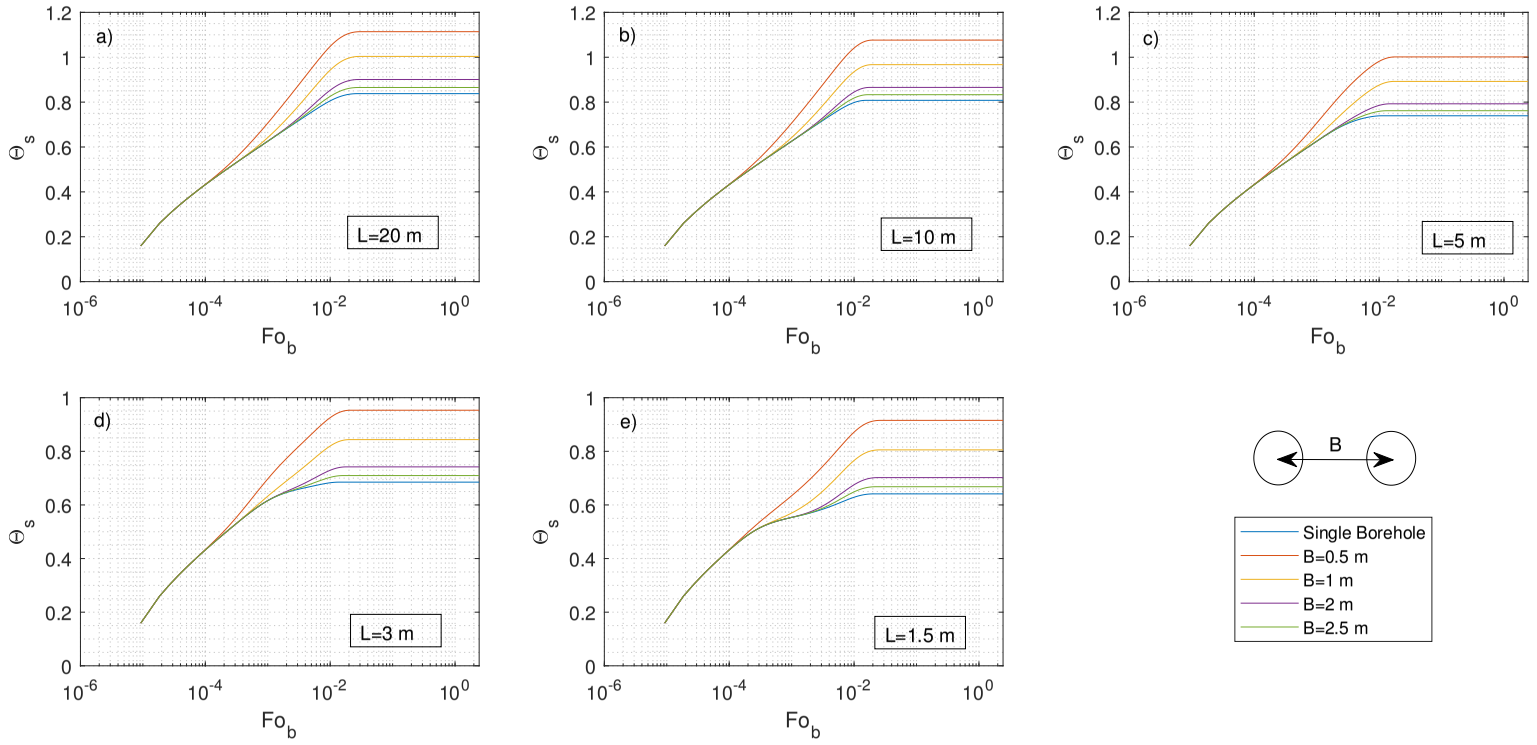

Figure 7.18: G-functions for arrays of two boreholes considering long-term axial effects and different borehole spacing

8. Conclusions

This chapter summarises the most relevant findings and results obtained in this research. Likewise, the main contributions to knowledge are highlighted in this section and the limitations and potential for further research are also shown.

As mentioned in section 1.3, the aim of this research was to develop a practical model of very shallow boreholes that is accurate enough to evaluate their thermal response in the short and long term. To achieve this aim, five specific objectives were proposed which were conducted along an experimental and numerical investigation developed in this research.

8.1 Main findings

8.1.1 Experimental investigation

An experimental study was conducted with data from 19 months of operation of the energy system in De Montfort University's 'Grasmere Street' project. Through this investigation, it was possible to observe the peculiarities of the operation of the seasonal thermal storage system or Earth Energy Bank (EEB). Although the EEB was conceived as a storage volume with negligible heat losses and gains through its base, it was experimentally determined that there is a considerable amount of heat exchange with the surrounding soil through the base. In fact, 18% of the heat flux into the EEB comes from the surrounding soil.

Likewise, the project has demonstrated that there is greater heat extraction in winter than heat injection in summer. This is due to the small size of the geothermal boreholes. Although the PVT collectors have a large capacity for gaining heat, much of this has not been transferred to the EEB due to the slow heat transfer rate caused by the small size of the boreholes. In addition, in summer, heat injection can only be done if there is a solar gain (daytime) since there is not a short-term storage tank for the heat gained. However, in winter,

heat extraction might occur at any time during the day.

By analysing the temperature profiles of the EEB, it was observed that the solar energy contribution during summer helps to improve the net balance of the EEB. The temperature at the centre of the EEB reaches up to 4 K more than the natural temperature of the soil. Thanks to this solar contribution, the temperature of the EEB does not decrease significantly in winter, reaching a minimum of 2°C, which prevents freezing of the water content in the soil which could lead to a dangerous expansion of the soil volume.

Although the system with very shallow boreholes limits the amount of heat that can be injected and extracted, a thermal store of this type is enough to meet the heat demands of a small well-insulated house of the same footprint as the EEB, which is the target of this type of system. With the current configuration, it was also possible to explore the potential improvements that can be made in this type of system. For example, for the temperatures typically reached, the use of the insulation at the sides of the EEB is irrelevant and even counterproductive as it prevents the system from gaining heat from the surroundings. However, the insulation would be more critical if a solar collector technology that injects heat at a higher temperature (e.g. flat plate or evacuated tube collectors) were used.

Finally, a potential improvement in the system, in order to maximise the heat storage, is the use of a short-term store. To do this, a water tank or phase change materials in the borehole backfill could help in storing heat in the EEB even at night.

8.1.2 Natural soil temperature variation

The natural variation of the soil temperature is very relevant in the performance of very shallow geothermal systems. However, not many studies that focus on the temperature variation of the very shallow soil in the short term were found in the literature. For this reason, different analytical and numerical models were evaluated. The analytical models studied were the sinusoidal and the semi-infinite heat conduction model. The numerical models studied were through the finite difference method (FDM) using air temperature as a boundary condition in the soil surface (FDM-T) and heat flow in the soil surface (FDM- HF), by the

energy balance in the soil surface.

It has been demonstrated that analytical models are not the most appropriate to study the behaviour of very shallow natural soil. The sinusoidal model is not able to predict temperature variations in the short term (daily or hourly) that are very important in the shallowest centimetres of the soil, while, the semi-infinite model is more accurate in the first centimetres but lacks accuracy at greater depths. Likewise, it was demonstrated that one of the most significant uncertainties in the study of the natural variation of the soil temperature is the undisturbed soil temperature. Typically, the average annual air temperature is used. However, according to the present study, it is much more accurate to use the empirical model of Badache et al. [84].

From the numerical models, it was shown that for a soil covered by light vegetation (e.g. grass) it is appropriate to use the air temperature as a proxy for the temperature at the soil surface. In fact, when comparing the FDM-T model with the experimental data of the Grasmere Street project, it was shown that this method was the most accurate, with an average error of less than 13%. Besides, it was shown that the FDM-HF model is much more complex to implement, and its average error exceeds 37%. This is mainly due to the greater uncertainty that exists in the input data.

These findings are very relevant not only for the study of geothermal systems but also for applications in agriculture and climate studies where it is crucial to define accurately the variation of the shallow soil temperature and its impact on different types of ecological systems.

8.1.3 Modelling of very shallow boreholes

The modelling of the thermal performance of arrays of very shallow geothermal boreholes is the core of this research. The main challenge of this part is to consider the impact of the natural variation of soil temperature on the thermal response of such boreholes. In the same way, considering variable loads in the short term and the interaction with adjacent boreholes makes the modelling of this system even more complex.

First, the research explored whether conventional analytical models such as

the Infinite Line Source (ILS) or Infinite Cylindrical Source (ICS) models are appropriate to study the thermal performance of such systems. For this, both analytical models were used together with the temporal superposition technique to represent the variable thermal loads. In addition, spatial superposition was also used to consider the influence of adjacent boreholes and the natural variation of soil temperature. It could be shown that both models have good accuracy to predict the soil temperature in the centre of the EEB with an efficiency (EF) of 95.6%. On the other hand, these models present greater error when used to estimate the temperature at the borehole wall, with EF less than 90% in the ILS and less than 86% in the ICS. The main reason for this is that none of these models considers the backfill material of the borehole, so they have greater uncertainty over small radial distances. However, the most significant limitation of these models is the high computational cost when considering variable thermal loads. Of the two analytical models studied, the ICS model is the one with the highest computational cost since its resolution uses more complex mathematics. In fact, in order to complete an annual simulation with the ICS model, it was necessary to work with daily thermal loads instead of hourly ones.

In contrast, the use of numerical models gave more promising results. Although the development of numerical models by the finite difference method (FDM) is more complex because it implies the discretisation of differential equations, this method has a lower computational cost and better accuracy. Given the flexibility of this method, the backfill material of the borehole and variable thermal loads can be considered more practically. When heat flow at the pipe wall was considered as boundary condition (FDM-HF), the EF was 98% and 96.5% when used to determine the temperatures in the centre of the EEB and the borehole wall respectively. When considering convection inside the pipe with variable inlet temperature (FDM-T), the EF is 93% for the temperatures of the centre of the EEB and the borehole wall, and 96% for determining the fluid outlet temperature.

The main advantage of the FDM is its fast computation. In the present research, the annual simulation that used hourly thermal loads took less than 20 seconds to finish on an ordinary personal computer. This makes the approach

practical for use with other transient models of complex systems, or for addition to building energy modelling software. It is important to mention that as part of this study, the hypothesis proposed in section 3.1 was tested. Therefore, it was shown that the use of the superposition technique together with the FDM is suitable for estimating the thermal response of very shallow boreholes quickly and accurately.

8.1.4 Performance of very shallow boreholes

The long-term thermal response of the EEB was studied using the FDM-HF model, developed in Chapter 6. It showed stable behaviour in which the annual imbalance of the system is minimal. This means that, with the current design, heat injection in summer compensates for heat extraction during winter. The storage of seasonal heat prevents the EEB from reaching very low temperatures in winter and thus prevents the heat pump from operating very inefficiently.

In addition, it was observed that if the system did not have heat injection it would also have a stable operation; however, the temperature of the EEB and the borehole wall would reach very low values (less than -3°C), which would force the working fluid to circulate at very low temperatures in order to extract heat in winter. This would decrease the COP of the heat pump considerably.

It was also demonstrated that in order to maximise heat storage, soil with low thermal conductivity is preferable. Likewise, it was shown that the backfill material is irrelevant in the performance of EEB in the long term and in the amount of heat that can be stored. This is because the backfill medium occupies a very small volume compared to the volume of the soil where heat is stored. However, it was also shown that the backfill material is of much more importance in the short term since it directly affects the operation of the heat pump. For this reason, in order to maximise the COP of the heat pump, it is preferable to use a high thermal conductivity backfill (greater than 2 W/mK). Consequently, the most desirable balance to have a better performance in the short and long term is to use a material of high thermal conductivity in the borehole backfill in soil of medium or low thermal conductivity (less than 2 W/mK).

Finally, G-functions were developed as a method for the study of the thermal

response of very shallow geothermal boreholes. This is the most common way to represent the thermal response of vertical boreholes graphically and in a dimensionless way. Thus, arrays of geothermal boreholes of different diameters, soil materials and time constants can be studied. Through this study, it was possible to demonstrate that, in order to maximise heat storage the spacing between the boreholes should not be greater than 2.5 metres. However, for systems without heat storage it is preferable that the spacing is greater than 2.5 metres to avoid a significant reduction in the soil temperature.

8.2 Contribution to knowledge

The main contribution to knowledge that is made through this research is the development of a numerical model for the evaluation of the thermal response of very shallow vertical boreholes. Although in the literature there are analytical models to evaluate the performance of conventional geothermal boreholes, these are not the most practical for study very shallow boreholes and for evaluating dynamic systems in the long term due to their high computational cost as shown in section 6.3.

The main advantage of the model developed in the present investigation is its fast resolution and high accuracy. Because of these, the model is suitable to be coupled to other numerical simulation software for energy systems such as TRNSYS, Modellica, Energyplus, etc. Therefore, complex thermal systems featuring very shallow boreholes can be studied in the long term at a low computational cost.

Also, through this research important evidence was provided concerning the operation of geothermal systems with very shallow boreholes and seasonal storage of heat in the shallow soil. This type of system has not been studied extensively because of its relatively low efficiency due to the influence of environmental variables on the soil near the surface. However, it was possible to demonstrate experimentally that this type of system can meet the energy demands of low-energy housing as seen in Chapter 4. Considering that the installation of the ground heat exchanger is very affordable compared to conventional bore-

holes, the potential that such systems may have in new constructions is very high. Indeed, systems of this type are currently being installed in new domestic developments, and this research will allow such designs to be optimised to improve the cost-benefits.

The model was developed based on heat transfer calculations and physics, therefore the application of this model is not limited to the geographic location and design of the current experimental research. This model could be easily extrapolated to other climates, borehole depth and borehole spacing.

8.3 Further research

The limitations of the current research (Chapters 4, 5, 6 and 7) and potential areas of improvement were shown both in the experimental part of the system and in the development of the different thermal response models. This section gives a brief summary of the potential future research areas that have become evident through the development of this research.

First, it is important to mention that there is a wide field for new research in the development of different types of system configurations that use very shallow vertical boreholes. This is due to the increasing number of innovative low-energy homes that are being constructed, mainly in countries such as the UK where the dominant thermal load is heating (see section 1.1). This has reduced energy demands, so that smaller systems are required to meet thermal loads. In this case, very shallow geothermal systems could play an important role due to their affordability. By including solar energy for heat recovery or storage, there would be even more interest due to the high sustainability of this system.

From the experimental study carried out, it was possible to show that given the small size of the ground heat exchanger (GHE), the solar contribution during daylight hours is limited. For this reason, future research may focus on improving the seasonal rate of heat injection into the EEB. Options such as the use of a water tank for short-term heat storage (diurnal) or the use of phase change materials in the borehole backfill would help to inject more of the heat from the solar thermal collectors into the EEB. There is also an opportunity for future re-

search into the control strategies for this type of system. Being a hybrid system (solar and geothermal), it is necessary to know the best strategy for using solar heat, which can be used directly to meet heating demands or to recover the soil temperature. The use of other types of solar collector technology is another field of future research. As evidenced, the GHE is not always able to store heat at the same rate as the solar gain. For this reason, the use of technologies such as flat plate collectors (FPC) or evacuated tube collectors (ETC) could increase the overall efficiency of the system through the higher working temperatures of the fluid in the solar thermal loop and therefore a higher temperature differential with the soil.

Potential areas of future research can also be identified through further development of heat transfer models created in this research. For example, a simple model to estimate the surface temperature of the soil for different types of surface (e.g. asphalt, concrete, dense vegetation, etc.) would be valuable. Thus, the natural temperature variation of different types of soil under different boundary conditions could be studied. This would be a great contribution not only in areas of geothermal systems but also in agriculture and climate change. Nowadays, artificial intelligence is often used to estimate the behaviour of very complex systems by using known input parameters. This could be one of the simplest and most accurate methods for developing this type of model.

Finally, a potential area of future research that would continue this investigation is the implementation of the thermal response model of very shallow boreholes in a transient simulation program such as TRNSYS or Modellica. That is, change the model developed into different programming languages that allow integration with models of other types of thermal systems. In this way, the interaction of an array of very shallow boreholes with different types of solar collector technologies, control strategies and short-term heat storage could be studied.

In summary, there is a high potential for further research, of different complexity and with practical application, which could be developed as research projects or as a thesis for doctoral or master's students.

A. Analytical Models for natural soil temperature variation

This appendix shows more details in the development of analytical models to estimate the temporal variation of the soil temperature at different depths. The two most commonly used analytical models for the study of heat diffusion in the soil are described: the sinusoidal model and the semi-infinite solid model.

A.1 Sinusoidal model

An example of a sinusoidal model is that of Kusuda and Achenbach [80, 84], which can be used to solve the heat transfer equation for the soil domain (Equation 5.4) assuming that the surface temperature of the soil has a sinusoidal variation throughout the year. This approximation enables quite an accurate derivation of the average temperature of the soil surface or evaluation of the temperature of very deep soil (more than 2 metres). However, this analytical model lacks precision if used to evaluate the temperature of very shallow soil (less than one metre deep) or to study the soil at sub-daily time steps, due to the sinusoidal shape of the function. This model only considers the one temperature amplitude (annual or daily) which is inadequate when studying sub-daily temperature fluctuations in very shallow soil.

The boundary condition of the soil surface temperature with sinusoidal variation is shown in Equation A.1.

$$T(0,t) = (T_s - \Delta T)\cos(\omega t - \varphi_s) \tag{A.1}$$

Considering this boundary condition, the resolution of Equation A.1, which can be used to determine the temperature at any time and depth, is expressed in Equation A.2:

$$T(z,t) = (T_s - \Delta T)\ e^{-z\sqrt{\frac{\omega}{2\alpha}}} \cos\left(\omega t - \varphi_s - \left(\sqrt{\frac{\omega}{2\alpha}}\right) z\right) \tag{A.2}$$

where $T_s(z,t)$ is the soil temperature at any depth z and time t, T_s is the average annual temperature of the soil surface (equivalent to the undisturbed ground temperature), ΔT is the average annual amplitude of the surface soil temperature, ω is known as the annual angular frequency and is equal to $\frac{2\pi}{t}$, α is the soil thermal diffusivity and φ_s is the phase angle in radians and corresponds to the time of the year in which the surface soil temperature is minimal [80,84].

Thus, to work with the sinusoidal analytical model, prior knowledge of T_s, ΔT, α and φ_s is required. Normally, this model is used to determine the annual behaviour of the soil, however, the same model can be used to determine the daily behaviour. In this case T_s corresponds to the average daily surface soil temperature, ΔT to the daily amplitude of the surface soil temperature, ω is the daily angular frequency and φ_s is the phase angle which corresponds to the time of day when the temperature of the soil surface is minimal.

Figure A.1 shows the variation of the temperature for soil with thermal diffusivity of 6.95 x10^{-7} m^2/s; average temperature of 12.5C, amplitude of 8°C and phase angle of $2\pi(31/365)$ rad. These input parameters were estimated from measured data (see section 4.2.1). As can be seen in the figure, at greater depths the soil temperature is less variable and there is a phase shift compared to the minimum and maximum temperature at the surface. This behaviour is due to the heat capacity of the soil, and the sinusoidal model is able to represent this. However, at the surface this model does not show the sub-daily temperature oscillation, hence this model is not appropriate for very shallow analysis. In general, this model is simple and accurate enough for the modelling of conventional borehole heat exchangers and most thermal simulation programs such as TRNSYS [135], RetScreen [153], DOE-2 [154], EnergyPlus [155], etc. use this type of model to predict soil temperature profiles.

A.2 Semi-infinite solid model

The semi-infinite solid model [81] is an analytical solution in which any solid is considered to be an infinite medium in all directions except one (the z-direction). This model is widely used for the study of thin elements like beams and metallic

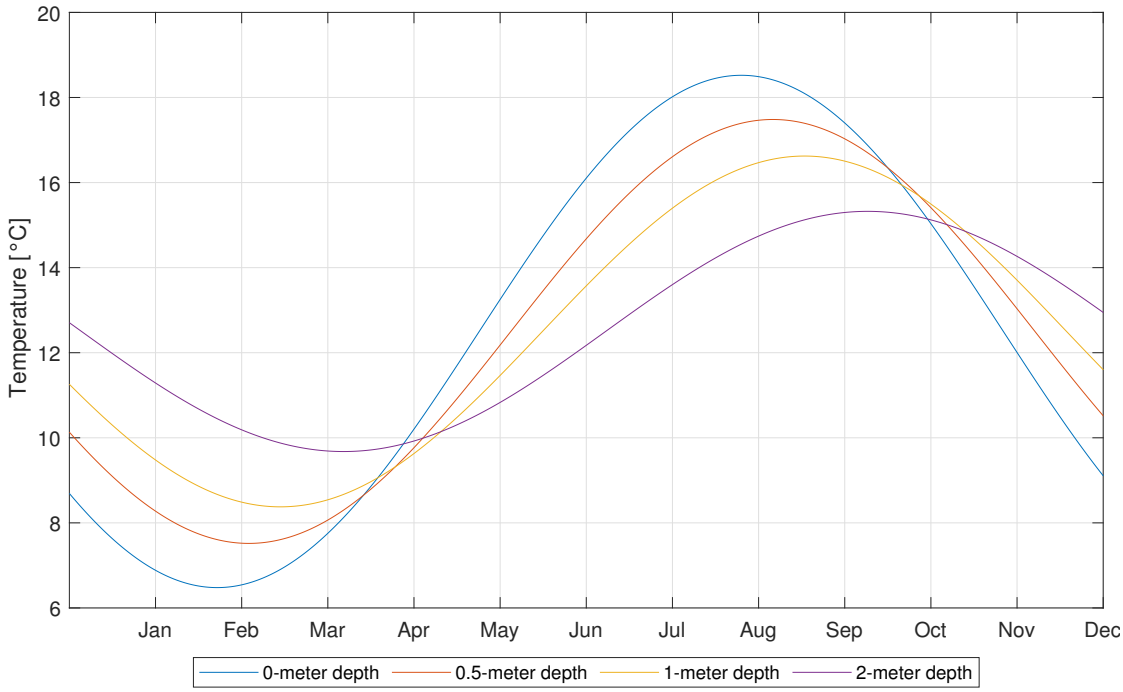

Figure A.1: Annual soil temperature variation: sinusoidal model

plates, and also for the study of the ground. Analytical solutions of the semi-infinite model are available for three different boundary conditions: constant surface temperature T_s (Equation A.3), surface exposed to convection and surface exposed to a constant heat flux q''_o (Equation A.4) [81]. The variation in the boundary conditions over time can be treated as a step function.

$$T(z,t) = \left[\text{erf}\left(\frac{z}{2\sqrt{\alpha t}}\right)(T_o - T_s)\right] + T_s \tag{A.3}$$

$$T(z,t) = \left[\frac{2q''_o(\alpha t/\pi)^{1/2}}{k}\exp\left(\frac{-z^2}{4\alpha t}\right) - \frac{q''_o z}{k}\,\text{erfc}\left(\frac{z}{2\sqrt{\alpha t}}\right)\right] + T_o \tag{A.4}$$

Where erf is the error function and erfc is the complementary function of error. The analytical semi-infinite solid model is very accurate when analysing the thermal response of a solid with a fixed boundary condition over a given time. However, this model is not appropriate for use with periodic boundary conditions since it does not accumulate the results from previous time steps.

For this reason, several authors such as Charpin et al. [82] and Florides and Soteris [156] make use of the 'thermal penetration depth' (δ_p) which corresponds to the distance over which changes in temperature are evidenced if a boundary condition is applied for a time t. In other words, the longer the exposure to a boundary condition, the greater the penetration depth and vice versa. This means that for very variable ambient conditions (hourly time step), temperature changes at depths greater than a few centimetres cannot be seen accurately through this model. Equation A.5 shows the thermal penetration depth for a given time ($\omega = 2\pi/t$) [157].

$$\delta_p = 4\sqrt{\frac{\alpha}{\omega}} \tag{A.5}$$

For example, for a soil with thermal diffusivity α=6.95 x10^{-7} m^2/s, the thermal penetration depth for different times of analysis is shown in Table A.1. As can be seen, in order to determine the influence of a boundary condition at a depth of 1 metre, the boundary condition must be applied for approximately 150 hours.

Table A.1: Thermal penetration depth at different analysis time

t **(hours)**	δp **(metres)**
0	0
1	0.05
15	0.3
40	0.5
157	1
354	1.5
628	2
981	2.5
1413	3

Figure A.2 shows the stepwise application of the semi-infinite solid model with constant surface temperature for each step as the boundary condition (Equa-

tion A.3). The boundary condition is variable each hour as a step function since the data from weather stations is normally collected on an hourly basis. This figure clearly shows the concept of the thermal penetration depth (Table A.1) where for time steps of 1 hour the penetration depth is 5 cm. This means that this model is very accurate to evaluate the temperature variation up to a depth of 5 cm. As the depth increases the accuracy is reduced so that for depths greater than 0.2 metres the model is inappropriate. Note that at depths greater than 0.5 metres, the model output is a horizontal line. At these depths, an approximate solution might be to consider the average temperature over a time step greater than one hour and apply that average temperature as a boundary condition. However, this would affect the analysis of the short-term temperature variation.

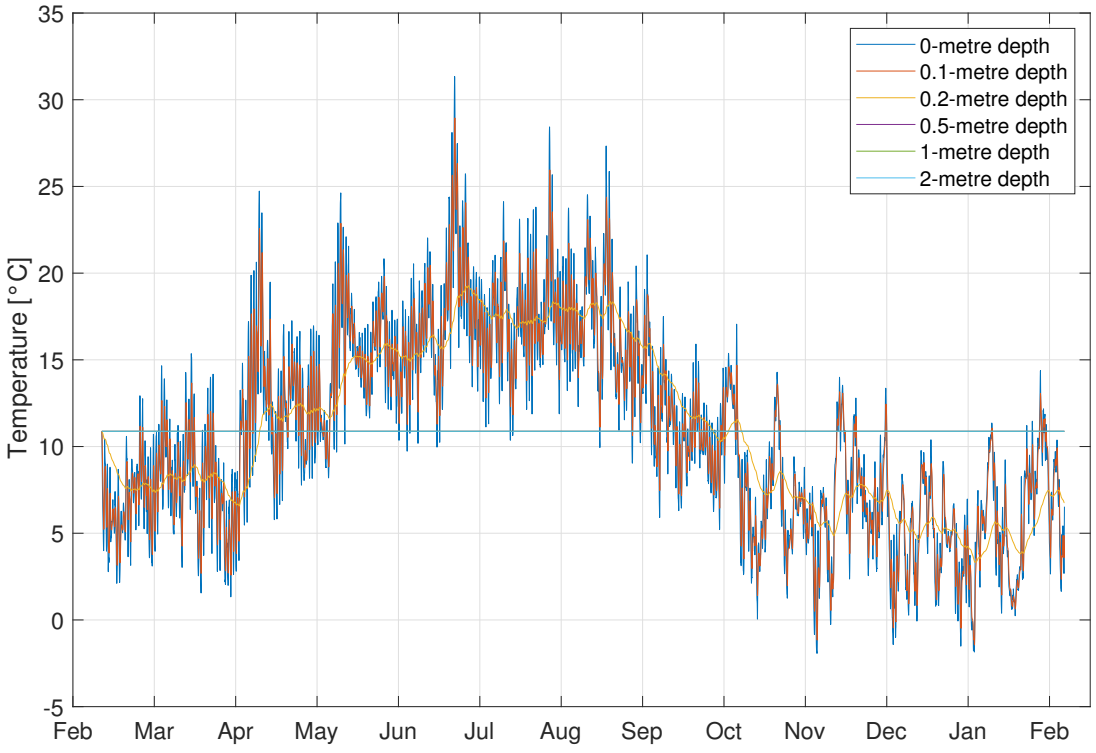

Figure A.2: Soil temperature variation: semi-infinite solid model

B. Methods for sizing borehole heat exchangers

Proper sizing of vertical ground heat exchangers (VGHE) is essential to ensure the long-term operation of the heat pump at a low cost. Undersized systems will cause heat pump failure since its entering fluid temperature (EFT) could be outside the operating ranges. On the other hand, oversized systems would imply excessive costs and profitability would be affected [158]. For this reason, the design must be "just" for a given installation. Also, the introduction of a VGHE into the soil will cause a variation in the soil temperature in the long-term (mainly in unbalanced loads). Therefore an appropriate design should consider the thermal loads as a function of time in the long-term [159]. Moreover, the VGHE sizing depends on the soil properties, the thermal resistance of the borehole R_b, the heat pump configuration, the borehole spacing (in the case of multiple arrangements) and the initial soil temperature [159, 160]. The last is very important when designing Solar Assisted VGHE because the average soil temperature is higher than the undisturbed ground temperature. Hence, the VGHE must be undersized compared to not Solar Assisted systems. Figure B.1 shows the typical geometrical configuration of multiple borehole arrangements in VGHE. An effective design should also focus on finding a suitable configuration of the borehole length H, the spacing between boreholes B, the borehole radius r_b, the shank spacing between in U-tubes S, the distance between the ground surface and the borehole top D and the number of boreholes N_b. The total length of the VGHE L is given by $N_b \times H$ [159].

While it is true that different types of VGHE configurations that differ from the standard design of Figure B.1 can be found (in-line arrangements, double U-tube, variable spacing), most practical designs fit on the standard configuration. For this reason, the review will focus on such arrangements.

The heat pump EFT, generally, should not be, in general, less than -7°C in

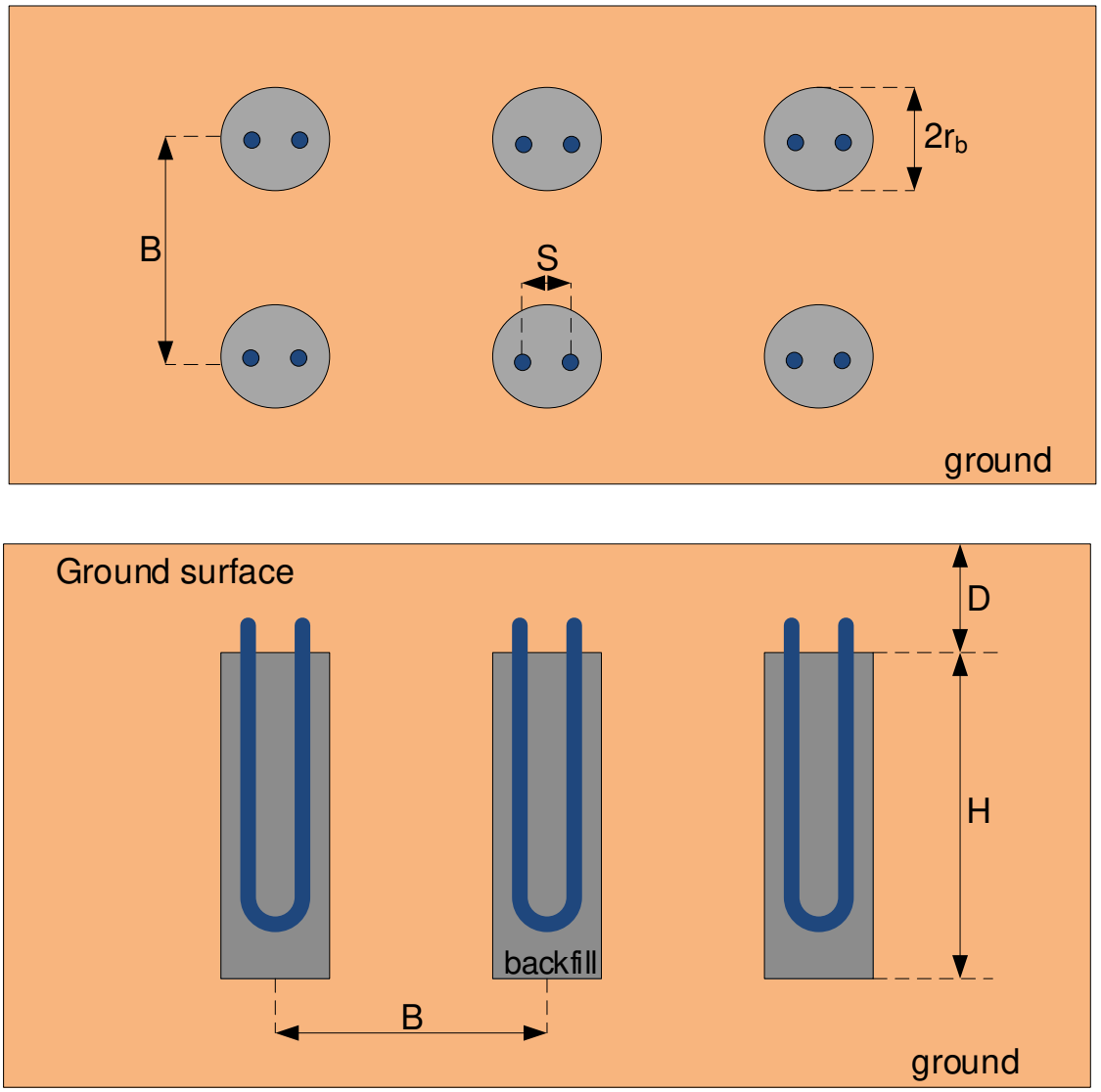

Figure B.1: Typical configuration of multiple boreholes VGHE

heating mode, and no more than 45°C in cooling mode. Therefore, considering a safety margin, VGHEs are dimensioned so that the heat pump EFT is maintained between 0 and 35°C [159]. For the heat pump of the Grasmere Street Project the admissible range is from -10 to 20°C.

B.1 Rules of thumb for VGHE sizing

The most common rules of thumb usually express an estimate for the total required borehole length as function of the heat pump capacity or the heat absorption rate from the soil [48]. These two can be related by the heat pump nominal

COP (Equation B.1).

$$q_{out} - \frac{q_{out}}{COP} = q_{in} \tag{B.1}$$

where: q_{out} (W) is the heat pump capacity; COP is the nominal coefficient of performance of the heat pump and q_{in} (W) is the heat absorption rate from the soil.

In this way, several domestic GSHP system installers use rules of thumb (e.g. 60 to 100 W peak installed heating capacity for each meter depth of borehole) adding some safety factor of a few meters. This rule of thumb is usually in agreement with most international studies. For example, in the USA, the specific installed heating capacity is usually between 68 to 82 W/m. In Switzerland, specific heat absorption rates from the ground above 75 W/m, are not recommended [48]. This type of rules of thumb is usually very simplistic since they do not consider the soil properties or the system location. In this context, some guidelines have extended this type of calculations considering other factors. For example, in Germany according to the VDI [161], specific heat absorption rates from the soil between 20 and 25 W/m are recommended for low thermal conductivity soils (<1.5 W/mK); between 50 and 60 W/m for soils with medium thermal conductivity and between 70 and 84 W/m for soils with high thermal conductivity (> 3 W/mK). In Austria, the specific heat absorption rate ranges from 30 W/m for dry sediment to 70 W/m for granite [48]. In the UK there are look-up tables supplied by the Department of Energy and Climate Change [129] to determine the maximum specific heat extraction rate (W/m) from different soil conditions.

Despite their easy application, rules of thumb are not recommended for VGHE design. As mentioned by Banks [48], a VGHE system will depend not only on the heat extraction rate but also on the thermal properties of the soil, the operation frequency, the heat pump operating temperature, thermal interference between boreholes in arrangements, among others. Applying rules of thumb can lead to design errors that may cause a system failure in the first few months or years of operation.

B.2 VGHE Design Standards and Guidelines

Nowadays there is an extended selection of guidelines and standards for the design of both vertical and horizontal GHE. Some of these guidelines are rather simplified and focus on the design of small systems (less than 45 kW) [129, 161, 162]. Some of them are only applicable in specific regions as they have charts or tables with values of temperatures or soil properties appropriate for a certain location such as the Austrian guide [162]. Few are standards based on analytical models, but mostly all of them are based on the Kavanaugh [163] models which are set out in the ASHRAE Standard Handbook of Applications, Chapter 34 [59]. Hence, in order to show methods that can be applied in different locations, the present review will show the simplified methods of the German VDI guideline [161], the British guideline [129] and the analytical method of the ASHRAE Handbook [59].

The German guide allows calculating the required borehole length L_b by a simple calculation (Equation B.2) as function of the specific heat extraction rate g, the number of boreholes N_b and the heat to be extracted from the soil q_{gr}.

$$L_b = \frac{q_{gr}}{N_b \times g} \tag{B.2}$$

The specific heat extraction rate g is obtained from tables based on the number of hours of operation of the heat pump and the thermal conductivity of the soil. On the other hand, the heat to be extracted from the soil is determined by Equation B.3.

$$q_b = q_{HP}\left(1 - \frac{1}{SPF}\right) \tag{B.3}$$

where: q_{HP} is the heat capacity of the pump and SPF is the seasonal coefficient of performance.

This guide is easy to implement. However, it has some restrictions that limit its use. The length of each borehole should be between 40 and 100 m, the separation between boreholes should be at least 5 m for lengths between 40 and 50 m and at least 6 m for lengths greater than 50 m and finally, only applies for double U-tubes boreholes. The Swiss standard SIA 384/6 proposes a correction

factor for single U-tubes, increasing the borehole length from 11 to 34% depending on the thermal conductivity of the soil [160]. Despite this, VDI guide does not consider the boreholes filling making its application very limited.

The British guideline MCS MIS 3005 suggests a simplified method like the German guide for determining the required borehole length (Equation B.4) as function of the amount of heat to be extracted from the soil q_b (Equation B.3) and the specific heat extraction rate g determined in look-up tables.

$$L_b = \frac{q_b}{g} \tag{B.4}$$

This methodology applies to single U-tubes which use a mixture of 25% Glycol Mono Ethylene and 75% water as a working fluid. It is also restricted to linear arrangements (with a minimum spacing of 6 m) and for small loads (less than 30 kW) in heating mode only.

B.3 ASHRAE Methodology

The VGHE design methodology of the ASHRAE Handbook [59] is based on the spatial and temporal superposition theorem mentioned in Kavanaugh's model [163]. This model, in turn, is based on the infinite cylindrical source (ICS) model proposed by Ingersoll et al. [103]. The ASHRAE method allows determining the required borehole length for VGHE based on successive heat transfers pulses in the long, medium and short-term (10 years, 1 month and 4 hours). The three heat pulses overlap assuming that a short peak load occurs right after a monthly peak load after 10 years of operation. In this way, robust design can be ensured in the long term. The method proposes to calculate the required length to satisfy both the cooling and heating loads. The final selection is made with the greater of these two lengths.

This method is applicable for heat pumps whose entering fluid temperature (EFT) is in the range of -5°C (in heating mode) to 40°C (in cooling mode). The design must be based on the previous knowledge of a) the peak heating and/or cooling loads; b) an estimate of the heat absorption or rejection from the soil; c) the heat pump technology to be used; d) the thermal properties of the soil and

e) maximum and minimum heat pump EFT. From this data, the sizing of the borehole length can be done through Equation B.5 (cooling) and Equation B.6 (heating).

$$L_c = \frac{q_a R_{ga} + (q_{lc} - W_c)\,(R_b + PLF_m R_{gm} + R_{gd} F_{sc})}{t_g - \frac{t_{wi}+t_{wo}}{2} - t_p} \tag{B.5}$$

$$L_h = \frac{q_a R_{ga} + (q_{lh} - W_h)\,(R_b + PLF_m R_{gm} + R_{gd} F_{sc})}{t_g - \frac{t_{wi}+t_{wo}}{2} - t_p} \tag{B.6}$$

where:

F_{sc} = short-circuit heat loss factor;

L_c = required borehole length for cooling, m;

L_h = required borehole length for heating, m;

PLF_m = part load factor during design month;

q_a = net annual average heat transfer to the ground, W;

q_{lc} = peak cooling load, W;

q_{lh} = peak heating load, W;

W_c = system power input at design cooling load, W;

W_h = system power input at design heating load, W;

R_{ga} = effective thermal resistance of the ground (annual pulse), (mK/W);

R_{gm} = effective thermal resistance of the ground (monthly pulse), (mK/W);

R_{gd} = effective thermal resistance of the ground (daily pulse: 1-6 hours), (mK/W);

R_b= effective thermal resistance of the borehole (filling, piping and fluid), (mK/W);

t_g = undisturbed ground temperature, °C;

t_p = temperature penalty for interference of adjacent boreholes, °C;

t_{wi} = liquid temperature at heat pump inlet, °C and

t_{wo} = liquid temperature at heat pump outlet, °C

In these equations, the thermal loads, heat transfer rates and temperature penalty are positive in heating mode and negative in cooling mode.

In Equations B.5 and B.6, the term $(q_{lc} - W_c)$ is equivalent to the heat rejected in the condenser q_{cond} while the term $(q_{lh} - W_h)$ is equivalent to the heat absorbed in the evaporator q_{eva}. These can be determined by Equations B.7 and B.8 respectively.

$$q_{cond} = q_{lc}\left(\frac{COP_c + 1}{COP_c}\right) \tag{B.7}$$

$$q_{eva} = q_{lh}\left(\frac{COP_h - 1}{COP_h}\right) \tag{B.8}$$

Where COP_c and COP_h are the nominal coefficient of performance in cooling and heating mode respectively.

As can be seen in Equations B.5 and B.6, three heat pulses are considered in three different time intervals through three time-varying ground thermal resistances. In the calculation, the required lengths in heating and cooling mode must be determined and the greater of the two must be selected.

Effective thermal resistances of the ground (R_{ga}, R_{gm}, R_{gd}) can be calculated graphically. To do this, the Fourier number Fo should be calculated and the G factor is determined by Equation B.9 and Figure B.2, respectively.

$$Fo = \frac{4\alpha_g \tau}{{d_b}^2} \tag{B.9}$$

In Equation B.9, α_g is the thermal diffusivity of the soil in m^2/day; τ is the operating time in days and d_b is the borehole diameter. Thus, to calculate the effective thermal resistances, three Fourier numbers must be considered: a) Fo_f (annual, τ= 3680.167 days); b) Fo_1 (monthly, τ= 30.167 days) and c) Fo_2 (daily, τ= 0.167 days). Then graphically the G factors G_f, G_1 and G_2 can be determined.

Once the G factors have been determined, the effective thermal resistances can be found through Equations B.10, B.11 and B.12.

$$R_{ga} = \frac{(G_f - G_1)}{k_g} \tag{B.10}$$

$$R_{gm} = \frac{(G_1 - G_2)}{k_g} \tag{B.11}$$

$$R_{gd} = \frac{G_2}{k_g} \tag{B.12}$$

where k_g is the effective thermal conductivity of the soil (W/mK).

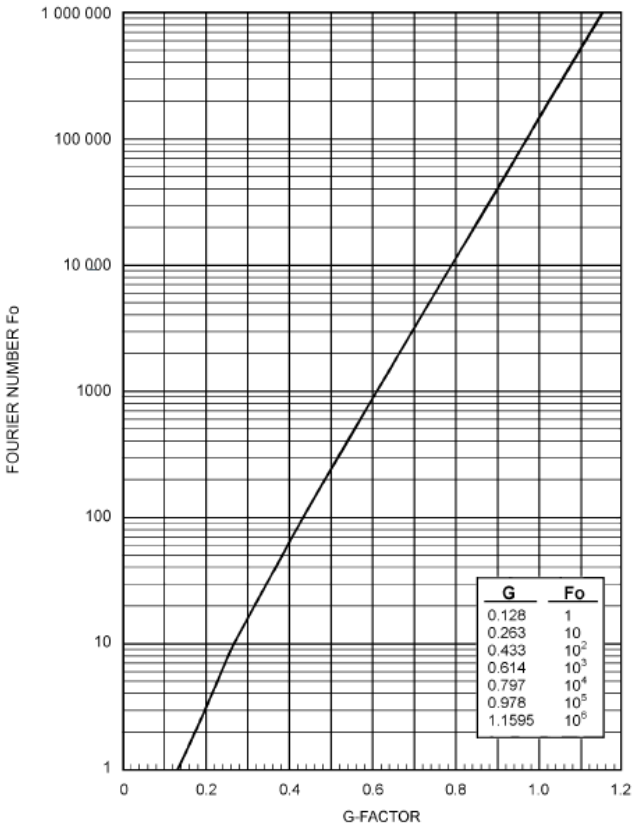

Figure B.2: G-factors in function of Fo number; Source: ASHRAE Handbook of applications, Chapter 34

On the other hand, the effective thermal resistance of the borehole can be expressed as a sum of the resistance of the pipe (including the fluid) and the resistance of the filling (Equation B.13).

$$R_b = R_p + R_{gr} \tag{B.13}$$

The thermal resistance of the pipe can be calculated from the knowledge of the convection coefficient of the fluid and the pipe h_{conv}, the inner and outer diameter of the pipe d_i and d_o, and the thermal conductivity of the pipe k_p (Equation B.14).

$$R_p = \frac{\frac{1}{\pi d_o h_{conv}} + \frac{1}{2\pi k_p} \ln\left(\frac{d_o}{d_i}\right)}{2} \tag{B.14}$$

The thermal resistance of the filling is determined by the Equation B.15.

$$R_{gr} = \left[\beta_o \left(\frac{d_b}{d_o} \right)^{\beta_1} \times k_{gr} \right]^{-1} \tag{B.15}$$

where: k_{gr} represents the thermal conductivity of the filling and the factors β_o and β_1 depend on the configuration of the borehole (Table B.1 and Figure B.3).

Table B.1: Paul's shape coefficients β_o,β_1; Adapted from: ASHRAE Handbook of applications, Chapter 34

β_0	β_1	**Case**
14.450872	-0.8176	A
17.44268	-0.605154	B
21.90587	-0.3796	C

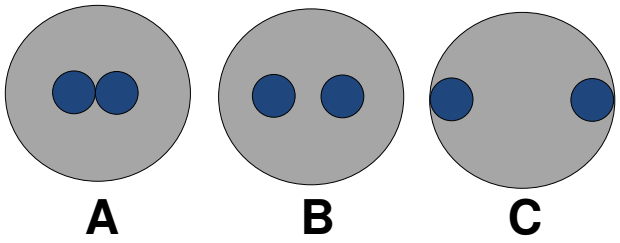

Figure B.3: Paul's coefficient cases

The short-circuit heat loss factor F_{sc} represents the heat loss between the inlet and outlet of the fluid in a loop. This can be determined by the number of boreholes per loop, the value varies from 1.01 for three boreholes in series to 1.06 for a single borehole per loop.

Finally, it is necessary to determine the temperature penalty that is due to the interference of a borehole with its adjacent boreholes. For this, ASHRAE provides a table according to the number of boreholes (and arrangement), the boreholes spacing and length. Other authors such as Bernier et al. [164] and Fossa [165] have developed methods for calculating the temperature penalty in a wider range of applications.

B.4 Alternative ASHRAE sizing method based on G-functions

As an alternative design method, the thermal response factors also known as g functions can be used. The g-functions were proposed by Eskilson [106] for long-term analysis and extended by Yavuzturk and Spitler [109] for short-term analysis. This is a graphical method in which the thermal response of a VGHE arrangement can be determined as a function of time through non-dimensional terms. The G-functions depend on four factors: a) t/t_s; b) B/H, c) r_b/H and d) D/H where t is the analysis time, t_s is a characteristic time t_s= $\frac{H^2}{9\alpha_g}$, B is the boreholes spacing, H is the borehole depth and D is the distance from the ground surface to the borehole top. Figure B.4 shows a typical graph of a G-function for a 3 x 2 borehole arrangement. Several curves of the G-functions have been proposed by Eskilson [106] and several authors have developed modifications of these functions. Also, design programs have integrated G-functions within databases.

The alternative ASHRAE method based on the g-functions proposes to use Equations B.5 and B.6 again for the design of the required borehole length. However, two modifications must be considered. The first is to eliminate the temperature penalty since this is implicit in the g-functions and the second is to calculate the effective thermal resistances (annual, monthly and daily) through the g-functions as shown in Equations B.16, B.17 and B.18.

$$R_{ga} = \frac{g\left(t_f\right) - g(t_f - t_1)}{2\pi k_{gr}} \tag{B.16}$$

$$R_{gm} = \frac{g\left(t_f - t_1\right) - g(t_f - t_2)}{2\pi k_{gr}} \tag{B.17}$$

$$R_{gd} = \frac{g(t_f - t_2)}{2\pi k_{gr}} \tag{B.18}$$

As can be seen, the complexity of this method is that the g-functions depend on the borehole length H and this in an unknown parameter in the design process ($L = N_b \times H$). Therefore, the design through this method is an iterative

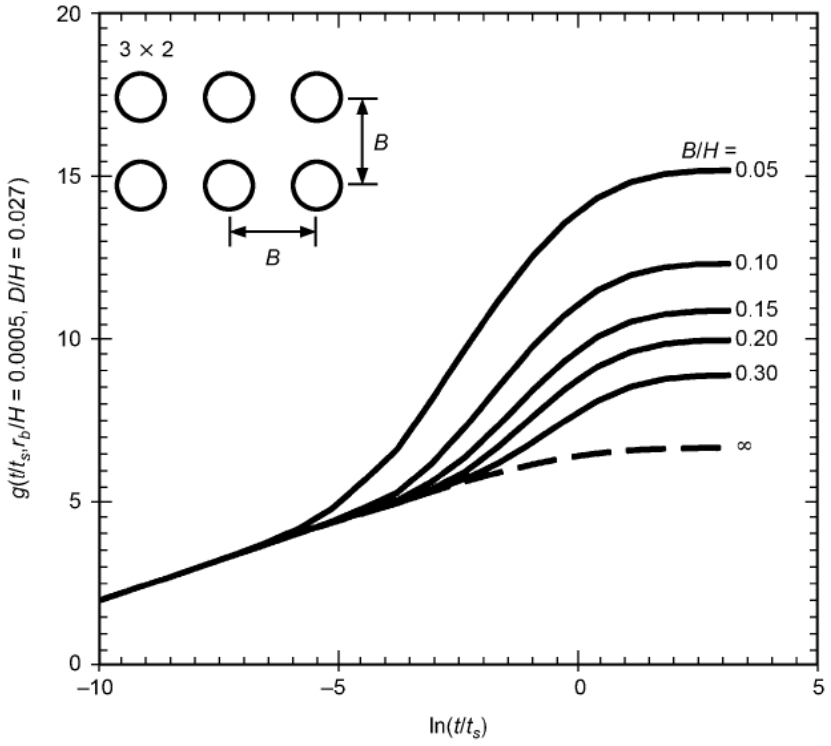

Figure B.4: Typical g-function curves (3x2 arrangement); Source: ASHRAE Handbook of applications, Chapter 34

process and requires computer assistance for an efficient resolution.

C. Heat balance in the soil surface

The study of heat transfer in the soil can be a very complex task depending on the accuracy required, as well as the depth of study. The ground temperature becomes more stable with depth. This can be seen in Figure C.1, which shows the variation of soil temperature at different depths. The data in Figure C.1 were obtained through monitoring in the soil of Leicester, UK. It is clear that the closer to the ground surface, the more unstable the thermal behaviour of the soil. Therefore, the thermal performance of shallow soil (depth less than 1 metre) is more difficult to predict. For this reason, it is important to perform an energy balance on the soil surface to have a clear idea of the variables that affect the thermal performance of the sub-surface soil.

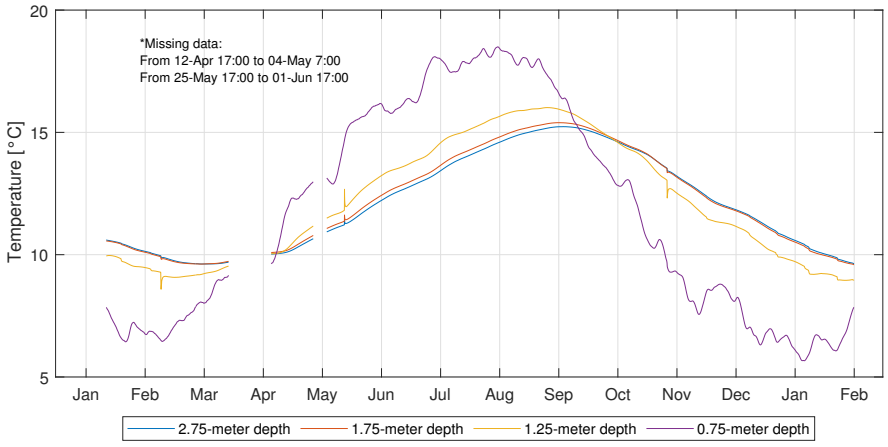

Figure C.1: Soil temperature variation with depth

Heat diffusion in soil is a transient phenomenon and can be accurately approximated as a one-dimensional flux. Equation C.1 (the Fourier heat equation in one dimension) describes this phenomenon and for its resolution, the appropriate temporal and boundary conditions must be considered.

$$\frac{\partial T}{\partial t} = \alpha \frac{\partial^2 T}{\partial z^2} \tag{C.1}$$

Typically, the soil is considered as a semi-infinite medium and the boundary conditions are as follows:

$T(z,0) = T_o$

$T(0,t) = T_s(t)\, or q_o''(0,t) = G(t)$

$T(\infty,t) = T_o$

where: $T(z,t)$ is the temperature of the soil at any depth and time; T_o is the initial soil temperature; $T_s(t)$ is the soil surface temperature which is highly variable over time, q_o'' is the conduction heat flux and $G(t)$ is the soil surface heat flux which is also variable according to the weather conditions.

If there are no soil surface temperature measurements, the surface soil temperature can be approximated as the air temperature. However, a more accurate calculation involves an analysis of heat transfer at the ground surface. Figure C.2 shows the main heat transfer mechanisms involved in the ground surface and Equation C.2 shows the existing energy balance.

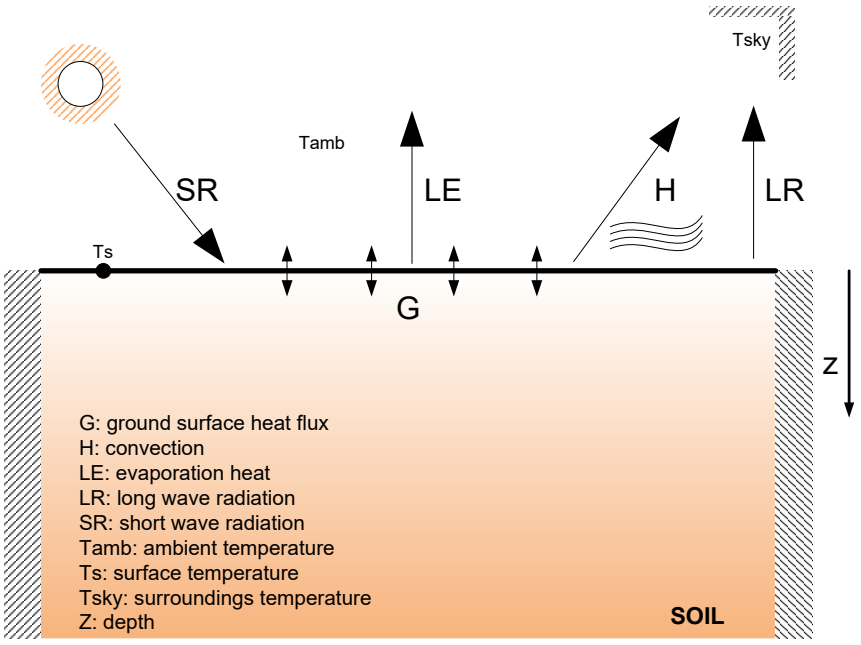

Figure C.2: Energy balance in the soil surface

$$SR - H - LR - LE - G = 0 \tag{C.2}$$

The solution of this energy balance serves to determine the boundary condition at the ground surface to be applied into Equation C.1. Two boundary

conditions are commonly used. The first is to consider the ground surface temperature, T_s, constant and the second is to consider the heat flux at the ground surface G constant. It is important to mention that such boundary conditions are constant only for a given time step, but they are dynamically or periodically variable. For the case of hourly numerical modelling, as proposed in this study, boundary conditions vary periodically every hour.

In Equation C.2, SR refers to the short-wave incident radiation (Equation C.3):

$$SR = abs\ I \tag{C.3}$$

where: abs is the soil absorptivity and I is the incident solar radiation.

H is the sensible heat by convection (Equation C.4) [89]:

$$H = \rho_a c_a \frac{(T_s - T_a)}{r_a} \tag{C.4}$$

where: ρ_a is the air density, c_a is the air specific heat, T_a is the air temperature and r_a is the aerodynamic resistance defined by Equation C.5 [166]:

$$r_a = \frac{\ln\left(\frac{z_m}{z_o}\right)}{K^2 u} \tag{C.5}$$

where: z_m is the standard height of measurement of wind speed (2 metres), z_o is the roughness length, K is the von Karman constant (0.41) and u is the wind speed.

LR refers to the long-wave radiation exchange with the surroundings (Equation C.6):

$$LR = \varepsilon\sigma({T_s}^4 - {T_{sky}}^4) \tag{C.6}$$

where: ε is the soil emissivity, σ is the Stephan-Boltzmann constant ($5.67e^{-8}$ W/m^2K^4) and T_{sky} is the sky temperature in K defined as $0.0552{T_a}^{1.5}$ [167]. LE is the heat transfer by evaporation (or latent heat) defined by Equation C.7:

$$LE = L\ E \tag{C.7}$$

where: L is the latent heat of evaporation of the water ($2.45e^6$ J/kg) and E is the evaporation rate. Before determining E, the evaporation rate potential E_p must

be determined through the Penman-Monteith method (Equation C.8) [166].

$$E_p = \frac{1}{L}\left[\frac{d\,(R_n - G) + \frac{\rho_a c_a (e_s - e_a)}{r_a}}{d + \gamma}\right] \tag{C.8}$$

where: R_n is the net radiation flux ($SR - LR$), γ is the psychrometric constant (≈ 0.066), e_s is the saturation vapour pressure, e_a is the actual vapour pressure and Δ is the slope of the saturation vapour pressure curve. These three variables can be determined following the Penman-Monteith method as stated in the work of Chalhoub et al. [89]. Then, E can be determined as a function of the rainfall P. If $P > E_p$ then $E = E_p$. If $P < E_p$, then E must be determined as stated in Equation C.9. The term β_d is function of the soil water content. The complete soil water balance and the evaporation model can be found in detail in the work of Chalhoub et al. [89].

$$E = P + \beta_d (E_p - P) \tag{C.9}$$

Finally, G is the heat transfer from or to the soil at the ground surface. The solution of Equation C.2 is an iterative process where the results of the surface temperature in a given time, affect the calculation of the surface heat flux in the following time. In this case, convection H, evaporation LE and long-wave radiation LR depend on the temperature at the soil surface.

References

[1] D. Mangold, T. Schmidt, A. Dohna, and D. Späh, "Guideline for the Seasonal Thermal Energy Storage Systems in the built environment," p. 62, 2016.

[2] C. Yavuzturk, "Modeling of vertical ground loop heat exchangers for ground source heat pump systems," p. 250, 1988.

[3] BEIS, "Energy Consumption in the UK," Tech. Rep. July, Department for Business, Energy & Industrial Strategy, 2019.

[4] C. Naranjo-Mendoza, R. M. Greenough, and A. J. Wright, "Integrating solar to ground seasonal heat storage for the small domestic heating sector in the UK: Experiments from a research prototype," in *Energising the Sustainable Development Goals through Appropriate Technology and Governance* (S. C. . Bhattacharyya, ed.), (Leicester), pp. 176–184, De Montfort University, 2019.

[5] T. You, W. Shi, B. Wang, W. Wu, and X. Li, "A new ground-coupled heat pump system integrated with a multi-mode air-source heat compensator to eliminate thermal imbalance in cold regions," *Energy and Buildings*, vol. 107, pp. 103–112, nov 2015.

[6] P. Eames, L. Dennis, H. Victoria, and P. Romanos, "The Future Role of Thermal Energy Storage in the UK Energy System: An assessment of the Technical Feasibility and Factors Influencing Adoption," *Research Report (UKERC: London)*, 2014.

[7] Y. Yuan, X. Cao, L. Sun, B. Lei, and N. Yu, "Ground source heat pump system: A review of simulation in China," *Renewable and Sustainable Energy Reviews*, vol. 16, pp. 6814–6822, dec 2012.

[8] S. E. Sofyan, E. Hu, and A. Kotousov, "A new approach to modelling of a horizontal geo-heat exchanger with an internal source term," *Applied Energy*, vol. 164, pp. 963–971, 2016.

[9] H. Yang, P. Cui, and Z. Fang, "Vertical-borehole ground-coupled heat pumps: A review of models and systems," *Applied Energy*, vol. 87, no. 1, pp. 16–27, 2010.

[10] A. Casasso and R. Sethi, "Efficiency of closed loop geothermal heat pumps: A sensitivity analysis," *Renewable Energy*, vol. 62, pp. 737–746, 2014.

[11] C. Naranjo-Mendoza, R. M. Greenough, and A. J. Wright, "Are shallow boreholes a suitable option for inter-seasonal ground heat storage for the small housing sector?," in *Proceedings of the IGSHPA Research Track 2018*, pp. 1–10, International Ground Source Heat Pump Association, sep 2018.

[12] C. Naranjo-Mendoza, A. J. Wright, M. A. Oyinlola, and R. M. Greenough, "A comparison of analytical and numerical model predictions of shallow soil temperature variation with experimental measurements," *Geothermics*, vol. 76, pp. 38–49, nov 2018.

[13] A. J. Wright, R. Talbot, and M. Goddard, "The solar house – a true low carbon solution for 2016?," in *CIBSE ASHRAE Technical Symposium*, no. April 2014, pp. 3–4, 2014.

[14] "Corby development to trial Earth Energy Bank · PHPD Online," 2019.

[15] National Statistics, "House building: new build dwellings, England: October to December 2017," p. 37, 2017.

[16] P. Conti, "Dimensionless Maps for the Validity of Analytical Ground Heat Transfer Models for GSHP Applications," *Energies*, vol. 9, p. 890, oct 2016.

[17] A. Prada, F. Cappelletti, P. Baggio, and A. Gasparella, "On the effect of material uncertainties in envelope heat transfer simulations," *Energy and Buildings*, vol. 71, pp. 53–60, mar 2014.

[18] J. Taler, "Superposition Method for Multidimensional Heat Conduction Problems," in *Encyclopedia of Thermal Stresses*, pp. 4708–4718, Dordrecht: Springer Netherlands, 2014.

[19] E. I. Sakellariou, A. J. Wright, P. Axaopoulos, and M. A. Oyinlola, "PVT based solar assisted ground source heat pump system: Modelling approach and sensitivity analyses," *Solar Energy*, vol. 193, pp. 37–50, nov 2019.

[20] G. Di Foggia, "Energy efficiency measures in buildings for achieving sustainable development goals," *Heliyon*, vol. 4, no. 11, 2018.

[21] J. Noailly, "Improving the energy efficiency of buildings: The impact of environmental policy on technological innovation," *Energy Economics*, vol. 34, pp. 795–806, may 2012.

[22] IEA, "World Energy Outlook 2017," *International Energy Agency*, 2017.

[23] S. Cao, A. Hasan, and K. Sirén, "Matching analysis for on-site hybrid renewable energy systems of office buildings with extended indices," *Applied Energy*, vol. 113, pp. 230–247, jan 2014.

[24] T. Pydych, M. Szydłowski, and J. Sowiński, "Forecast of power generation and heat production from renewable energy sources," in *E3S Web of Conferences*, 2017.

[25] J. Xu, R. Z. Wang, and Y. Li, "A review of available technologies for seasonal thermal energy storage," *Solar Energy*, vol. 103, pp. 610–638, may 2014.

[26] V. Basecq, G. Michaux, C. Inard, and P. Blondeau, "Short-term storage systems of thermal energy for buildings: a review," may 2013.

[27] A. Hesaraki, S. Holmberg, and F. Haghighat, "Seasonal thermal energy storage with heat pumps and low temperatures in building projects - A comparative review," *Renewable and Sustainable Energy Reviews*, vol. 43, pp. 1199–1213, mar 2015.

[28] L. Navarro, A. de Gracia, D. Niall, A. Castell, M. Browne, S. J. McCormack, P. Griffiths, and L. F. Cabeza, "Thermal energy storage in building integrated thermal systems: A review. Part 2. Integration as passive system," *Renewable Energy*, vol. 85, pp. 1334–1356, jan 2016.

[29] U. Stritih and U. Mlakar, "Technologies for Seasonal Solar Energy Storage in Buildings," *Advancements in Energy Storage Technologies*, vol. 125, no. Figure 1, 2018.

[30] E. Guelpa and V. Verda, "Thermal energy storage in district heating and cooling systems: A review," *Applied Energy*, vol. 252, p. 113474, 2019.

[31] P. A. Donkers, L. C. Sögütoglu, H. P. Huinink, H. R. Fischer, and O. C. Adan, "A review of salt hydrates for seasonal heat storage in domestic applications," aug 2017.

[32] C. Bott, I. Dressel, and P. Bayer, "State-of-technology review of water-based closed seasonal thermal energy storage systems," oct 2019.

[33] T. Schmidt and H. Muller-Steinhagen, "The Central Solar Heating Plant with Aquifer Thermal Energy Store in Rostock , Germany," *EuroSun 2004 – The 5th ISES Europe Solar Conference*, no. June, pp. 1–6, 2004.

[34] E. Nilsson and P. Rohdin, "Performance evaluation of an industrial borehole thermal energy storage (BTES) project – Experiences from the first seven years of operation," *Renewable Energy*, vol. 143, pp. 1022–1034, dec 2019.

[35] S. K. Shah, L. Aye, and B. Rismanchi, "Seasonal thermal energy storage system for cold climate zones: A review of recent developments," *Renewable and Sustainable Energy Reviews*, vol. 97, pp. 38–49, dec 2018.

[36] R. Fan, Y. Gao, Y. Pan, and Y. Zhang, "Research on cool injection and extraction performance of borehole cool energy storage for ground coupled heat pump system," *Energy and Buildings*, vol. 101, pp. 35–44, aug 2015.

[37] K. Allaerts, J. Al Koussa, J. Desmedt, and R. Salenbien, "Improving the energy efficiency of ground-source heat pump systems in heating dominated

school buildings: A case study in Belgium," *Energy and Buildings*, vol. 138, pp. 559–568, mar 2017.

[38] K. Allaerts, M. Coomans, and R. Salenbien, "Hybrid ground-source heat pump system with active air source regeneration," *Energy Conversion and Management*, vol. 90, pp. 230–237, jan 2015.

[39] L. Xu, J. I. Torrens, F. Guo, X. Yang, and J. L. Hensen, "Application of large underground seasonal thermal energy storage in district heating system: A model-based energy performance assessment of a pilot system in Chifeng, China," *Applied Thermal Engineering*, vol. 137, pp. 319–328, jun 2018.

[40] B. Welsch, L. Göllner-Völker, D. O. Schulte, K. Bär, I. Sass, and L. Schebek, "Environmental and economic assessment of borehole thermal energy storage in district heating systems," *Applied Energy*, vol. 216, pp. 73–90, apr 2018.

[41] N. Rapantova, P. Pospisil, J. Koziorek, P. Vojcinak, D. Grycz, and Z. Rozehnal, "Optimisation of experimental operation of borehole thermal energy storage," *Applied Energy*, vol. 181, pp. 464–476, nov 2016.

[42] B. Sibbitt, D. McClenahan, R. Djebbar, J. Thornton, B. Wong, J. Carriere, and J. Kokko, "The Performance of a High Solar Fraction Seasonal Storage District Heating System – Five Years of Operation," *Energy Procedia*, vol. 30, pp. 856–865, jan 2012.

[43] K. Tordrup, S. Poulsen, and H. Bjørn, "An improved method for upscaling borehole thermal energy storage using inverse finite element modelling," *Renewable Energy*, vol. 105, pp. 13–21, may 2017.

[44] M. Lundh and J.-O. Dalenbäck, "Swedish solar heated residential area with seasonal storage in rock: Initial evaluation," *Renewable Energy*, vol. 33, pp. 703–711, apr 2008.

[45] D. Bauer, R. Marx, J. Nußbicker-Lux, F. Ochs, W. Heidemann, and H. Müller-Steinhagen, "German central solar heating plants with seasonal heat storage," *Solar Energy*, vol. 84, pp. 612–623, apr 2010.

[46] L. Schibuola, C. Tambani, A. Zarrella, and M. Scarpa, "Ground source heat pump performance in case of high humidity soil and yearly balanced heat transfer," *Energy Conversion and Management*, vol. 76, pp. 956–970, dec 2013.

[47] Z. Qi, Q. Gao, Y. Liu, Y. Y. Yan, and J. D. Spitler, "Status and development of hybrid energy systems from hybrid ground source heat pump in China and other countries," *Renewable and Sustainable Energy Reviews*, vol. 29, pp. 37–51, jan 2014.

[48] D. Banks, *An introduction to thermogeology: Ground source heating and cooling: Second edition*. 2012.

[49] H. Biglarian, M. H. Saidi, and M. Abbaspour, "Economic and environmental assessment of a solar-assisted ground source heat pump system in a heating-dominated climate," *International Journal of Environmental Science and Technology*, no. Chiasson 2016, pp. 1–8, 2018.

[50] S. J. Self, B. V. Reddy, and M. A. Rosen, "Geothermal heat pump systems: Status review and comparison with other heating options," *Applied Energy*, vol. 101, pp. 341–348, 2013.

[51] P. Doherty, S. Al-Huthaili, S. Riffat, and N. Abodahab, "Ground source heat pump—description and preliminary results of the Eco House system," *Applied Thermal Engineering*, vol. 24, pp. 2627–2641, dec 2004.

[52] A. Hepbasli and Y. Kalinci, "A review of heat pump water heating systems," *Renewable and Sustainable Energy Reviews*, vol. 13, pp. 1211–1229, aug 2009.

[53] V. Trillat-Berdal, B. Souyri, and G. Fraisse, "Experimental study of a ground-coupled heat pump combined with thermal solar collectors," *Energy and Buildings*, vol. 38, no. 12, pp. 1477–1484, 2006.

[54] G. Emmi, A. Zarrella, M. De Carli, A. Galgaro, M. D. Carli, A. Galgaro, M. De Carli, and A. Galgaro, "Solar Assisted Ground Source Heat Pump in Cold Climates," *Energy Procedia*, vol. 82, pp. 623–629, dec 2015.

[55] S. J. Rees, *Advances in Ground-Source Heat Pump Systems*. Woodhead Publishing, 1 ed., 2016.

[56] G. Emmi, A. Zarrella, M. De Carli, and A. Galgaro, "An analysis of solar assisted ground source heat pumps in cold climates," *Energy Conversion and Management*, vol. 106, pp. 660–675, dec 2015.

[57] O. Ozgener and A. Hepbasli, "A review on the energy and exergy analysis of solar assisted heat pump systems," *Renewable and Sustainable Energy Reviews*, vol. 11, pp. 482–496, apr 2007.

[58] A. Franco and F. Fantozzi, "Experimental analysis of a self consumption strategy for residential building: The integration of PV system and geothermal heat pump," *Renewable Energy*, vol. 86, pp. 1075–1085, feb 2016.

[59] ASHRAE Standards, *ASHRAE handbook : heating, ventilating, and air-conditioning applications.* Atlanta: American Society of Heating, Refrigerating and Air-Conditioning Engineers, si edition ed., 2015.

[60] K. D. Rafferty, "Commercial Open Loop Heat Pump Systems," *ASHRAE Journal*, 2009.

[61] S. L. Do and J. S. Haberl, "A review of ground coupled heat pump models used in whole-building computer simulation programs," in *17th Symposium for Improving Building Systems in Hot and Humid Climates*, (Austin Texas), p. 9, 2010.

[62] J.-Y. Lee, "Current status of ground source heat pumps in Korea," *Renewable and Sustainable Energy Reviews*, vol. 13, pp. 1560–1568, aug 2009.

[63] N. Zhu, J. Wang, and L. Liu, "Performance evaluation before and after solar seasonal storage coupled with ground source heat pump," *Energy Conversion and Management*, vol. 103, pp. 924–933, oct 2015.

[64] M. Banjac, "Achieving sustainable work of the heat pump with the support of an underground water tank and solar collectors," *Energy and Buildings*, vol. 98, pp. 19–26, jul 2015.

[65] N. Zhu, P. Hu, L. Xu, Z. Jiang, and F. Lei, "Recent research and applications of ground source heat pump integrated with thermal energy storage systems: A review," *Applied Thermal Engineering*, vol. 71, pp. 142–151, oct 2014.

[66] X. Q. Zhai, M. Qu, X. Yu, Y. Yang, and R. Z. Wang, "A review for the applications and integrated approaches of ground-coupled heat pump systems," *Renewable and Sustainable Energy Reviews*, vol. 15, pp. 3133–3140, aug 2011.

[67] R. Thygesen and B. Karlsson, "Economic and energy analysis of three solar assisted heat pump systems in near zero energy buildings," *Energy and Buildings*, vol. 66, pp. 77–87, nov 2013.

[68] P. Eslami-Nejad and M. Bernier, "Coupling of geothermal heat pumps with thermal solar collectors using double U-tube boreholes with two independent circuits," *Applied Thermal Engineering*, vol. 31, pp. 3066–3077, oct 2011.

[69] E. Kjellsson, G. Hellström, and B. Perers, "Optimization of systems with the combination of ground-source heat pump and solar collectors in dwellings," *Energy*, vol. 35, pp. 2667–2673, jun 2010.

[70] Z. Han, M. Zheng, F. Kong, F. Wang, Z. Li, and T. Bai, "Numerical simulation of solar assisted ground-source heat pump heating system with latent heat energy storage in severely cold area," *Applied Thermal Engineering*, vol. 28, no. 11-12, pp. 1427–1436, 2008.

[71] A. D. Chiasson and C. Yavuzturk, "Assessment of the viability of hybrid geothermal heat pump systems with solar thermal collectors," *ASHRAE Transactions*, vol. 109, no. 2, pp. 487–500, 2003.

[72] N. Nord, L. H. Qvistgaard, and G. Cao, "Identifying key design parameters of the integrated energy system for a residential Zero Emission Building in Norway," *Renewable Energy*, vol. 87, pp. 1076–1087, mar 2016.

[73] F. Reda, N. Arcuri, P. Loiacono, and D. Mazzeo, "Energy assessment of solar technologies coupled with a ground source heat pump system for residential energy supply in Southern European climates," *Energy*, vol. 91, pp. 294–305, nov 2015.

[74] F. Reda and A. Laitinen, "Different strategies for long term performance of SAGSHP to match residential energy requirements in a cold climate," *Energy and Buildings*, vol. 86, pp. 557–572, 2015.

[75] C. Xi, Y. Hongxing, L. Lin, W. Jinggang, and L. Wei, "Experimental studies on a ground coupled heat pump with solar thermal collectors for space heating," *Energy*, vol. 36, pp. 5292–5300, aug 2011.

[76] K. Wang, J. Xiao, K. Li, and Y. Shi, "Experimental Research on Solar Assisted GSHP Heating System with a Latent Heat Storage Tank," in *2010 International Conference on E-Product E-Service and E-Entertainment*, pp. 1–4, IEEE, nov 2010.

[77] B. Stojanović and J. Akander, "Build-up and long-term performance test of a full-scale solar-assisted heat pump system for residential heating in Nordic climatic conditions," *Applied Thermal Engineering*, vol. 30, no. 2, pp. 188–195, 2010.

[78] L. Dai, S. Li, L. DuanMu, X. Li, Y. Shang, and M. Dong, "Experimental performance analysis of a solar assisted ground source heat pump system under different heating operation modes," *Applied Thermal Engineering*, vol. 75, pp. 325–333, 2015.

[79] T. T. Chow, H. Long, H. Y. Mok, and K. W. Li, "Estimation of soil temperature profile in Hong Kong from climatic variables," *Energy and Buildings*, vol. 43, pp. 3568–3575, dec 2011.

[80] T. Kusuda and P. Achenbach, "Earth temperature and thermal diffusivity at selected stations in the United States," *ASHRAE Transaction*, vol. 71, no. 1, pp. 61–75, 1965.

[81] F. P. Incropera, D. P. DeWitt, T. L. Bergman, and A. S. Lavine, *Fundamentals of Heat and Mass Transfer*, vol. 6th of *Dekker Mechanical Engineering*. John Wiley & Sons, 2007.

[82] J. Charpin, T. Myers, A. Fitt, Y. Ballim, and A. Patini, "Modelling Surface Heat Exchanges From a Concrete Block Into the Environment," *Mathematics in Industry Study Group South Africa*, pp. 51–58, 2004.

[83] P. J. Cleall, J. J. Muñoz-Criollo, and S. W. Rees, "Analytical Solutions for Ground Temperature Profiles and Stored Energy Using Meteorological Data," *Transp Porous Med*, vol. 106, pp. 181–199, jan 2015.

[84] M. Badache, P. Eslami-Nejad, M. Ouzzane, Z. Aidoun, and L. Lamarche, "A new modeling approach for improved ground temperature profile determination," *Renewable Energy*, vol. 85, pp. 436–444, jan 2016.

[85] F. Droulia, S. Lykoudis, I. Tsiros, N. Alvertos, E. Akylas, and I. Garofalakis, "Ground temperature estimations using simplified analytical and semi-empirical approaches," *Solar Energy*, vol. 83, pp. 211–219, feb 2008.

[86] T. R. Holmes, T. J. Jackson, R. H. Reichle, and J. B. Basara, "An assessment of surface soil temperature products from numerical weather prediction models using ground-based measurements," *Water Resources Research*, vol. 48, no. 2, 2012.

[87] T. Yilmaz, A. Özbek, A. Yilmaz, and O. Büyükalaca, "Influence of upper layer properties on the ground temperature distribution," *Journal of Thermal Science and Technology*, vol. 29, no. 2, pp. 43–51, 2009.

[88] S. D. Wullschleger, J. E. Cahoon, J. a. Ferguson, and D. M. Oosterhuis, "Simulation of Soil Surface Temperature Using the Energy Balance Equation," *Journal of Agronomic Education*, vol. 20, no. 1, 1991.

[89] M. Chalhoub, M. Bernier, Y. Coquet, and M. Philippe, "A simple heat and moisture transfer model to predict ground temperature for shallow ground heat exchangers," *Renewable Energy*, vol. 103, pp. 295–307, 2017.

[90] A. Kenan Tezcan, "Formula for the calculation of ground temperature at 1 m depth in Turkey," *Geothermics*, vol. 21, no. 3, pp. 415–417, 1992.

[91] G. Hu, X. Wu, L. Zhao, R. Li, T. Wu, C. Xie, Q. Pang, and G. Cheng, "An improved model for soil surface temperature from air temperature in permafrost regions of Qinghai-Xizang (Tibet) Plateau of China," *Meteorology and Atmospheric Physics*, pp. 1–11, jun 2016.

[92] D. Zheng, E. R. Hunt, and S. W. Running, "A daily soil temperature model based on air temperature and precipitation for continental applications," *Climate Research*, vol. 2, no. 1, pp. 183–191, 1993.

[93] K. Dolschak, K. Gartner, and T. W. Berger, "A new approach to predict soil temperature under vegetated surfaces," *Modeling Earth Systems and Environment*, vol. 1, p. 32, dec 2015.

[94] H. Tabari, P. Hosseinzadeh Talaee, and P. Willems, "Short-term forecasting of soil temperature using artificial neural network," *Meteorological Applications*, vol. 22, pp. 576–585, jul 2015.

[95] M. Li and A. C. Lai, "Review of analytical models for heat transfer by vertical ground heat exchangers (GHEs): A perspective of time and space scales," *Applied Energy*, vol. 151, pp. 178–191, 2015.

[96] J. Damiens, M. Li, Z. Pei, Y. Liu, and Y. Zhu, *Proceedings of the 8th International Symposium on Heating, Ventilation and Air Conditioning*, vol. 262 of *Lecture Notes in Electrical Engineering*. Berlin, Heidelberg: Springer Berlin Heidelberg, 2014.

[97] G. Hellström, "Ground heat storage: Thermal analyses of duct storage systems," *Lund University*, p. 310, 1991.

[98] E. Wang, A. S. Fung, C. Qi, and W. H. Leong, "Performance prediction of a hybrid solar ground-source heat pump system," *Energy and Buildings*, vol. 47, pp. 600–611, 2012.

[99] L. Lamarche and B. Beauchamp, "New solutions for the short-time analysis of geothermal vertical boreholes," *International Journal of Heat and Mass Transfer*, vol. 50, no. 7, pp. 1408–1419, 2007.

[100] Y. Li, L. Shuhua, W. Shu, M. Yucong, C. Bicheng, and L. Yuan, "Comparative Study on Methods for Computing Soil Heat Storage and Energy Balance in Arid and Semi-Arid Areas," *JOURNAL OF METEOROLOGICAL RESEARCH J. Meteor. Res*, vol. 28, no. 282, pp. 308–322.

[101] M. Li and A. C. Lai, "New temperature response functions (G functions) for pile and borehole ground heat exchangers based on composite-medium line-source theory," *Energy*, vol. 38, no. 1, pp. 255–263, 2012.

[102] M. He, "Numerical modelling of geothermal borehole heat exchanger systems," *De Montfort University*, no. February, p. 205, 2012.

[103] Ingersoll Leonard Rose, A. C. Ingersoll, and O. J. Zobel, *Heat conduction: with engineering, geological, and other applications*. London: Thames & Hudson London, 1955.

[104] W. T. Kelvin, *Mathematical and physical papers*. London: Cambridge, University Press, 1882.

[105] H. S. Carslaw and J. C. Jaeger, *Conduction of heat in solids*. Oxford: Clarendon Press, 2d ed., 1959.

[106] P. Eskilson, *Thermal Analysis of Heat Extraction Boreholes*. PhD thesis, University of Lund, 1987.

[107] H. Y. Zeng, N. R. Diao, and Z. H. Fang, "A finite line-source model for boreholes in geothermal heat exchangers," *Heat Transfer Asian Research*, vol. 31, pp. 558–567, nov 2002.

[108] M. Cimmino and M. Bernier, "A semi-analytical method to generate g-functions for geothermal bore fields," *International Journal of Heat and Mass Transfer*, vol. 70, pp. 641–650, 2014.

[109] C. Yavuzturk and J. D. Spitler, "A Short Time Step Response Factor Model for Vertical Ground Loop Heat Exchangers," *ASHRAE Transactions. ASHRAE Transactions*, vol. 105, no. 2, pp. 475–485, 1999.

[110] N. D. Paul, *The effect of grout thermal conductivity on vertical geothermal heat exchanger design and performance*. PhD thesis, 1996.

[111] M. G. Sutton, R. J. Couvillion, D. W. Nutter, and R. K. Davis, "An algorithm for approximating the performance of vertical bore heat," *ASHRAE Transactions*, vol. 108, 2002.

[112] T. R. Young, *Development, Verification, and Design Analysis of the Borehole Fluid Thermal Mass Model for Approximating Short Term Borehole Thermal Response*. PhD thesis, 2004.

[113] M. Li and A. C. Lai, "Analytical solution to heat conduction in finite hollow composite cylinders with a general boundary condition," *International Journal of Heat and Mass Transfer*, vol. 60, pp. 549–556, 2013.

[114] S. Javed, P. E. J. Claesson, and J. Claesson, "New analytical and numerical solutions for the short-term analysis of vertical ground heat exchangers," in *ASHRAE Transactions*, vol. 117, pp. 3–12, 2011.

[115] S. Javed, J. Claesson, and P. Fahlén, "Analytical Modelling of Short-term Response of Ground Heat Exchangers in Ground Source Heat Pump Systems," *10th REHVA World Congress, Clima 2010*, 2010.

[116] P. Pärisch, O. Mercker, P. Oberdorfer, E. Bertram, R. Tepe, and G. Rockendorf, "Short-term experiments with borehole heat exchangers and model validation in TRNSYS," *Renewable Energy*, vol. 74, pp. 471–477, 2015.

[117] F. Ruiz-Calvo, M. De Rosa, J. Acuña, J. M. Corberán, and C. Montagud, "Experimental validation of a short-term Borehole-to-Ground (B2G) dynamic model," *Applied Energy*, vol. 140, pp. 210–223, 2015.

[118] M. De Rosa, F. Ruiz-Calvo, J. M. Corberán, C. Montagud, and L. A. Tagliafico, "A novel TRNSYS type for short-term borehole heat exchanger simulation: B2G model," 2015.

[119] T. Sliwa, A. Gołas, J. Wołoszyn, and A. Gonet, "Numerical model of borehole heat exchanger in ansys CFX software," *Archives of Mining Sciences*, vol. 57, no. 2, pp. 375–390, 2012.

[120] J. Wołoszyn and A. Gołaś, "Experimental verification and programming development of a new MDF borehole heat exchanger numerical model," *Geothermics*, vol. 59, pp. 67–76, 2016.

[121] H. Biglarian, M. Abbaspour, and M. H. Saidi, "A numerical model for transient simulation of borehole heat exchangers," *Renewable Energy*, vol. 104, pp. 224–237, 2017.

[122] J. P. Fine, H. V. Nguyen, J. Friedman, W. H. Leong, and S. B. Dworkin, "A simplified ground thermal response model for analyzing solar-assisted ground source heat pump systems," *Energy Conversion and Management*, vol. 165, pp. 276–290, jun 2018.

[123] J. Holman, *Experimental methods for engineers*. McGraw-Hill/Connect Learn Succeed, 8th ed., 2012.

[124] "Convert Energy — Solar Hybrid PV-T range, https://www.convertenergy.co.uk/pv-t-hybrid-solar."

[125] British Standards Institution., *Thermal solar systems and components : solar collectors. Part 2, Test methods*. BSI British Standards Institution, 2006.

[126] IEC 61215, "International Standard IEC 61215: Crystalline silicon terrestrial photovoltaic (PV) modeules - design qualification and type approval," tech. rep., 2002.

[127] IEC 61730-1, "International Standard IEC 61730-1: Photovoltaic (PV) module safety qualification - Part 1: Requirements for construction," tech. rep., 2013.

[128] J. Schnieders, W. Feist, and L. Rongen, "Passive Houses for different climate zones," *Energy and Buildings*, vol. 105, pp. 71–87, oct 2015.

[129] Department of Energy and Climate Change, "MCS 3005-1: Microgeneration installation standard: MCS 022 Ground heat exchanger look-up tables: Supplementary material to MIS 3005: Issue 1.0," 2011.

[130] National Instruments and N. Instrument, "LabVIEW System Design Software - National Instruments," 2016.

[131] A. Anjomshoaa and M. Salmanzadeh, "Filling missing meteorological data in heating and cooling seasons separately," *International Journal of Climatology*, vol. 39, pp. 701–710, feb 2019.

[132] M. Oyinlola, G. Shire, and R. Moss, "Thermal analysis of a solar collector absorber plate with microchannels," *Experimental Thermal and Fluid Science*, vol. 67, pp. 102–109, oct 2015.

[133] E. W. Lemmon, M. O. McLinden, and D. G. Friend, "Thermophysical properties of fluid systems," *NIST chemistry webbook, NIST standard reference database*, vol. 69, 2005.

[134] R. Perez, R. Seals, P. Ineichen, R. Stewart, and D. Menicucci, "A new simplified version of the perez diffuse irradiance model for tilted surfaces," *Solar Energy*, vol. 39, no. 3, pp. 221–231, 1987.

[135] TRNSYS, "A transient system simulation program," 2010.

[136] D. Zenhäusern, E. Bamberger, A. Baggenstos, and A. Häberle, "PVT Wrap-Up: Energy Systems with Photovoltaic Thermal Solar Collectors," tech. rep., Swiss Federal Office of Energy, 2018.

[137] I. Guarracino, A. Mellor, N. J. Ekins-Daukes, and C. N. Markides, "Dynamic coupled thermal-and-electrical modelling of sheet-and-tube hybrid photovoltaic/thermal (PVT) collectors," *Applied Thermal Engineering*, vol. 101, pp. 778–795, may 2016.

[138] Z. Liu, J. Liu, X. Li, and J. Fang, "Experimental study on the volume and strength change of an unsaturated silty clay upon freezing," *Cold Regions Science and Technology*, vol. 157, pp. 1–12, jan 2019.

[139] M. Ouzzane, P. Eslami-Nejad, M. Badache, and Z. Aidoun, "New correlations for the prediction of the undisturbed ground temperature," *Geothermics*, vol. 53, pp. 379–384, 2015.

[140] D. Arias-Penas, M. P. Castro-García, M. A. Rey-Ronco, and T. Alonso-Sánchez, "Determining the thermal diffusivity of the ground based on subsoil temperatures. Preliminary results of an experimental geothermal borehole study Q-THERMIE-UNIOVI," *Geothermics*, vol. 54, pp. 35–42, 2015.

[141] Y. Gu and D. L. O'Neal, "An Analytical Solution to Transient Heat Conduction in a Composite Region With a Cylindrical Heat Source," *Journal of Solar Energy Engineering*, vol. 117, p. 242, aug 2008.

[142] R. A. Beier, "Equivalent Time for Interrupted Tests on Borehole Heat Exchangers," *HVAC&R Research*, vol. 14, pp. 489–505, may 2008.

[143] R. A. Beier and M. D. Smith, "Minimum duration of in-situ tests on vertical boreholes," in *ASHRAE Transactions*, vol. 109 PART 2, pp. 475–486, 2003.

[144] J. S. Claesson and P. E. Javed, "An Analytical Method to Calculate Borehole Fluid Temperatures for Time-scales from Minutes to Decades," *ASHRAE Transactions*, vol. 117, no. 2, pp. 279–288, 2011.

[145] T. Sivasakthivel, M. Philippe, K. Murugesan, V. Verma, and P. Hu, "Experimental thermal performance analysis of ground heat exchangers for space heating and cooling applications," *Renewable Energy*, vol. 113, pp. 1168–1181, 2017.

[146] L. Zhang, Q. Zhang, and G. Huang, "A transient quasi-3D entire time scale line source model for the fluid and ground temperature prediction of vertical ground heat exchangers (GHEs)," *Applied Energy*, vol. 170, pp. 65–75, 2016.

[147] F. Niu, Y. Yu, D. Yu, and H. Li, "Heat and mass transfer performance analysis and cooling capacity prediction of earth to air heat exchanger," *Applied Energy*, vol. 137, pp. 211–221, 2015.

[148] S. Chen, J. Mao, and X. Han, "Heat transfer analysis of a vertical ground heat exchanger using numerical simulation and multiple regression model," *Energy and Buildings*, vol. 129, pp. 81–91, 2016.

[149] R. A. Beier, M. S. Mitchell, J. D. Spitler, and S. Javed, "Validation of borehole heat exchanger models against multi-flow rate thermal response tests," *Geothermics*, vol. 71, pp. 55–68, 2018.

[150] T. Kurevija, M. Macenić, and S. Borović, "Impact of grout thermal conductivity on the long-term efficiency of the ground-source heat pump system," *Sustainable Cities and Society*, vol. 31, pp. 1–11, may 2017.

[151] J. D. Spitler and S. E. Gehlin, "Thermal response testing for ground source heat pump systems—An historical review," *Renewable and Sustainable Energy Reviews*, vol. 50, pp. 1125–1137, oct 2015.

[152] M. Cimmino, M. Bernier, and F. Adams, "A contribution towards the determination of g-functions using the finite line source," *Applied Thermal Engineering*, vol. 51, no. 1-2, pp. 401–412, 2013.

[153] Canmet Energy, "RETScreen International. Clean Energy Project Analysis," 2005.

[154] DOE-2.3, "Building Energy Use and Cost Analysis Tool," nov 2016.

[155] US Department of Energy, "EnergyPlus Engineering Reference: The Reference to EnergyPlus Calculations," 2010.

[156] G. Florides and S. Kalogirou, "Annual Ground Temperature Measurements at Various Depths," *8th REHVA World Congress*, no. May 2016, 2005.

[157] K. Roth, *Soil Physic: Lecture Notes*. Institute of Environmental Physics, Heidelberg University, first ed., 2012.

[158] P. Conti, *Sustainable design of ground-source heat pump systems: optimization of operative life performances*. PhD thesis, 2015.

[159] M. Ahmadfard and M. Bernier, "EVALUATION OF THE DESIGN LENGTH OF VERTICAL GEOTHERMAL BOREHOLES USING ANNUAL SIMULATIONS COMBINED WITH GENOPT," in *eSim 2016, IBPSA-Canada's biennial conference*, 2016.

[160] E. Sailer, D. M. G. Taborda, and J. Keirstead, "Assessment of Design Procedures for Vertical Borehole Heat Exchangers," *PROCEEDINGS, Fortieth Workshop on Geothermal Reservoir Engineering Stanford University*.

[161] B. Sanner, M. Reuss, and E. Konstantinidou, "VDI 4640 – a German guideline for shallow geothermal energy use," in *European Geothermal Congress 2013*, p. 1, 2013.

[162] Österreichische Wasser- und Abfallwirtschaftsverband, "ÖWAV-RB 207: Thermische Nutzung des Grundwassers und des Untergrunds," 2009.

[163] S. Kavanaugh, "A Design Method for Commercial Ground-Coupled Heat Pumps — ASHRAE Store," *Ashrae Transactions*, vol. 101, no. 2, 1995.

[164] M. A. Bernier, A. Chahla, and P. Pinel, "Long-Term Ground-Temperature Changes in Geo-Exchange Systems," *ASHRAE Transactions*, vol. 114, no. 2, pp. 342–350, 2008.

[165] M. Fossa, "The temperature penalty approach to the design of borehole heat exchangers for heat pump applications," *Energy and Buildings*, vol. 43, no. 6, pp. 1473–1479, 2011.

[166] R. G. Allen, L. Pereira, D. Raes, and M. Smith, "Crop evapotranspiration: Guidelines for computing crop water requirements," in *FAO*, p. 300, Food and Agriculture Organization of the United Nations, 1998.

[167] D. G. Krdgerl, "Convection heat transfer between a horizontal surface and the natural environment," *Research and Development Journal*, vol. 18, no. 3, pp. 49–54, 2002.